

2011-08  
10 11 1107  
1107

**Direct impact of atmospheric CO<sub>2</sub> enrichment on regional transpiration**

**Direct effect van de toenemende atmosferische CO<sub>2</sub> concentratie op regionale transpiratie**

CENTRALE LANDBOUWCATALOGUS



0000 0576 6940

**Promotor** : dr. ir. L. Wartena,  
emeritus hoogleraar in de landbouwweerkunde en  
omgevingsnatuurkunde

**Co-promotor** : dr. H.A.R. de Bruin  
universitair hoofddocent meteorologie

NN02201, 1772

C.M.J. Jacobs

## **Direct impact of atmospheric CO<sub>2</sub> enrichment on regional transpiration**

### **Proefschrift**

ter verkrijging van de graad van doctor  
in de landbouw- en milieuwetenschappen  
op gezag van de rector magnificus,  
dr. C.M. Karssen,  
in het openbaar te verdedigen  
op woensdag 11 mei 1994  
des namiddags te vier uur in de Aula  
van de Landbouwniversiteit te Wageningen.

621-599197

CIP-DATA KONINKLIJKE BIBLIOTHEEK, DEN HAAG

Jacobs, C.M.J.

Direct impact of atmospheric CO<sub>2</sub> enrichment on regional transpiration. / C.M.J. Jacobs.- [S.l.:s.n.]

Thesis Wageningen. - With ref. - With summary in Dutch.

ISBN 90-5485-250-X

Subject headings: planetary boundary layer / surface resistance / CO<sub>2</sub>.

**BIBLIOTHEEK  
LANDBOUWUNIVERSITEIT  
WAGENINGEN**

The logo for the Netherlands Organization for the Advancement of Research (NWO). It consists of the letters 'NWO' in a stylized, bold, sans-serif font. A curved line arches over the 'W' and 'O', connecting them.

The research described in this thesis was performed at the Department of Meteorology, Wageningen Agricultural University, The Netherlands. It was supported by the Netherlands Organization for the Advancement of Research (NWO).

Parts of this thesis which have been published elsewhere (Chapter 2) have been reproduced with permission of the publisher, the American Meteorological Society.

1. Modellen voor de oppervlakteweerstand van begroeide oppervlakken op basis van het door Jarvis (1976, *Phil. Trans. R. Soc. Lond., B, 273, 593-610*) en Stewart (1988, *Agric. For. Meteorol., 43, 19-35*) voorgestelde principe zijn niet geschikt voor gebruik in klimaatonderzoek.

*Dit proefschrift*

2. De door Holtslag & Moeng (1991, *J. Atmos. Sci., 48, 1690-1698*) voorgestelde parametrizatie van de "countergradient" term voor de beschrijving van niet-lokaal turbulent transport in de atmosferische grenslaag geldt alleen voor warmte.

*Dit proefschrift*

3. De in de media steeds vaker gebruikte zinsnede "het schadelijke koolstofdioxide" doet geen recht aan de ware aard van het betreffende gas.
4. De voor Noord-Afrika ontwikkelde methode om neerslaghoeveelheden te bepalen op basis van de zogenoemde "Cold Cloud Duration" (Bijv. G. Dugdale & J.R. Milford, 1986, *Proc. ISLSCP Conference, Rome, ESA SP-248, 315-319*) is verre van geschikt voor toepassing in Zuidelijk Afrika.

*Jacobs, C.M.J., 1987, Preliminary report on the applicability of the METEOSAT-system in rainfall mapping over Zambia. Internal report, Meteo Consult Wageningen.*

5. Om verwarring te voorkomen dient de term "interceptie" alleen gebruikt te worden in de letterlijke betekenis van het woord, en niet om verdamping van vrij water bij natte gewassen aan te duiden.
6. In tegenstelling tot de suggestie die de naam "Open Top Chamber" wekt, is in deze dakloze kassen de koppeling met de atmosfeer onvoldoende om de resultaten van bijvoorbeeld CO<sub>2</sub>-begassings experimenten rechtstreeks te extrapoleren naar grotere schalen.

*Bijv. Jetten, T.H., 1992, Physical description of transport processes inside an open top chamber in relation to field conditions. Proefschrift Landbouwniversiteit Wageningen.*

7. In de huidige koelkasten is de temperatuur vaak te hoog als gevolg van het foutief instellen van de thermostaat (bijv. Reitsma et al., 1986, *Verlag 1986-274, Vakgroep Gezondheidsleer, Landbouwniversiteit Wageningen*), zodat het beter is om koelkasten te voorzien van een niet-regelbare thermostaat, die een voldoende lage temperatuur waarborgt.
8. De verwaarlozing en onderdrukking van dialecten staan in schril contrast met de zorg die aan andere cultuuruitingen besteed wordt.
9. Rokers zouden regelmatig aan een longfunctietest onderworpen moeten worden om hen in een vroeg stadium met de gevolgen van roken voor hun gezondheid te confronteren.
10. Nederland is te vol met politici die roepen dat Nederland vol is.

12. Terwijl het Ministerie van Verkeer en Waterstaat de Betuwelijn presenteert als een panacee, is de vergelijking met een bittere pil uit de doordrukstrip meer op zijn plaats.
13. Durven uitkomen voor geen mening getuigt tegenwoordig van moed.
14. In het natuurwetenschappelijk onderwijs dient meer aandacht besteed te worden aan een correcte en consequente toepassing van het SI.
15. "Wetenschap" is een inflatoir begrip geworden.

*Stellingen behorende bij het proefschrift van C.M.J. Jacobs:  
"Direct impact of atmospheric CO<sub>2</sub> enrichment on regional transpiration"*

*Wageningen, 11 mei 1994*

## Abstract

Plant physiological research has revealed that stomatal aperture of many plant species is reduced by  $\text{CO}_2$ . Therefore, the question has been raised as to how transpiration will be affected if the ambient  $\text{CO}_2$  concentration increases. This study focuses on the prediction of changes in transpiration at the regional scale (10-100 km horizontal, 1-5 km vertical). A rather detailed, coupled vegetation-Planetary Boundary Layer (PBL) model has been constructed in order to identify important processes that control such changes.

The coupled model uses the well-known "big-leaf" model for the vegetation part. Surface resistance ( $r_s$ ) is described by means of an up-scaled "A- $g_s$ " model, where stomatal conductance is related to photosynthetic rate. The background of this model for  $r_s$  is outlined. A new parameterization to mimic stomatal humidity responses is proposed. The parameterization prescribes a linear relation between the specific humidity deficit at the leaf surface and the ratio of the internal  $\text{CO}_2$  concentration to the external  $\text{CO}_2$  concentration. The resulting A- $g_s$  model simulates stomatal responses to  $\text{CO}_2$ , light, temperature, humidity as well as their synergistic interactions. The model is tested using data for grapevines (*Vitis Vinifera* L., cv. Airen). The model is able to simulate the photosynthetic rate and the stomatal conductance of this species satisfactorily.

The PBL part of the coupled model is a 1D, first-order closure model, which takes into account nonlocal turbulent transport by means of a countergradient correction. The PBL model also simulates  $\text{CO}_2$  fluxes and concentrations. The surface flux of  $\text{CO}_2$  is driven by photosynthetic rate from the up-scaled A- $g_s$  model. The complete coupled model realistically simulates the state of the PBL,  $r_s$ , transpiration, and the most important aspects of the biosphere-atmosphere interaction for extensive, homogeneous, well-watered canopies with dry leaves.

Systematic sensitivity studies using the coupled model reveal that the interaction between vegetation and the PBL has a significant effect on transpiration and on  $r_s$ . On the one hand, the PBL provides a strong negative feedback on transpiration which reduces the change in the transpiration at given change in  $r_s$ . The influence of the PBL depends strongly on surface roughness. On the other hand, the simultaneous change of  $r_s$  and of the specific humidity deficit inside the canopy provides a positive feedback, thereby increasing the initial perturbation of  $r_s$  and transpiration. A second positive feedback mechanism is present if the optimum temperature for photosynthesis is exceeded.

The main conclusion is that the interaction between the PBL and vegetation has to be taken into account if transpiration and its changes due to changing surface characteristics are to be predicted at the regional scale.

Keywords: transpiration, planetary boundary layer, surface resistance,  $\text{CO}_2$

*de waereld blief drejje  
de wingk blief wejje  
jao, gluij mich, 't geit  
wie 't in de sjterre sjeit*

*P. van Bree & A. Geraeds*

*Vur moe en vur pa*



## Nawoord vooraf

Met een zucht van verlichting spuit de laserprinter deze laatste pagina's. Daarmee wordt dan het werk van jaren afgesloten. Werk, waaraan ik tot het einde toe met veel plezier bezig ben geweest. Die broodnodige lol in mijn werk werd gevoed met de hulp, steun en belangstelling van de mensen om mij heen. Daarom wil ik *iedereen* die op haar of zijn eigen manier bijgedragen heeft aan het tot stand komen van dit proefschrift heel hartelijk bedanken! Een aantal mensen wil ik hier speciaal noemen. Bevrijd van het Engels, dat ons dagelijks leven meer en meer terroriseert en ons taalgebruik zo onpersoonlijk maakt, kan dat des te beter.

Om te beginnen wil ik Bert Wartena, mijn promotor, bedanken. Bert, door jouw kennis van zaken en het enthousiasme waarmee je die kennis overbracht ben ik meteorologie écht leuk gaan vinden: dankzij jou heb ik de overstap van de arbeidshygiëne naar de meteorologie gemaakt. Jouw kijk op de materie was altijd fundamenteel én praktisch, een combinatie die mij menigmaal hoofdbrekens heeft bezorgd.

Zonder Henk de Bruin, mijn co-promotor, had ik waarschijnlijk nooit aan dit boekje kunnen beginnen. Henk, jij hebt mij geïntroduceerd in de internationale wereld van de micrometeorologie en de grenslaagmeteorologie. De ervaringen die ik daar heb opgedaan behoren tot de boeiendste uit de afgelopen periode. Ondanks de grijze haren die ik daaraan heb overgehouden wil ik je dan ook hartelijk bedanken voor je bijdrage aan mijn werk. Ik hoop dat we onze samenwerking nog kunnen voortzetten met het schrijven van een aantal publikaties.

Bert Holtslag van het KNMI wil ik bedanken voor het beschikbaar stellen van de oorspronkelijk versie van het in dit onderzoek gebruikte grenslaagmodel. De heren Schouwink van de vakgroep Tuinbouwplantenteelt van de Landbouwniversiteit en Stortelder van de KEMA wil ik bedanken voor het uitlenen van de porometers die gebruikt werden bij het veldexperiment in Spanje. Verder ben ik veel dank verschuldigd aan Jan van Kleef van CABO-DLO, voor het uitlenen van de fotosynthese-apparatuur en de daarbij geleverde unieke service. Proost, Jan!

Dan zijn er de mensen die badend in hun zweet en in het stof van Castilla-La-Mancha geholpen hebben bij het verzamelen van de porometer- en fotosynthese-data: Eric Beek, Harald van Dam, Laurens (bist du) Ganzeveld, Adrie (Señor) Jacobs, Ad (bijna Tegels) Jeuken, Berenice Michels, Arnold Moenen, Anne (tuuut) Verhoef, en natuurlijk de onovertroffen organisator van het Wagenings meteo-gebeuren bij Tomelloso: Bart van den Hurk. ¡Muchas gracias! Oh ja, het reisje naar de Maan heb ik nog even uitgesteld...

Jan Goudriaan wil ik bedanken voor het "op afstand", maar kritisch doorlezen van een groot deel van het manuscript. Bert van Hove van "Luvo" (mijn oude thuisbasis, tegenwoordig: "Lukwa") wil ik bedanken voor de stimulerende uitwisseling van gedachten over "plantjes". Nu de de rest nog, Bert!?

## Nawoord vooraf

---

Tot op het *allerlaatste* moment stond Kees van den Dries *altijd* klaar, zij het nu en dan verscholen. Als de computer weer eens een eigen wil bleek te hebben kreeg Kees 'm weer in het gareel! Bedankt Kees, ook voor je bakken stevige leut!

Op "Meteo" kan iedereen gewoon zichzelf zijn. In de unieke, informele sfeer op de vakgroep heb ik mij altijd thuis gevoeld. Ik wil dan ook alle medewerkers en ex-medewerkers (M/V) bedanken voor de prima tijd die ik op Duivendaal heb gehad, en nog heb. Bij een aantal mensen heb ik een heel speciale associatie met "promotie-tijd op Duivendaal": Anno van Dijken, ex-collega, kamergenoot, vriend en promotie-steun sinds mijn eerste uur op "Meteo". Samen hebben we een fantastische tijd gehad in de barak. Het lunch-halfuurtje en het middagkoffie-kwartiertje zijn nu niet meer weg te denken. Uiteraard, mede dankzij Theo (JeoVD) Jetten, voor mij een onverstaanbaar baken tijdens de afronding, en dat soort zaken. Salaam, Rushdi El-Kilani, how is your .ife...? Where do you live, Duivendaal, or what...? Tenslotte, tegen de sterspelers van "De Nattebollen", later "Rustenburg IV" en "Rustenburg V" zou ik willen zeggen: Vive la Victoire, Vive la Vie !

Van-eiges: moeder wil ich get zêgke op zich Tegels, mien *waore* moodertaal. Saame mêt pa leet geej mich altiéd mienen eige sjtudie-waég zeuke. Niks môs, alles kôs! Det is hiel belangriék vur mich gewaes. En ouch, ...efeng, neet vur niks is dit bukske aan uch opgedraage. Bedank!

Weej weite allemaol det ich noëts zoë wiéd gekômme kôs zien zônger mien liërmeisters van 't iërste oor: Antoon, Miek, Petra (in daen tiéd nag Nellie), Bella en José! ('t sjpiet mich, jônges, dao waart geej nag neet beej...)

Sneon, snein, knineblêdensmots, dao bösse den, Pluis! Als ik iemand moet noemen: c'est toi! Bedankt voor het hogere-orde plak- en knipwerk. Tige by tige, famke! Maar vooral: bedankt voor *meer* dan *alles*. Siiii, señora..., nu jij!

Cor, en ouch de groete van Kuëbes!

---

**Contents**

<b>List of symbols and abbreviations</b>	xv
<b>1 Introduction</b>	1
1.1 Background	1
1.1.1 General	1
1.1.2 Direct effects of atmospheric CO <sub>2</sub> enrichment on evapotranspiration	2
1.1.3 General features of transpiration and of the prediction of changes	3
1.1.4 Interactions at the regional scale	5
1.2 Objective and delimitation of the present study	6
1.3 Approach and organization of the thesis	7
<b>2 The sensitivity of regional transpiration to land-surface characteristics: significance of feedback</b>	11
2.1 Introduction	11
2.2 Theory	14
2.2.1 Sensitivity analyses	14
2.2.2 The sensitivity of $\lambda E$ without feedback	15
2.2.3 The sensitivity of $\lambda E$ with feedback	17
2.3 Setup of the sensitivity analyses	17
2.3.1 The models	17
2.3.2 Initial and boundary conditions	18
2.3.3 Reference surfaces and prescribed conditions	18
2.3.4 Variation of the surface characteristics; determination of sensitivities	19
2.4 Results	20
2.4.1 Influence of SL feedback	20
2.4.2 Influence of PBL feedback	22
2.4.3 Sensitivity with a box model for the PBL	27
2.5 Discussion and conclusions	28
2.5.1 Significance of PBL feedback	28
2.5.2 Coupling of the vegetation to the atmosphere	29
2.5.3 Control of transpiration	30
2.5.4 Influence of SL feedback on the sensitivities	30
2.5.5 Prediction of future changes in $\lambda E$	31
<b>3 Modelling stomatal responses to atmospheric CO<sub>2</sub> enrichment</b>	33
3.1 Introduction	33
3.2 Comparison of JS-models for $g_s$ versus A- $g_s$ models	34
3.2.1 General	34
3.2.2 JS models	35
3.2.3 A- $g_s$ models	36

---

3.3	Plant physiological background to the A-g <sub>s</sub> model	37
3.3.1	Basic features of photosynthesis	37
3.3.2	Stomatal behaviour	40
3.4	Physical limitations of the photosynthetic rate	44
3.4.1	General	44
3.4.2	Boundary layer conductance	45
3.4.3	Stomatal conductance	45
3.4.4	Cuticular conductance	45
3.4.5	Mesophyll conductance	46
3.5	The A-g <sub>s</sub> model part I: the photosynthesis model	46
3.5.1	General	46
3.5.2	Light as the limiting factor	47
3.5.3	CO <sub>2</sub> as the limiting factor	47
3.5.4	Synthesis: interaction of light responses and CO <sub>2</sub> responses	48
3.5.5	Temperature responses	48
3.5.6	Model characteristics: responses of A <sub>n</sub> to CO <sub>2</sub> , light and temperature	49
3.6	The A-g <sub>s</sub> model part II: stomatal responses	52
3.6.1	General	52
3.6.2	First approximation	52
3.6.3	Influence of light intensity on C <sub>i</sub> /C <sub>s</sub> ; C <sub>i</sub> as a virtual concentration	53
3.6.4	Effect of CO <sub>2</sub> concentration on C <sub>i</sub> /C <sub>s</sub>	53
3.6.5	Effect of air humidity on C <sub>i</sub> /C <sub>s</sub>	54
3.6.6	Influence of other factors on C <sub>i</sub> /C <sub>s</sub>	55
3.6.7	Effects of the interaction between E and A <sub>n</sub>	56
3.7	Parameterization of stomatal responses to air humidity	56
3.7.1	Description	56
3.7.2	Sample calculations	58
3.8	Discussion and conclusions	63
<b>4</b>	<b>Stomatal conductance and photosynthesis of unstressed grapevines under semi-arid conditions</b>	<b>67</b>
4.1	Introduction	67
4.2	Description of the measurements	68
4.2.1	General	68
4.2.2	Stomatal conductance measurements	70
4.2.3	Leaf photosynthesis measurements	72
4.3	General experimental results	74
4.3.1	Effects of leaf position and age on g <sub>s</sub> and A <sub>n</sub>	74
4.3.2	Diurnal variation of g <sub>s</sub> and A <sub>n</sub>	76
4.3.3	Comparison between porometer g <sub>s</sub> and gas-exchange g <sub>s</sub>	78
4.3.4	Combining results of porometer and gas-exchange measurements	80

4.4	Parameters in the A- $g_s$ model	81
4.4.1	General	81
4.4.2	Initial quantum use efficiency	81
4.4.3	Photosynthetic rate at optimum light intensity, $A_m$	82
4.4.4	The ratio $f$ as a function of specific humidity deficit, $D_s$	83
4.4.5	Mesophyll conductance, $g_m$ and maximum photosynthetic rate, $A_{m,max}$	84
4.4.6	Summary of the parameter values	85
4.5	Validation of the A- $g_s$ model	86
4.5.1	Introductory remarks	86
4.5.2	Photosynthetic rate, $A_n$	86
4.5.3	Stomatal conductance, $g_s$	86
4.6	Discussion and conclusions	91
<b>5</b>	<b>Direct impact of atmospheric CO<sub>2</sub> enrichment on surface resistance and regional transpiration: significance of the PBL-vegetation interaction</b>	<b>93</b>
5.1	Introduction	93
5.2	Extensions of the coupled PBL-vegetation model	94
5.2.1	General	94
5.2.2	Scaling the A- $g_s$ model up from the leaf to the canopy	95
5.2.3	Parameterization of turbulent transfer within the PBL	96
5.3	Setup of the analysis	98
5.3.1	General	98
5.3.2	Initial and boundary conditions	99
5.3.3	Characteristics of the simulations	100
5.3.4	Summary of the simulations	101
5.4	Results	102
5.4.1	Diurnal evolution of $r_s$ and $\lambda E$ , and the influence of LAI	103
5.4.2	Changes of $r_s$ and $\lambda E/Q^*$ : C <sub>3</sub> canopies	104
5.4.3	Changes of $r_s$ and $\lambda E/Q^*$ : C <sub>4</sub> canopies	106
5.4.4	Influence of diurnal evolution of CO <sub>2</sub> at reference height	107
5.5	Further analysis of the humidity responses	108
5.5.1	Introduction	108
5.5.2	Sensitivity of $r_s$ and $\lambda E/Q^*$ to $D_{max}$ and $f_0$	108
5.5.3	Concurrent changes of $D_s$ and ambient CO <sub>2</sub>	111
5.6	Discussion	113
5.6.1	Significance of PBL-vegetation interaction at the regional scale	113
5.6.2	Controls in the PBL-vegetation interaction	114
5.6.3	Simulation of stomatal responses	120
5.6.4	Final remarks	121
5.7	Summary of conclusions	122

<b>Samenvatting</b>	125
<b>Summary</b>	130
<b>Appendix 1</b> Anatomy of a leaf	135
<b>Appendix 2</b> The vegetation—surface-layer model	136
<b>Appendix 3</b> Extension of the vegetation model: PAR within the canopy	138
<b>Appendix 4</b> The planetary boundary layer model	139
<b>Appendix 5</b> Modifications of the PBL model (Chapter 5)	141
<b>Appendix 6</b> Test of the modified PBL model	146
<b>Appendix 7</b> The closed box model	148
<b>Appendix 8</b> Temperature responses	149
<b>Appendix 9</b> Characterization of micrometeorological conditions during EFEDA, site Tomelloso	152
<b>Appendix 10</b> Response test of gas-exchange system	153
<b>Appendix 11</b> Gas-exchange calculations	154
<b>Appendix 12</b> McClatchey profiles (specific humidity and potential temperature)	156
<b>Appendix 13</b> Results from sensitivity analyses (Chapter 5)	157
<b>References</b>	167
<b>Curriculum Vitae</b>	179

## List of symbols and abbreviations

### Abbreviations, acronyms and chemical symbols:

A	CO <sub>2</sub> Assimilation
ABA	ABscisic Acid
AMTEX	Air Mass Transformation EXperiment
B87	Ball <i>et al.</i> , (1987)
C <sub>3</sub>	with C <sub>3</sub> mechanism for photosynthesis
C <sub>4</sub>	with C <sub>4</sub> mechanism for photosynthesis
CAM	Crassulacean Acid Metabolism
CH <sub>2</sub> O	carbohydrate
CO <sub>2</sub>	carbondioxide
ECHIVAL	European International Project on Climatic and Hydrological Interactions between Vegetation, the Atmosphere and the Land Surface
EFEDA	ECHIVAL Field Experiment in Desertification-threatened Areas
G85	Goudriaan <i>et al.</i> (1985)
H <sub>2</sub> O	water
H&M	Holtslag & Moeng (1991)
HAPEX	Hydrological Atmospheric Pilot EXperiment
Helox	mixture of helium and oxygen
Ini	Initial conditions
IRGA	InfraRed Gas Analyzer
IPCC	Intergovernmental Panel on Climate Change
JS	Jarvis (1976), Stewart (1988)
KV91	Kim & Verma (1991)
LAI	Leaf Area Index
LES	Large Eddy Simulation
LT	Local (Standard) Time
ML	Mixed Layer
MLS	MidLatitude Summer
MOBILHY	MOdélisation du BILan HYdrique
NIR	Near Infrared Radiation
O <sub>2</sub>	Oxygen
PAR	Photosynthetically Active Radiation
PBL	Planetary Boundary Layer
Pho	Photosynthesis mechanism (C <sub>3</sub> or C <sub>4</sub> )
PP	Present Parameterization
Rubisco	Ribulose 1,5 biphosphate carboxylase oxydase
SAS	SubArctic Summer
SL	Surface Layer
T&M	Troen & Mahr (1986)
TRO	TROpical
UTC	Universal Time Code
WUE	Water Use Efficiency

### Symbols      *Description and [units]:*

#### Lower Cases

a	canopy albedo [-]
a	general coefficient, constant
b	general coefficient, constant
c	general coefficient, constant

---

c	CO <sub>2</sub> mole fraction [mol mol <sup>-1</sup> ], with subscript: o — in sample air r — in reference air r,c — in reference air, but corrected for humidification of the air
e	water vapour pressure [Pa], with subscript: r — at reference level
f	(C <sub>i</sub> -Γ)/(C <sub>s</sub> -Γ) [-], and with subscript: 0 f at D <sub>s</sub> = 0 min f at D <sub>s</sub> = D <sub>max</sub>
f	fraction of leaf area [-], with subscript: sh shaded sl sunlit
f <sub>x</sub>	response function, with subscript x denoting any variable
g	gravitational constant, 9.81 [m s <sup>-2</sup> ]
g	conductance, at leaf scale (exceptions indicated) [mm s <sup>-1</sup> ], with subscript: 0 initial — a aerodynamic — (canopy scale) bc boundary layer — for CO <sub>2</sub> bh boundary layer — for heat bv boundary layer — for water vapour c cuticular — cal calibration — (porometer calibration) m mesophyll — max maximum — s stomatal — for water vapour s,A from photosynthesis model, without stomatal humidity response sc stomatal — for CO <sub>2</sub>
g	dimensionless gradient of entity in PBL [-], with subscript: d — for top-down case u — for bottom-up case x — with x denoting any entity s
h	PBL height [m]
h	relative humidity (scale: 0-1) [-], with subscript: c — within porometer cup cycle — of porometer cycle operation s surface — (leaf); and with prefix: δ rise of — within porometer cup
k	general: coefficient of proportionality
l	distance [m]
p	power [-]
p	probability [-]
q	specific humidity [g kg <sup>-1</sup> ], and with subscript: cuv — in bulk air of leaf cuvette m — of mixed layer r — at reference level s — at surface (canopy or leaf); with superscript: * saturation —
r	resistance [s m <sup>-1</sup> ], with subscript: a aerodynamic — to heat and water vapour transport (between z <sub>0</sub> and z <sub>r</sub> ) ah aerodynamic — to heat transport (between z <sub>oh</sub> and z <sub>r</sub> ) av aerodynamic — to water vapour transport (between z <sub>ov</sub> and z <sub>r</sub> ) bh excess — to heat transport (between z <sub>oh</sub> and z <sub>0</sub> ) or — in leaf cuvette



>r	bv	excess — to water vapour transport (between $z_{oh}$ and $z_o$ ) or — in leaf cuvette
	s	surface —
	s,0	reference —
	s,crit	critical surface —
s		general, entity (in PBL), and with subscript:
	d	— for top-down case
	u	— for bottom-up case
	x	— with x denoting d or u
s		slope of saturation specific humidity versus temperature curve [ $K^{-1}$ ]
$s_l$		scattering coefficient of green leaves for PAR [-]
t		time [s]; and:
		porometer transition —, with prefix $\delta$
		porometer calibration —, with subscript c
u		wind speed along x-direction (east-west) [ $m\ s^{-1}$ ], and with subscript:
	*	friction velocity
	r	— at reference level
v		wind speed along y-direction (south-north) [ $m\ s^{-1}$ ]
w		vertical wind speed (z-direction) [ $m\ s^{-1}$ ], and with subscript:
	*	convective velocity scale
	s	PBL velocity scale, $u_w/\phi_m$
w		water vapour concentration [ $mol\ mol^{-1}$ ], with subscript:
	o	— in sample air
	r	— in reference air
x		general, variable
y		general, variable
z		height [m], and with subscript:
	l	— of first model level
	Hmin	— in PBL where minimum sensible heat flux is found
	o	aerodynamic roughness length
	oc	roughness length for $CO_2$
	oh	roughness length for heat
	ov	roughness length for water vapour
	r	reference —
	s	— of surface layer

**Capitals**

A		photosynthetic rate [ $mg\ m^{-2}\ s^{-1}$ or $\mu mol\ m^{-2}\ s^{-1}$ ], with subscript:
	g	gross —
	m	— at saturating light intensity
	m,g	$A_m + R_d$
	m,max	leaf photosynthetic capacity
	min	minimum $A_m$ , at $D_s = D_{max}$
	n	net — of leaf
	nc	net — of canopy
C		coefficient of proportionality
C		$CO_2$ concentration [ $\mu mol\ mol^{-1}$ or $mg\ m^{-3}$ ], and with subscript:
	a	ambient —
	cuv	— in bulk air cuvette
	i	intercellular — (realized)
	i,vir	intercellular — (virtual)
	min	minimum intercellular —, at $A_n = A_{min}$
	r	— at reference level
	s	— at surface (leaf or canopy)

C	bulk transfer coefficient [-], with subscript: h — for heat transport m — for momentum transport n — for neutral conditions x — denoting H or M
$C_p$	heat capacity of air at constant pressure (1005) [J kg <sup>-1</sup> K <sup>-1</sup> ]
$D^p$	displacement height [m]
D	specific humidity deficit [g kg <sup>-1</sup> ], and with subscript: max value of $D_s$ where stomata close completely r — at reference level s — at surface (leaf or canopy)
$D_v$	diffusion coefficient for water vapour in air [m <sup>2</sup> s <sup>-1</sup> ]
E	(Evapo)transpiration rate [kg m <sup>-2</sup> s <sup>-1</sup> or mg m <sup>-2</sup> s <sup>-1</sup> ], and: with prefix $\lambda$ : latent heat flux [W m <sup>-2</sup> ] with subscript max: maximum —, maximum latent heat flux, respectively
F	air flow through leaf cuvette [mol s <sup>-1</sup> ], with subscript: o — from cuvette, containing sample air r — towards cuvette, containing reference air
$F_i$	interpolation factor
$F_{x,y}$	ratio of sensitivities of x to y with and without PBL feedback, [-]
$F_y$	ratio of sensitivities of $\lambda E$ to y with and without PBL feedback, [-]
G	Soil heat flux [W m <sup>-2</sup> ]
H	Sensible heat flux [W m <sup>-2</sup> ], and with subscript: min minimum — in PBL
I	incident PAR [W m <sup>-2</sup> ], and with subscript: 0 — outside cuvette a absorbed PAR l — absorbed by leaf in cuvette t — at top of canopy
K	extinction coefficient for light in canopy [-], and with subscript: bl — containing black leaves df — , diffuse light dr — , direct light
K	Michaelis constant (to Rubisco), with subscript: c for CO <sub>2</sub> [ $\mu$ mol mol <sup>-1</sup> ] o for O <sub>2</sub> [mmol mol <sup>-1</sup> ]
K	turbulent diffusion coefficient [m <sup>2</sup> s <sup>-1</sup> ], with subscript: d top-down — h — for heat m — for momentum s — for entity s u bottom-up —
L	leaf area [m <sup>2</sup> ], and with subscript: a — in leaf cuvette c — above any level in canopy
$L_{\downarrow}$	downward longwave radiation [W m <sup>-2</sup> ]
$L_{\uparrow}$	upward longwave radiation [W m <sup>-2</sup> ]
$L_v$	virtual Monin-Obukhov length [m]
M	molecular mass [g mol <sup>-1</sup> ], with subscript: a — of air (28.9) v — of H <sub>2</sub> O (18.0)
O	O <sub>2</sub> concentration [mmol mol <sup>-1</sup> ]
Pr	Prandtl number [-]

$Q^*$	net radiation [ $W m^{-2}$ ], and with subscript: i isothermal —
$Q_{10}$	ratio of the rate at one temperature to that at a temperature 10 degrees lower
$R$	entrainment ratio [-], with subscripts: h — for sensible heat flux s — for flux of entity s
$R$	respiration [ $mg m^{-2} s^{-1}$ ] with subscripts: d dark — l photo—
$Ri$	Richardson bulk number [-], and with subscript: cr critical — (0.25)
$S$	flux of entity s
$S_{\downarrow}$	solar radiation [ $W m^{-2}$ ], and with subscript: l — absorbed by leaf in cuvette
$S_{g,A}$	slope of $A_n$ versus $g_{sc}$ relation [ $mg m^{-3}$ ]
$T$	temperature [K or $^{\circ}C$ ], and with subscripts: 1 lower reference — in inhibition function 2 upper reference — in inhibition function cuv in bulk air of leaf cuvette l leaf — r — at reference level s — at surface (leaf or canopy)
$V$	general, variable
$V(h)$	wind speed at top of PBL [ $m s^{-1}$ ]
$V_{c,max}$	maximum catalytic capacity of Rubisco [ $mg m^{-2} s^{-1}$ ]
$W_l$	leaf width [m]
$X$	general: parameter or variable

**Greek & special:**

$\alpha$	soil heat flux coefficient $G/Q^*$ [-]
$\beta$	solar elevation [rad]
$\beta g$	buoyancy parameter [ $m s^{-2} K^{-1}$ ]
$\gamma$	countergradient term, with subscript: d — for top-down case s — for any entity s u — for bottom-up case $\theta$ — for heat transport [ $K m^{-1}$ ]
$\gamma$	psychrometric constant, $C_p/\lambda$ [ $K^{-1}$ ]
$\Gamma$	$CO_2$ compensation concentration [ $\mu mol mol^{-1}$ ]
$\Delta$	difference [-], as prefix to x: difference of x
$\epsilon$	$M_v/M_a$ (0.622) [-]
$\epsilon$	emissivity [-], with subscript: a atmospheric — s surface —
$\epsilon$	initial quantum use efficiency [ $mg J^{-1} PAR$ ], and with subscript: o maximum initial quantum use efficiency
$\zeta$	dimensionless length scale, with subscript: r $(z_r - D)/L_v$ 0 $(z_0 - D)/L_v$
$\theta$	potential temperature [K or $^{\circ}C$ ], with subscript: *,c convective temperature scale 0 reference — 0v reference virtual — m — of mixed layer

xx *List of symbols*

---

$\theta$	s	— near surface or at surface
	T	scaled thermal temperature excess
	v	virtual —
$\kappa$		Von Kármán constant (0.4) [-]
$\lambda$		latent heat of vaporization 2.46 [J mg <sup>-1</sup> ]
$\xi_{x,y}$		sensitivity of x to y, with x and y denoting any variable
$\xi_y$		sensitivity of $\lambda E$ to y, with y denoting any variable
$\xi_{x,y}$		relative sensitivity of x to y, with x and y denoting any variable
$\xi_y$		relative sensitivity of $\lambda E$ to y, with y denoting any variable
$\rho$		density of air [kg m <sup>-3</sup> ], and with subscript: 0 reference —
$\sigma$		Stefan-Boltzman constant (5.67x10 <sup>-8</sup> ) [W m <sup>-2</sup> K <sup>-1</sup> ]
$\tau$		ratio of oxygenase to carboxylase activity of Rubisco
$\tau$		surface stress [N]
$\tau$		time constant [s]
$\phi$		dimensionless gradient [-] with subscript: h — of temperature m — of wind
$\Psi$		stability function in integrated flux-profile relationship, with subscript: h — heat transport m — for momentum transport x denoting h or m
$\Omega$		decoupling factor [-]
$\overline{w'x'}$		kinematic flux of x, with x denoting any variable; and with subscript: d top-down — e entrainment — s surface — u bottom-up —

# 1

## INTRODUCTION

### 1.1 Background

#### 1.1.1 General

Evaporation is a key process in meteorology, plant physiology and hydrology. As a component of the surface energy balance, it controls the amount of sensible and latent heat transferred to the atmosphere and, in addition, water vapour is the most important of the greenhouse gases. Thus, evaporation not only affects local and regional weather and climate, but also large-scale circulations and the global climate (see Schmugge & André, 1991, for examples on various scales). Second, as a component of the hydrological cycle, evaporation influences the distribution of water resources. Third, water is an indispensable element for plant growth. Therefore, changes in evaporation in a specific region will affect local agriculture and water management considerably. Also, the results of Global Circulation Models (GCMs) are sensitive to the parameterization of evaporation (Mintz, 1984; Rowntree, 1991).

In recent years, there has been considerable concern about changes in evaporation in relation to increased carbon dioxide (CO<sub>2</sub>) concentrations in the atmosphere. The International Panel on Climate Change (IPCC) estimated that ambient CO<sub>2</sub> concentration may be doubled by the end of the next century (Houghton *et al.*, 1990). Atmospheric CO<sub>2</sub> enrichment may affect evaporation *directly* and *indirectly*. The direct effects of CO<sub>2</sub> influence the physiological mechanisms that control evaporation from plants (see, Lemon, 1983; Strain & Cure, 1985; Enoch & Kimball, 1986; Rozema *et al.*, 1993). Indirect changes are evoked by possible *climate changes* (Houghton *et al.*, 1990). These affect the physical controls of evaporation and the ambient controls of plant physiological mechanisms (see, Rosenberg, 1981; Parry *et al.*, 1988).

This study is confined to the prediction problem concerning the *direct* effect of atmospheric CO<sub>2</sub> enrichment on evaporation. Thus, the study limits itself to *vegetated* surfaces.

### 1.1.2 Direct effects of atmospheric CO<sub>2</sub> enrichment on evapotranspiration

The evaporation of vegetated surfaces is usually denoted as *evapotranspiration*. It consists of three components:

1. evaporation of rainwater or dew intercepted by the canopy, often denoted as *interception*,
2. *evaporation from the bare soil*,
3. evaporation of water from dry plants and plant parts, denoted as the *transpiration*.

Obviously, interception occurs only when the canopy is wet or partially wet. It is, to a large extent, controlled by the aerodynamic properties of the vegetation. Therefore, the interception of tall canopies, such as forest, is much larger than that of short vegetation, such as grassland, under otherwise similar conditions (Thom & Oliver, 1977; Monteith & Unsworth, 1991). For forest areas, interception may be the most important component of *annual* evapotranspiration, although this depends on climate characteristics such as the frequency, intensity and duration of rainfall (Thom & Oliver, 1977; McNaughton & Jarvis, 1983). Interception is not likely to be *directly* influenced by CO<sub>2</sub> (De Bruin and Jacobs, 1993).

Evaporation in the soil occurs between soil particles, in the pores that are partly filled with liquid water. Water vapour then diffuses upward to the soil surface where it escapes into the air outside the soil. The evaporation from the soil is controlled by the characteristics of the soil such as its structure and texture, and the gradients of temperature and of soil moisture (Ten Berge, 1990). It contributes significantly to the evapotranspiration of sparsely vegetated surfaces. However, if the vegetation almost entirely intercepts the incoming radiation, needed to drive the evaporation, evaporation from the soil is insignificant (Shuttleworth & Wallace, 1985; Shuttleworth, 1991). This will be the case for densely vegetated surfaces. Direct effects of CO<sub>2</sub> on the soil evaporation have not been identified (De Bruin & Jacobs, 1993).

Evaporation from dry, densely vegetated surfaces consists almost entirely of transpiration. Water consumed by transpiration has passed the plant. It has been extracted from the soil and has subsequently been transported to the cells around the sub-stomatal cavity (see Appendix 1 for an outline of the anatomy of leaves). It evaporates from the walls of these cells into the sub-stomatal cavity. Next, it escapes through the stomatal pore into the air adjacent to the leaf. This is a diffusion process controlled by the stomata: the stomatal aperture can be adjusted by means of the guard cells. Two conflicting goals must be served here. On the one hand, the uptake of CO<sub>2</sub> has to be ensured. On the other, excessive transpiration has to be prevented. Thus, transpiration can be seen as an inevitable by-product of photosynthesis (Farquhar & Sharkey, 1982; Ziegler, 1987; Collatz *et al.*, 1991).

Atmospheric CO<sub>2</sub> enrichment can affect the transpiration of vegetated areas directly. First, the stomatal aperture of many plant species decreases as ambient CO<sub>2</sub> increases. This hampers transpiration (see, for example, Meidner & Mansfield, 1968; Mansfield *et al.*, 1981; Raschke, 1986; Morison, 1987). Second, CO<sub>2</sub> can stimulate leaf growth, and as a result the total canopy transpiration increases (Cure & Acock, 1986; Kimball, 1986; Kimball *et al.*, 1993). The two

effects can occur separately or they can occur in combination, depending on the plant species (Cure & Acock, 1986). Note that the second effect is probably less important because additional leaf area would contribute little to the transpiration of vegetations that were already dense (Shuttleworth & Wallace, 1985; Shuttleworth, 1991). Many other influences of CO<sub>2</sub> on plants have also been reported, but little consensus exists about these additional effects (see Strain & Cure, 1985, and Rozema *et al.*, 1993, for a review of the state of the art). By contrast, the aforementioned effects were found to occur consistently and among a wide range of plant species, so there is some consensus on these influences. This study is mainly confined to the effect of CO<sub>2</sub> on the stomata. Some attention will also be paid to the effect of the total amount of leaf area on canopy transpiration.

### 1.1.3 General features of transpiration and of the prediction of changes

In this section some general features of the transpiration of dense, dry canopies will be illustrated. The transpiration of such canopies can be described satisfactorily by means of the so called "big leaf" model (Monteith, 1965; McNaughton & Jarvis, 1983; Shuttleworth, 1991). The big leaf concept treats the canopy as a single big leaf, with the same optical and aerodynamic properties (albedo, emissivity, roughness length) as the vegetation that it represents. All the elements within the canopy face the same microclimate. The air in the stomata of the big leaf is assumed to be saturated with water, that is, the vapour pressure within the stomata is equal to the saturation vapour pressure at the mean surface temperature. The fluxes are described by means of the commonly used resistance analogues (see, for example, Monteith & Unsworth, 1991, and Shuttleworth, 1991, for recent reviews of this theory).

A surface resistance,  $r_s$ , is assigned to the diffusion of water vapour out of the sub-stomatal cavities of the big leaf.  $r_s$  is defined by  $E = \rho[q^*(T_1) - q_s]/r_s$ , in which  $E$  denotes the transpiration in  $\text{kg m}^{-2} \text{s}^{-1}$ ,  $q^*(T_1)$  is the saturation specific humidity at the leaf temperature,  $T_1 = T_s$  is the temperature of the surface, and  $q_s$  is the specific humidity at the leaf surface just outside the stomatal pore. Thus,  $r_s$  represents the control of the diffusion process through the stomatal pore, which depends on the stomatal aperture. For dry conditions, it may be assumed that  $r_s$  is equal to the bulk stomatal resistance, which is numerically similar to the integral value of component leaf resistances per layer (Monteith, 1965; Shuttleworth, 1991). The leaf resistance is defined on a unit leaf area basis. Thus,  $r_s$  also depends on the total leaf area per square meter ground (Leaf Area Index, LAI). It is  $r_s$  which may be directly affected by an increase of the CO<sub>2</sub> concentration. First, stomatal closure will cause  $r_s$  to increase. Second, increased leaf production will cause  $r_s$  to decrease. Therefore, in order to assess the direct effects of  $r_s$  on the transpiration,  $E$ , the change of  $r_s$  has to be predicted. An important part of the thesis is devoted to this problem.

Next, consideration is given to the problem of how to predict changes in  $E$  if the change of  $r_s$  is known.  $E$  can be calculated from routine weather data if the surface characteristics of the canopy are known. This is illustrated by means of the Penman-Monteith equation (Monteith, 1965), which is probably the most well-known representation of the big leaf model. This

equation describes E according to

$$\lambda E = \frac{s(Q^* - G) + \rho C_p \frac{D_r}{r_a}}{s + \gamma \left(1 + \frac{r_s}{r_a}\right)} \quad [1.1]$$

where  $\lambda$  is the latent heat of vaporisation,  $s$  is the slope of the saturation specific humidity versus temperature curve,  $Q^*$  is the net radiation,  $G$  represents the soil heat flux and other storage and metabolic terms,  $\rho$  is the density of the air,  $C_p$  is the heat capacity of the air at constant pressure,  $D_r$  is the specific humidity deficit ( $D_r \equiv q^*(T_r) - q_r$ , with  $T$  and  $q$  temperature and the specific humidity, respectively),  $r_a$  is the aerodynamic resistance to heat and water vapour transport between the surface and the reference height,  $z_r$ ,  $\gamma$  is the psychometric constant ( $\equiv C_p/\lambda$ ) and the subscript  $r$  denotes reference height (usually screen height). Note that  $Q^*-G$  is the "available energy" for the sensible heat flux density ( $H$ ) and latent heat flux density ( $\lambda E$ ) (viz.  $Q^* - G = H + \lambda E$ ).

It was pointed out by De Bruin (1983, 1989), McNaughton (1976, 1989) and by McNaughton & Jarvis (1983), for example, that  $E$  is expressed in dependent variables. This makes evaporation models, of which [1.1] is an example, *diagnostic rather than predictive*. Also, changes in  $E$  cannot just be predicted from the derivative of [1.1] with respect to one of the controlling variables. Neither can they be predicted from finite changes if conditions at the reference level are taken as being constant.  $D_r$  and  $E$  are correlated in particular because of the interaction between  $\lambda E$ ,  $H$ , and the lowest layer of the atmosphere, the planetary boundary layer (PBL). The following example from De Bruin (1989) and McNaughton (1989) illustrates this interaction and the associated prediction problem.

In the example, the PBL is described by means of the "closed box model." The box has the height,  $h$ , of the PBL. In the PBL the following layers are distinguished. The first one, the "surface layer" (SL), is the layer of the PBL that is found adjacent to the surface. The SL is typically about one tenth of the height of the PBL. Here, gradients of the potential temperature and the specific humidity are allowed. [1.1] applies in this layer. Above the SL the air is well mixed so that the potential temperature ( $\theta_m$ ) and specific humidity ( $q_m$ ) are constant with height. This layer is called the "mixed layer" (ML). The saturation specific humidity deficit of the ML is defined as  $D_m \equiv q^*(\theta_m) - q_m$ . The top of the PBL is an inversion layer assumed impermeable to water vapour and heat. In the box  $\theta_m$  and  $q_m$  will change according to

$$\frac{d\theta_m}{dt} = \frac{H}{\rho C_p h} \quad \text{and} \quad \frac{dq_m}{dt} = \frac{E}{\rho h} \quad [1.2]$$

respectively. Using [1.1], [1.2] and the definition of  $D_m$  it can be shown that



$$\frac{dD_m}{dt} = \frac{sH - \gamma\lambda E}{\rho C_p h} = \frac{s(Q^* - G) - (s + \gamma)\lambda E}{\rho C_p h} \quad [1.3]$$

(De Bruin, 1989; McNaughton, 1989). Thus, if  $\lambda E$  decreases due to an increasing  $r_s$ , the PBL will be a little drier than in the case where  $\lambda E$  remains unchanged. Furthermore, noting that a decrease of  $\lambda E$  is accompanied by an increasing  $H$  if the available energy remains equal, the PBL will become warmer. As a result,  $D_m$  increases, which enhances  $\lambda E$  again. It can be shown that, in this example,  $\lambda E$  ultimately reaches the so called "equilibrium rate," defined as  $\lambda E_{eq} = (Q^* - G) / (s + \gamma)$ .  $\lambda E_{eq}$  depends primarily on  $Q^*$  (McNaughton & Jarvis, 1983; De Bruin, 1989; McNaughton, 1989).

In reality,  $h$  is not fixed and during PBL growth warm, dry air from above the PBL is entrained into the PBL. The entrainment process is, to a large extent, controlled by  $H$  (Tennekes, 1973; Tennekes & Driedonks, 1983). Other changes, such as changes in the surface temperature and the wind speed might also occur. All of these changes are related to each other and their total effect depends on the interaction of processes within the PBL (see Stull (1988) and Garratt (1992) for a recent description of physical aspects of the PBL). In addition, several dependences within the SL and relations between  $r_s$  and the environment have to be dealt with. For example, the humidity response of the stomata can be described as a function of the specific humidity deficit (Choudhury & Monteith, 1986; Aphalo & Jarvis, 1991), which introduces an additional dependence in [1.1].

In conclusion, the interactions lead to a set of highly non-linear relationships. Their total effect can only be estimated properly using a realistic model for the PBL, coupled to a vegetation model that includes a description of the physiological responses of  $r_s$  to the environment. The principal objective of this study is to construct such a model and to estimate the importance of the main feedback processes.

#### 1.1.4 Interactions at the regional scale

The atmospheric feedback discussed above is present at all scales. Its importance depends, among other things, on the scale that is being considered (Jarvis & McNaughton, 1986; McNaughton & Jarvis, 1991). If the horizontal scale becomes large enough, the entire PBL will be affected. Shuttleworth (1988) called this an "organized response." If the typical surface elements are smaller than a certain distance, the PBL will average out the contributions from the different surface elements. If they are larger than this distance, the PBL adapts to the underlying surface. Experimental evidence for such an adaptation was found during HAPEX in southwest France (André *et al.*, 1986; Shuttleworth, 1988). Shuttleworth (1988) suggested taking ten times the height of the PBL as the horizontal extension at which an organized response becomes possible. For a typical PBL, this would imply a horizontal distance of 10-20 km. Raupach (1991) estimated the adjustment length scale to be 1 - 10 km for the convective PBL. However, for conditions other than convective conditions, the typical length scale for adjustment may be larger, corresponding to a longer travelling distance.

The conclusion of this argument is that the interaction of the surface fluxes and the PBL may become important at the regional scale, that is, a horizontal scale of 10-100 km and a vertical scale of 1-5 km. This was clearly pointed out by De Bruin (1983), McNaughton & Spriggs (1986), and McNaughton (1989), who used a simple slab model for the PBL, coupled to the big leaf model to estimate regional evapotranspiration, and by Brutsaert (1986) and Shuttleworth (1988). Others coupled a model of the PBL to a model for the bare soil (Pan and Mahrt, 1987; Ten Berge, 1990). However, a systematic sensitivity study on the effect of the interaction between the PBL and the surface fluxes and its consequences for the *prediction* of changes of the regional transpiration has not been reported yet. It is one of the purposes of this study to provide such a sensitivity study. Note that previous studies on the effect of surface changes on transpiration ignored the interaction between the PBL and vegetation (for example, Martin *et al.*, 1989; Rosenberg *et al.*, 1989). Also, it cannot be included in controlled experiments in glasshouses (Jarvis & McNaughton, 1986).

The regional scale is of particular importance to climatologists and meteorologists who need to improve the predictions from GCMs. Furthermore, the large-scale output of their models needs to be translated to scales smaller than their grid distance. For example, much of the present knowledge about the effects of CO<sub>2</sub> enrichment is obtained either at the small scale of the leaf or the plant, or at the large scale of the grid distance of climate models. Extrapolating or interpolating the results from one scale to the other leads to theoretical and practical problems (Parry *et al.*, 1988). The regional scale is a convenient intermediate scale. It is suitable for studying the interaction between "downward influences", that is, large-scale influences on small-scale processes, and "upward influences", that is, small-scale effects on large-scale processes (Raupach, 1991). Agronomists and hydrologists who would also like to estimate regional transpiration will be interested in interactions at this scale. Finally, the interaction between the surface fluxes and the PBL is of importance because the PBL and its parameterizations affects the results of climate models (Garratt, 1992, 1993).

## 1.2 Objective and delimitation of the present study

The main objectives of the present study are:

- to construct a coupled model for the PBL and the vegetation, which also accounts for responses of the stomata to the environment, in particular to CO<sub>2</sub>,
- to assess the effect of the interaction between the atmosphere and the vegetation on the sensitivity of the regional transpiration to surface characteristics, and to evaluate its impact on *predicted changes*.

Many variables and aspects of the PBL as well as aspects of the vegetation could be considered. For example, the most relevant surface characteristics are roughness, albedo and  $r_s$ . The latter characteristic is at least related to CO<sub>2</sub>, light, atmospheric humidity and temperature. These will have an impact on H,  $\lambda E$ ,  $Q^*$ , etc. In the PBL, the impact of various parameterizations could be studied, as well as different initial and boundary conditions for temperature, air humidity, CO<sub>2</sub> concentration, and wind speed. Clearly, it is impossible to

cover all aspects in one study. Therefore, the main delimitation is chosen as follows:

- only the *transpiration* of dry vegetation is examined,
- dense, well-watered canopies are assumed, so that the influence of the soil may be ignored,
- only *direct* effects of  $\text{CO}_2$  on  $\lambda E$  are considered,
- the study is limited to the *regional scale* (10-100 km horizontal scale, 1-5 km vertical scale),
- in general, fair-weather summer conditions will be considered so that the PBL is mostly in a convective state. Note that a substantial amount of transpiration occurs under such conditions.

Other delimitations are given at the appropriate places. In summary, the following aspects are considered:

- feedback mechanisms that are active in the atmosphere-vegetation interaction and their control of  $r_s$  and  $\lambda E$ ,
- influences of different atmospheric conditions and surface characteristics (albedo, roughness, plant class) on the PBL-vegetation interaction,
- the estimation of the effect of  $\text{CO}_2$  on  $r_s$ , and the role of atmospheric feedback.

### 1.3 Approach and organization of the thesis

To investigate the interaction between the atmosphere and the vegetation at the regional scale, a model for the vegetation is coupled to a model for the PBL. The intention is to construct a model that is realistic enough from the perspective of various scientific disciplines. In addition, its use should not be limited by the amount of computational time required: it should not be necessary to run it on a super computer. Therefore, the components of the coupled model are chosen such that they are simple, but physically realistic.

#### *a) Physical aspects: the coupled model, first version (Chapter 2)*

In the present study, the big leaf model is used as the vegetation model. Its principles were already described in Section 1.1.2. Further details are given in Appendix 2.

The big leaf model is the best known and perhaps the most successful vegetation model for describing the transpiration of extensive dry canopies. The big leaf concept is attractive because it is simple and yet physically realistic. It has been widely tested experimentally, numerically, and theoretically (see Shuttleworth, 1991, for a review and for comparison with other evapotranspiration models). It is, therefore, used in climate models (for example, Rowntree, 1991) as well as in mesoscale models (for example, Segal *et al.*, 1989; Mascart *et al.*, 1991). Note that it is not able to describe the microclimate of the canopy (see Finnigan & Raupach, 1987, Baldocchi, 1989, Baldocchi *et al.*, 1991, and Lhomme, 1991, for a critical discussion of the big leaf concept). Because it is not the intention of the present study to describe the processes within the canopy, this restriction on the big leaf concept is accepted.

The model of Troen & Mahrt (1986) is used as the PBL model. This is a 1D, first order closure model. The model accounts for nonlocal turbulent transport by means of a countergradient term (Deardorff, 1972) related to surface fluxes. At each time step, the model diagnoses the height of the PBL by means of a bulk Richardson formulation. It also accounts for the entrainment that is related to the growth of the PBL. Further details are given in Appendix 4.

The PBL model of Troen & Mahrt (1986) has been tested and used for different purposes in several studies (Mahrt *et al.*, 1987; Pan & Mahrt, 1987; De Bruin & Jacobs, 1989; Holtslag *et al.*, 1989; Jacobs *et al.*, 1991). It simulates the development of the PBL reasonably well.

The choice of a 1D model for the PBL implies that results of the study apply to homogeneous vegetation with a horizontal extension of, say, 10 km or more. In reality, only a few such areas exist. In addition, mesoscale circulations that are induced by surface inhomogeneities cannot be described. However, these disadvantages need not to be a problem. It is not the goal of this study to come to precise predictions for existing areas, but to identify important *processes* that influence such predictions. Furthermore, surface parameters are imposed as independent boundary conditions that do not necessarily refer to real surfaces. Therefore, the surface characteristics can be assumed to be *perfect, representative averages*. Note that, in reality, it is not at all easy to find such averages (see, for instance, Wieringa, 1986; Mason, 1988; Claussen, 1990; Raupach, 1991).

The coupled model PBL-vegetation model is used to investigate the significance of PBL feedback to the sensitivity of regional transpiration to land-surface characteristics. This sensitivity study is described in Chapter 2, which is adapted from Jacobs & De Bruin (1992). Biological feedback is excluded here, in order to be able to concentrate on atmospheric feedback, that is,  $r_s$  is imposed as an independent variable. Sensitivity to the roughness length,  $z_0$ , and to the albedo,  $a$ , are also studied, as is their influence on atmospheric feedback.

*b) Biological aspects: the model for  $r_s$  (Chapter 3 and 4)*

A model is used to describe the responses of  $r_s$  to environmental variables, which assumes a firm correlation between the photosynthetic rate of plants and their leaf *conductance*.  $r_s$  can then be modelled using a model for the photosynthesis. Again, a simple but realistic model is chosen. This is basically the model of Goudriaan *et al.* (1985).

The model for  $r_s$  will be called the A- $g_s$  model, where A refers to  $\text{CO}_2$  assimilation and  $g_s$  to stomatal conductance. The approach has been chosen because it describes the responses of the stomata to  $\text{CO}_2$ , light, and temperature as well as the interaction between responses to these stimuli. A new parameterization that accounts for the humidity responses is proposed. Also, the A- $g_s$  model generates fluxes of  $\text{CO}_2$  at the surface, which can be used to drive fluxes in the PBL.

Chapter 3 addresses the question of how the responses of the stomata to  $\text{CO}_2$ , in relation to responses other variables, can be predicted. A theoretical background to the A- $g_s$  model is

also given and an important part of the chapter is devoted to the inclusion of stomatal humidity responses in the model. A new parameterization of these responses will be described.

In Chapter 4, the model is tested against observations in the field. The data were obtained during an experiment in central Spain where there was a wide range of light intensities, air temperatures, and air humidities.

*c) Biosphere-atmosphere interactions: extensions of the coupled model (Chapter 5)*

In both Chapter 3 and 4, the A- $g_s$  model is described at the leaf scale. The A- $g_s$  model so described has been scaled up to the canopy level, in order to couple it to the big leaf vegetation model. In addition, the PBL model has been extended with a description of CO<sub>2</sub> fluxes and concentrations. The surface flux of CO<sub>2</sub> is driven by canopy photosynthesis, evaluated with the A- $g_s$  model. Also, the model of Troen & Mahrt (1986) has been modified to include recent ideas with respect to the transport of heat and tracers in the PBL. This followed the ideas of Holtslag & Moeng (1991). The basic features of the extensions are described in Section 5.2. More details on the extension of the big leaf model are given in Appendix 3. Extensions of the PBL model are further described in Appendix 5.

Chapter 5 presents an analysis of regional transpiration with the extended coupled model. It focuses on the effect of a doubled atmospheric CO<sub>2</sub> concentration on  $r_s$  and on  $\lambda E$ . Contrary to the analysis presented in Chapter 2,  $r_s$  now becomes a dependent variable. Thus, physical aspects and biological aspects are considered. Special attention is paid to the influence of:

- PBL feedback
- stomatal humidity responses
- differences between plant classes (C<sub>3</sub> or C<sub>4</sub>, see Chapter 3)
- different atmospheric conditions
- CO<sub>2</sub> fluxes in the PBL
- Leaf Area Index, LAI, and roughness length,  $z_0$

The discussion in section 5.6 is a general discussion of the thesis.

## 2

**THE SENSITIVITY OF REGIONAL TRANSPIRATION TO LAND-SURFACE CHARACTERISTICS: SIGNIFICANCE OF FEEDBACK<sup>1</sup>****2.1 Introduction**

To estimate changes of the evapotranspiration in a specific region, many parameters and mechanisms must be considered. Therefore, several soil—vegetation—surface-layer models have been used to evaluate the sensitivity of evapotranspiration to various parameters of the soil, the vegetation, and the atmosphere (Saxton, 1975; Beven, 1979; Luxmoore *et al.*, 1981; Sellers & Dorman 1987; Wilson *et al.* 1987; Martin *et al.*, 1989; Rosenberg *et al.*, 1989; Rowntree, 1991). The aforementioned sensitivity studies have in common that the atmospheric conditions is *prescribed* at a reference level some height above the surface ( $z_r$ , often at 2 m). The sensitivities are calculated from the first derivative of the Penman-Monteith equation ([1.1], Monteith, 1965), or a finite, fixed change is applied to one or more of the boundary conditions. The static stability of the surface layer (SL) is often ignored and the surface temperature,  $T_s$ , is not updated.

However, evapotranspiration is expressed in dependent variables (see Section 1.1.3). As a consequence, a change of the surface fluxes implies changes within the SL as well as changes at  $z_r$ . Consider, for example, a surface of which the surface resistance,  $r_s$ , changes from  $r_s(I)$  to  $r_s(II)$  (Fig. 2.1A). The surface fluxes change accordingly and therefore  $T_s$  changes. Assume that the conditions at  $z_r$  (wind speed,  $u_r$ , temperature,  $T_r$ , and specific humidity,  $q_r$ ) are fixed. The temperature profile of the SL changes from profile I to profile II, which implies a change of the static stability within the SL, and also a change of the aerodynamic resistance,  $r_a$ , of the layer. Net radiation,  $Q^*$ , is affected because the portion of outgoing longwave radiation is altered (Appendix 2, [A3.b]). In addition, the surface specific humidity,  $q^*(T_s)$ , changes ( $q^*$  denotes the saturation specific humidity). All of these changes directly affect the surface fluxes.

---

1) Adapted from Jacobs & De Bruin (1992).

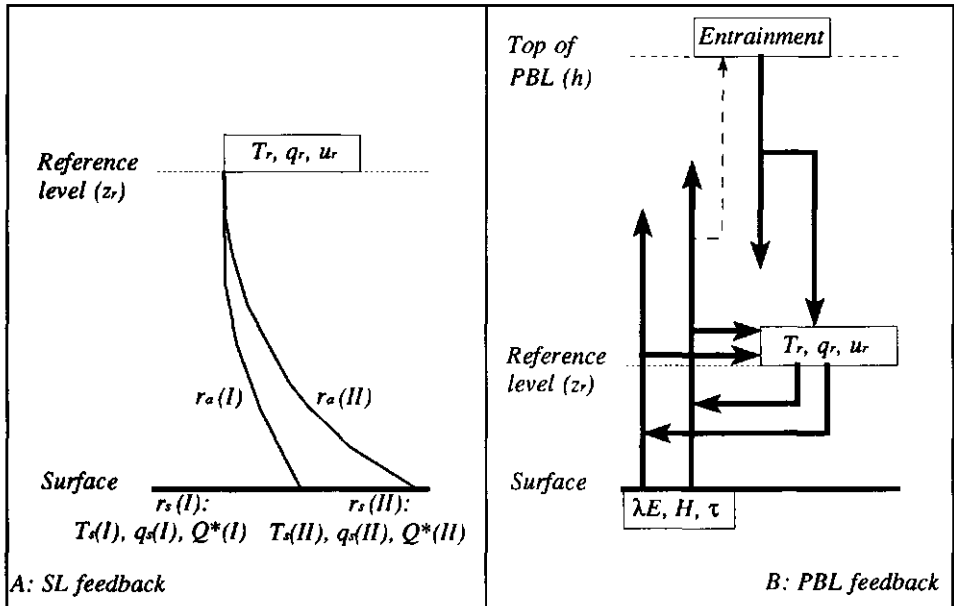


FIGURE 2.1. Schematic illustration of the feedback mechanisms considered in this study. A): Surface Layer feedback (SL feedback). The surface resistance is changed from  $r_s(I)$  to  $r_s(II)$ , which causes a change of the surface fluxes. As a result, the surface temperature changes from  $T_s(I)$  to  $T_s(II)$  and the surface humidity from  $q_s(I)$  to  $q_s(II)$ . The net radiation,  $Q^*$ , the aerodynamic resistance,  $r_a$ , etc., will change accordingly. These changes affect the surface fluxes. The conditions at  $z_r$ , ( $T_r, q_r$ , and  $u_r$ ) are considered as fixed conditions. B): Feedback in the PBL above the surface layer (PBL feedback): The surface fluxes,  $H$ ,  $\lambda E$ , and  $\tau$  influence the conditions within the PBL and therefore  $T_r, q_r$ , and  $u_r$ . Moreover,  $H$  influences the entrainment flux, which also affects  $T_r$  and  $q_r$  (and  $u_r$ ). In return, the conditions at  $z_r$  affect the surface fluxes. Note that, for clarity, the feedback through  $\tau$  and  $u_r$  is not made explicit here.

The mechanism illustrated here is a feedback mechanism. This mechanism, which acts by means of changing conditions of the SL, with fixed conditions at  $z_r$ , is called *SL feedback*.

In reality, the conditions at  $z_r$  will change if the fluxes change. As was illustrated in Section 1.1.3 for transpiration, the surface fluxes directly affect the conditions (for example, temperature, humidity) of the Planetary Boundary Layer (PBL), which includes  $z_r$ . Because the atmospheric conditions influence the surface fluxes, the conditions at  $z_r$  and the surface fluxes are related to one another (see [1.1]-[1.3]). Consider, for example, a case where transpiration decreases. Then, the atmosphere will be drier than in the case where no change of the transpiration occurs. In addition, more energy is available for the sensible heat flux, and hence, the PBL will be heated more. Thus, the humidity deficit will *increase* which in its turn causes the *transpiration to increase*, etc. Moreover, entrainment of warm, dry air from above the PBL considerably affects the conditions of the PBL. This provides an additional feedback because entrainment is also related to the surface fluxes (Tennekes, 1973; Tennekes

& Driedonks, 1981). The feedback mechanism related to the PBL development (temperature, humidity, PBL depth, entrainment, etc.) and its interaction with the surface fluxes through *changing conditions at the reference level* is called here the *PBL feedback*. The PBL feedback is illustrated in Fig. 2.1B. Note that now the conditions of the free atmosphere well above the PBL are regarded as fixed conditions.

Several authors pointed out the significance of the interaction between the PBL and the surface fluxes at the regional scale (for example, De Bruin, 1983, 1989; Brutsaert, 1986; McNaughton & Spriggs, 1986; Shuttleworth, 1988; De Bruin & Jacobs, 1989; McNaughton, 1989; Jacobs *et al.*, 1991). However, to the author's knowledge, a systematic sensitivity analysis with a detailed description of the PBL has not yet been reported. It is the main objective of this chapter to provide such an analysis for transpiration ( $\lambda E$ ;  $r_s > 0$ ) and to evaluate the effect of PBL feedback on the sensitivity of  $\lambda E$  to various surface characteristics quantitatively.

Like in Martin *et al.* (1989), Rosenberg *et al.* (1989), and Rowntree (1991) the Penman-Monteith big-leaf model (Monteith, 1965) is used as the vegetation-SL model (see Chapter 1 and Appendix 2). However, in contrast to their sensitivity studies, the present study includes SL as well as PBL feedback. The vegetation-SL model has been coupled to the PBL model of Troen & Mahrt (1986). This PBL model is rather detailed (see Appendix 4). At present, such detail cannot be used in climate studies with a Global Circulation Model (GCM). Therefore, the question of how detailed the PBL needs to be described is briefly considered as well. For this purpose, additional sensitivity studies have been performed with the so called "box model" for the PBL replacing the detailed PBL model.

The analyses presented in this chapter can be regarded as an extension of the studies by De Bruin (1983), De Bruin & Jacobs (1989), Martin *et al.* (1989), Rosenberg *et al.* (1989), and Jacobs *et al.* (1991). It is also related to the studies by, for example, Jarvis & McNaughton (1986), McNaughton & Spriggs (1986, 1989), Pan & Mahrt (1987), Ten Berge (1990), and McNaughton & Jarvis (1991).

Here, the sensitivity is calculated for:

1.  $\lambda E$  to net radiation,  $Q^*$ , as obtained from an albedo change,
2.  $\lambda E/Q^*$  (the relative transpiration) to aerodynamic resistance,  $r_a$ , between the roughness length,  $z_0$ , and  $z_r$ , as obtained from a change in  $z_0$ ,
3.  $\lambda E/Q^*$  to surface resistance,  $r_s$ .

The influence of SL feedback and PBL feedback on the sensitivities is estimated by comparing:

1. the sensitivity of  $\lambda E$  or  $\lambda E/Q^*$  without accounting for SL feedback or PBL feedback (like, for example, Saxton, 1975; Beven, 1979; Luxmoore *et al.*, 1981; Martin *et al.*, 1989; Rosenberg *et al.*, 1989);
2. the sensitivity of  $\lambda E$  or  $\lambda E/Q^*$  while accounting for *SL feedback*, with prescribed conditions at  $z_r$ ;
3. the sensitivity of  $\lambda E$  or  $\lambda E/Q^*$ , while accounting for both *SL and PBL feedback*.



The emphasis lies on the influence of PBL feedback. Physiological influences are ignored, that is,  $r_s$  is treated like an independent surface parameter. The plant-physiological component of the vegetation-atmosphere interaction is dealt with in Chapter 5. Further delimitations (scale, boundary conditions) are as described in Chapter 1.

## 2.2 Theory

### 2.2.1 Sensitivity analyses

For a general definition of sensitivity, consider the variable  $V$ , which is a function of the input variables  $x_1 \dots x_n$ :

$$V = f(x_1, \dots, x_n) \quad [2.1]$$

If the variables  $x_1 \dots x_n$  are *independent* of  $V$ , it may be written

$$V + \Delta V = f(x_1 + \Delta x_1, \dots, x_n + \Delta x_n) \quad [2.2]$$

Now, from a Taylor series expansion, neglecting higher order terms:

$$\Delta V = \frac{\partial V}{\partial x_1} \Delta x_1 + \dots + \frac{\partial V}{\partial x_n} \Delta x_n \quad [2.3]$$

By definition, the partial differentials,  $\partial V / \partial x_i$ , are the sensitivities,  $\xi_{xi}$ , of the dependent variable  $V$  to the independent input variable  $x_i$  (McCuen, 1974; Saxton, 1975; Beven, 1979). It denotes the change in  $V$  per *unit* change in  $x_i$ .

It follows from [2.3] that

$$\xi_{x_i} = \frac{\partial V}{\partial x_i} = \frac{\Delta V}{\Delta x_i} \quad [2.4]$$

which shows that  $\xi_{x_i}$  may be obtained by calculating directly the value of the partial differential, or by applying a step change in  $x_i$ , while leaving the variables other than  $x_i$  constant.

$\xi_{x_i}$  may be sensitive to the relative magnitude of  $V$  and  $x_i$ . Therefore,  $\xi_{x_i}$  may be divided by the ratio  $V/x_i$ , which leads to the *relative* sensitivity, or sensitivity coefficient  $\Xi_{xi}$ :

$$\Xi_{x_i} = \frac{\partial V}{\partial x_i} \frac{x_i}{V} \quad [2.5]$$

Now, the *relative* change in  $V$  can be expressed as

$$\frac{\Delta V}{V} = \Xi_{x_1} \frac{\Delta x_1}{x_1} + \dots + \Xi_{x_n} \frac{\Delta x_n}{x_n} \quad [2.6]$$

(Saxton, 1975), which shows that the relative sensitivity coefficient denotes the part of the relative change in  $x_i$  that is transferred to the relative change in  $V$ . If, for instance,  $\Xi_{x_i} = 0.25$ , a 10% change in  $x_i$  will result in a 2.5% change in  $V$ .

## 2.2.2 The sensitivity of $\lambda E$ without feedback

The sensitivity of  $\lambda E$  without accounting for feedback can be obtained if [2.4] is applied to the Penman-Monteith equation ([1.1]; Monteith, 1965). All of the variables are assumed to be *independent* of  $\lambda E$  and of each other. In earlier sensitivity studies, partial derivatives of the Penman-Monteith equation (the sensitivity equations) as well as finite differences have been used to determine the sensitivity of  $\lambda E$  to various parameters. Here, the sensitivity equations for the sensitivity of  $\lambda E$  to  $Q^*$ ,  $\lambda E/Q^*$  to  $r_a$ , and of  $\lambda E/Q^*$  to  $r_s$  are given. The sensitivities can be calculated directly from these equations. Furthermore, useful insight can be gained from the sensitivity equations.

In the case of the sensitivities of  $\lambda E/Q^*$  to  $r_a$  and to  $r_s$ , the Penman-Monteith equation is divided by  $Q^*$ . This is reasonable because  $Q^*$  is the driving force for  $\lambda E$ . Also, the sensible heat flux,  $H$ , is defined in terms of potential temperatures (Appendix 2, [A2.4a]). Hence, the combination equation is written:

$$\frac{\lambda E}{Q^*} = \frac{s(1 - \alpha)r_a + \frac{\rho C_p D_r}{Q^*}}{(s + \gamma)r_a + \gamma r_s} \quad [2.7]$$

where  $\lambda$  is the latent heat of vaporization ( $2.46 \times 10^6 \text{ J kg}^{-1}$ ),  $E$  is the transpiration rate in  $\text{kg m}^{-2} \text{ s}^{-1}$ ,  $s = dq^*(T)/dT$  is the slope of the saturation specific humidity,  $q^*$ , versus the temperature,  $T$ ,  $\alpha = G/Q^*$  (where  $G$  is the soil heat flux; see Appendix 2),  $\rho$  is the density of dry air,  $C_p$  is the heat capacity of dry air at constant pressure ( $1005 \text{ J kg}^{-1} \text{ K}^{-1}$ ),  $\gamma = C_p/\lambda$ ,  $D_r$  is the specific humidity deficit at  $z_r \equiv q^*(\theta_r) - q_r$ , where  $\theta_r$  denotes the potential temperature at  $z_r$ . For simplicity, it is assumed in [2.7] that the aerodynamic resistance to heat transport,  $r_{ah}$ , is equal to that of moisture transport,  $r_{av}$ , and that the source and sink heights for heat and moisture,  $z_{oh}$  and  $z_{ov}$  respectively, are equal to  $z_o$ , so that  $r_{ah} = r_{av} = r_a$ . Note that these assumptions have often been made in earlier sensitivity studies. However, in the present calculations with feedback (SL feedback or both SL and PBL feedback) a distinction is made between  $z_o$ ,  $z_{oh}$  and  $z_{ov}$  (see Appendix 2).

### a) Sensitivity of $\lambda E$ to $Q^*$

The sensitivity of  $\lambda E$  to  $Q^*$ ,  $\xi_{Q^*}$ , is given by

$$\xi_{Q^*} = \frac{\partial \lambda E}{\partial Q^*} = \frac{(1 - \alpha)}{1 + \frac{\gamma}{s} \left(1 + \frac{r_s}{r_a}\right)} \quad [2.8]$$

and the relative sensitivity,  $\Xi_{Q^*}$ , by

$$\Xi_{Q^*} = \frac{\partial \lambda E / Q^*}{\partial Q^*} = \frac{1}{1 + \rho C_p \frac{D_r}{s(1-\alpha)r_a Q^*}} \quad [2.9]$$

From [3.8] it can be seen that the sensitivity is always positive ( $\lambda E$  increases with increasing  $Q^*$ ) and that it is determined by the temperature and by the ratio  $r_s/r_a$ . Thus, it is expected to be lower for rougher and "drier" surfaces than for smoother and "wetter" surfaces, while lower temperatures will result in lower sensitivities than do higher temperatures (also see Rowntree, 1991).  $\xi_{Q^*}$  depends neither on  $\lambda E$  nor on  $Q^*$ . Because  $\xi_{Q^*}$  is independent of  $Q^*$  and  $\lambda E$ ,  $\Xi_{Q^*}$  is, by definition, dependent on these variables, but it is independent of  $r_s$ .

*b) Sensitivity of  $\lambda E/Q^*$  to  $r_a$ ; critical surface resistance*

It follows from [2.7] that the sensitivity of  $\lambda E/Q^*$  to  $r_a$ ,  $\xi_{r_a}$ , can be written as

$$\xi_{r_a} = \frac{\partial(\lambda E/Q^*)}{\partial r_a} = \frac{\gamma s(1-\alpha)[r_s - r_{s,crit}]}{[(s+\gamma)r_a + \gamma r_s]^2} \quad [2.10]$$

where the critical surface resistance,  $r_{s,crit}$  is defined as:

$$r_{s,crit} = \frac{(s+\gamma)\rho\lambda D_r/Q^*}{s(1-\alpha)} \quad [2.11]$$

For  $r_s > r_{s,crit}$  the transpiration will *increase* with increasing  $r_a$ , for example, at lower wind speed or at a lower aerodynamic roughness length. If  $r_s < r_{s,crit}$  the transpiration *decreases* with increasing  $r_a$ . Moreover, if  $r_s \approx r_{s,crit}$ , a change in  $r_a$  is expected to have hardly any influence on  $\lambda E$ . From [2.11] it is seen that  $r_{s,crit}$  decreases with increasing temperature while it increases with an increasing ratio  $D_r/Q^*$  (cf. Rowntree, 1991; see also McNaughton & Spriggs, 1986, for a slightly different approach). Note that  $r_{s,crit}$  depends on  $D_r$  and is therefore influenced by PBL feedback.

Like  $\xi_{r_a}$ , the relative sensitivity,  $\Xi_{r_a}$ , depends on  $\lambda E/Q^*$  and  $r_a$ . Using [2.4] and [2.7],  $\Xi_{r_a}$  can be written as

$$\Xi_{r_a} = \frac{\partial(\lambda E/Q^*)}{\partial r_a} \frac{r_a}{(\lambda E/Q^*)} = \frac{\frac{s}{(s+\gamma)} \frac{(1-\alpha)}{(\lambda E/Q^*)} - 1}{1 + \frac{\gamma}{(s+\gamma)} \frac{r_s}{r_a}} \quad [2.12]$$

For dry canopies it can be shown that  $\xi_{r_a}$  is less dependent on both  $\lambda E/Q^*$  and  $r_a$  than is  $\Xi_{r_a}$ .

*c) Sensitivity of  $\lambda E/Q^*$  to  $r_s$*

The sensitivity of  $\lambda E/Q^*$  to  $r_s$ ,  $\xi_{r_s}$ , is given by:

$$\xi_{rs} = \frac{\partial(\lambda E/Q^*)}{\partial r_s} = \frac{-\gamma(\lambda E/Q^*)}{(s + \gamma)r_a + \gamma r_s} \quad [2.13]$$

Thus,  $\xi_{rs}$  strongly depends on  $\lambda E/Q^*$  and on  $r_s$ . It is also dependent on the temperature and on  $r_a$ . The dependence of the sensitivity on  $\lambda E/Q^*$  is avoided if the relative sensitivity,  $\Xi_{rs}$ , is taken:

$$\Xi_{rs} = \frac{\partial(\lambda E/Q^*)}{\partial r_s} \frac{r_s}{(\lambda E/Q^*)} = \frac{-1}{1 + (1 + \frac{s}{\gamma}) \frac{r_a}{r_s}} \quad [2.14]$$

Thus, the transpiration always *decreases* with increasing  $r_s$ , and the relative sensitivity depends only on the temperature and on the ratio of  $r_a$  to  $r_s$ .

### 2.2.3 The sensitivity of $\lambda E$ with feedback

Due to the interaction between the surface and the atmosphere, the variables from which the transpiration is calculated are *dependent* on the transpiration itself (also see Section 1.1.3). Then, a change of one variable implies a change of one or more of the other variables. The interactions are highly nonlinear and there are many variables involved in the problem. Therefore, the sensitivities cannot be derived analytically and must be calculated from finite differences. Due to the interrelated changes, the sensitivity with feedback (SL or PBL) contains the effect of many changes that cannot be separated any more. Therefore, the influence of the PBL feedback on the sensitivities is estimated by calculating a feedback factor  $F_x$  for the sensitivity of the transpiration to the variable  $x$  as:

$$F_x = \frac{\xi_{x,PBL}}{\xi_{x,SL}} \text{ or } \frac{\Xi_{x,PBL}}{\Xi_{x,SL}} \quad [2.15]$$

where the additional subscript PBL denotes PBL feedback + SL feedback and the subscript SL denotes SL feedback only.

## 2.3 Setup of the sensitivity analyses

### 2.3.1 The models

The sensitivity *without feedback* is obtained from the first derivative of the Penman-Monteith equation [1.1 or 2.7]. In order to account for the *SL feedback* the equations are used of which [1.1] and [2.7] are an approximate solution (Appendix 2, [A2.1]-[A2.4]). This set of equations is solved numerically for  $T_s$ , using the incoming *solar* radiation,  $S\downarrow$ , as the driving force and for a set of fixed conditions at  $z_r$ . (Note that errors because of the linearizations necessary to obtain the Penman-Monteith equation are avoided; see Paw U & Gao, 1988; McArthur, 1990). Here  $r_a$  is corrected for stability. Moreover, the difference between  $z_o$ ,  $z_{oh}$ , and  $z_{ov}$  is accounted for. The vegetation-SL model is outlined in Appendix 2.

Both *SL* and *PBL* feedback are taken into account by coupling the vegetation-SL model to a model of the PBL. Each time step, the conditions at  $z_r$  are updated by the PBL part of the coupled model. The model of Troen & Mahrt (1986) is used as the PBL model. This is a detailed, 1D, first-order closure model, which takes into account non-local turbulent transport. The model is outlined in Appendix 4. For a complete description and model validation the reader is referred to Troen & Mahrt (1986), Mahrt *et al.* (1987), Pan & Mahrt (1987), and Holtslag *et al.* (1990). Appendix 4 also gives some information on how the PBL model and the vegetation-SL model are coupled. The coupled model realistically simulates the evolution of the surface fluxes and the development of the PBL (De Bruin & Jacobs, 1989).

### 2.3.2 Initial and boundary conditions

*Observed* temperature, humidity, and wind profiles from HAPEX-MOBILHY (Hydrologic Atmospheric Pilot Experiment and Modélisation du Bilan Hydrique; André *et al.*, 1986, 1988) are taken as initial conditions of the sensitivity experiments. The HAPEX radiosonde data of 25 May 1986 and 13 June 1986, 6.00 UTC (44°07'N, 00°03'W) serve as the initial atmospheric conditions for Case I and Case II, respectively. The weather on both days was rather fair, except that some cumulus (<0.3) appeared in the afternoon of 25 May. The PBL characteristics were different, especially with respect to PBL depth, mixed-layer temperature, and wind speed. Some of the observed PBL characteristics are compared in Table 2.1.

The solar radiation,  $S_{\downarrow}$ , is calculated for clear sky conditions according to Holtslag and Van Ulden (1983) for the geographic position given above, but using the atmospheric transmissivity typical of De Bilt (The Netherlands, 52°06'N, 5°11'E). The simulations are carried out for daylight hours, between 6.00 and 18.00 UTC. Large-scale motions are neglected. The geostrophic wind speed is taken to be the average observed wind speed between 3.5 and 4.0 km (which is at the upper boundary of the model grid).

### 2.3.3 Reference surfaces and prescribed conditions

Two reference surfaces have been chosen. The first is a rough surface,  $z_0 = 2.0$  m, with low albedo,  $a = 0.1$ . This surface resembles the Les Landes forest in the southwest of France (see André *et al.*, 1986, 1988). In order to determine an appropriate  $r_s$  for this surface, a

TABLE 2.1. Comparison of PBL characteristics, observed during HAPEX-MOBILHY (André *et al.*, 1986, 1988) on 25 May 1986 (Case I) and 13 June 1986 (Case II), 12.00 UTC (from Hildebrand, 1988).

<i>PBL characteristics</i>	<i>Case I</i> 25 May, 12.00 UTC	<i>Case II</i> 13 June, 12.00 UTC
Inversion height [ km ]	1.1-1.2	1.8-2.1
Mixed-layer potential temperature [ °C ]	24-25	18-19
Mixed-layer specific humidity [ g kg <sup>-1</sup> ]	6-7	7-8
Wind speed at $z = 100$ m [ m s <sup>-1</sup> ]	4-5	7-8

TABLE 2.2. Prescribed conditions at  $z_r$ , average solar radiation ( $S\downarrow$ ), and transpiration ( $\lambda E$ ,  $\lambda E/Q^*$ ) for the two test cases and reference surfaces, from the simulations with the coupled model. Rough surface:  $z_0 = 2.0$  m,  $a = 0.1$ ,  $r_s = 130$  s  $m^{-1}$  (Case I) or  $100$  s  $m^{-1}$  (Case II); smooth:  $z_0 = 0.025$  m,  $a=0.2$ ,  $r_s = 60$  s  $m^{-1}$ . The average wind speed for  $z_0 = 0.25$  m is also given.

Case	Reference surface	$T_r$ [°C]	$q_r$ [g $kg^{-1}$ ]	$u_r$ [m $s^{-1}$ ]	$S\downarrow$ [W $m^{-2}$ ]	$\lambda E$ [W $m^{-2}$ ]	$\lambda E/Q^*$ [-]
I	Rough	22.4	8.2	3.4	599	238	0.511
	Smooth	20.0	9.3	5.7	599	267	0.682
	$z_0=0.25$ m			4.7			
II	Rough	18.8	6.7	7.0	624	240	0.500
	Smooth	17.3	7.1	11.3	624	267	0.653
	$z_0=0.25$ m			9.6			

simulation was carried out in which  $r_s$  was evaluated following Stewart (1988) and Gash *et al.* (1989). The average simulated  $r_s$  is taken as  $r_s$  for the reference surface:  $130$  s  $m^{-1}$  for Case I and  $100$  s  $m^{-1}$  for Case II. The second is a smooth surface,  $z_0 = 0.025$  m, with  $a = 0.2$  and  $r_s = 60$  s  $m^{-1}$ , resembling a typical pasture grassland of midlatitude regions. The reference surfaces will be denoted according to their roughness as "rough" and "smooth."

From the simulations for the reference surfaces with the coupled model, including SL and PBL feedback, the predicted average temperature, specific humidity, and the wind speed at  $z_r$  and the average simulated global radiation at the surface are calculated. These are used as the *prescribed conditions* required for the sensitivity calculations without PBL feedback. This procedure has been followed in order to obtain a fair comparison between the results of the different models. The used averages are listed in Table 2.2. Note that the conditions at  $z_r$  as predicted by the coupled model are different for the various surfaces, which is an illustration of the interaction between the PBL and the surface fluxes.

### 2.3.4 Variation of the surface characteristics; determination of sensitivities

Table 2.3 presents the scheme for the variation of the surface characteristics during the sensitivity experiments. For each simulation,  $z_0$ ,  $a$ , and  $r_s$  take one of the combinations of values as indicated in Table 2.3.

In the sensitivity studies with SL feedback only, two series of calculations have been carried out for each case (see Table 2.2):

1.  $T_r$  and  $q_r$  are as for the rough reference surface;
2.  $T_r$  and  $q_r$  are as for the smooth reference surface.

In both cases  $u_r$  is changed with the roughness length as denoted in Table 2.2. The finite differences and the sensitivities are calculated directly from the fluxes.

TABLE 2.3. Scheme for the variation of the surface characteristics in the sensitivity experiments.  $r_{s,0}$  denotes the reference value of  $r_s$ :  $130 \text{ s m}^{-1}$  (rough, Case I),  $100 \text{ s m}^{-1}$  (rough, Case II), or  $60 \text{ s m}^{-1}$  (smooth, both cases).

$z_0$ [ m ]	$a$	$r_s$
2.000	0.1	$r_{s,0}, r_{s,0} \pm 12.5\%, r_{s,0} \pm 25\%, r_{s,0} \pm 50\%$
	0.2	
	0.3	
0.250	0.1	$r_{s,0}, r_{s,0} \pm 12.5\%, r_{s,0} \pm 25\%, r_{s,0} \pm 50\%$
	0.2	
	0.3	
0.025	0.1	$r_{s,0}, r_{s,0} \pm 12.5\%, r_{s,0} \pm 25\%, r_{s,0} \pm 50\%$
	0.2	
	0.3	

From the sensitivity studies with feedback (SL, or SL plus PBL), the predicted averages of the fluxes, temperatures, etc., are calculated from the simulated evolutions between 6.00 and 18.00 UTC. The finite differences and the sensitivities are calculated from these averages.

To determine the sensitivities *without feedback*  $T_r$ ,  $q_r$ , and  $u_r$  are taken as in the experiments with SL feedback (Table 2.2). Now  $Q^*$ , instead of  $S\downarrow$ , and  $r_a$  have to be prescribed. The  $Q^*$  values as obtained in the sensitivity experiments with SL feedback are used. Moreover, the average wind speeds at  $z_r$  from the simulations with the coupled model are used to compute  $r_a$  for neutral conditions. As such, these results are comparable with those of the "classical" sensitivity experiment.

## 2.4 Results

### 2.4.1 Influence of SL feedback

#### a) Albedo change: sensitivity of $\lambda E$ to $Q^*$

The sensitivities of  $\lambda E$  to  $Q^*$ ,  $\xi_{Q^*}$ , as presented in this section are obtained for an albedo change from 0.1 to 0.3. Table 2.4 shows  $\xi_{Q^*}$ , for the two cases and for various surfaces. For completeness, the results of all models (without feedback, SL feedback only, and SL feedback + PBL feedback) are presented. It is recalled that, for a given set of prescribed conditions,  $\xi_{Q^*}$  is independent of  $\lambda E$  and  $Q^*$  ((2.8)). The values of  $S_{Q^*}$  are calculated from finite differences. For the approach without feedback, it can be shown that the analytical sensitivities ((2.8)) are exactly equal to those obtained with finite differences.

SL feedback has a small but notable influence on  $\xi_{Q^*}$ , which is either reduction or enlargement, depending on the boundary conditions. SL feedback plus PBL feedback systematically enlarges  $\xi_{Q^*}$  in the cases considered here.

TABLE 2.4. Sensitivity of  $\lambda E/Q^*$ ,  $\xi_{ra}$ : 1) without feedback, 2) with SL feedback, and 3) with SL + PBL feedback. The results are obtained from finite differences. The first column refers to the prescribed conditions at  $z_r$  in the cases without feedback and with SL feedback: rough reference surface or smooth reference surface (see Table 2.2).

Conditions		Feedback		
$T_r, q_r, u_r,$ $r_s$	$z_o$ [ m ]	—	SL	SL + PBL
<i>Case I:</i>				
Rough	2.000	0.230	0.191	0.403
	0.025	0.447	0.431	0.531
Smooth	2.000	0.322	0.301	0.563
	0.025	0.517	0.527	0.623
<i>Case II:</i>				
Rough	2.000	0.142	0.167	0.339
	0.025	0.329	0.356	0.449
Smooth	2.000	0.190	0.231	0.452
	0.025	0.386	0.419	0.538

*b) Change of surface roughness: sensitivity of  $\lambda E/Q^*$  to  $r_a$*

The sensitivity of  $\lambda E/Q^*$  to  $r_a$ ,  $\xi_{ra}$ , is calculated from the difference in  $r_a$  resulting from a change in  $z_o$  from 2.0 to 0.025 m. The analytical sensitivity ([2.10]) was determined for the average value of  $r_a$  at  $z_o = 2.0$  and  $r_a$  at  $z_o = 0.025$  m. Note that for dry canopies and a given set of prescribed conditions,  $\xi_{ra}$  is less sensitive to  $\lambda E/Q^*$  and to  $r_a$  than is  $\Xi_{ra}$  (Section 2.2.2).  $r_{s,crit}$  ([2.11]) was determined using the prescribed conditions and the results of the simulations with SL feedback only. Next,  $\xi_{ra}$  was calculated for one  $r_s < r_{s,crit}$  and another  $r_s > r_{s,crit}$ . The albedo is taken 0.2. The results are shown in Table 2.5. They include  $r_{s,crit}$  without PBL feedback as well as the analytical value for  $\xi_{ra}$ . It can be seen that SL feedback considerably increases  $|\xi_{ra}|$ , while PBL feedback counteracts the effect of SL feedback.

TABLE 2.5. As in Table 2.4, but for the sensitivity of  $\lambda E/Q^*$  to  $r_a$ ,  $\xi_{ra}$ , in millimetres per second. The analytical values of  $\xi_{ra}$  are given between parentheses. The critical surface resistance,  $r_{s,crit}$ , is calculated for the prescribed conditions, without feedback.

Conditions			Feedback		
$T_r, q_r,$ $u_r$	$r_s$ [s m <sup>-1</sup> ]	$r_{s,crit}$ [s m <sup>-1</sup> ]	—	SL	SL + PBL
<i>Case I:</i>					
Rough	65	100	-2.18 (-1.90)	-3.14	-0.20
	195	100	+2.09 (+1.98)	+3.62	+2.79
Smooth	30	67	-3.62 (-5.41)	-5.41	-1.74
	90	66	+1.15 (+1.03)	+2.59	+0.68
<i>Case II:</i>					
Rough	50	81	-5.16 (-4.70)	-6.34	-1.33
	100	81	+3.22 (+3.04)	+4.42	+3.08
Smooth	30	66	-9.00 (-7.87)	-10.34	-3.26
	90	65	+2.16 (+2.05)	+2.74	+1.35



c) Sensitivity of  $\lambda E/Q^*$  to  $r_s$ 

The relative sensitivities of  $\lambda E/Q^*$  to  $r_s$ ,  $\Xi_{rs}$ , are calculated for a change in  $r_s$  from  $r_{s,0} + 12.5\%$  to  $r_{s,0} - 12.5\%$ , at  $a = 0.2$ ,  $z_0 = 2.0$  m, and 0.025 m, respectively.  $\Xi_{rs}$  is presented because it does not depend on  $\lambda E/Q^*$  and  $r_s$  is prescribed ([2.14]). The results are listed in Table 2.6. The analytical results are also given.

As with  $\xi_{Q^*}$  the SL feedback can affect  $|\Xi_{rs}|$  either by reduction or by enlargement, depending on the boundary conditions, whereas PBL feedback systematically reduces  $\Xi_{rs}$  in the cases shown here.

TABLE 2.6. As in Table 2.4, but for the relative sensitivity of  $\lambda E/Q^*$  to  $r_s$ ,  $\Xi_{rs}$ . The analytical sensitivities are given between parentheses.

Conditions		Feedback			
$T_r, q_r, u_r,$ $r_s$	$z_0$ [ m ]	—		SL	SL + PBL
<i>Case I:</i>					
Rough	2.000	-0.660	(-0.656)	-0.708	-0.462
	0.025	-0.351	(-0.351)	-0.369	-0.284
Smooth	2.000	-0.497	(-0.496)	-0.531	-0.259
	0.025	-0.218	(-0.217)	-0.224	-0.158
<i>Case II:</i>					
Rough	2.000	-0.783	(-0.775)	-0.745	-0.534
	0.025	-0.494	(-0.493)	-0.451	-0.366
Smooth	2.000	-0.694	(-0.688)	-0.639	-0.386
	0.025	-0.385	(-0.385)	-0.343	-0.257

## 2.4.2 Influence of PBL feedback

a) Albedo change: sensitivity of  $\lambda E$  to  $Q^*$ 

From the results of the simulations with SL feedback and with both SL and PBL feedback, the sensitivity  $\xi_{Q^*}$  is calculated for an albedo change from 0.1 to 0.3 at  $z_0 = 2.0$  m,  $z_0 = 0.25$  m, and  $z_0 = 0.025$  m. In Fig. 2.2,  $\xi_{Q^*}$  is plotted versus  $r_s$ . The results shown for the simulations with only SL feedback are obtained with the conditions of the smooth reference surface as the prescribed conditions at  $z_1$  (see Table 2.2).

Qualitatively, the results for Case I and Case II are similar. Here  $S_{Q^*}$  as calculated with only SL feedback shows a sharp increase toward low  $r_s$  for  $z_0 = 2.0$  m. A negative sensible heat flux is obtained, which implies a stable stratification of the SL and a high  $r_a$ , leading to a high sensitivity (see [2.8]). It can be seen that  $\xi_{Q^*}$  as obtained from the coupled model (SL + PBL feedback) is significantly *higher* than without PBL feedback. The ratio of the two sensitivities,  $F_{Q^*}$ , is plotted as a function of  $r_s$  in Fig. 2.3.  $F_{Q^*}$  ranges from about 1.1 at low  $r_s$  and low  $z_0$  to about 2.8 at  $r_s = 195 \text{ s}^{-1}$  and  $z_0 = 2.0$  m (Fig. 2.3, Case I).

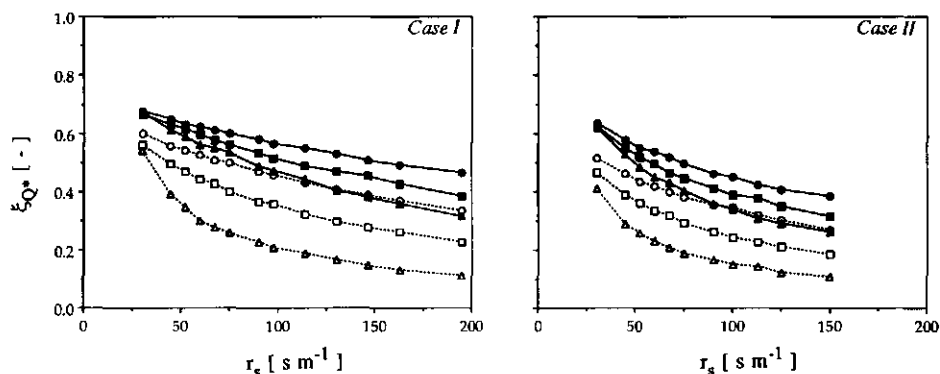


FIGURE 2.2 Sensitivity of  $\lambda E$  to  $Q^*$ ,  $\xi_{Q^*}$ , versus  $r_s$ , for Case I (left) and Case II (right). Albedo change from 0.1 to 0.3. Prescribed conditions at  $z_r$  as for smooth reference surface. Dashed lines: SL feedback only; solid lines: SL and PBL feedback. Circles:  $z_o = 0.025$  m; squares:  $z_o = 0.25$  m; triangles:  $z_o = 2.0$  m.

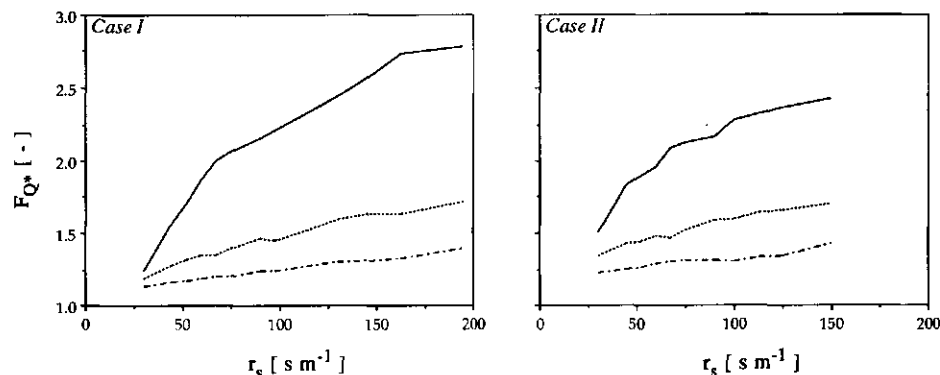


FIGURE 2.3. Feedback factor  $F_{Q^*}$  for the sensitivity of  $\lambda E$  to  $Q^*$ , versus  $r_s$ , for Case I (left) and Case II (right). Albedo change from 0.1 to 0.3. Prescribed conditions at  $z_r$  as for smooth reference surface. Dashed-dotted line:  $z_o = 0.025$  m; dashed line:  $z_o = 0.25$  m; solid line  $z_o = 2.0$  m.

b) Change of surface roughness: sensitivity of  $\lambda E/Q^*$  to  $r_a$

The sensitivity of  $\lambda E/Q^*$  to  $r_a$ ,  $\xi_{ra}$ , is determined for a change in  $z_o$  from 2.0 to 0.025 m. Figure 2.4 shows the sensitivity versus  $r_s$  for  $a = 0.1, 0.2$ , and 0.3. Again, the results shown for the simulations with only SL feedback are obtained using the prescribed conditions of the smooth reference surface (see Table 2.2). Note that at  $r_s = r_{s,crit}$  the sensitivity becomes zero. As an example,  $r_{s,crit}$  is indicated in Fig. 2.4 for an albedo of 0.3, while accounting for both SL and PBL feedback. The values for  $r_{s,crit}$  are about the actual  $r_s$  for short vegetation in midlatitude regions, which implies that  $\lambda E$  of such crops is not very sensitive to  $r_a$ .

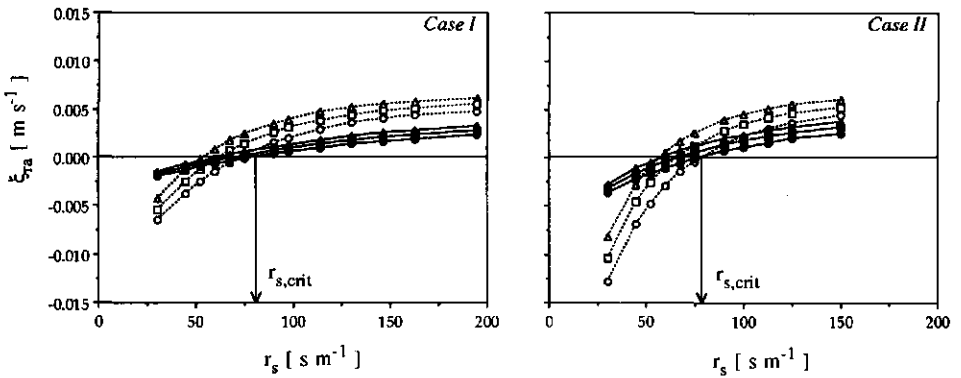


FIGURE 2.4. The sensitivity of  $\lambda E/Q^*$  to  $r_a$ ,  $\xi_{ra}$ , versus  $r_s$ , for Case I (left) and Case II (right). Change in  $z_o$  from 2.0 to 0.025 m. Prescribed conditions at  $z_r$  as for smooth reference surface.  $r_{s,crit}$  is found where  $\xi_{ra} = 0$ , as indicated by the arrows for  $a = 0.3$ . Dashed lines: SL feedback only; solid lines: SL feedback + PBL feedback. Circles:  $a = 0.3$ ; squares:  $a = 0.2$ ; triangles:  $a = 0.1$ .

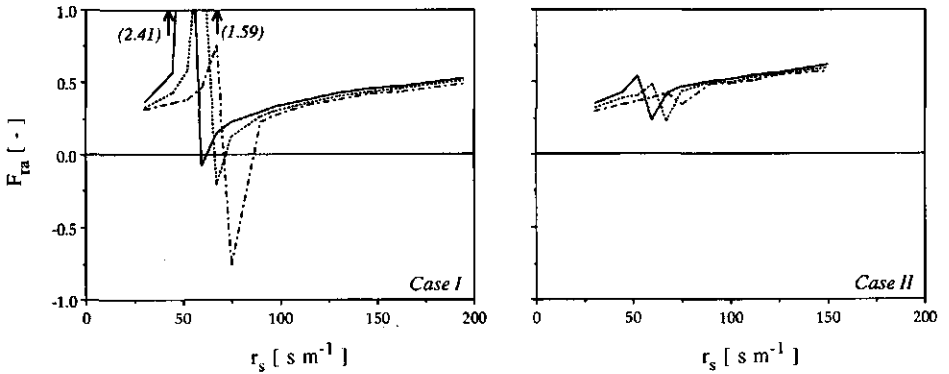


FIGURE 2.5. Feedback factor  $F_{ra}$  for the sensitivity of  $\lambda E/Q^*$  to  $r_a$ , versus  $r_s$ , for Case I (left) and Case II (right). Change in  $z_o$  from 2.0 m to 0.025 m. Prescribed conditions at  $z_r$  as for smooth reference surface. Dashed-dotted line:  $a = 0.3$ ; dashed line:  $a = 0.2$ ; solid line:  $a = 0.1$ .

With only SL feedback,  $|\xi_{ra}|$  is systematically higher than with  $|\xi_{ra}|$  with SL feedback + PBL feedback, except for  $r_s \approx r_{s,crit}$ . Both approaches show a decrease of the sensitivity if the albedo increases, but the differences are smaller if PBL feedback is taken into account.

The ratios of  $\xi_{ra}$  with and without PBL feedback,  $F_{ra}$ , are depicted versus  $r_s$  in Fig. 2.5. The effect of PBL feedback on  $\xi_{ra}$  is to reduce it to 25-50 % of the sensitivity without PBL feedback. For  $r_s \approx r_{s,crit}$   $F_{ra}$  behaves poorly. Because  $r_{s,crit}$  differs for the two approaches, an asymptotic value of  $F_{ra}$  is reached at  $r_s = r_{s,crit}$  with SL feedback only. However, the present simulations yield finite values because the prescribed  $r_s$  is never exactly equal to  $r_{s,crit}$  and thus,  $\xi_{ra}$  is never exactly equal to zero.

c) Sensitivity of  $\lambda E/Q^*$  to  $r_s$ 

Results for the sensitivity of  $\lambda E/Q^*$  to  $r_s$  are presented as the percentage change in  $\lambda E/Q^*$  as a function of the percentage change in  $r_s$ , using  $r_{s,0}$  and  $\lambda E/Q^*$  at  $r_{s,0}$  as the reference values. Then, the ratio of the relative change in  $\lambda E/Q^*$  to the relative change in  $r_s$  represents  $\Xi_{rs}$ . Some examples of the results are plotted in Figs. 2.6 and 2.7. The albedo had almost no influence on  $\Xi_{rs}$ . Therefore, only the results for  $a = 0.2$  are shown. Furthermore, only the results for  $z_0 = 2.0$  m and  $z_0 = 0.025$  m are depicted. Again,  $\Xi_{rs}$  is decreased by PBL feedback. Furthermore, the effect of  $z_0$  on the sensitivities is stronger if PBL feedback is ignored.

The ratio of the sensitivities,  $F_{rs}$ , is determined using the relative sensitivity.  $F_{rs}$  is depicted in Fig. 2.8 versus the relative change in  $r_s$ . It can be seen that  $\Xi_{rs}$  is reduced by the PBL feedback to 40-85% of  $\Xi_{rs}$  as calculated without PBL feedback.

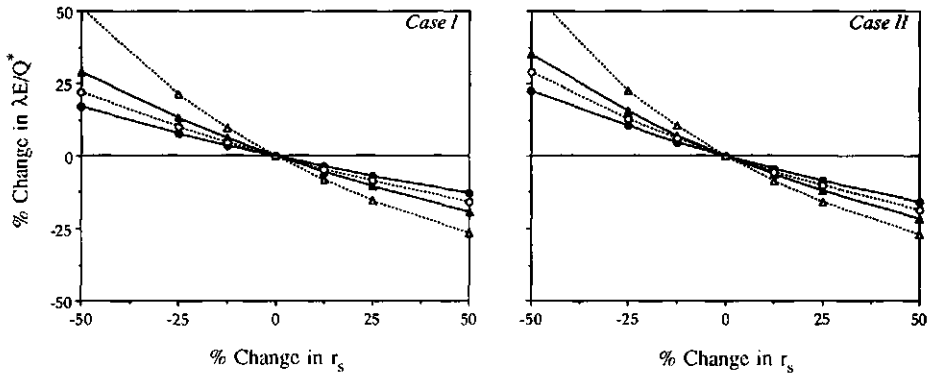


FIGURE 2.6 The relative change in  $\lambda E/Q^*$ , versus the relative change in  $r_s$ , for Case I (left) and Case II (right). Prescribed conditions at  $z_r$  as for rough reference surface. Reference values:  $r_{s,0}$  and  $\lambda E/Q^*$  at  $r_s = r_{s,0}$ ,  $r_{s,0} = 130 \text{ s m}^{-1}$  (Case I) or  $100 \text{ s m}^{-1}$  (Case II). Albedo = 0.2. Dashed lines: SL feedback only; solid lines: SL + PBL feedback. Circles:  $z_0 = 0.025$  m; triangles:  $z_0 = 2.0$  m.

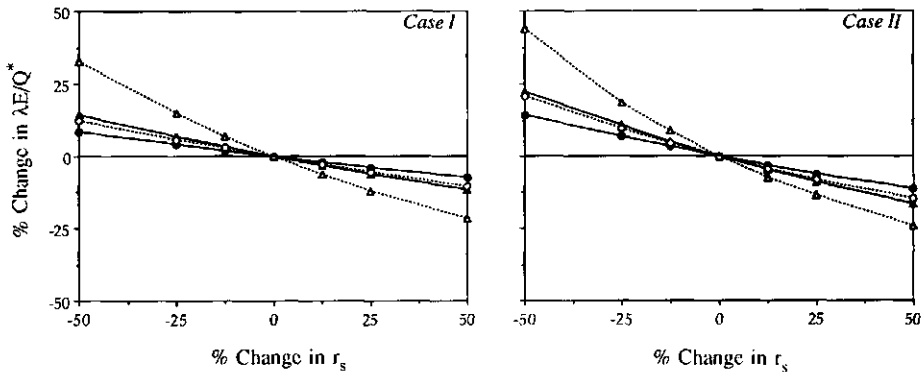


FIGURE 2.7. As in Fig. 2.6, but prescribed conditions at  $z_r$  are as for smooth reference surface.  $r_{s,0} = 60 \text{ s m}^{-1}$ .

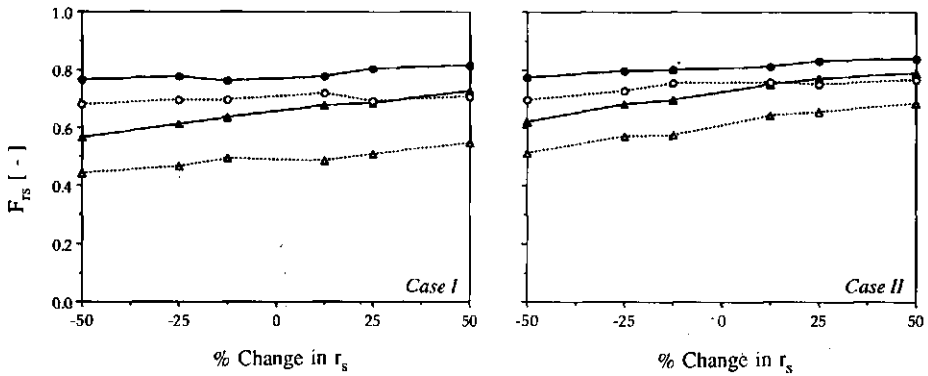


FIGURE 2.8. Feedback factor  $F_{rs}$  for the relative sensitivity of  $\lambda E/Q^*$  to  $r_s$ , versus the relative change in  $r_s$ , for Case I (left) and Case II (right). Dashed lines: prescribed conditions at  $z_r$ , as for smooth reference surface. Solid lines: prescribed conditions at  $z_r$ , as for rough reference surface. Circles:  $z_o = 0.025$  m; triangles:  $z_o = 2.0$  m.

d) Special case: changes in  $\lambda E$  due to a combination of changes

Changes in surface characteristics will hardly ever occur separately. In this subsection an example is considered of a combination of changes that may occur if a forest is "replaced" by a pasture grassland or the reverse:  $r_s$  is changed from 130 or 100  $s\ m^{-1}$  to 60  $s\ m^{-1}$ ,  $z_o$  is changed from 2.0 to 0.025 m, and the albedo from 0.1 to 0.2. The average  $\lambda E$  between 6.00 UTC and 18.00 UTC is determined for both vegetations. Two "predictions" are made: one in which only SL feedback is accounted for and one that accounts for both SL and PBL feedback. In the first case,  $T_r$  and  $q_r$  of the grassland are used to predict the transpiration of the grassland as well as of the forest. However,  $u_r$  is adapted to  $z_o$  (see Table 2.2). Note that it is common practice to use data measured above grassland. The results and the "predicted" changes are given in Table 2.7.

The predicted change in  $\lambda E$  appears to be much less if PBL feedback is taken into account. The air over grassland becomes cooler and more humid than over forest. The coupled model

TABLE 2.7. Average transpiration of a forest and a grassland, and the predicted change in  $\lambda E$  if forest is replaced by grassland or the reverse. Averaging period: 12 hours (6.00 UTC - 18.00 UTC). Forest:  $a = 0.1$ ,  $z_o = 2.0$  m,  $r_s = 130\ s\ m^{-1}$  (Case I) or  $100\ s\ m^{-1}$  (Case II). Grassland:  $a = 0.2$ ,  $z_o = 0.025$  m,  $r_s = 60\ s\ m^{-1}$ . Prescribed conditions at  $z_r$ , as for smooth reference surface.

	Feedback SL + PBL	SL	Feedback SL + PBL	SL
	Case I:		Case II:	
Forest	238	174	240	208
Grassland	267	261	267	271
CHANGE	29	87	27	63

is able to predict such differences, contrary to the model with SL feedback only. In the latter case,  $T_r$  above the forest is taken too low and  $q_r$  too high. This causes  $\lambda E$  of the forest to be underestimated if feedback is ignored and the change in  $\lambda E$  is overestimated.

### 2.4.3 Sensitivity with a box model for the PBL

Even the use of a simple, multilayer, 1D PBL model has its drawbacks with respect to complexity and required computational time. Thus, the question of what level of complexity is needed and what mechanisms must be described in a PBL model to reach the desired accuracy at a minimum effort is relevant. Only a very coarse-grid spacing is allowed in PBL "schemes" that are designed to be incorporated into a GCM. Thus, a related question is whether or not these schemes are able to describe properly the existing feedback mechanisms.

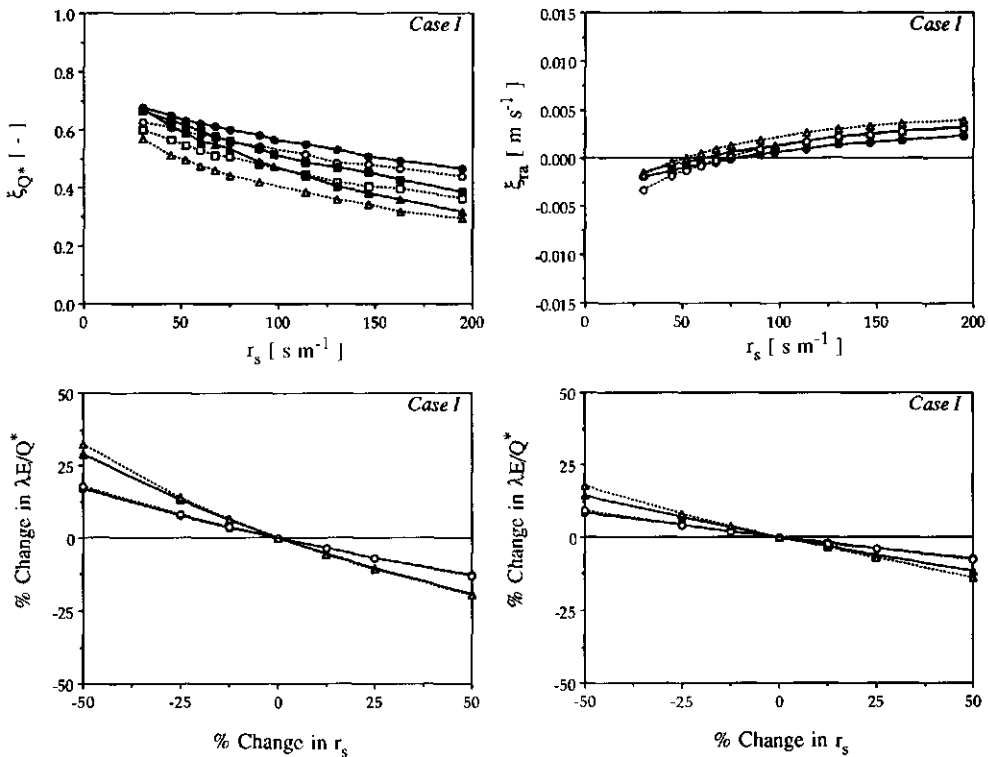


FIGURE 2.9. Comparison of sensitivities determined using the vegetation-SL model coupled to: 1) a box model for the PBL (dashed lines), and 2) the PBL model of Troen & Mahrt (1986) (solid lines). Upper left:  $\xi_{Q^*}$  versus  $r_s$ , albedo change from 0.1 to 0.3. Circles:  $z_o = 0.025$  m; squares:  $z_o = 0.25$  m; triangles:  $z_o = 2.0$  m. Upper right:  $\xi_{Tra}$  versus  $r_s$ , change in  $z_o$  from 2.0 to 0.025 m. Circles:  $a = 0.3$ ; triangles:  $a = 0.1$ . Lower left: relative change of  $\lambda E/Q^*$  versus relative change of  $r_s$ ,  $r_{s,\rho} = 130$   $s\ m^{-1}$ ;  $a = 0.2$ . Circles:  $z_o = 0.025$  m, triangles:  $z_o = 2.0$  m. Lower right: as for lower left but with  $r_{s,\rho} = 60$   $s\ m^{-1}$ . All results apply to Case 1.

Additional sensitivity calculations were performed with the PBL represented by the simple box model (Jarvis & McNaughton, 1986; De Bruin, 1989; McNaughton, 1989). Parts of the PBL feedback included in the box model are the adaptation of  $T_r$  and  $q_r$  to different surfaces. However, it does not describe entrainment (PBL growth), nor the adaptation of  $u_r$ . The box model and its coupling to the vegetation-SL model, as well as the determination of initial and boundary conditions, are outlined in Appendix 7.

Examples of the results are given in Fig. 2.9. The results shown apply to Case I. It can be seen that the sensitivities are much improved in comparison to those obtained with SL feedback only (Section 2.4.2). Improvements are similar for Case II (not shown here).

## 2.5 Discussion and conclusions

### 2.5.1 Significance of PBL feedback

Results of the sensitivity experiments clearly show that the PBL feedback has a significant influence on the sensitivity of  $\lambda E$  to the tested variables. This influence can be seen in two ways. First, for equal boundary conditions at the surface, the magnitude of the sensitivity with and without PBL feedback is different. Second, the differences between the sensitivities for different sets of surface characteristics are smaller if PBL feedback is accounted for. Both with and without PBL feedback, the results are in qualitative agreement with the predictions by the sensitivity equations ([2.8]-[2.14]).

The PBL feedback changes conditions at the reference level of the SL, by which the sensitivity of  $\lambda E$  to  $Q^*$  is enhanced, but the sensitivities of  $\lambda E/Q^*$  to  $r_a$  and  $r_s$  are reduced. This can be explained as follows.

If  $Q^*$  is reduced, both  $\lambda E$  and  $H$  will become smaller. Because of the reduction of  $H$ ,  $T_r$  will become lower, which will damp  $\lambda E$  in addition to the direct reduction by the change in  $Q^*$ . (Note that this temperature effect is partly compensated because the humidity of the atmosphere will also be less if transpiration decreases.) If  $Q^*$  is increased the reverse is true. Without PBL feedback, the change of  $T_r$  is not accounted for. Then, the changes in  $\lambda E$  for a given change in  $Q^*$  reflect only the impact of the modification of  $Q^*$ , and are therefore underestimated.

Now consider the changes in  $\lambda E$  due to changes in  $r_a$  or  $r_s$  at given  $Q^*$ . If  $\lambda E$  decreases,  $H$  increases. This combination of changes of the fluxes will result in an increase of the humidity deficit (rising temperature, decreasing moisture content), which will enhance  $\lambda E$ . The reverse is true for an increase in  $\lambda E$ . Thus, if PBL feedback is ignored the changes in  $\lambda E$  are overestimated.

Similar explanations are valid with respect to the differences between the sensitivities at various surface boundary conditions. In general, the coupled model accounts for the adaptation of the PBL to the surface underneath, which affects the surface fluxes.

The feedback factors  $F_x$  quantitatively show the importance of PBL feedback. For  $r_a$  and  $r_s$ , PBL feedback reduces the sensitivity to 40% - 85% of the sensitivity without PBL feedback. For  $Q^*$ , the sensitivities are increased by a factor 1.1 at low  $z_0$  and  $r_s$ , up to a factor 2.5 at high  $z_0$  and  $r_s$ .

Somewhat different ratios of the sensitivities are found for Case I and Case II. This influence of the atmospheric conditions may be expected: the initial profile for wind ( $r_a$ ), temperature, and humidity affect the average conditions at  $z_p$ , and thus the interaction between the PBL and the surface fluxes. Furthermore, the entrainment flux is determined by the atmospheric conditions. The effect of the entrainment on the surface fluxes can be considerable (De Bruin & Jacobs, 1989; McNaughton & Spriggs, 1989), but it is not always large (McNaughton & Spriggs, 1986). The interaction between entrainment and the surface fluxes as well as its influence on the sensitivities merit further study (see also Chapter 5).

The results presented in this chapter are obtained with constant  $r_s$  during the day. In reality,  $r_s$  shows a diurnal variation that depends, among other things, on atmospheric conditions. This may introduce an *additional* feedback mechanism, which tends to reduce the effects of PBL feedback. An example is given in Jacobs *et al.* (1991). The influence of the additional feedback is a major subject in Chapter 5.

### 2.5.2 Coupling of the vegetation to the atmosphere

The effect of the PBL feedback depends on the surface characteristics: it increases with increasing  $z_0$  and, in most cases, there is a slight increase in  $F_x$  with increasing  $r_s$ . For  $S_{Q^*}$ , this means an increase of the influence of the PBL feedback ( $F > 1$ ). However, with respect to the resistances the reverse is true ( $F < 1$ ).

It is interesting here to refer to the  $\Omega$  concept of Jarvis & McNaughton (1986) (see also McNaughton & Jarvis, 1983). The "decoupling factor,"  $\Omega$ , is derived from the Penman-Monteith equation, for *prescribed* boundary conditions at the reference level. It is defined as (McNaughton & Jarvis, 1983):

$$\Omega = \left[ 1 + \frac{\gamma}{s + \gamma} \frac{r_s}{r_a} \right]^{-1} \quad [2.15]$$

Thus, the value of  $\Omega$  varies between 0 and 1 and is determined by the ratio of  $r_s$  to  $r_a$  and by the temperature. If  $\Omega \rightarrow 0$ , the transpiration is mainly controlled by the conditions at the reference level. Then, the PBL feedback is expected to have a large influence on the sensitivity of  $\lambda E$ . Low values of  $\Omega$  are found for tall (high  $z_0$ , low  $r_a$ ), dry (high  $r_s$ ) vegetation, such as forest, whereas high values are found for low agricultural crops with high  $r_a$  and low  $r_s$ .

In the case of  $\xi_{Q^*}$ , the results are consistent with the  $\Omega$  concept: the atmospheric influence increases with increasing roughness length (decreasing  $r_a$ ) and with increasing  $r_s$ . For  $\xi_{r_a}$  and



$\Xi_{rs}$  however, the influence of the PBL feedback increases with increasing  $z_0$ , but it tends to decrease with increasing  $r_s$ . Monteith & Unsworth (1990) remark that "the term 'coupling' must not be taken too literally." Indeed, for several reasons it may be questioned whether  $\Omega$  is a suitable parameter to describe the "coupling" of vegetation to the atmosphere.  $\Omega$  depends on the PBL feedback because it is a sensitivity. Without feedback, it can be shown that  $\Xi_{rs} = \Omega - 1$  (see Jarvis, 1986; Jarvis & McNaughton, 1986; McNaughton & Jarvis, 1991). Therefore, and because of other objections (as discussed by, for example, Monteith & Unsworth, 1990; McNaughton & Jarvis, 1991) it is recommended to use  $\Omega$  only for diagnostic purposes. The description of the coupling between the vegetation and the atmosphere is discussed further in Section 5.6.

### 2.5.3 Control of transpiration

Radiation is considered as the main controlling mechanism of  $\lambda E$  for low canopies, whereas for forests it is assumed to be much less important (Beven, 1979; McNaughton & Jarvis, 1983; Stewart, 1983). Results without PBL feedback are in agreement with these earlier findings. Without PBL feedback,  $\xi_{Q^*}$  for  $z_0=0.025$  m and  $r_s=60$  s  $m^{-1}$  (comparable to grassland) is found to be about 0.5. In contrast,  $\xi_{Q^*}$  for  $z_0=2.0$  m and  $r_s=100-130$  s  $m^{-1}$  (comparable to forest) is only 0.10-0.20. However, with PBL feedback the sensitivities are about 0.6 for "grassland" and 0.4-0.5 for "forest." Thus, according to the results with the coupled model, radiation is important both for forest and grassland. Differences in radiation imply differences in atmospheric temperature and humidity which act indirectly to increase the effect of the radiation.

The sensitivity of  $\lambda \dot{E}/Q^*$  to  $r_a$  is found to be very small, which is in agreement with the results of others (McNaughton & Spriggs, 1986; Martin *et al.* 1989; Rosenberg *et al.*, 1989; Rowntree, 1991). The PBL feedback reduces the sensitivity to even lower values. The critical surface resistance,  $r_{s,crit}$ , is apparent with and without PBL feedback. If  $r_s \approx r_{s,crit}$  both approaches predict the transpiration to be rather insensitive to  $r_a$ . Such an insensitivity of  $\lambda E$  to  $r_a$  around  $r_s \approx 60$  s  $m^{-1}$  has also been reported by De Bruin (1983) and by McNaughton & Spriggs (1986).

### 2.5.4 Influence of SL feedback on the sensitivities

The results presented in Section 2.4.1, show that the SL feedback has a notable influence on the sensitivity of  $\lambda E$ . The effect of the SL feedback depends strongly on the boundary conditions as is demonstrated in the case of the sensitivity of  $\lambda E$  to  $Q^*$ . In case I,  $\xi_{Q^*}$  is reduced by up to 20% (prescribed conditions as for rough reference surface,  $z_0 = 2.0$  m), while in Case II  $\xi_{Q^*}$  is enlarged by up to 20% (prescribed conditions as for smooth reference surface,  $z_0 = 2.0$  m). Similarly,  $|\Xi_{rs}|$  is reduced in Case I, while it is enlarged in Case II. The sensitivity  $\xi_{ra}$  is systematically enhanced by SL feedback (by up to a factor 2). SL feedback has only a minor influence on  $\xi_{Q^*}$  and  $\Xi_{rs}$  as compared to PBL feedback. The PBL and SL feedback have an opposite effect on  $\xi_{ra}$  and in some cases on  $\Xi_{rs}$  and  $\xi_{Q^*}$ .

### 2.5.5 Prediction of future changes in $\lambda E$

The early studies on the sensitivity of evapotranspiration to various parameters were mainly concerned with error analysis, model performance and system analysis (McCuen, 1974; Saxton, 1975; Coleman & DeCoursey, 1976; Beven, 1979; Luxmoore *et al.*, 1981). Most of these results were obtained using observed values for the variables involved. The evapotranspiration models were used *diagnostically*. Such results are affected only by the existence of SL feedback.

During the last decade however, the *prediction* of climatic change and its consequences for, say,  $\lambda E$  has gained more and more attention. Beside error analysis of evapotranspiration models in GCM's (Sellers & Dorman, 1987, Wilson *et al.*, 1987) the question arises as to how the evapotranspiration models can be used in a *predictive* way (Martin *et al.*, 1989; Rosenberg *et al.*, 1989). Then, the interaction with the PBL becomes important. Several authors already mentioned the possibility that the sensitivity of  $\lambda E$  is influenced by the feedback between the atmosphere and the surface fluxes (Sellers & Dorman, 1987; Wilson *et al.*, 1987; Rosenberg *et al.*, 1989). The results of the present analysis confirm the existence of a significant influence of PBL feedback on the sensitivity of  $\lambda E$  at the regional scale. Without accounting for PBL feedback, *predictions* may be erroneous. This has been demonstrated in the "deforestation case" where the *change in  $\lambda E$*  is overestimated by up to a factor of 2-3 if PBL feedback is ignored. Thus, future sensitivity studies aimed at the *prediction* of changes should take PBL feedback into account.

It must be stressed that the present analysis is only a first extension of the work by others (for example, Martin *et al.*, 1989; Rosenberg *et al.*, 1989) and that much work has yet to be done. The complete set of feedback mechanisms in the soil-vegetation-atmosphere continuum can probably be described properly only in a rather detailed coupled soil-vegetation-atmosphere model. However, which feedback mechanisms are important and what level of detail is required in order to obtain reliable estimates on future changes in the evapotranspiration? For the cases presented here, coupling the vegetation-SL model to the box model has been found to be much of an improvement with respect to the sensitivities. This is an indication that reliable results might be obtained with relatively simple means. Note that the results obtained using the box model are valid only without a significant effect of entrainment (PBL growth) and for convective conditions. Furthermore, the estimate of the important parameter  $h$  (PBL height) was obtained from the results of the detailed coupled model.

Items that merit further investigation and are not covered in this study are, for example, the influence of mesoscale circulations (for example, Segal *et al.*, 1988; Pinty *et al.*, 1990), effects of local advection (De Bruin *et al.*, 1991; see also Martin *et al.*, 1989), the influence of the soil and the interaction between the soil and the plants (Luxmoore *et al.*, 1981; Pan & Mahrt, 1986; Wilson *et al.*, 1987) as well as the description of the fluxes and the PBL under stable and night-time conditions. The influence of stomatal behaviour is considered in the following chapters.

## 3

**MODELLING STOMATAL RESPONSES TO ATMOSPHERIC CO<sub>2</sub> ENRICHMENT****3.1 Introduction**

In the sensitivity analysis presented in the previous chapter surface resistance,  $r_s$ , was considered to be an independent variable with a fixed value. In reality, stomatal aperture will be adjusted to environmental conditions, so that  $r_s$  shows a diurnal variation. A crucial question is how do plants respond to an increasing atmospheric CO<sub>2</sub> concentration and how do these responses affect  $r_s$ . These plant physiological aspects of vegetation-atmosphere interaction are considered theoretically in this chapter. A model is described which accounts for stomatal behaviour at the leaf scale. In Chapter 4, the model is tested against experimental data. Subsequently, in Chapter 5, an explanation will be given as to how this leaf-scale model can be scaled up to the canopy level in order to couple it to the vegetation-PBL model of the previous chapter.

The change in subject is accompanied by a change in terminology. Plant physiologists are inclined to use "conductances" rather than "resistances". Here this "cultural" difference will be followed and will be used to indicate the difference between the stomatal control at the leaf level versus that at the canopy level:  $g_s$  for "leaf stomatal conductance" versus  $r_s$  for "surface resistance."

Plant physiological research has revealed that CO<sub>2</sub> enrichment can cause a reduction in stomatal aperture in most plant species (Raschke, 1986; Morison, 1987; see also reviews by Lemon, 1983; Strain & Cure, 1985; Warrick *et al.*, 1986; Idso, 1989; Rozema *et al.*, 1993), although some species, especially conifers, are relatively insensitive to CO<sub>2</sub> (Shugart *et al.*, 1986; Eamus & Jarvis, 1989). This chapter considers how the effect of CO<sub>2</sub> on the stomata can be accounted for, while still taking the effects of other stimuli into account. It will be argued that using a model for  $g_s$  based on a model for photosynthesis (A) is the most suitable strategy here (Section 3.2). This type of model will be called the "A- $g_s$ " model. To appreciate

the present model, some background information on the physiological principles of photosynthesis and stomatal behaviour is required. Therefore, Section 3.3 summarizes some basic plant physiological features, while physical limitations to the photosynthetic rate are briefly discussed in Section 3.4. The actual A- $g_s$  model is described in Sections 3.5 and 3.6. The photosynthesis part of the model is essentially the model of Goudriaan *et al.* (1985), which has been tuned here to the widely used biochemical model of Farquhar *et al.* (1980) and its follow-ups. Special attention is paid to the parameterization of stomatal responses to humidity that are not implicitly accounted for in A- $g_s$  models. It will be shown (Section 3.6) that the humidity responses may result in a ratio of the internal  $CO_2$  concentration ( $C_i$ ) to the external  $CO_2$  concentration ( $C_s$ ),  $C_i/C_s$ , which decreases with the leaf surface specific humidity deficit. It is proposed to directly use this relationship to parameterize stomatal humidity responses in the context of A- $g_s$  models. The new parameterization is explained and compared to existing parameterizations in Section 3.7. There is a discussion of the chapter in Section 3.8.

## 3.2 Comparison of JS-models for $g_s$ versus A- $g_s$ models

### 3.2.1 General

Stomatal behaviour is influenced by many environmental conditions and plant factors (as summarized in Table 3.1). A model for  $g_s$  should properly describe the responses of stomata to each of these stimuli. Moreover, one factor may influence the sensitivity of the stomata to one or more of the other factors. Therefore, a  $g_s$  model should also describe these synergistic interactions between separate stimuli. This becomes especially important in the present study, because  $CO_2$  has long been known as a factor which alters the sensitivity of the stomata to light, temperature and perhaps other stimuli (Meidner & Mansfield, 1968). At present it is virtually impossible to describe stomatal behaviour by means of a mechanistic model. Therefore empirical approaches have to be followed.

The most frequently used modelling strategy in meteorological research is to use a phenomenological model of the type proposed by Jarvis and Stewart (hereafter called "JS models"; see, for example, Jarvis, 1976; Stewart, 1988). It is used in micrometeorological

TABLE 3.1. Summary of plant factors and environmental factors that control stomatal behaviour.

Plant Factors	Environmental Factors
	$CO_2$
	Light
Leaf temperature	Temperature (air, soil)
Water status/turgidity	Air humidity (transpiration rate)
Plant hormones (e.g., ABA)	Soil moisture content (pF)
Leaf age/Development	Soil air concentration
Growth stage/Development stage	Pollution (air, soil)
Growth conditions	
	Nutrients

research (see Lynn & Carlson, 1990, for a review), in mesoscale models (for example, Noilhan & Planton, 1989; Mascart *et al.*, 1991) as well as in climate models (see Dickinson *et al.*, 1991). It will be argued that the currently available JS models do not meet the requirements mentioned above. Therefore, an alternative is used, which is based on the observed correlation between photosynthetic rate,  $A$ , and stomatal conductance,  $g_s$  ( $A$ - $g_s$  model). In plant physiology, this type of model is already becoming quite common (see, for example, Farquhar & Sharkey, 1982; Goudriaan *et al.*, 1985; Collatz *et al.*, 1991). In this section, the JS models and  $A$ - $g_s$  models are compared and evaluated in the framework of the present study.

### 3.2.2 JS models

The first step in the use of JS models is to determine the factors which control stomatal behaviour over a particular period of time, usually about one hour. Most of the models include a description of the response to a subset of the environmental factors listed in Table 3.1. Often plant water status is also considered.

A general response function of  $g_s$  to each of the driving variables is selected. The form of these relations is best established in controlled environments (Jarvis, 1976). Furthermore, it has to be decided how the response functions will be combined to yield the total conductance. In most of the models, the functions are combined in a multiplicative fashion (Lynn & Carlson, 1990). Then, the response functions for variables  $X_1 \dots X_n$  are normalized with the function value at the optimum so that function values ( $f_{X_1} \dots f_{X_n}$ ) are between 0 (complete limitation) and 1 (no limitation). Now,  $g_s$  can be described as:

$$g_s = g_{\max} \cdot f_{X_1} \cdot \dots \cdot f_{X_n} \quad [3.1]$$

Here,  $g_{\max}$  is the maximum conductance (or minimum resistance) which is obtained if none of the selected controlling variables  $X_1 \dots X_n$  is limiting. JS models usually exclude any synergistic interaction, that is,  $f_{X_1} \dots f_{X_n}$  are considered to be independent of each other. In theory, some interaction can be allowed for (Löscher & Tenhunen, 1981), but this would complicate the parameterization and the derivation of the function parameters probably much.

$g_{\max}$  and the parameters in the response functions (slopes, maxima etc.) are to be determined from a statistical analysis of a data set acquired in the field which contains  $g_s$ , or  $r_s$ , together with the simultaneously measured controlling variables  $X_1 \dots X_n$ . A successful statistical analysis of the data requires a large data set. Furthermore, the range of values of the controlling variables must be sufficiently large in order to obtain the function parameters. Ideally, this range would extend from values at which  $g_s$  is completely limited up to the optimum at which no limitation occurs. Such data can rarely be obtained in the field (Jarvis, 1976).

The currently available JS models for  $g_s$  or  $r_s$  will not meet the requirements of the present study, because:

1. The  $\text{CO}_2$  concentration in or near a canopy typically varies between 320 and  $450 \mu\text{mol mol}^{-1}$  (Verma & Rosenberg, 1976; Reicosky, 1989). Such a range of values in the ambient  $\text{CO}_2$  concentration is too small to establish reliable function parameters (Burrows & Milthorpe, 1976; Jarvis, 1976; Stewart, 1988). Moreover, most of the observed variation occurs during the night (Pearman & Garratt, 1973; Verma & Rosenberg, 1976), when the stomata usually are closed. Therefore, most studies ignore the effect of  $\text{CO}_2$  (Lynn & Carlson, 1990). In conclusion, although some information is available for greenhouse crops (see Stanghellini, 1987), reliable function parameters for field crops are not available, and it may be doubted whether they can be established.
2.  $\text{CO}_2$  is known to influence the stomatal responses to other conditions, notably light and temperature (Meidner & Mansfield, 1968). This interaction is not dealt with in the current JS models. Therefore, previously determined function parameters stimuli are only valid for the present ambient  $\text{CO}_2$  concentration. In general, the fact that JS models do not account for synergistic interactions is a serious shortcoming of these models.

### 3.2.3 A- $g_s$ models

Starting point for A- $g_s$  models are observations that show a strong correlation between photosynthetic rate,  $A_n$ , and  $g_s$ . This correlation is accompanied by a somewhat conservative ratio between the intercellular  $\text{CO}_2$  concentration ( $C_i$ ) and the  $\text{CO}_2$  concentration of the ambient air ( $C_a$ , or  $C_s$  at the leaf's surface) (Goudriaan & Van Laar, 1978; Wong *et al.*, 1979; Louwse, 1980). Although the correlation between  $A_n$  and  $g_s$  is probably not of a truly causal nature (Jarvis & Morison, 1981; Morison, 1987) it is observed under a wide range of conditions in the field (see reviews by, for example, Schulze & Hall, 1982; Tenhunen *et al.*, 1987), including less favourable conditions like shortage of water and nutrients, environmental pollution, and senescence (Goudriaan & Unsworth, 1990). Therefore, it is thought to reflect the strategy of plants to optimize the relation between water use and carbon assimilation (Cowan, 1982).

Upon accepting the observed relation between  $A$ ,  $g_s$  and  $C_i/C_s$  as the outcome of some kind of a general strategy of plants, modelling  $g_s$  becomes in essence equivalent to modelling  $A$ . As a first approximation:

$$g_s = 1.6 \frac{A_n}{C_s - C_i} \quad [3.2]$$

where the net photosynthetic rate,  $A_n$ , is defined positive towards the leaf. The factor 1.6 appears because of the different diffusivities of  $\text{CO}_2$  and  $\text{H}_2\text{O}$  in air. Note that  $C_s$  applies directly at the leaf's surface. The effects of the controlling variables on  $g_s$  are now accounted for through the A-model. A satisfactory A-model will at least include effects of  $\text{CO}_2$ , light and temperature. It may be a model directly describing biochemical processes (see Farquhar *et al.*, 1980) that even includes factors such as nitrogen supply and oxygen content of the air (Farquhar & Wong, 1984; Friend, 1991), or it may be a simpler model (see, for example, Goudriaan *et al.*, 1985). In all cases, the A-model will allow for the synergistic interactions

between the variables accounted for by the model. Thus, the modelled stomatal behaviour will also take into account the response to this set of variables, including  $\text{CO}_2$ , and their nonlinear interactions (see also Collatz *et al.*, 1991).

Now the question remains as to how the stomatal responses to stimuli independent of photosynthesis (for instance, responses to air humidity) should be accounted for. Here, it will be proposed to directly prescribe a relationship between the specific humidity deficit at the leaf surface and the ratio  $C_i/C_s$  in order to account for humidity responses. This parameterization is further addressed in Section 3.7, where it will be compared to some previously described alternatives (Ball *et al.*, 1987; Kim & Verma, 1991).

It must be stressed that, like JS models, A- $g_s$  models are of an *empirical* nature. However, at the cost of a somewhat greater degree of complexity, applying the simple assumption of the relation between  $A_n$  and  $g_s$  has several advantages.

1. A- $g_s$  models describe stomatal responses to  $\text{CO}_2$ .
2. The description of synergistic interactions is an *implicit* characteristic of A- $g_s$  models. The interactions include the influence of  $\text{CO}_2$  on sensitivity to other stimuli.
3. A- $g_s$  models may be expected to be more generally (in time and in place) applicable because they rely more on the very nature of plants (for example, the observed correlation between  $A_n$  and  $g_s$ , responses to  $\text{CO}_2$ , synergistic interactions) and less on statistics. It is noted that several of the key parameters of photosynthesis models are based on generally observed characteristics (for instance, of widespread proteins). As a result, some of these parameters show relatively little variation among species and in different circumstances. Often they respond rather uniformly to changing conditions (for example, to temperature).

### Conclusion

Unlike the JS models, A- $g_s$  models include a description of stomatal responses to  $\text{CO}_2$  and the synergistic interaction between  $\text{CO}_2$  and other stimuli. Therefore, an A- $g_s$  model is used in the present study.

## 3.3 Plant physiological background to the A- $g_s$ model

This section presents the plant physiological background to the A- $g_s$  model described in later sections. It serves to recall some basic, rather well-known features of photosynthesis and stomatal behaviour. Important terminology related to the anatomy of a leaf is reproduced in Appendix 1.

### 3.3.1 Basic features of photosynthesis

#### a) General: photosynthesis and dark respiration

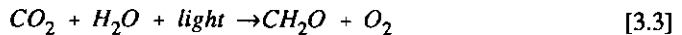
Photosynthesis of green plants is a highly complicated set of interactive reactions in which

the energy of light is trapped and used to convert  $\text{CO}_2$  into carbohydrates ( $(\text{CH}_2\text{O})_n$ ). Two groups of reactions can be distinguished: the *light reactions* and the *dark reactions*.

In the light reactions, solar energy is trapped and stored into carriers of chemical energy. Only light of wavelength bands between 400 and 700 nm is utilized in photosynthesis. Solar radiation in this part of the spectrum may be referred to as *Photosynthetically Active Radiation (PAR)* (McCree, 1981). Usually, the energy contained in PAR constitutes about half of the total solar energy received at the Earth's surface (Ross, 1975; Goudriaan, 1977).

The dark reactions utilize the energy trapped in the light reactions to convert  $\text{CO}_2$  into carbohydrates (Arnon, 1977). The most important pathway of the dark reactions is the so-called Calvin cycle (Bassham, 1979). The first step in this chain of reactions is the fixation of  $\text{CO}_2$ , which is catalyzed by the enzyme ribulose 1,5 bi-phosphate carboxylase oxygenase, *Rubisco*. The subsequent steps result in the formation of the required carbohydrate products (Stryer, 1981).

The complete set of light and dark reactions results in a strikingly simple overall reaction:



(Stryer, 1981). The ratio of the number of fixed  $\text{CO}_2$  molecules (or  $\text{O}_2$  produced) to the amount of photons used is the *quantum efficiency* or the light conversion efficiency (Radmer & Kok, 1977). The quantum efficiency near zero light intensity (the *initial quantum use efficiency*,  $\epsilon$ ) is an important parameter in photosynthesis models because it determines the initial slope of the light response curve.

Part of the fixed carbon is used as an energy source for plant processes and as material to build structural dry matter. These processes all result in the release of  $\text{CO}_2$ . They are often considered together under the name *dark respiration* because it takes place in the dark (Beer, 1986; Amthor, 1989) and to distinguish it from photorespiration, which only takes place in the light (see below). There are indications that dark respiration in leaves is suppressed by light (Graham & Chapman, 1979; Amthor, 1989).

#### b) $C_3$ and $C_4$ plants.

$\text{CO}_2$  which has passed the intercellular spaces and has entered the mesophyll cells will have to be fixed into an organic carbon product (carboxylation). In one plant class this primary carboxylation occurs by introducing the  $\text{CO}_2$  from the air directly into the Calvin cycle. Because the first product of the Calvin cycle is a 3-carbon product, plants of this class are called  $C_3$  plants.

In plants of another class, the  $C_4$  plants, the Calvin Cycle is situated in a special type of photosynthetic cells. These so called *bundle sheath cells* are embedded in the mesophyll tissue of these plants, around the vascular strands (not shown in Fig. A1.1). In  $C_4$  plants the primary fixation of  $\text{CO}_2$  in the mesophyll cells results in a 4-carbon product. This product carries  $\text{CO}_2$  to the site of the Calvin cycle in the bundle sheath cells. Here,  $\text{CO}_2$  is released again to be introduced in the Calvin cycle (Ray & Black, 1979; Leegood & Osmond, 1990).



The vast majority of the plants are of the  $C_3$  class. However, a number of important and productive crop species (for example, *Zea Mays*) and quite a few grassland species and shrubs of tropical, warm-temperate and semi-arid regions are of the  $C_4$  type (Percy & Björkman, 1983). Other plant classes are plants with a so-called crassalacean acid metabolism (CAM plants) and intermediates between CAM,  $C_3$  and  $C_4$  plants (Canvin, 1990; Leegood & Osmond, 1990). These will not be discussed here.

### c) Photorespiration

Because the carbon fixing enzyme of the Calvin cycle, Rubisco, is not only a carboxylase, but also an oxidase,  $CO_2$  and  $O_2$  compete for the same active site of Rubisco (Canvin, 1979; Stryer, 1981). Therefore, photosynthesis will be inhibited in the presence of  $O_2$ . At the same time, the oxidase activity of Rubisco will trigger a process that, like photosynthesis, depends on the availability of light and ultimately results in the release of previously fixed  $CO_2$ . This process is called *photorespiration*. Upon consuming three  $O_2$ , one  $CO_2$  is produced in the photorespiration cycle (Canvin, 1990). Because as yet no clear function of photorespiration has been identified, it is often considered to be a waste of energy (Canvin, 1990).

The ratio of photosynthesis to photorespiration depends on the concentration of  $CO_2$  and  $O_2$  at the location of the Calvin cycle and on the affinity of Rubisco to  $CO_2$  and  $O_2$ . At the current atmospheric  $CO_2$  concentration,  $C_4$  plants appear to be able to maintain a much higher  $CO_2$  concentration at the active site of Rubisco than do  $C_3$  plants (Bassham, 1979; Canvin, 1990), thanks to their special mechanism for fixing carbon. Therefore, photorespiration is virtually absent in  $C_4$  plants. By contrast,  $C_3$  plants may lose up to 50% of the newly fixed  $CO_2$  by photorespiration (Stryer, 1981; Tolbert & Zelitch, 1983; Canvin, 1990). The affinity of Rubisco for  $O_2$  increases much faster with increasing temperature than its affinity for  $CO_2$ . Thus, photorespiration rate increases with temperature (Canvin, 1990), which makes the  $C_4$  mechanism particularly advantageous in warmer environments (see Percy & Ehleringer, 1984, for a critical discussion of the ecophysiology of  $C_3$  and  $C_4$  plants).

### d) Net assimilation of a leaf and $CO_2$ compensation concentration

The net photosynthetic rate of a leaf,  $A_n$ , is the balance between the amount of carbon fixed by photosynthesis (the gross photosynthetic rate,  $A_g$ ) and the losses due to the photorespiration ( $R_l$ ) and dark respiration ( $R_d$ ):

$$A_n = A_g - R_l - R_d \quad [3.4]$$

If an *illuminated* leaf is placed in a closed chamber, the air in the chamber will be depleted of  $CO_2$  until a stable  $CO_2$  concentration is established. Then, the influx of  $CO_2$  due to  $CO_2$  assimilation is exactly balanced by the efflux due to respiratory processes ( $A_n=0$ ). The  $CO_2$  concentration in this experimental situation is called the  $CO_2$  *compensation concentration*, denoted by  $\Gamma$  (Canvin, 1979).

$\Gamma$  is an important parameter in models for  $A_n$ . Its value is mainly determined by the rate of photorespiration. For  $C_3$  plants,  $\Gamma$  is typically between 40 and 60  $\mu\text{mol mol}^{-1}$  at 25 °C and at the ambient  $O_2$  concentration of 210  $\text{mmol mol}^{-1}$  (Canvin, 1979, 1990).  $\Gamma$  increases linearly

with an increasing ambient  $O_2$  concentration and it also increases with increasing temperature (Canvin, 1979).  $C_4$ -plants lack a significant photorespiration. In addition, they are able to recycle  $CO_2$  which is released by respiratory processes (Bassham, 1979; Beer, 1986; Canvin, 1990). Therefore,  $\Gamma$  of  $C_4$ -plants approaches zero ( $< 5\text{-}10 \mu\text{mol mol}^{-1}$ ) and is not influenced by temperature or  $O_2$  (Canvin, 1979, 1990).

### 3.3.2 Stomatal behaviour

The description of stomatal behaviour in this section is mainly restricted to responses to those stimuli accounted for in the A- $g_s$  model:  $CO_2$ , light, temperature and humidity. Furthermore, responses to soil water status and plant water status will be discussed briefly, because they have often been considered in models for  $g_s$ .

#### a) $CO_2$

Plants of which the stomata are sensitive to  $CO_2$  reduce stomatal aperture upon an increase of the  $CO_2$  concentration. This  $CO_2$  response of stomata has been observed by many authors for a variety of species (see Meidner and Mansfield, 1968). However, some species, including conifers in particular, turn out to be rather insensitive to  $CO_2$  (Raschke, 1986; Shugart *et al.*, 1986; Morison, 1987; Earnus & Jarvis, 1989).

The question has arisen as to where the stomata sense the  $CO_2$  concentration. Recently, it has been demonstrated that stomata are sensitive to the *intercellular*  $CO_2$  concentration,  $C_i$ , and not to the concentration outside the leaf or inside the stomatal pore (Mott, 1988). However, the exact mechanism of the  $CO_2$  response is still unknown.

The existence of a response to  $CO_2$  is independent of the availability of light: in  $CO_2$  free air complete closure of the stomata in darkness is prevented (see, for example, Gaastra, 1959). However, the actual sensitivity of stomata to  $CO_2$  is influenced by light (Meidner & Mansfield, 1968). Other conditions that influence the  $CO_2$  response include, for example, leaf age and growth conditions (Morison, 1987). It has been shown that sometimes stress (drought stress, chilling) is required to sensitize the stomata with respect to  $CO_2$ . Such a stress signal may be mediated by the plant hormone abscisic acid, ABA (Dubbe *et al.*, 1978; Raschke, 1987).

The following pattern of response to  $C_i$  has often been observed (Raschke, 1986; Morison, 1987). A maximum stomatal aperture occurs at low  $C_i$  ( $0\text{-}100 \mu\text{mol mol}^{-1}$ ). At somewhat higher concentrations up to  $300 \mu\text{mol mol}^{-1}$  the stomata show the largest sensitivity to  $CO_2$ , with maximum sensitivities at  $C_i$  between  $150$  and  $250 \mu\text{mol mol}^{-1}$ . If  $C_i > 300 \mu\text{mol mol}^{-1}$ , the stomata continue to close, but the sensitivity decreases. Closure will not be completed as long as the stomata remain illuminated. The response of  $g_s$  to  $C_i$  might be characterized with a hyperbola (Burrows & Milthorpe, 1976; Jarvis, 1976). Response *times* may vary from less than a minute to several hours (Morison, 1987). In the former case, the stomata would be able to sense some of the turbulent concentration fluctuations. However, because a complete response would take a few minutes, it will be assumed that a description of the response to average concentrations is sufficiently accurate.

### b) Light

Generally, stomata close in the darkness and open if exposed to light. Exceptions occur in the case of the stomata of CAM plants, or may occur because of endogenous rhythms (Meidner & Mansfield, 1968).

Stomata are often more sensitive to light flux density at low intensities than at high intensities (Burrows & Milthorpe, 1976). The response of  $g_s$  to light may be described using a rectangular hyperbola (Burrows & Milthorpe, 1976; Jarvis, 1976). The response time to a step change in photon flux density varies from one species to another. A complete response may take from a few minutes to several hours. The opening response may be faster than the closing response (Turner, 1991). Furthermore, a rapid initial response may be followed by some oscillatory movements before a stable aperture is reached (Raschke, 1979).

CO<sub>2</sub> is well-known for its influence on the light response. Furthermore, the light response depends strongly on other environmental conditions, species, and the history of the plant like weather and growth conditions (Gaastra, 1959; Meidner & Mansfield, 1968; Ng & Jarvis, 1980; Lösch & Tenhunen, 1981).

Stomata not only respond to light *quantity*, but also to light *quality*. Generally, stomata show a greater sensitivity to blue light than to red light (Meidner & Mansfield, 1968; Mansfield *et al.*, 1981; Sharkey & Ogawa, 1987). The blue light response already occurs at extremely low light intensities and seems to be required for maximum stomatal aperture. On the other hand, the red light response is thought to be important at high light intensities (Sharkey & Ogawa, 1987).

Stomatal sensitivity to the quality of light shows that the light response has an important *direct* component. In addition, stomata may respond *indirectly* by means of a depletion of internal CO<sub>2</sub>, which is due to photosynthesis (Meidner & Mansfield, 1968; Mansfield *et al.*, 1981; Sharkey & Ogawa, 1987). It is very difficult to distinguish between these response types. Although the indirect response cannot be completely neglected (Raschke, 1979), it is thought at present that the direct response is by far the most important one (Sharkey & Ogawa, 1987). A third role of light might be that it provides some of the energy required to perform the stomatal movements. However, this role must be considered as a marginal one (Raschke, 1979; Meidner *et al.*, 1981; Zeiger *et al.*, 1987).

### c) Leaf temperature

It is rather difficult to determine an independent temperature response of stomata. This is because the temperature of a leaf is closely linked to light intensity,  $I$ , the leaf surface specific humidity deficit,  $D_s$ , and with  $C_i$  (through the influence of temperature on metabolic activity). Therefore,  $I$ ,  $D_s$  and  $C_i$  act as confounding variables in the temperature response. Much of these influences can be avoided by maintaining a high wind speed near the leaf, which prevents large gradients between the leaf and the surrounding air (see Ball, 1987). In spite of the difficulty mentioned above, it has been shown that higher temperatures increase the speed of stomatal movements as well as the final aperture (Meidner & Mansfield, 1968; Burrows

& Milthorpe, 1976). For some species, such an increase may continue up to very high temperatures, above the optimum for photosynthesis (Schulze & Hall, 1982). In other cases very high temperatures may cause a reduction of stomatal aperture so that the temperature response appears as an optimum curve (Burrows & Milthorpe, 1976; Lösch & Tenhunen, 1981; see also Jarvis, 1976).

*d) Air humidity (evaporation rate)*

Stomata tend to close if the vapour pressure deficit of the surrounding air increases. This behaviour has been documented for a variety of species, with a variety of plant-physiological and micrometeorological techniques (see reviews by Lösch & Tenhunen, 1981; Schulze & Hall, 1982; Schulze *et al.*, 1987; Grantz, 1990; Turner, 1991). The response can be so strong that in dry air the transpiration may decrease with increasing humidity deficit (Farquhar, 1978; Choudhury & Monteith, 1986; Mott & Parkhurst, 1991). Species with high maximum conductances are more sensitive to humidity but relative responses are similar (Schulze & Hall, 1982). Also, the sensitivity is higher at lower vapour pressure deficit (Grantz, 1990; Grantz & Meinzer, 1990).

The exact mechanism for the humidity response is still unresolved. This is one of the reasons for the confusion surrounding the interpretation and modelling of the humidity response. Therefore, some attention will be paid to this issue in the following paragraphs.

An important question related both to resolving the mechanism and to modelling strategies is which humidity parameter or which process triggers the humidity response. Part of the confusion about the humidity response has arisen because this response is easily confounded by other variables such as light intensity (Grantz & Meinzer, 1990, 1991) and leaf temperature (Schulze & Hall, 1982). Furthermore, in nature it seems impossible to break the intrinsic relation between  $g_s$ ,  $E$  and  $D_s$ :

$$E = \rho g_s D_s \quad [3.5]$$

Here,  $D_s$  is defined by the saturation specific humidity ( $q^*$ ) at the leaf temperature ( $T_l$ ) and the specific humidity of the air just outside the stomatal pore ( $q_s$ ):  $D_s = q^*(T_l) - q_s$ .

Recently, Mott & Parkhurst (1991) were able to vary  $D_s$  and  $E$  independently. They replaced air by a mixture of helium and oxygen (Helox) to which they added  $H_2O$  and  $CO_2$ . Because of the differences in diffusivity of  $H_2O$  and  $CO_2$  in air and Helox, the same stomatal aperture and air humidity (at constant leaf temperature) result in a different  $E$  in the two mixtures. Their results show that stomata do not respond to the humidity of the air but to the water vapour flux,  $E$ . Therefore, the response should, in fact, be called *evaporation response*. However, due to the relation between  $E$  and  $D_s$ , the latter variable might still be appropriate to describe the humidity response in nature. Therefore, and to avoid confusion, the response will still be called humidity response here.

Indeed,  $D_s$  is usually taken as the descriptor of humidity responses. However, probably because the sensitivity of the stomata to  $D_s$  decreases at higher temperatures, Ball *et al.*

(1987) found that the relative humidity at the leaf surface ( $h_s$ ) is a good descriptor of the humidity response. This descriptor would, in fact, account for a combined humidity-temperature response (Grantz, 1991). Nevertheless, this relationship between  $h_s$  and  $g_s$  must be considered as a purely correlative relation and not as a mechanistic one (Aphalo & Jarvis, 1991; Mott & Parkhurst, 1991).

A straightforward explanation of the *mechanism* of stomatal humidity responses is the so-called hydraulic feedback hypothesis. In dry air, the transpiration rate tends to be higher. If the evaporated water cannot be replenished by the plant, the water potential of the cells will decrease. Now, the stomata close due to the related loss of turgor.

However, the response of the stomata to the internal bulk water status is too weak to explain the range of changes in stomatal aperture that is usually observed (Raschke, 1979; Schulze & Hall, 1982; Schulze *et al.*, 1987). Furthermore, hydraulic feedback can never account for the observed decreases in  $E$  at high values of  $D_s$ . This phenomenon requires a "feedforward" loop, which implies a mechanism acting somewhat independent of  $E$ . Note that McNaughton & Jarvis (1991) were able to describe the phenomenon as a *feedback*: the observed phenomenon of a decreasing  $E$  with increasing  $D_s$  occurs because the humidity response causes an increased sensitivity of transpiration to stomatal conductance. However, "feedforward" will be used here because it has become a commonly used term in plant physiology.

Peristomatal transpiration (cuticular water loss from guard cells and subsidiary cells) could be a mechanism providing the feedforward response (Farquhar, 1978; see also Lange *et al.*, 1971, Tenhunen & Lösch, 1981). Mott & Parkhurst (1991) propose the existence of two interdependent processes: at high humidity ( $E$  increases with  $D_s$ ), the response is controlled by hydraulic feedback. At low humidity ( $E$  decreases with  $D_s$ ) heterogeneous stomatal closure accounts for the necessary feedforward control. In the latter case, a limited number of stomata close almost completely, while the others respond only weakly. Both the assimilation and the transpiration rate are reduced in this case. Nonami *et al.* (1990) propose that an internal cuticula prevents water from moving from the bulk leaf tissue to the guard cells. Whatever proposal is correct, for modelling purposes the feedforward response can be described if an appropriate response function to  $D_s$  (Choudhury & Monteith, 1986), or  $h_s$  (Ball *et al.* 1987) is used.

#### *e) Soil water*

Stomata close in response to drying of the soil, but closure starts only if the soil water potential drops down to rather low values. There is accumulating evidence that the response to soil drought is mediated through metabolites from the roots and not through the bulk water status of the plant (Schulze *et al.*, 1987; Turner, 1991). This is clearly demonstrated in experiments where the soil is allowed to dry, but the water status of the shoot is kept intact:  $g_s$  decreases in spite of a constant bulk leaf water potential (for example, Gollan *et al.*, 1986; Gollan *et al.*, 1992). The simulations in this study are all performed assuming a well-watered soil. Therefore, no further attention will be paid to responses to soil moisture content.

#### f) Plant water status

Often, a correlation is reported between the bulk water status of a plant and stomatal aperture or  $g_s$  (see Jarvis, 1976). Indeed, the stomata can close only if the guard cells lose turgor (Raschke, 1979). However, in the field the observed correlation is very weak or even absent (Schulze *et al.*, 1987; Turner, 1991). Furthermore, the observed ranges in bulk leaf water potential are far from being sufficient to explain the variations in  $g_s$  which are observed at timescales ranging from several hours to a day (see humidity responses). Therefore, it must be concluded that turgor loss of guard cells is controlled, to a large extent, independent of bulk leaf water potential. This may be achieved by means of an active exchange of solutes between the guard cells and the subsidiary cells (Raschke, 1979, 1987; Bradford & Hsiao, 1982) or by the internal resistance to water supply to the guard cells (Nonami *et al.*, 1990). Thus, variations in the bulk plant water status are not a cause of changing stomatal aperture, but a *result* of the balance between water uptake from the soil and the transpiration which is controlled by stomatal action (Schulze & Hall, 1982).

Although in the short term plant water status has probably no significant *direct* effect on stomatal conductance, plant water status may determine the maximum stomatal conductance in the longer term (Lösch & Tenhunen, 1981), for example, by releasing ABA (Bradford & Hsiao, 1982; Raschke, 1987). This longer term effect is ignored in the present study.

### 3.4 Physical limitations of the photosynthetic rate

#### 3.4.1 General

Photosynthetic rate ([3.4]) does not only depend on the biochemical processes described in the previous section. The diffusion process which controls the transport of  $\text{CO}_2$  from the atmosphere to the carboxylation sites inside the leaf sets a physical limit to photosynthetic rate (Gaastra, 1962; Farquhar & Sharkey, 1982; Bravdo, 1986). In the terminology of Raschke (1979), the "physical supply" has to be equated with the "biochemical demand" in order to find the actual photosynthetic rate.

The flux of  $\text{CO}_2$  towards the leaf is driven by the  $\text{CO}_2$  concentration difference between the turbulent air just outside the leaf and the  $\text{CO}_2$  concentration at the sites of the carboxylation and is controlled by many conductances. Some of these conductances are physical in nature. Others are related to chemical processes, and are also called "conductance" in order to allow a convenient comparison of limitations imposed by chemical and physical processes (Monteith, 1963; Jarvis, 1971; Farquhar & Sharkey, 1982). A detailed description of the conductances is provided by, for example, Jarvis (1971) and Nobel (1991). Here, the following conductances are distinguished:

1. the leaf boundary layer conductance ( $g_{bc}$  for  $\text{CO}_2$ ,  $g_{bv}$  for water vapour,  $g_{bh}$  for heat)
2. the stomatal conductance ( $g_{sc}$  for  $\text{CO}_2$ ,  $g_s$  for water vapour)
3. the cuticular conductance ( $g_c$ )
4. the mesophyll conductance ( $g_m$ )

### 3.4.2 Boundary layer conductance

The boundary layer conductance controls the diffusion through the layer of air adjacent to the leaf. It applies to the transport of  $\text{CO}_2$ , water vapour and heat. From a dimensional analysis it can be shown that  $g_{bv}$  may be written as a function of the wind speed in the bulk air,  $u$ , and of the leaf's dimension parallel to the direction of the wind speed,  $W_l$ , (Gates, 1980):

$$g_{bv} = k \cdot \left( \frac{u}{W_l} \right)^{0.5} \quad [3.6]$$

where  $k$  is an empirical constant (taken  $5.6 \times 10^{-3} \text{ m s}^{-0.5}$  for a one-sided conductance, see Goudriaan, 1977). In order to model  $\text{CO}_2$  fluxes, the difference in the diffusivities of water vapour and  $\text{CO}_2$  through the leaf boundary layer has to be accounted for. This difference in diffusivity is partly determined by some convection, so that (Ball, 1987):

$$g_{bv} = 1.37 g_{bc} \quad [3.7]$$

The boundary layer conductance for heat,  $g_{bh}$ , is 1.86 times  $g_{bv}$  in the case of a hypostomatous leaf (Monteith & Unsworth, 1990).

### 3.4.3 Stomatal conductance

Stomatal conductance is used to describe diffusion through the stomatal pore. It is controlled by stomatal aperture (see the previous section) and applies to both  $\text{CO}_2$  and  $\text{H}_2\text{O}$ . Again, the difference in diffusivity between  $\text{CO}_2$  and  $\text{H}_2\text{O}$  has to be accounted for. In this case, the diffusion is assumed to be strictly normal to the concentration gradient, so that the conversion factor between  $g_s$  and  $g_{sc}$  becomes equal to the ratio of the binary diffusivities of  $\text{CO}_2$  and  $\text{H}_2\text{O}$  in air (Ball, 1987):

$$g_s = 1.6 g_{sc} \quad [3.8]$$

In order to calculate transpiration, the water vapour concentration within the sub-stomatal cavity must be known. For convenience, the walls of the mesophyll cells can be considered as the source of water vapour. Moreover, the air in the sub-stomatal cavity may be assumed to be saturated with water vapour, so that the water vapour concentration can be calculated from the leaf temperature as the saturation water vapour concentration. The errors associated with these assumptions are usually very small (Ball, 1987; Nobel, 1991).

### 3.4.4 Cuticular conductance

The cuticular conductance describes the diffusion of water and  $\text{CO}_2$  through the waxy cuticle. For convenience,  $g_c$  is assumed equal for  $\text{CO}_2$  and  $\text{H}_2\text{O}$ . It is a quantity parallel to stomatal conductance, so that the total conductance through the epidermis can be calculated as  $(g_c + g_s)$  and  $(g_c + g_{sc})$ , respectively. Usually, if the stomata are fully open,  $g_c$  is much smaller than  $g_s$ . Therefore, it is often neglected. However, when the stomata are nearly closed,

$g_c$  may become larger than  $g_s$ .  $g_c$  is typically between 0.1 and 0.4 mm s<sup>-1</sup> for crops, but is usually smaller for trees and xerophytes. It may increase when the cuticle is mechanically damaged or develops cracks, due, for example, to rain, hail or growth (Nobel, 1991).

### 3.4.5 Mesophyll conductance

The mesophyll conductance,  $g_m$ , describes the transport of CO<sub>2</sub> between the sub-stomatal cavity and the site of the carboxylation. This conductance does not apply to water vapour transport, because the mesophyll cells may be considered as being the source of water vapour (see above).  $g_m$  includes a variety of conductances which arise from physical or chemical processes (Jarvis, 1971; Nobel 1991). Because the value of some of these component conductances is very uncertain (Nobel, 1991)  $g_m$  is most conveniently treated as one residual resistance (see Gaastra, 1959).  $g_m$  appears to be an important parameter for modelling the photosynthetic rate. It will be defined more precisely in the next section.

## 3.5 The A-g<sub>s</sub> model part I: the photosynthesis model

### 3.5.1 General

The photosynthesis part of the A-g<sub>s</sub> model is in essence the model of Goudriaan *et al.* (1985) and will be referred to here as G85. This model satisfactorily describes most of the essential response characteristics of photosynthesis. It can be used to evaluate photosynthesis of C<sub>3</sub> and C<sub>4</sub> plants.

G85 is less detailed than the model of Farquhar *et al.* (1980). The latter, biochemical model and its variants are at present more widely used for purposes similar to those of the present study (Farquhar & Wong, 1984; Ball *et al.*, 1987; Leuning, 1990; Collatz *et al.*, 1991; Friend, 1992; Collatz *et al.*, 1992, Harley *et al.*, 1992, Reynolds *et al.*, 1992). Evidently, it requires somewhat more knowledge of biochemistry and plant physiology. Furthermore, a larger number of input parameters need to be known. For these reasons and because G85 *directly* relies on conductances to describe the diffusion of CO<sub>2</sub> between the air and chloroplasts, it is felt that G85 has more links with current meteorological research than has a biochemical model. Therefore, G85 has been selected for use in the present study.

The modelling approach of G85, is based on the distinction between two essentially different conditions:

1. Light is the limiting factor (at relatively high CO<sub>2</sub> concentrations)
2. CO<sub>2</sub> is the limiting factor (at relatively high light intensity)

These conditions essentially determine the shape of the light response curve used to calculate  $A_n$ .



Throughout, it will be assumed that  $R_d$  is suppressed at high light intensities (Graham & Chapman, 1977; Amthor, 1989). It will also be assumed that  $R_d$  has no significant influence on  $\Gamma$ . As explained by Goudriaan *et al.* (1985), the error involved with the latter assumption is typically less than  $3 \mu\text{mol mol}^{-1}$  in  $\Gamma$  and the concurrent error in  $A_n$  will be negligible.

### 3.5.2 Light as the limiting factor

$A_n$  at very low light intensity is linearly related to the amount of absorbed PAR,  $I_a$ :

$$A_n = \epsilon I_a - R_d \quad [3.9]$$

where  $\epsilon$  denotes the initial quantum use efficiency, quantifying the slope of the light response curve.  $\epsilon$  is affected by photorespiration. It can be shown that  $\epsilon$  may be calculated as (Goudriaan *et al.*, 1985):

$$\epsilon = \epsilon_0 \frac{C_s - \Gamma}{C_s + 2\Gamma} \quad [3.10]$$

where the parameter  $\epsilon_0$  denotes the maximum quantum use efficiency and  $C_s$  the  $\text{CO}_2$  concentration at the leaf surface. [3.10] is derived from biochemical considerations and is similar to the result obtained by Farquhar *et al.* (1980). In fact, the internal  $\text{CO}_2$  concentration,  $C_i$ , should be used in [3.10]. However, [3.10] applies close to  $I_a = 0$ , so that  $C_i \approx C_s$ ,  $\Gamma$  represents the effect of photorespiration on  $\epsilon$  so that  $\epsilon$  depends on temperature and  $\text{O}_2$  concentration. Furthermore, it can be seen that  $\epsilon$  increases with an increasing  $\text{CO}_2$  concentration, which is due to a suppression of photorespiration. Note that [3.10] can also be applied in the case of  $C_4$  species. For plants of this class  $\Gamma \rightarrow 0$ , so that  $\epsilon$  becomes nearly a constant (Ehleringer and Björkman, 1977).

$\epsilon_0$  is based on the theoretical quantum requirement of the Calvin cycle ( $\approx 0.025 \text{ mg J}^{-1} \text{ PAR}$ ). This theoretical requirement must be corrected by a loss factor, which is mainly due to absorption by tissues not taking part in photosynthesis (Farquhar *et al.*, 1980, Goudriaan *et al.*, 1985). Therefore,  $\epsilon_0$  of  $C_3$  plants is taken  $0.017 \text{ mg J}^{-1} \text{ PAR}$  (Goudriaan *et al.*, 1985).  $\epsilon_0$  of  $C_4$  species is further reduced because of the energy requirement of the  $\text{CO}_2$  concentrating mechanism, so that in this case  $\epsilon_0$  becomes about  $0.014 \text{ mg J}^{-1} \text{ PAR}$  (see Collatz *et al.*, 1992).

### 3.5.3 $\text{CO}_2$ as the limiting factor

At high light intensities and limiting  $\text{CO}_2$  concentrations, it may be assumed that the photosynthetic rate coincides with the asymptotic value of the light response curve,  $A_m$  (Thornley, 1976). Then, at low  $C_i$ ,  $A_m$  is linearly related to the  $\text{CO}_2$  concentration according to (Goudriaan *et al.*, 1985):

$$A_m = (C_i - \Gamma) \cdot g_m \quad [3.11]$$

[3.11] shows that  $\Gamma$  can be regarded as the apparent concentration at the bottom of the conductance chain, near the carboxylation site in the chloroplast. [3.11] also defines  $g_m$ . It can be seen that  $g_m$  may be derived from the light-saturated rate of photosynthesis. Furthermore,  $g_m$  quantifies the slope of the  $\text{CO}_2$  response curve at high light intensity. As such, it can be interpreted as a parameter to model the activity of Rubisco under these conditions (see Farquhar *et al.*, 1980; see also Appendix 8).

### 3.5.4 Synthesis: interaction of light responses and $\text{CO}_2$ responses

An empirical light response function of  $A_n$  is used to combine the above described effects of  $\text{CO}_2$  and light. As in G85, the asymptotic exponential is used here:

$$A_n = (A_m + R_d) \cdot \left(1 - \text{EXP}\left(\frac{-\epsilon I_a}{A_m + R_d}\right)\right) - R_d \quad [3.12]$$

Here,  $R_d$  is parameterized by taking  $R_d = A_m/9$  (van Heemst, 1986).

Equations [3.9]-[3.12] predict an unlimited photosynthesis at high light intensities and high  $\text{CO}_2$  concentrations. In reality, the photosynthetic rate will be bound to a maximum,  $A_{m,\max}$ , which is related to the ability of plants to allocate the products of the Calvin cycle and to regenerate ribulose 1,5 biphosphate (Stitt, 1991). Here,  $A_{m,\max}$  is accounted for using a saturation response, similar to [3.12], that provides a smooth transition between [3.11] and  $A_{m,\max}$  (see Thornley, 1976):

$$A_m = A_{m,\max} \cdot \left(1 - \text{EXP}\left(\frac{-g_m(C_i - \Gamma)}{A_{m,\max}}\right)\right) \quad [3.13]$$

### 3.5.5 Temperature responses

The temperature dependence of photosynthesis is accounted for through the temperature dependence of  $\Gamma$ ,  $g_m$ , and  $A_{m,\max}$ . The temperature response of these variables is based on a  $Q_{10}$  response function.  $Q_{10}$  is defined as the proportional increase of a parameter value for a 10 degrees increase in temperature (Berry & Raison, 1982), so that:

$$X(T) = X(@25) \cdot Q_{10}^{\frac{T-25}{10}} \quad [3.14]$$

where  $T$  denotes temperature (in  $^{\circ}\text{C}$ ),  $X(T)$  is the value of any variable  $X$  at temperature  $T$ , and  $X(@25)$  the value of  $X$  at  $T = 25^{\circ}\text{C}$ . [3.14] is used directly to describe the temperature response of  $\Gamma$ . In the case of  $g_m$  and  $A_{m,\max}$ , [3.14] is modified using the inhibition functions given by Collatz *et al.* (1992):

$$X(T) = \frac{X(@25) \cdot Q_{10}^{\frac{T-25}{10}}}{(1 + \text{EXP}(0.3(T_1 - T)))(1 + \text{EXP}(0.3(T - T_2)))} \quad [3.15]$$

where  $T_1$  and  $T_2$  denote reference temperatures. Note that  $X(@25)$  is the value of  $X$  at 25 °C without inhibition.  $T_1$  and  $T_2$  can be adjusted to mimic species-specific features (for instance, the lower temperature optimum of  $C_3$  species than of  $C_4$  species).

The set of parameter values and reference temperatures can be chosen such that the temperature dependence of  $\Gamma$ ,  $g_m$ , and  $A_{m,max}$  reflects the properties of their equivalents in the biochemical models. This procedure is outlined in Appendix 8. The resulting default values used in the present study are summarized in Table 3.2.

### 3.5.6 Model characteristics: responses of $A_n$ to $CO_2$ , light and temperature

Some examples of model simulations are shown in Figs. 3.1A-3.1C. The examples are chosen to illustrate the model's ability to simulate some well-known features of  $C_3$  and  $C_4$  photosynthesis. Furthermore, some predictions of responses to a doubled ambient  $CO_2$  concentration are illustrated. The aspects of  $C_3$  and  $C_4$  photosynthesis shown and the possible responses to  $CO_2$  enrichment are more thoroughly discussed elsewhere (Lemon, 1983; Strain & Cure, 1985; Enoch & Kimball, 1986; Warrick *et al.*, 1986; Idso, 1989; Bowes, 1991; Rozema *et al.*, 1993).

Fig. 3.1A depicts the predicted responses to  $C_i$  at a temperature of about 25 °C and at light intensities of 125, 250 and 500  $W m^{-2}$  PAR respectively (500  $W m^{-2}$  PAR represents full sunlight). Typical operational  $C_i$  values under the current ambient  $CO_2$  concentration (1x: 350  $\mu mol mol^{-1}$ ) and for a doubled  $CO_2$  concentration (2x: 700  $\mu mol mol^{-1}$ ) are indicated by the arrows.  $C_4$  plants show a steeper initial response to  $C_i$  than  $C_3$  plants due to the high  $g_m$ . This feature is related to their  $CO_2$  concentrating mechanism, which enables them to optimally use  $CO_2$  at low concentrations. At the current operational  $C_i$ ,  $C_4$  plants have almost reached

TABLE 3.2. Parameter values used in the present study (see also Appendix 8).

	Parameter (X)	X(@25)	$Q_{10}$	$T_1$ [°C]	$T_2$ [°C]
$C_3$	$\epsilon_0$ [mg J <sup>-1</sup> PAR]	0.017	-	-	-
	$\Gamma$ [ $\mu mol mol^{-1}$ ]	45	1.5	-	-
	$g_m$ [mm s <sup>-1</sup> ]	7.0	2.0	5	28
	$A_{m,max}$ [mg m <sup>-2</sup> s <sup>-1</sup> ]	2.2	2.0	8	38
$C_4$	$\epsilon_0$ [mg J <sup>-1</sup> PAR]	0.014	-	-	-
	$\Gamma$ [ $\mu mol mol^{-1}$ ]	2.8	1.5	-	-
	$g_m$ [mm s <sup>-1</sup> ]	17.5	2.0	13	36
	$A_{m,max}$ [mg m <sup>-2</sup> s <sup>-1</sup> ]	1.7	2.0	13	38

saturation of  $A_n$  to  $C_i$ . Little more is gained at a doubled ambient  $\text{CO}_2$  concentration. Differences in light intensity become much more important. By contrast,  $\text{C}_3$  plants show a much slower response to  $C_i$ . Upon increasing  $C_i$ , photorespiration becomes more and more suppressed, which causes an increase of  $A_n$  up to rather high values of  $C_i$ . If the atmospheric  $\text{CO}_2$  concentration is doubled,  $\text{C}_3$  plants will not only profit at high light intensities but also at low light intensities, due to the increased light use efficiency ([3.11]).

Some of the phenomena described above are also visible from the light response curves (Fig. 3.1B). The initial slope of the curve for  $\text{C}_3$  plants increases markedly upon a doubling of the ambient  $\text{CO}_2$  content. Furthermore, the saturation value for  $\text{C}_3$  plants is increased by about 45%. As a result, the  $\text{C}_3$  light response curve at  $700 \mu\text{mol mol}^{-1}$  is much like the  $\text{C}_4$  light response curves. In the latter case, the light response changes only if the  $\text{CO}_2$  concentration is doubled.  $\text{C}_4$  plants may show a non-saturating light response up to full sunlight (Ray & Black, 1979). In order to simulate that feature more pronounced  $A_{m,\text{max}}$  should be increased (not shown here).

Finally, Fig. 3.1C depicts the simulated temperature responses of  $\text{C}_3$  and  $\text{C}_4$  plants in full sunlight ( $500 \text{ W m}^{-2}$  PAR). The simulated optimum temperature for  $\text{C}_3$  photosynthesis is about  $25^\circ\text{C}$  at an ambient  $\text{CO}_2$  concentration of  $350 \mu\text{mol mol}^{-1}$  and shifts towards  $26^\circ\text{C}$  in  $700 \mu\text{mol mol}^{-1}$   $\text{CO}_2$ . Such a shift of the optimum temperature is a rather well-known feature and may become as much as  $3\text{--}5^\circ\text{C}$  for some species (Berry & Raison, 1982; Long, 1991). The optimum temperature for  $\text{C}_4$  photosynthesis is about  $34\text{--}35^\circ\text{C}$  at  $350 \mu\text{mol mol}^{-1}$  and at  $700 \mu\text{mol mol}^{-1}$ . If  $C_s = 350 \mu\text{mol mol}^{-1}$ ,  $A_n$  at the optimum temperature is about twice as high for  $\text{C}_4$  plants than for  $\text{C}_3$  plants. This difference between the two plant classes has largely disappeared for the simulations at  $C_s = 700 \mu\text{mol mol}^{-1}$ . The temperature response curves also illustrate that the predicted increase in photosynthetic rate for a doubling of the ambient  $\text{CO}_2$  concentration depends strongly on temperature. This confirms the conclusion of Long (1991) that growth or yield predictions based on models or observations that ignore the interaction between temperature and  $\text{CO}_2$  (for example, Parry *et al.*, 1988) should be reconsidered.

It must be stressed that the results shown for the enriched atmosphere are only valid if the plants do not acclimatize to the higher  $\text{CO}_2$  concentration. If plants are not able to create new sinks for photosynthetic products, acclimatization will result in an inhibition of photosynthesis, which counteracts the beneficial effect of ambient  $\text{CO}_2$  enrichment (Percy & Björkman, 1983; Bowes, 1991; Stitt, 1991). Also, photosynthesis can be reduced by a decreased production of photosynthetic enzymes such as Rubisco (Stitt, 1991). As a result of adaptation, the characteristics of the photosynthesis response ( $A_{m,\text{max}}$ ,  $g_m$ ) are altered (Stitt, 1991; Long *et al.*, 1993). However, the variability of these features is very large among plant species. Furthermore, it has been suggested that the acclimatization found in enrichment experiments is, in fact, an experimental artifact (Harley *et al.*, 1992). Acclimatization is ignored in the present study.

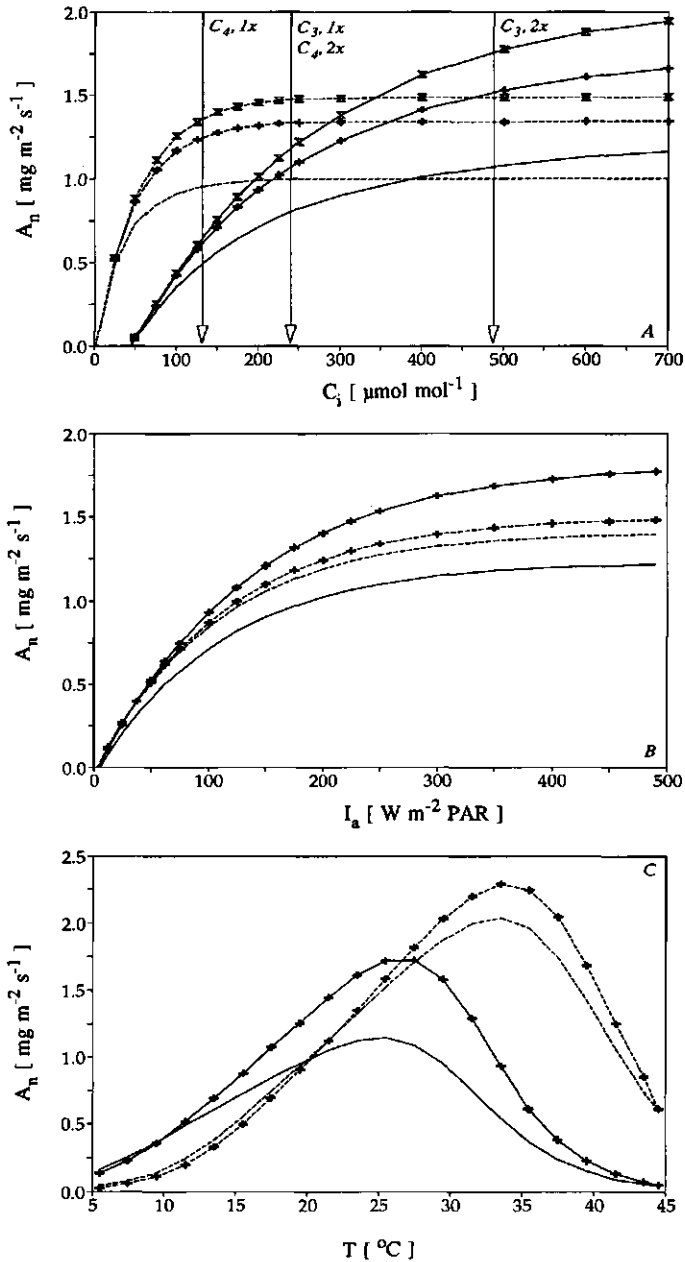


FIGURE 3.1. Simulated photosynthetic rate,  $A_n$ , of  $\text{C}_3$  species (solid lines) and  $\text{C}_4$  species (dashed lines) as a function of: A) internal  $\text{CO}_2$  concentration,  $C_i$ , at  $T = 25^{\circ}\text{C}$  and  $I_a = 125, 250,$  and  $500 \text{ W m}^{-2} \text{ PAR}$  (unlabelled, pluses, and hourglasses, respectively); B) light intensity,  $I_a$ , at  $T = 25^{\circ}\text{C}$  and  $C_s = 350 \mu\text{mol mol}^{-1}$  (unlabelled) and  $700 \mu\text{mol mol}^{-1}$  (pluses); C) temperature,  $T$ , at  $I_a = 500 \text{ W m}^{-2} \text{ PAR}$  and  $C_s = 350 \mu\text{mol mol}^{-1}$  (unlabelled) and  $700 \mu\text{mol mol}^{-1}$  (pluses). The arrows indicate typical operational internal  $\text{CO}_2$  concentrations. See text for further explanation.

## 3.6 The A-g<sub>s</sub> model part II: stomatal responses

### 3.6.1 General

So far, the assimilation part of the A-g<sub>s</sub> model has been considered. Stomatal conductance, g<sub>s</sub>, has to be evaluated from the photosynthetic rate calculated in the assimilation part. This section describes how assimilation and stomatal control are linked in the present A-g<sub>s</sub> model.

The assumption that stomatal behaviour and CO<sub>2</sub> assimilation are coupled is based on the fundamental premise that plants will operate their stomata such that carbon gain is maximized while minimizing water loss. It is believed that it is this strategy which results in the strong observed correlation between A<sub>n</sub> and g<sub>s</sub>. The correlation is observed in the laboratory as well as in the field, including under such unfavourable conditions as senescence, water stress, nutrient shortage and air pollution (for example, Goudriaan & van Laar, 1978; Wong *et al.*, 1979; Tenhunen *et al.*, 1987; Goudriaan and Unsworth, 1990; Van Hove, 1989). It should be stressed that a correlation between A<sub>n</sub> and g<sub>s</sub> does not necessarily imply a causal relation (Jarvis & Morison, 1981), nor does it imply large stomatal control of A<sub>n</sub> (Farquhar & Sharkey, 1982; Jones, 1985). It should be regarded as the outcome of a plant "strategy" in the field, which can be used as a valuable working hypothesis (Cowan, 1982).

### 3.6.2 First approximation

In order to be able to calculate g<sub>s</sub> from A<sub>n</sub> the concentration difference (C<sub>s</sub> - C<sub>i</sub>) has to be known, because (neglecting cuticular conductance, g<sub>c</sub>, and effects of water vapour transport):

$$g_s = 1.6g_{sc} = \frac{1.6A_n}{C_s - C_i} \quad [3.16]$$

In order to complete the set of equations, the observation is used that the correlation between A<sub>n</sub> and g<sub>s</sub> results a somewhat conservative ratio C<sub>i</sub>/C<sub>s</sub>. The tendency to maintain a constant C<sub>i</sub>/C<sub>s</sub> has been demonstrated experimentally (Goudriaan & Van Laar, 1978; Wong *et al.*, 1979; Louwse, 1980; reviews: Raschke, 1986; Morison, 1987) as well as theoretically (Farquhar *et al.*, 1978). This result can be used to complete the A-g<sub>s</sub> model by taking:

$$\frac{C_i}{C_s} = \text{constant} \quad [3.17]$$

[3.17] generates the internal CO<sub>2</sub> concentration used to calculate A<sub>m</sub> ([3.11] and [3.13]) as well as the difference between the ambient and the internal CO<sub>2</sub> concentration to use in [3.16]. C<sub>i</sub>/C<sub>s</sub> is about 0.7 for C<sub>3</sub> species and 0.4 for C<sub>4</sub> species (Wong *et al.*, 1979).

[3.17] is crucial to A-g<sub>s</sub> models of the type presented here. Therefore, the assumption made in [3.17] is investigated in somewhat more detail in the following paragraphs.

### 3.6.3 Influence of light intensity on $C_i/C_s$ ; $C_i$ as a virtual concentration

[3.16] shows that  $C_s - C_i$ , and therefore the ratio  $C_i/C_s$ , can be derived from a plot of  $A_n$  versus  $g_{sc}$ . The slope of the regression line,  $S_{g,A}$ , yields the average concentration difference  $C_s - C_i$  (Goudriaan & van Laar, 1978).  $S_{g,A}$  does not depend on light intensity (Goudriaan & van Laar, 1978; Louwse, 1980), which is in agreement with [3.17]. However, an increase of  $C_i/C_s$  may be expected towards low light intensities. This can be seen as follows.

At low light intensity  $g_c$  may not be neglected any more, because  $g_s \rightarrow 0$  while  $g_c$  remains constant. Therefore,  $C_i/C_s$  will become:

$$\frac{C_i}{C_s} = 1 - \frac{A_n}{(g_{sc} + g_c)C_s} \quad [3.18]$$

[3.18] shows that  $C_i/C_s \rightarrow 1$  if  $A_n \rightarrow 0$ . It follows that  $C_i/C_s$  increases towards low light intensities. In addition, if  $I_a = 0$ ,  $A_n = -R_d$  ([3.12]) and  $g_{sc} \approx 0$ , so that  $C_i/C_s > 1$ . For  $R_d = 0.05 \text{ mg m}^{-2} \text{ s}^{-1}$ ,  $C_s = 640 \text{ mg m}^{-3}$  ( $350 \text{ } \mu\text{mol mol}^{-1}$  at  $20^\circ\text{C}$ ) and  $g_c = 0.25 \text{ mm s}^{-1}$ , [3.18] results in  $C_i/C_s \approx 1.3$ . Increases of  $C_i/C_s$  towards low light intensity have been found experimentally (Meinzer, 1982; Fuentes & King, 1989; Van Hove *et al.*, 1992), as well as with simulations using biochemical models for photosynthesis (Farquhar & Wong, 1984; Friend, 1991).

The example shows that  $S_{g,A}$  is *not* a real concentration difference. It should be interpreted as a virtual concentration difference, which will approach the real concentration difference at high light intensity. Nevertheless, this virtual concentration difference should be used to calculate  $g_{sc}$  and  $g_s$  at all light intensities, because by definition:

$$g_{sc} = \frac{A_n + R_d}{S_{g,A}} \quad [3.19]$$

where  $R_d$  appears because the regression line will originate from  $A_n$  at  $I_a = 0$ , which is  $-R_d$ . Similarly, the corresponding internal  $\text{CO}_2$  concentration appearing in [3.17] is a virtual concentration. Note that the virtual concentration can also be used to calculate  $A_m$ , because it approaches the realized  $C_i$  at high light intensities.

### 3.6.4 Effect of $\text{CO}_2$ concentration on $C_i/C_s$

$S_{g,A}$  generally increases with increasing  $\text{CO}_2$  concentration such that [3.17] is satisfied (Goudriaan & Van Laar, 1978; Louwse, 1980; see also Wong *et al.*, 1979) bearing in mind that  $C_i$  is a virtual concentration. However, even at high light intensities [3.18] predicts that  $C_i/C_s \rightarrow 1$  if  $A_n \rightarrow 0$ , which will be the case if  $C_i = C_s = \Gamma$ . The following ratio,  $f$ , appears to be a more appropriate constant to use (Goudriaan *et al.*, 1985; see also Monteith, 1991):

$$f = \frac{C_i - \Gamma}{C_s - \Gamma} \quad [3.20]$$

so that:

$$\frac{C_i}{C_s} = f + (1 - f)\frac{\Gamma}{C_s} \quad [3.21]$$

The value of  $f$  is about 0.7 for  $C_3$  plants and 0.4 for  $C_4$  plants.

In the A- $g_s$  model, [3.21] is used instead of [3.17]. It predicts a strong increase of  $C_i/C_s$  for  $C_s \rightarrow \Gamma$  and  $C_i = \Gamma$  if  $C_s = \Gamma$ . At the current ambient  $CO_2$  concentration and at 25 °C,  $C_i/C_s$  will become about 0.74 for  $C_3$  plants. These features are in reasonable agreement with the data presented by Mott (1988).

### 3.6.5 Effect of air humidity on $C_i/C_s$

The humidity of the air (or transpiration; Mott & Parkhurst, 1991), directly affects  $g_s$  (see Section 3.3.3), independent of  $A_n$ . The resulting relation between  $D_s$  and  $C_i/C_s$  is determined by the concurrent change in  $A_n$  and  $g_{sc}$  (or  $g_s$ ). If only  $D_s$  changes while other conditions, such as leaf temperature and  $C_s$ , are unchanged, three scenarios can be envisaged. In order to explore these possibilities, consider an *increase* of  $D_s$  which results in a *decrease* of  $g_{sc}$ . Fig. 3.2 shows an example of a such a situation in which  $g_{sc}$  is reduced by about a factor 2. The scenarios are as follows.

First, if  $A_n$  is not affected, [3.18] predicts a decrease of  $C_i/C_s$ . However, this scenario would not lead to the strong correlation between  $g_{sc}$  and  $A_n$  that is often observed (see Tenhunen *et al.*, 1987). It requires that the operational internal  $CO_2$  concentration remains in the saturation region of the response of  $A_n$  to  $CO_2$ . For plants which have an operational  $C_i$  *below* saturation (as in Fig. 3.2) this behaviour would imply either an increased mesophyll conductance,  $g_m$ , or a greatly increased saturation level,  $A_{m,max}$  (or both). These requirements point towards a stimulation of the photosynthetic apparatus, which is unlikely to occur under dry conditions.

Second, if  $A_n$  and  $g_{sc}$  are both affected in the same proportion,  $C_i/C_s$  will remain constant. This convenient assumption satisfies [3.17]. It implies a decrease in  $g_m$  or a decrease in  $A_{m,max}$  (or both). However, the assumption is contradictory to observations that  $C_i/C_s$  changes if  $D_s$  changes (Wong *et al.*, 1979; Morison & Gifford, 1983; Van Hove, 1989; Monteith, 1991; reviewed by: Raschke, 1986; Morison, 1987; see also Chapter 4).

Third, both  $A_n$  and  $g_{sc}$  decrease but the  $A_n$ - $C_i$  response curve is not altered. Then, the proportional decrease of  $g_{sc}$  is more than that of  $A_n$ . The resulting decline in  $A_n$  depends on the initial operational  $C_i$ . At first, the relative decline may be weak, but it can become stronger as  $C_i$  drops further (Bradford & Hsiao, 1982). This scenario implies a correlation



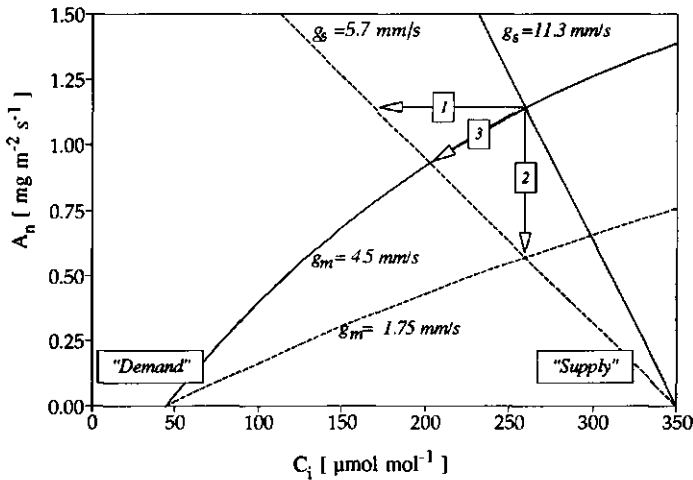


FIGURE 3.2. Illustration of concurrent changes in photosynthetic rate,  $A_n$ , and internal  $\text{CO}_2$  concentration,  $C_i$ . In the example given, a 50% change in  $g_{sc}$  is assumed. Two  $C_i$  response curves, the "demand" functions, are depicted: one for  $g_m = 4.5 \text{ mm s}^{-1}$  and one for  $g_m = 1.75 \text{ mm s}^{-1}$ . These are calculated using the  $A_n$  model described above, at a temperature of  $25^\circ\text{C}$  and at a light intensity of  $500 \text{ W m}^{-2}$  PAR. The "supply" ( $g_{sc}[C_s - C_i]$ ) is calculated for  $g_{sc} = 11.3$  and  $5.7 \text{ mm s}^{-1}$ , respectively. The numbered arrows refer to the scenarios discussed in the text. In the case of scenario 1 ( $A_n$  is unchanged), the reduction of  $g_{sc}$  would have to be accompanied by an increase of  $g_m$ , while  $C_i/C_s$  decreases by about 35%. In scenario 2 ( $A_n$  and  $g_{sc}$  change in the same proportion (50%), and  $C_i/C_s$  does not change), the change in  $g_{sc}$  would have to be accompanied by a 61% decrease of  $g_m$  if  $A_{n,max}$  remains the same. Scenario 3 results in a 17% decrease of  $A_n$  and a 20% decrease of  $C_i/C_s$ , but  $g_m$  does not change.

between  $A_n$  and  $g_{sc}$ , although less than in the previous case, as well as a decline of  $C_i/C_s$  with  $D_s$ . It is also consistent with the results of, for example, Wong *et al.* (1979). In their study,  $A_n$  responded to  $C_i$  when stomatal aperture was directly affected without a direct influence on  $A_n$  (for example, by air humidity or ABA). Therefore, in the present study it is assumed that this scenario occurs if stomata respond to humidity. In Section 3.7 the resulting relationship between  $C_i/C_s$  and  $D_s$  and how this can be used to mimic stomatal humidity responses will be discussed.

### 3.6.6 Influence of other factors on $C_i/C_s$

$\text{CO}_2$ , light and humidity of the air are considered to cause most of the variation in  $C_i/C_s$ . Factors such as nutrient deficiency or water stress due to soil water depletion are thought to change  $g_s$  and  $A_n$  in proportion to each other so that  $C_i/C_s$  is not reduced further (Wong *et al.*, 1979; Goudriaan *et al.*, 1985; Raschke, 1986; Monteith, 1991). Direct effects of plant hormones such as ABA (Dubbe *et al.*, 1978; Wong *et al.*, 1979) are ignored in the present study. It is assumed that such effects are implicitly accounted for through the responses to the modelled environmental stimuli.

### 3.6.7 Effects of the interaction between E and $A_n$

The model presented so far treats the  $\text{CO}_2$  flux as a diffusion in a binary system, that is, only interactions between  $\text{CO}_2$  and air are taken into account. However, Jarman (1974) and Leuning (1983) pointed out that the interaction between water vapour and  $\text{CO}_2$  has a significant influence on the diffusion process and may not be neglected. Fortunately, the effect of oxygen evolution may be ignored (Jarman, 1974).

Leuning (1983) also considered the interactions between diffusing molecules and the wall of the stomatal pore. In addition, he considered the viscous flow arising from the small pressure gradient within the leaf. Such a pressure gradient may be expected in any transpiring leaf (see also Nobel, 1991). These effects lead to significant errors in the calculated  $g_s$  and  $C_i$  only for pore sizes less than  $0.5 \mu\text{m}$ . Fully open stomata may have widths of a few tens of  $\mu\text{m}$  (Meidner & Mansfield, 1968). Therefore, the effects of gas-wall collisions and the internal pressure gradient can usually be neglected (Leuning, 1983). Other sources of error are probably dominant in calculations of gas-exchange under the conditions where they become important (Ball, 1987).

Here, the effects of the interaction between the diffusion of  $\text{H}_2\text{O}$  and  $\text{CO}_2$  are accounted for following Von Caemmerer & Farquhar (1981) and Ball (1987).  $g_{sc}$  ([3.17]) is calculated as:

$$g_{sc} = \frac{A_n + \frac{EM_a(C_s + C_i)}{\rho M_v} 10^{-6}}{C_s - C_i} \quad [3.22]$$

where  $A_n$  and  $E$  are both in  $\text{mg m}^{-2} \text{s}^{-1}$ ,  $M_v$  and  $M_a$  are the molecular weights of water and air respectively and  $10^{-6}$  is a conversion factor (between kg and mg). For  $A_n = 1 \text{ mg m}^{-2} \text{s}^{-1}$ ,  $E = 100 \text{ mg m}^{-2} \text{s}^{-1}$  ( $246 \text{ W m}^{-2}$ ),  $C_s = 640 \text{ mg m}^{-3}$ ,  $C_i/C_s = 0.7$  and  $\rho = 1.2 \text{ kg m}^{-3}$  the water vapour flux correction amounts to about 7.5% of  $g_{sc}$ .

## 3.7 Parameterization of stomatal responses to air humidity

### 3.7.1 Description

The parameterization of stomatal humidity responses in the context of the present A- $g_s$  model relies on the following observations and assumptions:

1.  $f$  decreases almost linearly with  $D_s$ , at least at low  $D_s$  (Raschke, 1986; Morison, 1987; Friend, 1991; Chapter 4);
2. at the timescale of interest to this study (a day or less) the independent humidity effects do not affect the potential activity of photosynthetic apparatus, that is,  $g_m$  and  $A_{m,\text{max}}$  remain constant at otherwise unchanged conditions;
3. the minimum epidermal conductance is equal to  $g_c$ . This is the case if  $I_a = 0$  or if  $D_s = D_{\text{max}}$ .

2) implies that changes in  $C_i/C_s$  are evaluated as changes of the virtual internal concentration.  
 3) defines  $D_{\max}$ . This definition of  $D_{\max}$  differs somewhat from that of Choudhury & Monteith (1986): a small transpiration rate and a minimum photosynthetic rate are allowed after stomatal closure (where  $g_s = 0$ ). The minimum photosynthetic rate at full light intensity is denoted as  $A_{\min}$ .  $A_{\min}$  will be established at a minimum internal  $\text{CO}_2$  concentration  $C_{\min}$  corresponding to a minimum value of  $f$ ,  $f_{\min}$ . Note that, as before,  $A_n = -R_d$  if  $I = 0$ .

$f_{\min}$  can be estimated as follows. It is assumed that  $A_{\min}$  and the corresponding  $C_{\min}$  are found in the quasi-linear part of the  $C_i$ -response curve. Then,  $A_{\min}$  may be estimated as

$$A_{\min} = g_m(C_{\min} - \Gamma) \quad [3.23]$$

from which follows (using [3.16] and neglecting possible effects of transpiration)

$$C_{\min} = C_s - \frac{g_m(C_{\min} - \Gamma)}{g_c} \quad [3.23a]$$

or

$$C_{\min} = \frac{g_c C_s + g_m \Gamma}{g_c + g_m} \quad [3.23b]$$

Now  $f_{\min}$ , defined as  $f$  at  $D_{\max}$  will be

$$f_{\min} = \frac{g_c}{g_c + g_m} \quad [3.24]$$

while  $f$  is written as a linear function of  $D_s$ :

$$f = f_o \left(1 - \frac{D_s}{D_{\max}}\right) + f_{\min} \left(\frac{D_s}{D_{\max}}\right) \quad [3.25]$$

Here,  $f_o$  denotes the value of  $f$  which is obtained after a linear extrapolation to  $D_s = 0$ . Finally, the virtual value of  $C_i$  is calculated from insertion of [3.25] in [3.21]. The description of  $f$  chosen here ([3.25]), necessary because of the third assumption made above, causes  $C_i/C_s$  to increase at very high temperatures ( $g_m$  and  $A_n \rightarrow 0$ ), despite a high light intensity. This phenomenon, which is also predicted by [3.21] and which can be derived from the data presented by, for example, Tenhunen *et al.* (1987), contributes to the conservative nature of  $C_i/C_s$ . Other A- $g_s$  models which account for a humidity response (for example, Ball *et al.*, 1987; Kim & Verma, 1991) also predict such behaviour for  $C_i/C_s$  (see Figs. 3.3 and 3.4 for examples). At low temperatures,  $D_{\max}$  cannot be reached so that the second term of [3.25] is relatively unimportant. A smooth approach towards the limit at  $D_s = D_{\max}$  requires:

$$g_{sc} + g_c = g_c + \frac{A_n - A_{\min}}{C_s - C_{i,vir}} \quad [3.26]$$

Here, the subscript "vir" has been added to stress that the virtual value of  $C_i$  should be used. Note that [3.26] will only be valid in the quasi linear part of the  $C_i$  response curve. Usually, this will only be the case if  $D_s \rightarrow D_{\max}$ . Furthermore, it will only be valid at high light intensities. At low light intensities, the other limit must be approached which requires:

$$g_{sc} + g_c = g_c + \frac{A_n + R_d}{C_s - C_{i,vir}} \quad [3.27]$$

[3.26] conflicts with [3.27] at high light intensities. Therefore, a formulation is used that correctly describes both extremes and provides a smooth transition between [3.26] and [3.27]:

$$g_{sc} + g_c = g_c + \frac{A_n - A_{\min} \cdot \frac{D_s}{D_{\max}} \cdot \frac{A_g}{A_{m,g}} + R_d \left(1 - \frac{A_g}{A_{m,g}}\right)}{C_s - C_{i,vir}} \quad [3.28]$$

Here,  $A_{m,g} \equiv A_m + R_d$  and  $A_g$  is the gross assimilation rate ( $= A_n + R_d$ ). As before, the formulation can be adjusted to account for the effect of transpiration on the diffusivity of  $\text{CO}_2$ .

The current approach needs two parameters to be determined,  $D_{\max}$  and  $f_0$ .  $D_{\max}$  can be estimated from the available literature on the stomatal humidity response. For the time being,  $D_{\max}$  is taken  $45 \text{ g kg}^{-1}$ , which is a value typical for agricultural crops and deciduous forest (Choudhury and Monteith, 1986). Obviously,  $D_{\max}$  can be adjusted to reflect species-specific features of the stomatal humidity responses.

Using the given value for  $D_{\max}$ ,  $f_0$  can be estimated as follows. Many reports on the ratio  $C_i/C_s$  apply to conditions where  $D_s$  is between about 7.5 and  $12.5 \text{ g kg}^{-1}$  (for example, Wong *et al.*, 1979; Louwse, 1980; Mott, 1988). Assuming that the standard values of  $f$  (0.7 for  $C_3$  plants and 0.4 for  $C_4$  plants) are valid at  $D_s \approx 10 \text{ g kg}^{-1}$  and neglecting  $f_{\min}$ , it follows that  $f_0$  is about 0.85 for  $C_3$  plants and about 0.5 for  $C_4$  plants. The resulting intercept for  $C_3$  plants is in reasonable agreement with the data shown by Morison & Gifford, (1983). For  $C_4$  plants,  $C_i/C_s$  seems to be underestimated at low values of  $D_s$ . However, it is noted that the curves for  $C_4$  plants as given by Morison & Gifford (1983) lead to values of  $C_i/C_s$  much higher than 0.4 over the entire range of  $D_s$ . As such, they are in contradiction with evidence presented by others (Wong *et al.*, 1979). Furthermore, the data of Morison & Gifford (1983) were obtained at rather low light intensity ( $\approx 150 \text{ W m}^{-2} \text{ PAR}$ ).

### 3.7.2 Sample calculations

In order to illustrate some features of the current parameterization of humidity responses, results of simulations will be compared to the results of two other approaches recently proposed. The two alternatives are:

1. The approach proposed by Kim & Verma (1991), denoted by KV91. They used

$$g_s = g_{s,A} \cdot f_{D_s} \quad [3.29]$$

where  $g_{s,A}$  is given by [3.16] and  $f_{D_s}$  is a response function for the effect of  $D_s$  on  $g_s$ . For comparison,  $f_{D_s}$  is taken to be the linear function proposed by Choudhury & Monteith (1986):

$$f_{D_s} = 1 - \frac{D_s}{D_{\max}} \quad [3.30]$$

Furthermore, [3.19] is used with  $f=0.7$ .  $C_{i,vir}$  as evaluated from [3.19] is used to make a first guess of  $A_n$  and to determine  $g_{s,A}$  from [3.28], with  $A_{\min} = 0$  and  $g_c = 0$ . Then,  $g_{s,A}$  is multiplied with  $f_{D_s}$  to yield  $g_s$ . This value of  $g_s$  is then used to recalculate  $C_i$ , which now becomes the *realized*  $C_i$ , and  $A_n$ . The solution must be determined numerically, as is done in the examples presented below. It is noted that Kim & Verma (1991) approximate the solution using a second order equation in  $C_i$ , of which the coefficients contain  $C_{i,vir}$ . The smaller root of this second order equation is then used to recalculate  $A_n$ .

2. The so called stomatal index, denoted by B87:

$$g_s + g_c = a \frac{A_n h_s}{C_s - \Gamma} + b \quad [3.31]$$

where  $h_s$  is the relative humidity at the leaf surface. [3.31] was first proposed by Ball *et al.* (1987) and modified by Leuning (1990) to the form presented above. The regression coefficient  $b$  must be equal to  $g_c$  to give  $g_s + g_c = g_c$  at very low air humidity. However, it must be slightly *larger* than  $g_c$  to have  $g_s + g_c = g_c$  if  $I_a = 0$ . Here,  $b$  is taken equal to  $g_c$ . Furthermore, the value of  $a$  is taken 10 (Leuning, 1990) and  $\Gamma$  is calculated as described in Appendix 8. These values of  $a$  and  $b$  give values of  $g_s$  values which are comparable to those of the present parameterization. To obtain the final solution of  $g_s$ ,  $A_n$  and  $C_i$ , the equations [3.12], [3.16], and [3.31] have to be solved simultaneously. In principle, using  $C_s$  and  $h_s$  instead of the bulk properties of the air, analytical solutions can be obtained but these are very cumbersome (Leuning, 1990). As in Collatz *et al.* (1991), the solution is determined numerically. It is noted that although [3.31] seems to describe the general behaviour of  $g_s$  rather well (Ball *et al.*, 1987; Norman & Polley, 1988; Leuning, 1990; Collatz *et al.*, 1991; Collatz *et al.*, 1992), objections have been raised to the use of  $h_s$  as the descriptor of humidity responses (Aphalo & Jarvis, 1991; Mott & Parkhurst, 1991).

Note that the present parameterization (denoted by PP) uses  $D_s$  as a humidity descriptor. Furthermore, no additional iteration is required if  $C_s$  is used as the  $CO_2$  concentration outside the leaf. For convenience, the parameterizations compared in the sample calculations are summarized in Table 3.3.

TABLE 3.3. Summary of humidity response parameterizations. In the sample calculations,  $g_s$  is corrected for the influence of transpiration on  $A_n$ .

Parameterization:	Humidity descriptor:	Humidity response by:
1. PP (Present study)	$D_s$	$g_s \approx g_c + 1.6A_n/(C_s - C_{i,vir})$ $f = (C_{i,vir} - \Gamma)/(C_s - \Gamma) = f_0(1 - D/D_{max}) + f_{min}(D/D_{max})$
2. KV91 (Kim & Verma, 1991)	$D_s$	$g_s \approx g_c + (1 - D/D_{max}) \cdot 1.6A_n/(C_s - C_{i,vir})$ $C_{i,vir}/C_s = 0.7$
3. B87 (Ball <i>et al.</i> , 1987; Leuning, 1990)	$h_s$	$g_s = aA_n h_f / (C_s - \Gamma) + b$

In the examples given below  $C_3$  photosynthesis is assumed. The parameters used to drive the photosynthesis model are as in Table 3.2.  $g_c$  is taken  $0.25 \text{ mm s}^{-1}$ . Furthermore,  $C_s$  is taken  $630 \text{ mg m}^{-3}$  ( $\approx 340 \text{ } \mu\text{mol mol}^{-1}$  at  $20^\circ\text{C}$  and  $1000 \text{ hPa}$ ), and  $I_a = 500 \text{ W m}^{-2}$  PAR (full sunlight).

The examples differ in the way that  $D_s$  is varied. In the first example  $D_s$  has been increased by decreasing the humidity of the air at the leaf surface ( $q_s$ ), while keeping the leaf temperature constant. Thus, the  $C_i$  response curve is unchanged throughout the simulation. In the second example,  $D_s$  has been varied by increasing the leaf temperature, while maintaining  $q_s$  constant. In this case, the  $C_i$  response curve will change because  $g_m$  and  $A_{m,max}$  change.

Results of the simulations are shown in Fig. 3.3 (Example 1) and Fig. 3.4 (Example 2). The graphs depict  $A_n$ , the realized ratio  $C_i/C_s$ , ( $g_s + g_c$ ), and  $E$  as a function of  $D_s$ .

*Example 1:  $D_s$  is increased by decreasing the humidity of the air.*

The model predictions are shown in Fig. 3.3 for a leaf temperature of  $15^\circ\text{C}$  (dashed lines) and  $35^\circ\text{C}$  (solid lines), respectively. At each temperature, the range of  $D_s$  shown corresponds to  $h_s = 1 \rightarrow 0$ .

KV91 and PP predict an almost linear decrease of  $A_n$  and  $C_i$  with  $D_s$  (Figs. 3.3 A and B), but the relation between ( $g_s + g_c$ ) and  $D_s$  is a hyperbola (Fig. 3.3C). These parameterizations yield about the same value of ( $g_s + g_c$ ) at both values of  $T_l$ . By contrast, B87 predicts a sudden collapse of  $A_n$  and  $C_i/C_s$  at  $h_s < 0.3$ , irrespective of the temperature (Figs. 3.3 A and B). Furthermore, B87 simulates an almost linear decrease of ( $g_s + g_c$ ) with  $D_s$ . At one value of  $D_s$ , ( $g_s + g_c$ ) is different for  $T_l = 15^\circ\text{C}$  and  $T_l = 35^\circ\text{C}$  respectively.

PP and B87 simulate a declining  $E$  at high  $D_s$ . KV91 predicts a continuously increasing  $E$  over the entire range of  $D_s$ , which is in contradiction with observations that  $E$  decreases again at high  $D_s$  (Farquhar, 1978; Choudhury & Monteith, 1986; also see discussion, Section 3.8).

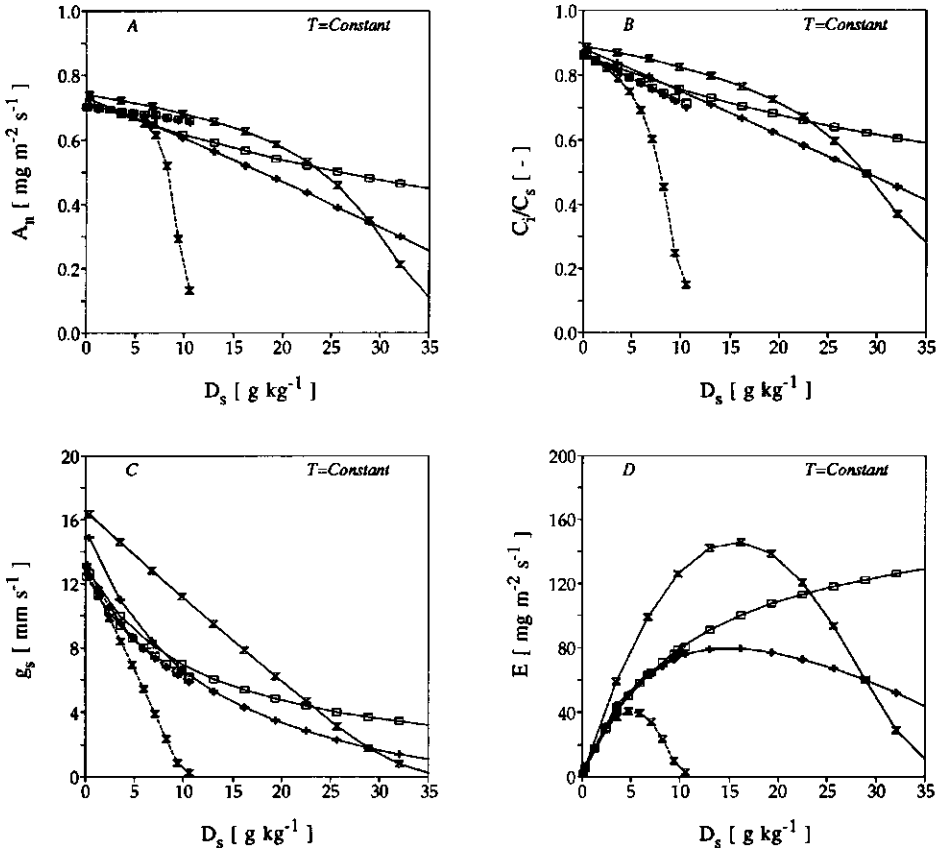


FIGURE 3.3. Modelled net photosynthetic rate ( $A_n$ : A), realized ratio  $C_i/C_s$  (B), epidermal conductance ( $g_s + g_c$ : C) and transpiration ( $E$ : D) as a function of leaf surface specific humidity deficit,  $D_s$ .  $D_s$  was increased by decreasing the air humidity at a leaf temperature of 15 °C and 35 °C (dashed lines and solid lines, respectively). Parameterization of stomatal humidity responses: PP (pluses); KV91 (open squares); B87 (hour glasses).

KV91 and PP result in a similar  $E$  at 15 °C and 35 °C at one value of  $D_s$  (Fig. 3.3D). Given the similar assimilation rates at the two temperatures, it follows that the water use efficiency ( $\text{WUE} = \text{ratio of dry matter production to amount of water used}$ ) is similar at both temperatures. B87 allows a much higher  $E$  at the higher temperature, while  $A_n$  is similar at low  $D_s$ . This points towards a strongly decreasing WUE at higher temperatures in this case.

*Example 2:  $D_s$  is increased by increasing the leaf temperature.*

Results of this example are shown in Fig. 3.4 for  $q_s = 6 \text{ g kg}^{-1}$  (dashed lines) and  $q_s = 18 \text{ g kg}^{-1}$  (solid lines) respectively. In the simulations for  $q_s = 6 \text{ g kg}^{-1}$ ,  $T_1$  varies between 7 and 42 °C, which results in  $D_s$  ranging between 0.2 and 45.5  $\text{g kg}^{-1}$  while  $h_s$  ranges between 0.97 and 0.12. At  $q_s = 18 \text{ g kg}^{-1}$  the respective ranges are from 24 to 45 °C for  $T_1$ ,

from 0.6 to 42.3 g kg<sup>-1</sup> for  $D_s$  and from 0.97 to 0.30 for  $h_s$ . It is noted that  $A_n$  and  $(g_s + g_c)$  are higher for  $q_s = 18$  g kg<sup>-1</sup> than for  $q_s = 6$  g kg<sup>-1</sup> at low values of  $D_s$  because of the lower temperature in the latter case.

In this example, all parameterizations simulate similar relationships between  $D_s$  and the variables shown. They agree rather well in the calculated photosynthetic rates. Furthermore, an almost linear decline of  $C_i/C_s$  is obtained at low  $D_s$ . The decline levels off towards a rather broad minimum. At very high values of  $D_s$ ,  $C_i/C_s$  rises again. According to PP and B87 the minimum  $C_i/C_s$  may be less than 0.5. PP predicts this minimum at higher values of  $D_s$  than do other models (Fig. 3.4B). B87 results in large differences in  $C_i/C_s$  between both values of the humidity, over the entire range of  $D_s$ . The other models predict that such differences will become apparent only if  $D_s > 10 - 15$  g kg<sup>-1</sup> (Fig. 3.4B).

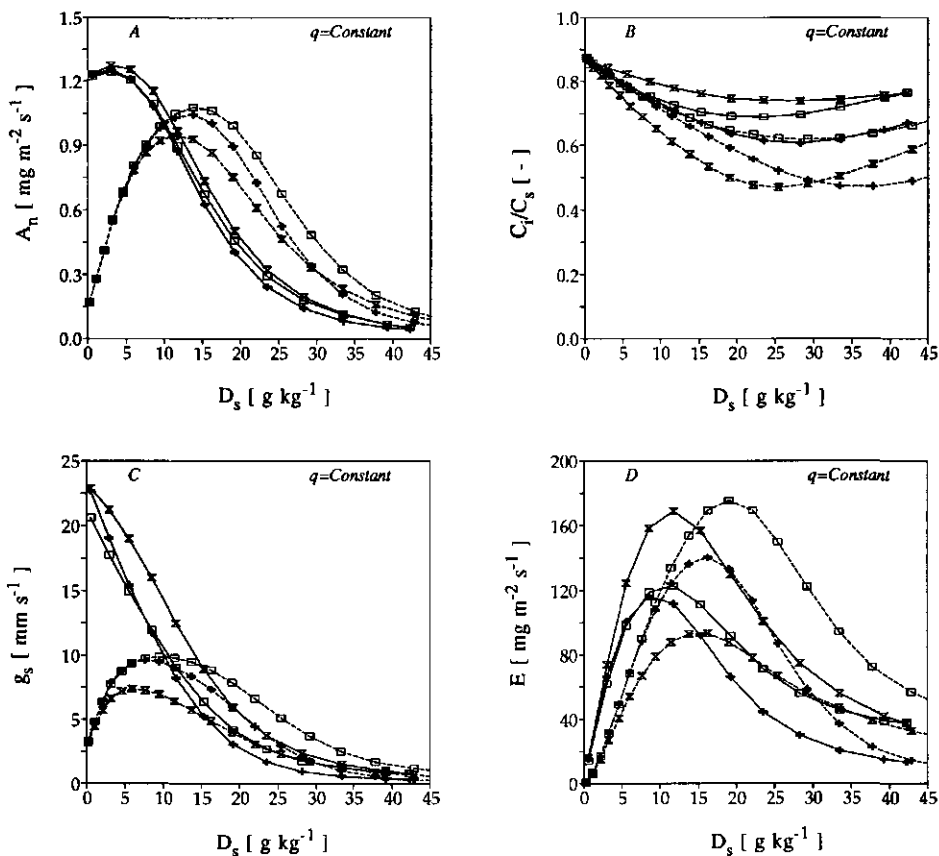


FIGURE 3.4. As in Fig. 3.3, except that  $D_s$  was increased by increasing the leaf temperature at a constant air humidity of 6 and 18 g kg<sup>-1</sup> (dashed lines and solid lines, respectively).



PP and KV91 agree rather well in their simulations of  $(g_s + g_c)$  and  $E$ , up to  $D_s = 10$  to  $15 \text{ g kg}^{-1}$ . At higher  $D_s$ ,  $(g_s + g_c)$  and  $E$  tend to remain higher in the PP simulations. The behaviour of  $(g_s + g_c)$  and  $E$  as predicted by B87 differs from both PP and KV91. Again, the WUE seems to decrease at high temperatures (high values of  $D_s$ ), where the lower photosynthetic rate is linked up with the higher transpiration rate.

### 3.8 Discussion and conclusions

A- $g_s$  models are better suited for use in meteorological research than are models of the Jarvis and Stewart type (JS models; Jarvis, 1976; Stewart, 1988). Unlike JS models, the description of synergistic interactions between stimuli and of stomatal responses to  $\text{CO}_2$  are implicit characteristics of A- $g_s$  models. Thus, A- $g_s$  models are advantageous in particular in predictive studies where  $\text{CO}_2$  is involved, including the present study.

It is doubted whether the problems related to JS models can be solved rigorously. Variations of the  $\text{CO}_2$  concentration in the field are, in general, too low to establish reliable parameters for the response function to  $\text{CO}_2$ . Furthermore, massive amounts of high quality data would be required to derive parameters for additional functions to describe synergistic interactions. Furthermore, because  $\text{CO}_2$  in particular is well-known for its interaction with other responses such as light (Meidner & Mansfield, 1968), the currently available coefficients of the response functions used in JS models are only valid for present-day atmospheric  $\text{CO}_2$  concentration. The changing atmospheric conditions imply that previously determined coefficients probably would have to be re-evaluated on a regular basis. From this argument it follows that the predictive power and future use of JS models may be questioned.

A- $g_s$  models are based on the observed correlation between  $A_n$  and  $g_s$  (Farquhar & Sharkey, 1982; Goudriaan *et al.*, 1985; Collatz *et al.*, 1991). Although these models are also empirical models, it is believed that the observed correlation between  $A_n$  and  $g_s$  indicates a plant strategy, which is of a more fundamental nature. These models can be based on the large record of results from fundamental photosynthesis research. Some of the parameter values appear to be relatively constant among different species, at least among species of one plant class.

The A- $g_s$  model used in the present study is basically that of Goudriaan *et al.* (1985). This model is closely linked up with the micrometeorological research practice. Here, the parameters of this model are tuned to the results of the biochemically based models (for example, Farquhar *et al.*, 1980). The resulting description remains relatively simple, but effective in its simulation of most of the well-known features of photosynthesis.

The photosynthetic rate can be coupled to stomatal behaviour if the difference between the sub-stomatal  $\text{CO}_2$  concentration and that outside the leaf is known. Most convenient is to assume that  $C_i/C_s$  is a constant. However,  $C_i/C_s$  may vary with light intensity,  $\text{CO}_2$  concentration and humidity. Furthermore, the internal  $\text{CO}_2$  concentration used to calculate  $g_s$  from  $A_n$  must be considered as a virtual concentration, which approaches the real concentration only at high light intensities.

The variation of  $C_i/C_s$  with  $D_s$  can be used to mimic stomatal humidity responses. In the present study, the relationship between  $f$ , defined by [3.20], and  $D_s$  is assumed to be linear. Experimental evidence for such relationship will be given in Chapter 4. The cuticular conductance,  $g_c$ , is not ignored. Then, a minimum assimilation rate  $A_{\min}$  can be assumed to occur at  $D_s = D_{\max}$ .  $A_{\min}$  is defined for saturating light intensity. It implies a minimum value of the ratio  $f$ ,  $f_{\min}$ , by which  $C_i/C_s$  is prevented from becoming too low. Once  $C_s$  has been determined, the present parameterization prescribes a simultaneous solution of  $C_i/C_s$  and  $A_n$ , by which iterations to determine this solution (Ball *et al.*, 1987; Collatz *et al.*, 1991) or cumbersome analytical solutions (Leuning, 1990; Collatz *et al.*, 1992) are avoided. In modelling studies, the determination of  $C_s$  will not be a problem.

Two parameters are required:  $D_{\max}$ , which is the value of  $D_s$  where the stomata are closed, and  $f_0$ , which is the extrapolated value of  $f$  at  $D_s=0$ . Here, values of  $D_{\max}$  and  $f_0$  have been estimated from literature. As a first guess  $D_{\max}$  may be taken  $45 \text{ g kg}^{-1}$  for  $C_3$  as well as  $C_4$  crops.  $f_0$  is about 0.85 for  $C_3$  species and 0.5 for  $C_4$  species. The value of  $f_{\min}$  in [3.26] follows from the magnitude of the cuticular conductance and the mesophyll conductance ([3.25]). In practice  $f_{\min}$  may be difficult to determine. Furthermore, its influence becomes only apparent under very extreme conditions, which probably seldom occur. Therefore, the form of [3.26] should be considered as a theoretical tool to explore implications of the present treatments in the extremes. Its possible role for practical purposes should be evaluated by means of experimental data from which  $g_c$  and  $g_m$  can be determined.

The relationship between  $D_s$  and  $C_i/C_s$  which results from the present parameterization is slightly curved. This is consistent with the data reported by Morison & Gifford (1983), although these authors fit a linear curve. It is also consistent with the simulations by Friend (1991), who uses a biochemical model and optimizes  $C_i/C_s$  and  $g_s$ . The present parameterization simulates an increase of  $C_i/C_s$  towards very high values of  $D_s$ . A qualitatively similar result is obtained by parameterizations of others if  $g_c$  is not ignored (Ball *et al.*, 1987; Kim & Verma, 1991). Well-known characteristics of stomatal humidity responses are simulated satisfactorily using the new parameterization. These characteristics include a decrease of transpiration at high values of  $D_s$ . Furthermore the relationship between  $g_s$  and  $D_s$  resembles a hyperbola.

The correlation between the stomatal index ([3.31]) and  $g_s$  (Ball *et al.*, 1987) is not a causal one (Mott & Parkhurst, 1991; Aphalo & Jarvis, 1991). The use of  $D_s$  as the humidity descriptor is preferred because it is related more closely to the true cause of the humidity response, which is evaporation rate. However, if the empirical nature of  $g_s$  models is accepted, the stomatal index could still be useful if it accounts for a generally occurring combined humidity-temperature response (Mott & Parkhurst, 1991; Grantz, 1991). In the present study it has been shown that use of the stomatal index implies an "inconsistent" water use efficiency (WUE). However, it also implies a relatively large transpirational cooling under warm conditions. Both a consistent WUE and a larger cooling to prevent overheating of the leaves could be useful survival strategy of plants, depending on the environmental conditions. More experiments are required to determine which strategy is followed in nature and whether the combined humidity-temperature response implied by the stomatal index actually occurs.

In the present study,  $D_s$  has been used as the descriptor of the humidity response. Recently, Monteith (personal communication; also see Monteith, 1993) proposed to directly use the result by Mott & Parkhurst (1991), that  $g_s$  is related to the transpiration rate  $E$ . He re-analyzed data *at the canopy scale* by scaling  $g_s$  (canopy conductance) by  $g_{\max}$ , denoting a maximum canopy conductance, and  $E$  (canopy transpiration) by  $E_{\max}$ , denoting a maximum transpiration rate. Most of the data he investigated collapsed into one straight line, so that

$$\frac{g_s}{g_{\max}} = 1 - \frac{E}{E_{\max}} \quad [3.32]$$

Introducing [3.32] into the Penman-Monteith equation (Monteith, 1965) yields a quadratic function of  $\lambda E$ , that can be solved analytically. This interesting new approach calls for further research. Fundamental questions related to this approach need to be answered. For example, at what time scale and at what spatial scale can it be used? How should the parameters  $g_{\max}$  and  $E_{\max}$  be interpreted and how can they be determined properly? Also, using the simple linear relation given by [3.32] does not lead to the often observed decrease of  $E$  at high  $D_s$  (Farquhar, 1978; Choudhury & Monteith, 1986). So, how should this feature be taken into account?

## 4

## STOMATAL CONDUCTANCE AND PHOTOSYNTHESIS OF UNSTRESSED GRAPEVINES UNDER SEMI-ARID CONDITIONS

## 4.1 Introduction

In the previous chapter a model for the stomatal conductance,  $g_s$ , was presented. This model is based on the relation between photosynthetic rate,  $A_n$ , and  $g_s$ . To a first approximation, this relation can be written:

$$1.6A_n = g_s(C_s - C_i) \quad [4.1]$$

Thus, a model for  $A_n$  can also serve as a model for  $g_s$ .

However, [4.1] shows that the  $\text{CO}_2$  concentration difference between the air at the leaf surface and the air in the sub-stomatal cavity,  $C_s - C_i$ , must also be known. The ratio  $C_i/C_s$  provides a convenient way of parameterizing  $C_s - C_i$ . While exploring the characteristics of  $C_i/C_s$ , it was argued that  $C_i/C_s$  may decrease almost linearly with specific humidity deficit at the leaf surface,  $D_s$  (Raschke, 1986; Morison, 1987; Friend, 1991). Furthermore, it is slightly influenced by the  $\text{CO}_2$  concentration (Goudriaan *et al.*, 1985; Mott, 1988). These characteristics of  $C_i/C_s$  can be expressed by writing:

$$f = \frac{C_i - \Gamma}{C_s - \Gamma} = f_o \left(1 - \frac{D_s}{D_{\max}}\right) + f_{\min} \left(\frac{D_s}{D_{\max}}\right) \quad [4.2]$$

where  $\Gamma$  is the  $\text{CO}_2$  compensation concentration,  $f_o$  is the value of  $f$  at  $D_s = 0$ , and  $f_{\min}$  is the value of  $f$  at  $D_s = D_{\max}$  ( $D_{\max}$  being the value of  $D_s$  where the stomata are completely closed). The magnitude of  $f_{\min}$  depends on cuticular conductance,  $g_c$ , and mesophyll conductance,  $g_m$ .

The A- $g_s$  model applied in the present study uses [4.2] to complete the model and in the mean time to mimic stomatal humidity responses (see Chapter 3 for a description of the A- $g_s$

model). The resulting relation between  $g_s$  and  $D_s$  resembles a hyperbola, while  $E$  decreases at very high values of  $D_s$ . In the model,  $A_n$  is calculated following Goudriaan *et al.* (1985), but with the model parameters tuned to the biochemical photosynthesis model of Farquhar *et al.* (1980).

The main purpose of this chapter is to provide experimental evidence for [4.1]-[4.2]. It serves as a test of the A- $g_s$  model described in Chapter 3. As in the previous chapter, the A- $g_s$  model is considered at leaf scale. In the next chapter, it will be scaled up to the canopy level in order to include it in the coupled model described in Chapter 2.

The data shown in this chapter were collected at grapevines (*Vitis Vinifera* L. cv. Airen) during the EFEDA pilot study in Spain, June 1991 (Bolle *et al.*, 1993). The semi-arid conditions at the experimental site resulted in a wide range of air temperatures and air humidities. However, thanks to the deep roots of the plants, no evidence of serious drought stress or temperature stress could be observed during the experimental period. Therefore, the collected data provide an excellent basis to test the present A- $g_s$  model and in particular [4.1]-[4.2].

## 4.2 Description of the measurements

### 4.2.1 General

The measurements described here were performed within the framework of the EFEDA pilot study in Spain, June 1991 (EFEDA = ECHIVAL Field Experiment in a Desertification-threatened Area; ECHIVAL = European International Project on Climatic and Hydrological Interactions between the Vegetation, the Atmosphere and the Land Surface). A general description of this experiment can be found in Bolle *et al.* (1993). Here, only the measurements of  $g_s$  and of  $A_n$  are described.

The experimental site was a vineyard near Tomelloso in the Spanish district of Castilla-La Mancha (2°55'48" W, 39°08'30" N, 693 m above sea level). The grapevines in this vineyard (*Vitis Vinifera* L. cv. Airen) were grafted on root-stocks which were placed in a square grid with an average spacing of about 2.5 m. The row orientation was 10° with respect to the North/South axis. The vegetative period of the plants had been delayed somewhat because of ground frost earlier in the season. However, in June they showed a rapid growth. The total ground cover increased from less than 5% on 15 June to about 10% on 25 June. The one sided LAI increased from 0.21 on 14 June to 0.38 on 28 June (Bolle *et al.*, 1993). By the end of June, the fruiting stage had been reached by most of the plants.

Simultaneous measurements of leaf conductance and leaf photosynthesis started on 15 June. These measurements were performed every other day, and on 22 June and 28 June as extra days. Afterwards, the data of 17, 19, 21, 23, 25, 27 and 28 June were selected for further analyses. A (micro)meteorological characterization of these days is presented in Appendix 9.

TABLE 4.1. *Performance of conductance measurements and photosynthesis measurements. Numbers between parentheses apply to the days which were selected for further analyses.*

	<i>Conductance</i>	<i>Photosynthesis</i>
total number of days	9 (7)	9 (7)
frequency of measurements	every two hours	every two hours
number of plants per measurement	2	1
number of sample leaves per plant layer	3-6	5-10
number of sample leaves per plant	12-18	15-25
total number of samples	2317 (1940)	1469 (1265)

On the selected days, cloud cover was usually less than 4/8, except on 19 June and in the afternoon of 21 June (4/8-6/8). No rain was observed during the entire period between 14 and 29 June. The measurements were carried out from sunrise to sunset at intervals of about 2 hours. For each measurement, sample plants were randomly selected with the only restriction being that the two types of measurement were carried out on different plants at any one time. Details such as the frequency of the measurements, the number of selected plants and number of sample leaves per plant are given in Table 4.1. The plants were sampled in layers of 20 cm each. Sample leaves were selected in each layer and classified in terms of height above the ground, age, and light conditions. The characteristics of the sample leaves were judged according to Table 4.2.

TABLE 4.2. *Classification scheme for sample leaves*

<i>Characteristic or Condition</i>	<i>Categories</i>	<i>Code</i>
Age before 20 June	young: small, slack, light green	1
	old: not young	3
Age after 20 June	young: small, slack, light green	1
	normal: not young or old	2
	old: large, rigid, dark green	3
Position/Layer; height above soil surface:	0-20 cm	1
	20-40 cm	2
	40-60 cm	3
	60-80 cm	4
	80-100 cm	5
	>100 cm	6
Light	shaded (by other plant parts)	0
	sunlit	1
	intermediate	2
	cloudy during measurement	3

## 4.2.2 Stomatal conductance measurements

## a) Principle

Stomatal conductance was measured using a dynamic diffusion porometer (Delta-T automatic porometer, Mk3). This instrument has a cup containing a relative humidity sensor. The cup must be clamped onto a leaf surface. Due to the transpiration of the leaf the relative humidity within the cup will rise. The instrument automatically records the transit time,  $\delta t$ , needed for the relative humidity in the cup to rise from a predetermined starting value,  $h_{\text{cycle}}$ , to  $h_{\text{cycle}} + 0.05$ . Hereafter, dry air is automatically pumped into the cup. If a critical value of  $h$  is reached below  $h_{\text{cycle}}$ , the relative humidity is allowed to rise again and the porometer cycle is repeated (see Fig. 4.1).

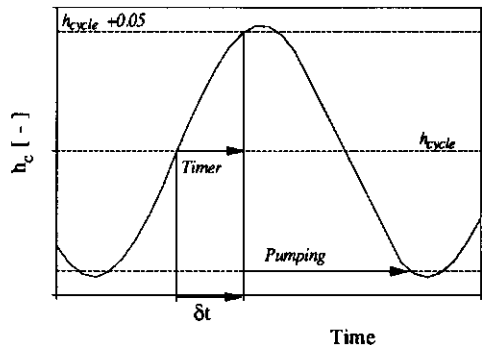
The measured transit time  $\delta t$  will be a measure of the epidermal conductance,  $g_s + g_c$ . At a given leaf temperature, the transpiration rate of leaves which have a low conductance will be relatively small so that the transit time will be longer. The reverse will also be true. It can be shown that a first approximation of the transit time is given by (Monteith *et al.*, 1988)

$$\delta t = \left( \frac{4l}{\pi^2 D_v} + \frac{1}{g_s + g_c} \right) \frac{l \delta h}{(1 - h_{\text{cycle}})} \quad [4.3]$$

in which  $l$  is the distance between the source of water vapour and the place where the humidity is measured,  $D_v$  is the diffusion coefficient for water vapour in air,  $\delta h$  is the rise of the relative humidity within the cup. However, three serious causes for deviations from [4.3] can be identified (Stigter *et al.*, 1973; Monteith *et al.*, 1988).

The first important cause of deviations from [4.3] is a difference between the leaf temperature and the temperature of the air in the porometer cup,  $\Delta T \neq 0$ . This feature can be corrected for by using (Monteith *et al.*, 1988)

FIGURE 4.1. Illustration of the porometer cycle during stomatal conductance measurements.  $h_c$  denotes the relative humidity in the porometer cup. See text for further explanation.



$$\frac{1}{\delta t} \frac{d(\delta t)}{dT} = \frac{-1}{(1 - h_{cycle})} \frac{1}{q^*(T_l)} \frac{dq^*(T_l)}{dT} \quad [4.4]$$

where  $q^*$  is the saturation specific humidity and  $T_l$  leaf temperature. The second major cause of deviations from [4.3] is the finite response time of the humidity sensor. The third cause is adsorption of water vapour by the walls of the porometer cup and by the sensor. Due to the latter feature, the sensitivity of the porometer becomes temperature dependent. Furthermore, it increases the response time of the instrument and leads to deviations from the linear relationship between  $1/(g_s + g_c)$  and  $\delta t$ . Parameters describing adsorption and sensor response time are difficult to obtain or predict and therefore, calibration of the porometer in the field remains necessary (Monteith *et al.*, 1988). More detailed information on the theory and operation of diffusion porometers can be found in, for example, Jarvis (1971), Stigter (1972), Stigter *et al.* (1973), Stigter & Lammers (1974) and Monteith *et al.* (1988).

#### b) Calibration

The actual conductance of the leaf must be calculated by comparing  $\delta t$  with similar calibration times,  $\delta t_c$ . During a calibration, the sensor is clamped onto a calibration plate. The plate is perforated with holes of known geometry. A wetted blotting paper fixed onto the plate, behind the holes, serves as the water vapour source. The conductance of the holes,  $g_{cal}$ , is determined from theory.

During the experiment the porometer was calibrated before each measurement session (one or two plants). The calibration times  $\delta t_c$  were determined for  $g_{cal} = 1/40, 1/130, 1/290, 1/650$  and  $1/1090 \text{ m s}^{-1}$ , respectively. At each conductance, five subsequent readings of  $\delta t_c$  were recorded after stabilization of the transit time. This procedure was performed twice. The observed values of  $\delta t_c$  were corrected later for the cup-to-"leaf" temperature difference following Monteith *et al.* (1988; [4.4]). An average of the five recorded and corrected values of  $\delta t_c$  was taken for further processing.

Next, a linear regression analysis of  $\delta t_c$  versus  $1/g_{cal}$  was carried out in order to determine the calibration curves from which the actual conductance can be calculated. Calibration curves were rejected if  $r^2 < 0.9$ . Of the remaining double calibration curves the one with the highest  $r^2$  was selected to calibrate the actual conductance measurements.

#### c) Leaf conductance measurements and initial processing of the data

In order to perform the actual conductance measurements, the porometer cup was clamped onto the centre of the abaxial surface of the sample leaf. Attempts to measure transit time at the adaxial side of the leaves failed because no significant increase of the relative humidity was observed for at least half a minute. Therefore, it was concluded that the cuticular conductance of the adaxial surface added no significant contribution to the total conductance of the leaf. Thus, the measured conductances may be considered as stomatal conductances and this term will be used here.



For each leaf the transit time,  $\delta t$ , was allowed to stabilize. Usually a stable value was obtained after two or three drying cycles. Then, three subsequent readings of  $\delta t$  were recorded. The temperature in the cup,  $T_c$ , and the cup-to-leaf temperature difference were recorded after the transit time measurements.

The observed values of  $\delta t$  were corrected for the cup-to-leaf temperature difference. Furthermore, they were corrected to the temperature of the calibration ([4.4], Monteith *et al.*, 1988). The average of the three recorded and corrected values of  $\delta t$  was used to calculate the actual stomatal conductance from the predetermined calibration curves. If both calibration curves for a particular measurement series had been rejected, the calibration curve belonging to the previous measurements was taken. Note that this procedure will not lead to serious calibration errors because of the applied temperature corrections.

### 4.2.3 Leaf photosynthesis measurements

#### a) Principle

The leaf photosynthesis measurements were carried out with an open flow differential gas-exchange unit. Such a system samples air from a certain height above the surface. The air stream is divided into two parts. The first part, the reference air, is sent directly to a gas analyzer, where its  $\text{CO}_2$  concentration is determined. The second part, the sample air, is first pumped through a transparent cuvette which is clamped onto a leaf. Hereafter, it is also pumped to the gas analyzer and its  $\text{CO}_2$  concentration is measured. Because of photosynthesis, the air passing over the leaf in the cuvette will be somewhat depleted in  $\text{CO}_2$  so that the  $\text{CO}_2$  concentration of the reference air and that of the sample air becomes different. The photosynthetic rate can be calculated from this concentration difference. As a first approximation (Ball, 1987)

$$A_n = \frac{F(C_r - C_o)}{L_a} \quad [4.5]$$

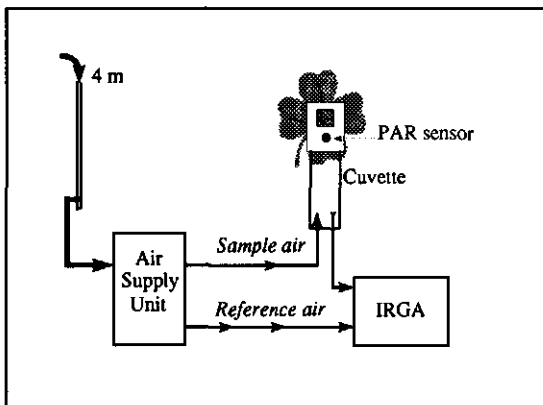


FIGURE 4.2. Schematic representation of the ADC open air gas-exchange system (after Van Kleeff, 1991). See text for explanation.

where  $F$  is the air flow through the chamber,  $C$  is the  $\text{CO}_2$  concentration and  $L_a$  is the leaf area enclosed by the cuvette. The subscripts  $r$  and  $o$  denote "reference" (that is, towards cuvette) and "out" (that is, from cuvette), respectively. [4.5] must be corrected for the influence of transpiration, which dilutes the  $\text{CO}_2$  concentration by adding  $\text{H}_2\text{O}$  to the airstream (Ball, 1987; see also Appendix 11).

A more detailed description on the background and the theory of this type of gas-exchange measurements can be found in Ball (1987).

*b) Equipment*

The gas-exchange unit used in this study is schematically represented in Fig. 4.2. It consists of an Infra Red Gas Analyzer (IRGA; ADC LCA-2), an air supply unit (ADC ASUM-2), and a leaf cuvette which encloses a leaf area of  $2.5 \times 2.5 \text{ cm}^2$ . In the cuvette, the relative humidity and temperature of the sample air is measured. Furthermore, a PAR sensor near the leaf chamber measures the incident PAR outside the cuvette. Air is sampled from a height of about 4 m. The systems pump divides the air stream such that the air flow through the leaf cuvette is about  $7 \text{ ml s}^{-1}$ . The  $\text{CO}_2$  concentrations as determined in the IRGA, the temperature, and relative humidity of the sample air in the cuvette as well as the air flow through the cuvette and the incident PAR are continuously monitored by means of a data logger (ADC DL-2).

*c) Actual photosynthesis measurements*

Before each measurement series (1 plant, see Table 4.1) a reference temperature and a reference humidity were determined with an empty cuvette. These data are required to calculate, amongst other things, transpiration, leaf temperature, stomatal conductance, and internal  $\text{CO}_2$  concentration. Next the cuvette was clamped onto the centre of the sample leaves such that the cuvette was entirely filled. Data were stored on the systems data-logger if the measured difference in  $\text{CO}_2$ -concentration between reference air and sample air had stabilized. A response test showed that stabilization of the concentration difference occurred within 20-30 seconds after enclosing the leaf and that no significant concentration changes occurred until at least 1 minute after stabilization (see Appendix 10 for the results of this response test).

*d) Initial processing and selection of data*

Since the IRGA becomes unreliable if it is exposed to very high temperatures, assimilation data were rejected if the recorded temperature of the air in the cuvette was higher than  $40^\circ\text{C}$ . Furthermore, data were rejected if the average flow through the cuvette was less than  $6.5 \text{ ml s}^{-1}$ . For the retained data,  $A_n$  was calculated using the software provided with the gas-exchange system (Van Kleef, 1991). Apart from the instrumental corrections, this software yields virtually the same results for  $A_n$  as the equations proposed by Ball (1987). The procedure takes into account the influence of transpiration on the flow through the cuvette. For the calculation of  $E$ ,  $g_s$  and  $C_i$ , the equations given by Ball (1987) were used, which take into account the influence of transpiration on the diffusion of  $\text{CO}_2$  (Jarman, 1974; Leuning, 1983). The basic equations related to the gas-exchange calculations are given in Appendix 11. These include the equations used to calculate the leaf's energy balance.

### 4.3 General experimental results

#### 4.3.1 Effects of leaf position and age on $g_s$ and $A_n$

The effects of leaf age and position on  $g_s$  and  $A_n$  were studied using the data of 21 to 28 June. The data of 17 and 19 June were not used here because of the slightly different age classification (see Table 4.2). First, the data were ordered according to light conditions. Those of sunlit leaves and of shaded leaves were selected for further processing (Table 4.2, classification 0 or 1).

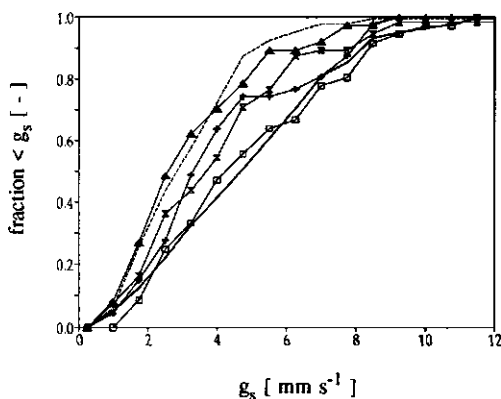
In the analyses presented below, no assumptions were made with respect to the shape of response curves (for example, the light response curve) or data frequency distribution (for example, Gaussian distribution). The Kruskal-Wallis test has been used to test for differences between the populations (Van der Laan, 1982).

##### a) Effect of leaf position

First, the influence of leaf position on  $g_s$  was investigated while retaining the distinction according to leaf age. No significant differences were found between  $g_s$  for leaves of different layers, except in the case of sunlit, normal (age 2) leaves ( $p < 0.05$ ).

The exception was analyzed further because it was suspected that an age difference was involved in reality. That is, in the plants investigated position correlates somewhat with age. This is illustrated in Fig. 4.3. For each layer, the cumulative frequency distribution of  $g_s$  for normal sunlit leaves is shown. Furthermore, the cumulative frequency distribution of sunlit young leaves and of sunlit old leaves are given for all layers together. Statistically, the population of sunlit, normal leaves of the lowest layer (layer 1) can no longer be distinguished from the population of old leaves. Similarly, the population of normal sunlit leaves of the upper layer (layer 4), can no longer be distinguished from the population of young leaves. At the same time, the combined population of sunlit, normal leaves of layer 1 and layer 4 and that of layer 2 and layer 3 cannot be distinguished statistically. It is concluded that the influence of layer number as found for sunlit, normal leaves is an age difference in reality.

FIGURE 4.3. Cumulative frequency distribution of stomatal conductance,  $g_s$ , of: 1) all sunlit old leaves (solid line, unlabelled); 2) all sunlit young leaves (dashed line, unlabelled); 3) normal sunlit leaves in layer 1, layer 2, layer 3 and layer 4 (solid lines with squares, pluses, hourglasses, and triangles, respectively). See text for explanation and Table 4.2 for leaf classification scheme.



No significant influence of position on  $A_n$  was found. A slight indication for such an influence was found in the case of shaded old leaves ( $0.05 < p < 0.1$ ). The leaves in the bottom layer had relatively low assimilation rates, possibly because of dust. Furthermore, a slight indication for a position-related difference was found for sunlit normal leaves ( $0.05 < p < 0.1$ ). As in the case of  $g_s$ , the population characteristics of normal leaves in the upper layer were similar to those of the entire population of young leaves. No such parallel with the  $g_s$  data could be identified in the case of normal sunlit leaves in the lowest layer, possibly because of a compensating effect of dust.

#### b) Effect of age

In order to investigate effects of leaf age, a distinction was no longer made between leaves of different plant layers. Fig. 4.4 shows the cumulative frequency distributions of  $g_s$  for the various leaf classes. The values of the medians are given in the figure caption. For the sunlit leaves the differences between age classes were significant at the 0.1% confidence level while those for shaded leaves were significant at the 5% confidence level. In the latter case, this is, in fact, a difference between old leaves on the one hand and normal and young leaves on the other. The  $g_s$  frequency distributions of the latter age classes cannot be distinguished statistically.

A significant effect of leaf age on  $A_n$  was found for sunlit leaves ( $p < 0.001$ ), but not for shaded leaves. The effect of leaf age on the assimilation rate was further analyzed as follows.

For each age class, the negative exponential curve ([3.12]) was fitted using a non-linear, parametric least square method (Ruckdeschel, 1981). It was assumed that  $R_d = A_{max}/9$  (Van Heemst, 1986) so that only the light use efficiency,  $\epsilon$ , and the asymptotic value of  $A_n$ ,  $A_m$ , remained to be optimized. The parameter values and their 95% confidence limits (calculated following Mead & Curnow, 1983) are given in Table 4.3.

The light response curve of the young leaves deviates considerably from that of old leaves and normal leaves, respectively ( $p < 0.01$ ). The fits for normal leaves and old leaves will

FIGURE 4.4. Cumulative frequency distribution of  $g_s$  for: 1) young shaded leaves (solid line with squares): median =  $1.64 \text{ mm s}^{-1}$ ; 2) normal shaded leaves (solid line, unlabelled): median =  $1.57 \text{ mm s}^{-1}$ ; 3) old shaded leaves (solid line with triangles): median =  $1.94 \text{ mm s}^{-1}$ ; 4) young sunlit leaves (dashed line with squares): median =  $2.82 \text{ mm s}^{-1}$ ; 5) normal sunlit leaves (dashed line, unlabelled): median =  $3.29 \text{ mm s}^{-1}$ ; 6) old sunlit leaves (dashed line with hourglasses): median =  $4.47 \text{ mm s}^{-1}$ .

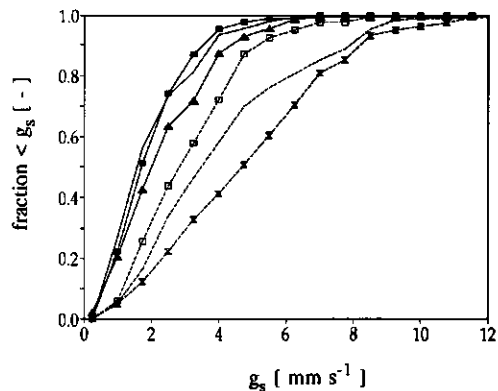


TABLE 4.3. Parameters of the fitted light response curves (see Fig. 4.5). The 95% confidence limits are given between parentheses (lower limit-upper limit; Mead & Curnow, 1983).

Leaf class / age	fitted $A_m$ [ $\text{mg m}^{-2} \text{s}^{-1}$ ]	fitted $\epsilon$ $\text{mg J}^{-1} \text{PAR}$
1. Young	0.484 (0.439-0.535)	0.0069 (0.0056-0.0089)
2. Normal	0.599 (0.578-0.621)	0.0102 (0.0093-0.0113)
3. Old	0.650 (0.608-0.697)	0.0096 (0.0084-0.0130)

yield almost the same assimilation rates, although there is an indication that they are different ( $0.05 < p < 0.1$ ). This difference will be ignored in further analyses and for modelling purposes.

The comparison of the 95% confidence intervals of the fitted parameters (Table 4.3) suggests that the observed population differences are mainly caused by difference at higher light intensities, which is consistent with the earlier result of the parameter free test.

#### c) Discussion and conclusions

The effects of leaf position (layer) on  $g_s$  and on  $A_n$  may be ignored for the plants investigated in this study. Furthermore, there is a significant effect of age on  $g_s$  and on  $A_n$  which comes to full expression only if the leaves are exposed to direct sunlight. On average, younger leaves have lower conductances and lower assimilation rates, although the actual difference in assimilation rate between normal leaves and old leaves is small. Reports of other research have shown that  $g_s$  and  $A_n$  typically show a maximum at intermediate leaf ages. Thus, a decrease is expected if leaves become very old (reviewed by: Field, 1987). The reason that no such evidence of decline was found here might be that all the leaves were relatively young.

#### 4.3.2 Diurnal variation of $g_s$ and $A_n$

The observed diurnal variation of  $g_s$  on 6 days (17, 19, 21, 23, 25, and 27 June) is depicted in Fig. 4.5. The values shown are the averages of at least three single leaf observations (all age classes). The observed diurnal variation of the average  $A_n$ , measured inside the leaf cuvette, is depicted in Fig. 4.6 for the same six days. Again, the average values are calculated from at least three single leaf observations (all age classes).

Neither in the case of  $g_s$ , nor in the case of  $A_n$  was a systematic decrease observed during the experimental period, although the observed  $g_s$  was relatively high on 17 June. The reason for the very high  $g_s$  in the morning of this particular day is not clear. Note that the average has been computed out of data for all age classes, which may cause some of the scatter. It is concluded that the diurnal variation of  $g_s$  and of  $A_n$  is similar on all days. This is consistent with the observation that no significant drought stress occurred during the experimental period.

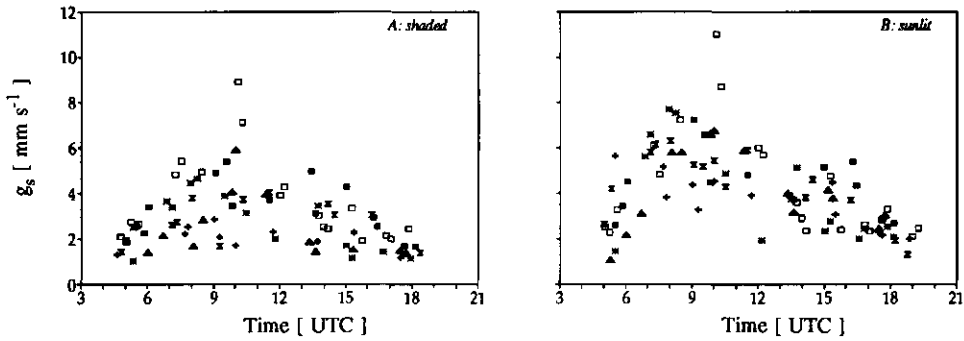


FIGURE 4.5. Diurnal variation of the average stomatal conductance,  $g_s$ , determined by porometer measurements. A) shaded leaves and B) sunlit leaves. Days: 17 June (open squares), 19 June (filled squares), 21 June (hourglasses), 23 June (filled triangles), 25 June (asteriks) and 27 June (pluses).

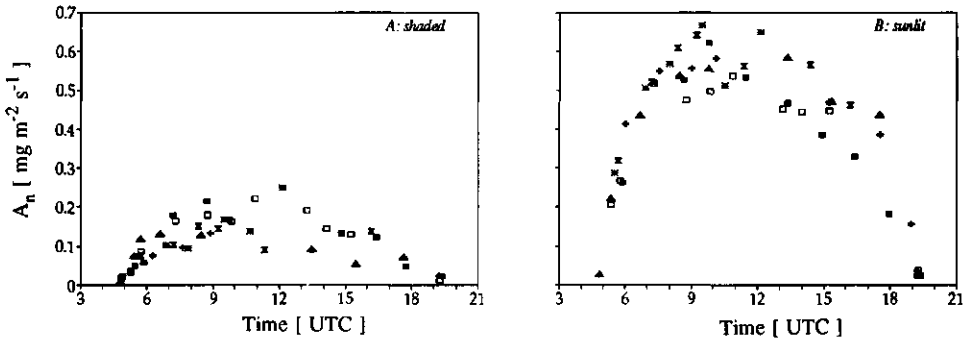


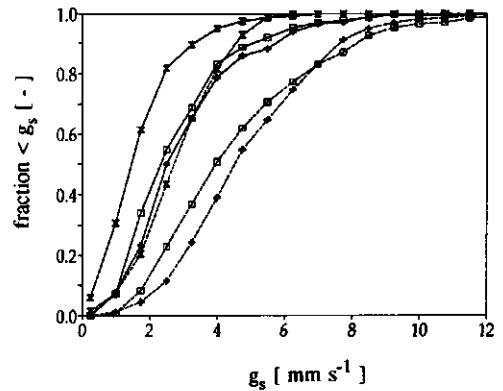
FIGURE 4.6. Diurnal variation of the average photosynthetic rate,  $A_n$ , determined by gas-exchange measurements: A) shaded leaves and B) sunlit leaves. Days: 17 June (open squares), 19 June (filled squares), 21 June (hourglasses), 23 June (filled triangles), 25 June (asteriks) and 27 June (pluses).

The data support the assumption that  $A_n$  and  $g_s$  are correlated. Both  $g_s$  and  $A_n$  of sunlit leaves reach their maximum well before noon. In addition, the maximum in the case of shaded leaves tends to shift towards noon in both cases. However, the decrease in  $A_n$  between 9 UTC and 15 UTC is somewhat more pronounced than the decrease in  $g_s$  during this period of the day.  $A_n$  at 15 UTC is on average about 80% of  $A_n$  at 9 UTC, while  $g_s$  at 15 UTC is on average about 60% of  $g_s$  at 9 UTC. Similar differences between the diurnal variation of  $g_s$  and  $A_n$  for grapevines were reported by Rodrigues *et al.* (1993). It follows that the ratio  $C_i/C_s$  must have decreased because, as a first approximation:

$$\frac{C_i}{C_s} = 1 - \frac{A_n}{C_s g_s} \tag{4.6}$$

where the cuticular conductance and the effect of transpiration have been ignored. The ratio  $C_i/C_s$  is further investigated in Section 4.4.

FIGURE 4.7. Cumulative frequency distribution of  $g_s$  values according to different methods. 1) from gas-exchange, uncorrected: shaded leaves (solid line with hourglasses) and sunlit leaves (dashed line with hourglasses); 2) from porometer: shaded leaves (solid line with pluses) and sunlit leaves (dashed line with pluses); 3) from gas-exchange, corrected: shaded leaves (solid line with squares) and sunlit leaves (dashed line with hourglasses).



### 4.3.3 Comparison between porometer $g_s$ and gas-exchange $g_s$

Fig. 4.7 compares the cumulative frequency distribution of  $g_s$  using the gas-exchange method, to that obtained by the porometer measurements. It can be seen that the gas-exchange method applied in this experiment yields much lower conductance values than does the porometer. The mean ratio of the average  $g_s$  from the porometer measurements and the average  $g_s$  from the gas-exchange measurements is about 1.5, but may vary from somewhat less than 1 to 4 or 5 in exceptional cases. Additional tests and data analyses showed that the empty chamber measurements resulted in a temperature and humidity similar to those measured by the aspirated psychrometer at 1.4 m (Fig. A9.1, C-F), so that the reference temperature and humidity were not a significant error source. Furthermore, a cuvette response test revealed that  $g_s$  may be underestimated by 10-20% because  $g_s$  has not yet reached an equilibrium at the time the measured values are stored (see Appendix 10). The latter effect is far from being sufficient to explain the observed differences. So, the question of where this difference between the methods comes from and how the gas-exchange data should be interpreted remains.

The most important difference between the two methods is that the assimilation measurements are *equilibrium* measurements, whereas the measurements by porometry are *dynamic* measurements. During the gas-exchange measurements the environment of the sample leaf is altered for a much longer period of time, typically half a minute to a minute. In the case of the dynamic porometer measurements the time of enclosure is typically 10 seconds or less.

It is suggested that the longer deprivation of light in the case of the gas-exchange measurements is the main cause of the observed differences. As an illustration of the possible impact of this feature, consider the following example.

Assume that the leaf is placed in complete darkness. The darkness will ultimately cause  $g_s$  to approach zero. Now assume that the response of  $g_s$  to the enclosure may be described by:

$$g_s = g_o \text{EXP}\left(-\frac{t}{\tau}\right) \quad [4.7]$$

which is a general response function to describe responses to step changes without delay (see Thornley, 1976). In [4.7]  $\tau$  is the response time of the stomatal action (s), while  $t$  is the time during which the leaf is enclosed. Furthermore,  $g_o$  is the initial value of  $g_s$ . Taking  $\tau = 60$  seconds, which is typical of stomatal responses to light,  $g_s$  would be reduced to 85% - 92% of its original value in the case of porometry (with  $t = 5 - 10$  s), and to about 37% - 61% in the case of the gas-exchange method (with  $t = 30 - 60$  s).

The measurements with the leaf cuvette require an additional analysis, because the cuvette is transparent at the top but opaque at the bottom. Therefore, a radiation gradient will exist through an enclosed leaf. The light intensity will be at a minimum at the bottom side, near the abaxial surface of the leaf. For PAR, the transmissivity of the top of the cuvette may be taken 0.85 (Van Kleef, 1991). Assuming a leaf reflectance to PAR of 0.1, a leaf transmittance of 0.1, so that the leaf absorptance = 0.8 (Goudriaan, 1977), the PAR intensity felt by the stomata (neglecting contributions from reflection by the bottom of the cuvette) will on average be about  $0.85 \cdot 0.1 = 0.085$  times PAR intensity measured outside the cuvette. Such a reduction in light intensity is enough to cause a significant stomatal response, assuming that they possess independent light receptors (see Section 3.3.3). Note that the assumption of independent light receptors in the stomata is *not* in contradiction with a possible *correlation* between  $A_n$  and  $g_s$  under *natural* circumstances.

Now the important question arises as to how the change in light intensity influences the quality of the assimilation measurements. The photosynthetic apparatus is distributed more or less throughout the leaf. The amount of radiation absorbed by the leaf tissue will on average be  $0.85 \cdot 0.8 = 0.68$  times the outside intensity of PAR if the leaf is enclosed by the cuvette. Therefore, photosynthetic rate can still be determined over a wide range of light intensities, in fact, up to saturating light intensities in direct sunlight. Hence, the photosynthetic characteristics, such as  $\epsilon_o$ ,  $A_{max}$ , can still be established. If desired, the reduction in light intensity by the cuvette can be corrected for using the obtained light response characteristics.

Note that effects of the reduced light intensity on  $g_s$  may be compensated somewhat because of the increased humidity and a reduced  $\text{CO}_2$  concentration in the cuvette. The latter feature may theoretically reduce  $A_n$  further. However, the  $\text{CO}_2$  effect on  $A_n$  is expected to have a far larger time constant than the effect on the stomata, because of the  $\text{CO}_2$ -pool in the leaf tissue. This assumption is confirmed by the response test of the cuvette, which showed no reduction in  $A_n$  up to at least one minute after enclosure of the leaf (Appendix 10).

The conclusion is that the stomata may be deprived of light both in the porometer cup and also in the leaf cuvette of the type used here. This alteration of light intensity reduces the measured  $g_s$  especially in the case of gas-exchange measurements, because these are equilibrium measurements. Fortunately,  $A_n$  is much less affected, and the reduction in light



intensity can be corrected for. However, the best solution is to use a cuvette which has also a transparent bottom. This should improve the quality of the  $g_s$  data as well as that of the  $A_n$  data.

#### 4.3.4 Combining results of porometer and gas-exchange measurements

In the previous section the reliability of the  $g_s$  data obtained by the gas-exchange measurements was questioned. This implies that the values of  $C_i/C_s$  derived from the combination of the  $A_n$  and  $g_s$  ([4.6]) would also be unreliable if  $g_s$  data from the gas-exchange measurements are used. Therefore,  $g_s$  from the porometer is combined with  $A_n$  from the gas-exchange measurements to derive  $C_i/C_s$ .

The analysis in Section 4.3.3 shows that it may be assumed that:

1. the porometer yields the correct values of  $g_s$ , where "correct" should be interpreted as " $g_s$  for leaves in their unaltered environment,"
2. the assimilation characteristics of the leaves can reliably be determined from the gas-exchange measurements.

In addition, further analysis of the data showed that:

3.  $g_s$  from the gas-exchange measurements shows an essential correlation with  $g_s$  from porometry (for instance,  $g_s$  for sunlit leaves is higher than that of shaded leaves).

Therefore, the results of the two methods were combined as follows. First, for both methods and per measurement series (1 or 2 plants at a time) the average  $g_s$  was calculated for sunlit leaves and for shaded leaves. At least three observations were used to determine the averages. The ratio of the porometer value and of the gas-exchange value was then determined. New single leaf  $g_s$  values for gas-exchange measurements were now obtained by multiplying the uncorrected values with this ratio, thereby retaining the distinction between shaded and sunlit leaves. This method leads to averages which equal the averages obtained with the porometer, but leaves intact most of the variation between individual leaves. From a comparison between the cumulative frequency distributions it can be seen that the corrected  $g_s$  values from the gas-exchange measurements are now much more similar to those of the porometer (Fig. 4.7). This indicates that the method can be applied with reasonable confidence.

$A_n$  and the leaf energy balance were also corrected in accordance with the new value of  $g_s$  and with the environmental conditions outside the cuvette. This was done as follows.

A light response curve was established from observations of  $A_n$  and PAR. The characteristics of this curve were applied to recalculate the individual results as if they were obtained outside the cuvette. Finally, the corrected  $A_n$  and  $g_s$  were combined to yield derived results, including  $C_i$  and  $C_s$ .  $C_a$  was taken  $325 \mu\text{mol mol}^{-1}$ , which is close to the average measured  $\text{CO}_2$  concentration of the reference air. Furthermore, leaf boundary layer conductance  $g_{bc}$ ,  $g_{bv}$  or  $g_{bh}$ , was calculated using the measured wind speed at 1.4 m (Fig. A9.1, A-B), and a leaf width of  $W_l = 0.075 \text{ m}$  ([3.6]). The energy balance of the leaves was also recalculated in accordance with the corrected values. The equations used are given Appendix 11.

## 4.4 Parameters in the A-g<sub>s</sub> model

### 4.4.1 General

The assimilation characteristics of the grapevines and their temperature dependencies were determined using the g<sub>s</sub> and A<sub>n</sub> data of 17, 21, 25 and 28 June. The data were divided into classes of similar leaf temperatures, using intervals of 3 °C between 13 °C and 40 °C. The negative exponential curve ([3.12]) was fitted in each of these temperature intervals by means of a parametric least-square method (Ruckdeschel, 1981). During these analyses, R<sub>d</sub> was prescribed as R<sub>d</sub> = A<sub>m</sub>/9 (Van Heemst, 1986). The resulting parameter values were assumed to be valid at the average leaf temperature of the respective intervals.

The analyses presented below were performed for normal and old leaves, taken as one population. This will not cause serious errors because the photosynthesis characteristics of old and normal leaves are similar, and because g<sub>s</sub> data are only taken as individual values, not as averages.

### 4.4.2 Initial quantum use efficiency

The resulting initial quantum use efficiencies,  $\epsilon$ , are shown as a function of temperature in Fig. 4.8. It should be born in mind that the optimization of  $\epsilon$  will be very dependent on the quality of the A<sub>n</sub> measurements at low light intensity. Here, the measurements are generally less reliable than at high light intensity, because only a small difference in CO<sub>2</sub> concentration will be measured inside the leaf cuvette. The optimized values are compared to the theoretical values, given by [3.10], using  $\epsilon_0 = 0.017 \text{ mg J}^{-1} \text{ PAR}$ , C<sub>s</sub> = 325  $\mu\text{mol mol}^{-1}$ , and with  $\Gamma$  calculated as described in Appendix 8. Furthermore, the average values for C<sub>3</sub> plants, as reported by Ehleringer & Björkman (1977) are plotted. Two clear outliers can be distinguished, one at 17.6 °C and one at 38.2 °C. The high value of  $\epsilon$  at 17.6 °C is probably caused by the fact that relatively little data were available in this interval. At 38.2 °C, the optimized value of  $\epsilon$  seems too low and is accompanied by a rather high value of A<sub>m</sub> (see below) and the percentage of variance explained by the optimized model is relatively low:

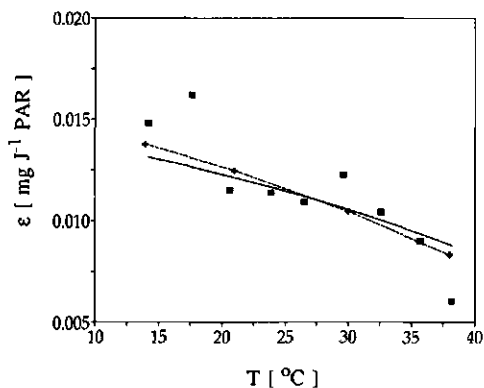


FIGURE 4.8. Initial quantum use efficiency,  $\epsilon$ , as a function of temperature, T: 1) from optimization of light response curves (squares); 2) data of Ehleringer & Björkman (1977) (dashed line with pluses); 3) according to present parameterization ([3.10], Goudriaan et al., 1985) (solid line).

60% as compared to 77% or more in each of the other temperature intervals. Again, this may be due to the fact that in this temperature interval only a few data were taken at low light intensities, which makes the estimate of  $\epsilon$  unreliable. Furthermore, a large scatter was found near high light intensities. This may be caused by the high temperature at which the observations were made, so that the IRGA was less reliable.

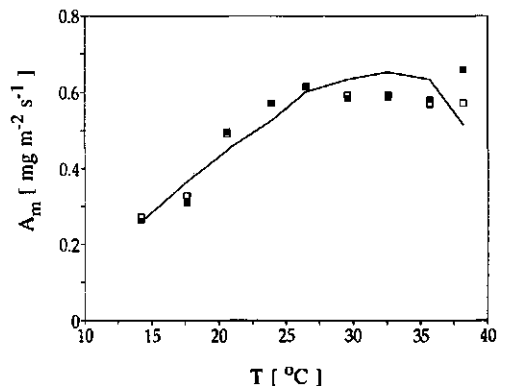
From the evidence presented above it can be concluded that the theoretical temperature dependence is in reasonable agreement with the values found by optimization ( $r^2=0.65$  and slope=1.05 with forced zero intercept [n=9]; without outliers:  $r^2=0.73$  and slope=1.03 with forced zero intercept [n=7]). Furthermore, is quite close to the observations from the controlled laboratory experiments by Ehleringer and Björkman (1977). Therefore, the theoretical relationship will be used in the further analyses of the data.

#### 4.4.3 Photosynthetic rate at optimum light intensity, $A_m$

The optimized values of  $A_m$  are shown as a function of temperature in Fig. 4.9. Two optimization procedures are compared. In the first optimization procedure both  $A_m$  and  $\epsilon$  were found by optimization, as described above (solid squares). In the second one  $\epsilon$  was calculated according to [3.10], with the values for  $\epsilon_0$  and  $C_s$  given above (open squares), so that only one free parameter remained to be optimized. It can be seen that the two procedures yield only slightly different values for  $A_m$ . At 38.2 °C  $A_m$  seems to have improved by prescribing  $\epsilon$ . The difference in the percentage of explained variance for the two optimization procedures was within 0.6% except at 17.6 °C and at 38.2 °C. The solid line shown in Fig. 4.9 results from a parameterization of  $g_m$  and  $A_{m,max}$  and is discussed in Section 4.4.5.

The broad temperature optimum of  $A_m$  for the grapevines is typical of  $C_3$  plants at the current atmospheric  $CO_2$  concentration (Berry & Raison, 1982). However, the optimum occurs at rather high temperatures, which may indicate an adaptation to warm environments. The results for  $A_m$  confirm that the model for  $\epsilon$  can fairly safely be used in the case of the grapevines investigated here.

FIGURE 4.9. Photosynthetic rate at saturating light intensities,  $A_m$ , as a function of temperature,  $T$ . 1)  $A_m$  by optimization of the light response curves for  $A_m$  as well as for  $\epsilon$  (solid squares); 2)  $A_m$  by optimization of light response curves with prescription of  $\epsilon$  according to [3.10] (open squares); 3) from a parameterization of  $g_m$  (see Section 4.4.5 and Fig. 4.11) and  $A_{m,max}$ , using [3.13] with  $A_{m,max}(@25)=2.2 \text{ mg m}^{-2} \text{ s}^{-1}$ ,  $T_1=15 \text{ °C}$  and  $T_2=42 \text{ °C}$  (solid line).



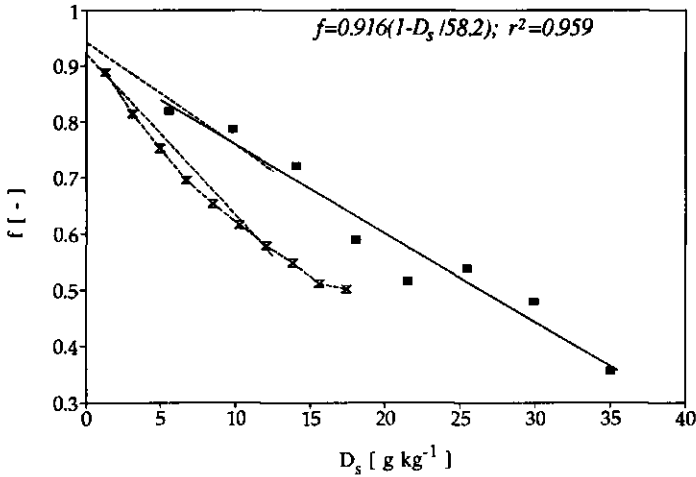


FIGURE 4.10. The ratio  $f$  as a function of specific humidity deficit at the leaf surface,  $D_s$ . 1) from present data set (data: solid squares; linear regression fit: solid line); 2) recalculated from Morison & Gifford (1983) for observations at two  $C_3$  species (dashed lines); 3) recalculated from model results by Friend (1991) (dashed line with hourglasses).

#### 4.4.4 The ratio $f$ as a function of specific humidity deficit, $D_s$

In order to determine the ratio  $f$  ([4.2]), the data of  $A_n$  and  $g_s$  from the gas-exchange measurements were recalculated using the porometer measurements, as described in Section 4.3.3. Next, the data were distinguished according to  $D_s$ , using intervals of  $4 \text{ g kg}^{-1}$  for values of  $D_s$  between 4 and  $32 \text{ g kg}^{-1}$ . An additional class was created in which  $D_s > 32 \text{ g kg}^{-1}$ . In each class the slope of  $A_n$  versus  $g_s$  was determined by linear regression of the individual leaf data. The regression line must originate between  $(g_c, -R_d)$  and  $(g_c, +A_{\min})$  ([3.27] and [3.28]). However, due to the large scatter and the relatively large errors in low values of  $A_n$  and  $g_s$ , this origin cannot be estimated with satisfactory accuracy. Therefore, the regression line was forced through  $A_n=0$  and  $g_s=0$ , assuming  $g_c=0 \text{ mm s}^{-1}$ . The latter assumption implies that  $A_{\min}$  ([3.27]) and  $f_{\min}$  ([3.26]) are both taken equal to zero.

For each  $D_s$  class, the virtual internal  $\text{CO}_2$  concentration,  $C_{i,\text{vir}}$ , was calculated from the slope of the regression lines, following Goudriaan & Van Laar (1978) with minor adaptations (also see Section 4.4.3). Correlation coefficients ranged from 0.5 at low values of  $D_s$  up to 0.84 at high values of  $D_s$ . Note that better correlations could have been obtained by not forcing the regression line through  $(g_s=0, A_n=0)$  and that  $g_s$  values had to be corrected afterwards. Therefore, it was concluded that  $A_n$  and  $g_s$  were well correlated.  $C_{i,\text{vir}}$  as obtained from the regression analysis was first corrected for the influence of transpiration on the  $\text{CO}_2$  diffusion. Finally,  $f$  ([3.20]) was calculated using  $\Gamma$  at the average leaf temperature in each class (see also Appendix 8). Fig. 4.10 depicts  $f$  as a function of the average  $D_s$  of each class. It shows

that  $f$  is linearly related to  $D_s$  with  $f=0.916(1 - D_s/58.2)$  ( $r^2=0.959$ ). Thus, according to the present data  $f_0$  is 0.916 and  $D_{max} \approx 60 \text{ g kg}^{-1}$  (see also Section 4.4.4). This value of  $D_{max}$  is at the higher end of the range given by Choudhury & Monteith (1986) for  $C_3$  crops. Again, this can be interpreted as an adaptation to warm, dry environments.

Fig. 4.10 also depicts the relation between  $f$  and  $D_s$  as reported by Morison & Gifford (1983) for two other  $C_3$  species. In a recalculation of their  $C_i/C_s$  to the values of  $f$  shown in Fig. 4.10,  $\Gamma$  was assumed  $45 \mu\text{mol mol}^{-1}$  ( $T_1 = 25^\circ\text{C}$ ) and  $C_s = 340 \mu\text{mol mol}^{-1}$ . Some model results by Friend (1991) are also given. This author used a biochemical model for photosynthesis which optimizes  $C_i/C_s$  and  $g_m$  for a given set of environmental conditions. Again,  $f$  has been recalculated from  $C_i/C_s$  taking  $\Gamma=45 \mu\text{mol mol}^{-1}$  and  $C_s=340 \mu\text{mol mol}^{-1}$ . It is seen that his model predicts an almost linear decrease of  $f$  with  $D_s$ , which deflects somewhat at higher  $D_s$ , where  $A_n$  decreases. Apart from species specific differences, the present results are consistent with the earlier results of Morison & Gifford (1983) and of Friend (1991). However, they extend over a much wider range of  $D_s$  values.

#### 4.4.5 Mesophyll conductance, $g_m$ and maximum photosynthetic rate, $A_{m,max}$

The most convenient method to determine  $g_m$  is to assume that the internal  $\text{CO}_2$  concentration at full light intensity is in the quasi linear part of the  $\text{CO}_2$  response curve. In this case,  $g_m$  can be determined from  $A_m$  and  $C_{i,vir}$  using [3.11]. However, if  $C_{i,vir}$  and  $A_m$  are outside the quasi linear region of the  $\text{CO}_2$  response curve,  $g_m$  will be underestimated. An alternative in the context of the present model is to rewrite [3.13] which shows that  $g_m$  is given by:

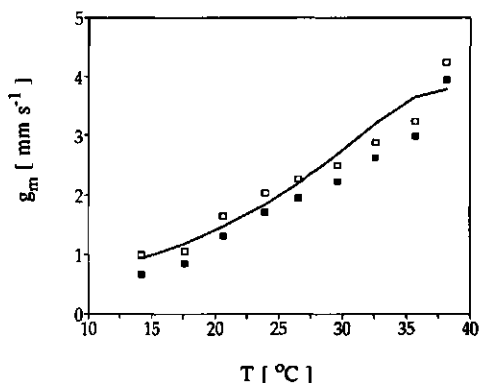
$$g_m = \frac{A_{m,max} \ln\left(1 - \frac{A_m}{A_{m,max}}\right)}{C_i - \Gamma} \quad [4.8]$$

When using [4.8],  $A_{m,max}$  has to be known.

Because the  $C_i$  response curve of the grapevines of the present study was unknown, the following procedure was established to determine  $g_m$ .  $C_{i,vir}$  was calculated using the relationship between  $f$  and  $D_s$ , from the average value of  $D_s$  in each temperature class (Fig. 4.10). Now,  $g_m$  was calculated for each temperature interval according to [3.11], using the optimized values of  $A_m$  with prescribed  $\epsilon$  (see Section 4.4.3, Fig. 4.9). These first estimates are shown in Fig. 4.11 as the solid squares.

Next, the temperature response function for  $g_m$ , given by [3.15] was fitted on the first estimates of  $g_m$ . The response function was used with  $Q_{10}=2$  (see Appendix 8), but the characteristic temperatures  $T_1$  and  $T_2$  were adjusted to reflect an adaptation of the grapevines to higher temperatures (see Section 4.4.3). Using this response function for  $g_m$ , the temperature response function for  $A_{m,max}$  was adjusted so that  $A_m$  as calculated with [3.13] resembled the optimized values  $A_m$  as closely as possible. Hereby,  $A_{m,max}(@25)$  was taken as  $2.2 \text{ mg m}^{-2} \text{ s}^{-1}$  and  $Q_{10}=2$ , which are "standard" values for  $C_3$  plants (see Table 4.2). Using

FIGURE 4.11. Mesophyll conductance,  $g_m$ , as a function of temperature,  $T$ . 1) values derived from photosynthesis data using [3.13], that is, not corrected for nonlinearity of the  $C_i$  response curve (solid squares); 2) as for 1), but corrected for the nonlinearity of the  $C_i$  response curve, using [4.8] (open squares); 3) parameterization using [3.15] for  $g_m$  and  $A_{m,max}$  with  $g_m(@25) = 2.0 \text{ mm s}^{-1}$ ,  $T_1 = 0^\circ\text{C}$  and  $T_2 = 42^\circ\text{C}$  (solid line) and  $A_{m,max}(@25) = 2.2 \text{ mg m}^{-2} \text{ s}^{-1}$ ,  $T_1 = 15^\circ\text{C}$ ,  $T_2 = 42^\circ\text{C}$ .



the optimized temperature function for  $A_{m,max}$ , new values for  $g_m$  can be calculated, but this time from [4.8]. These values will yield a slightly different temperature response function for  $g_m$ , etc.. The final estimates and temperature dependences for  $g_m$  are also depicted in Fig. 4.11 (the results for  $A_{m,max}$  are given in the figure caption). It can be seen that the final values of  $g_m$  are slightly above the values according to [3.11]. The final result for  $A_m$  which is calculated from the parameterizations of  $g_m$  and  $A_{m,max}$ , is shown as the solid line in Fig. 4.9.

#### 4.4.6 Summary of the parameter values

Table 4.4 summarizes the final results for the different parameters and their temperature responses for the grapevines under investigation. The A- $g_s$  model described in Chapter 3 is tested in the next section, using these parameter values.

TABLE 4.4. Parameters in the A- $g_s$  model, described in Chapter 3, derived from the present data for *Vitis Vinifera L. cv Airen*. Values at 25 °C are without accounting for inhibition (see Appendix 8).

	Parameter (X)	X(@25)	Q <sub>10</sub>	T <sub>1</sub> [°C]	T <sub>2</sub> [°C]
C <sub>3</sub>	$\epsilon_o$ [mg J <sup>-1</sup> PAR]	0.017	-	-	-
	$\Gamma$ [ $\mu\text{mol mol}^{-1}$ ]	45	1.5	-	-
	$g_m$ [mm s <sup>-1</sup> ]	2.0	2.0	0	42
	$A_{m,max}$ [mg m <sup>-2</sup> s <sup>-1</sup> ]	2.2	2.0	15	42
	$D_{max}$ [g kg <sup>-1</sup> ]	58.2	-	-	-
	$f_o$	0.916	-	-	-
	$g_c$ [mm s <sup>-1</sup> ]	0.0	-	-	-

## 4.5 Validation of the A- $g_s$ model

### 4.5.1 Introductory remarks

In this section, the A- $g_s$  model is tested. The model tests consist of two parts. The first part is a self-consistency test for the days from which the data were drawn in order to derive the model parameters (17, 21, 25, and 28 June, called set A). The second part is a test for three independent days (19, 23, and 27 June, called set B). The results for set A and set B will be presented together.  $A_n$  and  $g_s$  are presented as follows.

First, the model performance for individual leaves is shown. The test-leaves are all of age classes normal (2) and old (3) (Table 4.2). The photosynthetic rate is calculated for the conditions *inside the leaf cuvette*. Hence, it is a *direct* test of the model.  $g_s$  will be tested for the conditions *outside* the leaf cuvette, using the corrected observations from the gas-exchange measurements (Section 4.4.3). Therefore, this is an *indirect* test.

Ultimately, the model must be scaled up to the canopy level. Then, the averages of  $A_n$  and  $g_s$  as well as the diurnal variation of these averages become more important, and therefore these will be presented next. The averages presented are the mean of at least three individual observations. Again,  $A_n$  is calculated for the conditions inside the leaf cuvette.  $g_s$  is calculated for the conditions in the natural leaf environment and tested against the porometer averages. Therefore, the test of  $A_n$  as well as that of  $g_s$  is a *direct* test of the model.

### 4.5.2 Photosynthetic rate, $A_n$

Fig. 4.12 depicts the calculated  $A_n$  versus the observed  $A_n$  for the days of set A and of set B. Fig. 4.13 depicts the calculated and observed averages of  $A_n$ . The slope and the correlation coefficients from the linear regression analysis are given in the figure captions. In all cases, the photosynthetic rate is reasonably well simulated. Due to the fact that the derived  $A_n$  (Section 4.4.5) is an *average*,  $A_n$  for the individual leaves will level off at higher values. This feature is visible in both plots for the individual leaves. As may be expected, it has virtually disappeared in the case of the average photosynthetic rates.

The diurnal variation of the average  $A_n$  is depicted in Fig. 4.14 (A to D for set A and E to G for set B). The diurnal variation is reasonably well simulated in most cases. The performance is somewhat less on 19 June, where  $A_n$  is systematically overestimated during the second half of the day. Furthermore, little can be said for 27 June, where data are available only to around noon.

### 4.5.3 Stomatal conductance, $g_s$

The model performance with respect to  $g_s$  is shown in Fig. 4.15 for the individual leaves, in Fig. 4.16 for the averages, and in Fig. 4.17 for the diurnal variations. The performance is

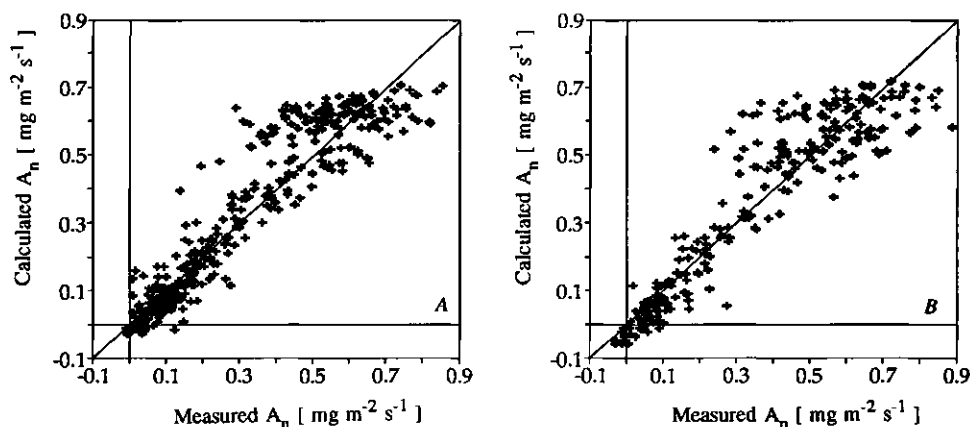


FIGURE 4.12. Scatter plot of calculated  $A_n$  versus observed  $A_n$  inside the leaf cuvette: values for single leaves, set A (dependent days, left) and set B (independent days, right). Linear regression analysis with forced zero intercept: Set A:  $y=1.01x$ ,  $r^2=0.878$ ; Set B:  $y=0.98x$ ,  $r^2=0.864$ .

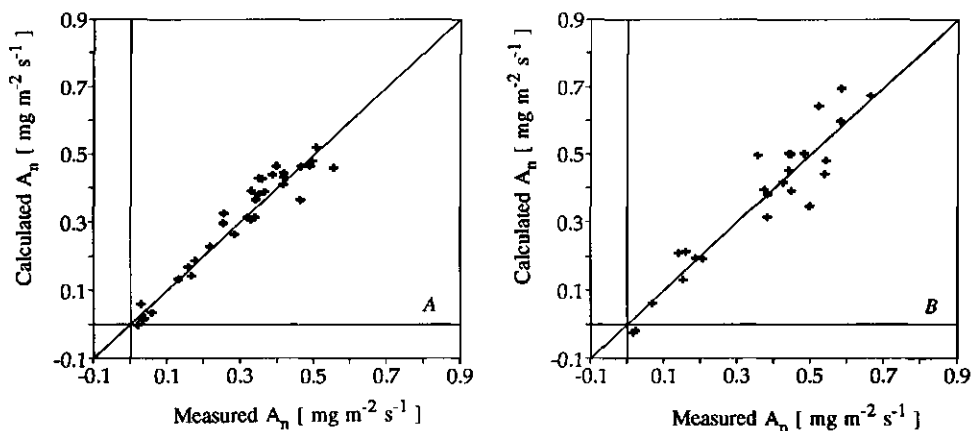


FIGURE 4.13. As in Fig. 4.12, but for averaged values of  $A_n$ . Set A:  $y=1.01x$ ,  $r^2=0.931$ ; Set B:  $y=1.02x$ ,  $r^2=0.890$ .

much less than for  $A_n$ . This was to be expected because of the extra step in the model, the relation of  $f$  versus  $D_s$ , and because these results partly rely on the reliability of the method for combining the porometer data with the gas-exchange data. Nevertheless, the correlation coefficients and slopes for the averages, given in the figure captions, are similar to the performances of models of the Jarvis-Stewart type (for example, Winkel & Rambal, 1990; see also Stewart, 1988).



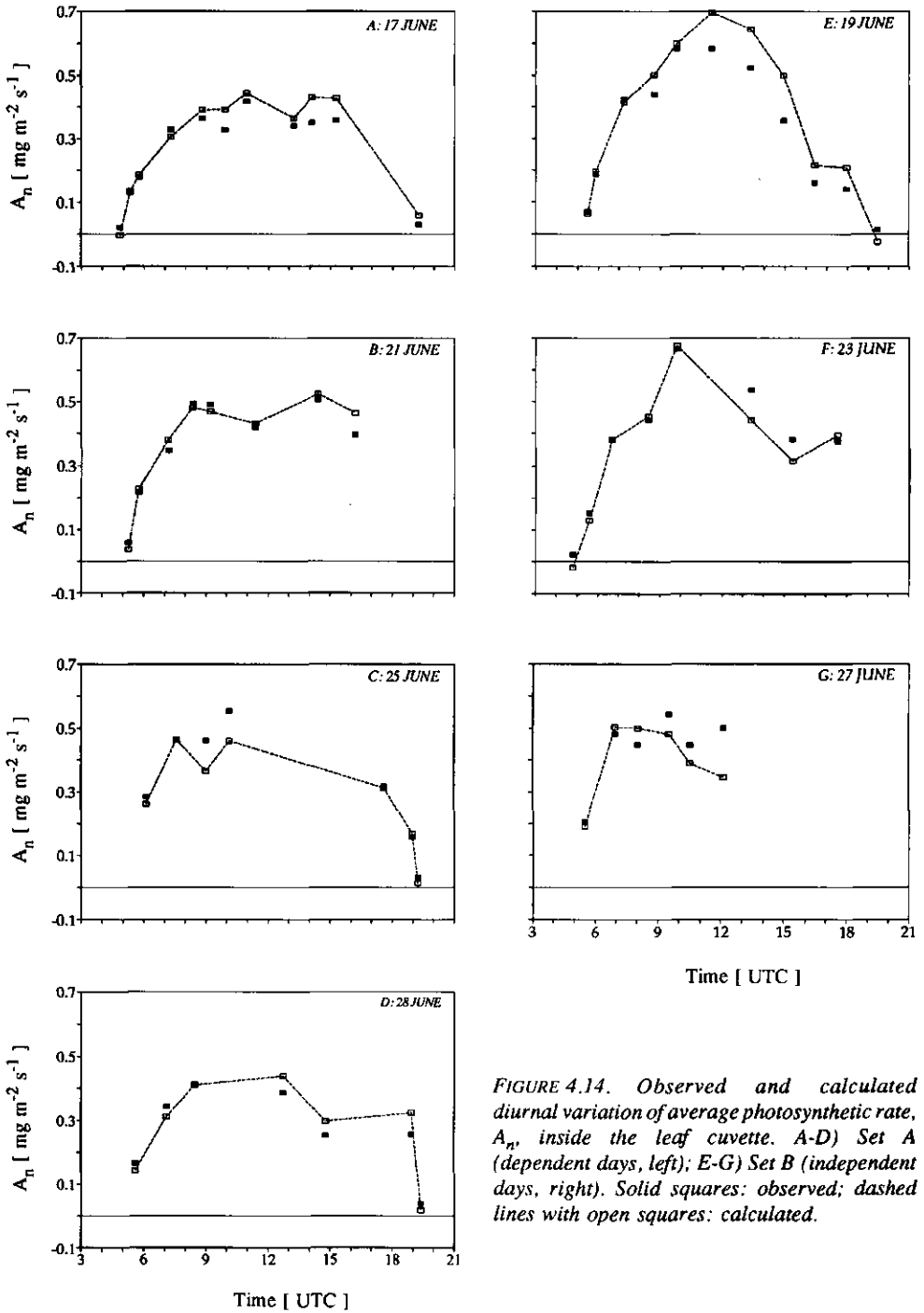


FIGURE 4.14. Observed and calculated diurnal variation of average photosynthetic rate,  $A_n$ , inside the leaf cuvette. A-D) Set A (dependent days, left); E-G) Set B (independent days, right). Solid squares: observed; dashed lines with open squares: calculated.

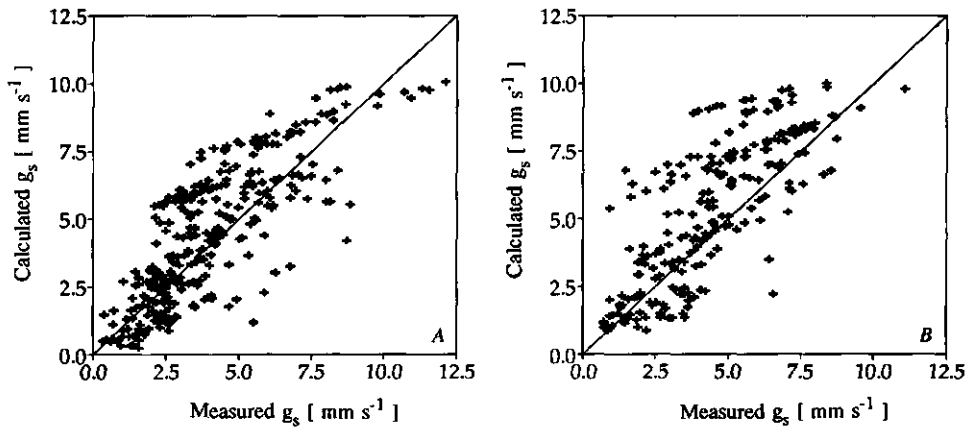


FIGURE 4.15. Scatter plot of calculated stomatal conductance,  $g_s$ , versus observed  $g_s$ : single leaf values. A) dependent days (left) and B) independent days (right). Linear regression with forced zero intercept: Set A:  $y=1.06x$ ,  $r^2=0.619$ ; Set B:  $y=1.15x$ ,  $r^2=0.585$ .

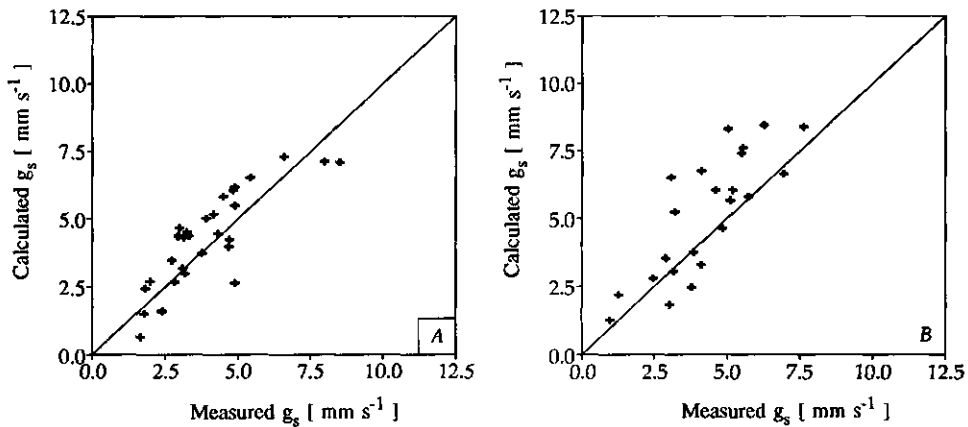


FIGURE 4.16. Scatter plot of calculated stomatal conductance,  $g_s$ , versus observed  $g_s$ : averaged values. A) dependent days (left) and B) independent days (right). Linear regression with forced zero intercept: Set A:  $y=1.04x$ ,  $r^2=0.667$ ; Set B:  $y=1.18x$ ,  $r^2=0.653$ .

There is a clear core of observations that are rather well simulated both for the independent and the dependent days. Elsewhere, there are clusters of data for which the simulation is much worse. The formation of the clusters arises partly because the photosynthetic rate is limited to a maximum value which might be too low for some individual leaves. However, this does not explain the fact that  $g_s$  is mostly *overestimated* in these clusters of data. It is noted that, interestingly, a similar overestimation is visible from modelling studies by authors who used a JS model, for example, Stewart (1988, coniferous forest), and Winkel & Rambal

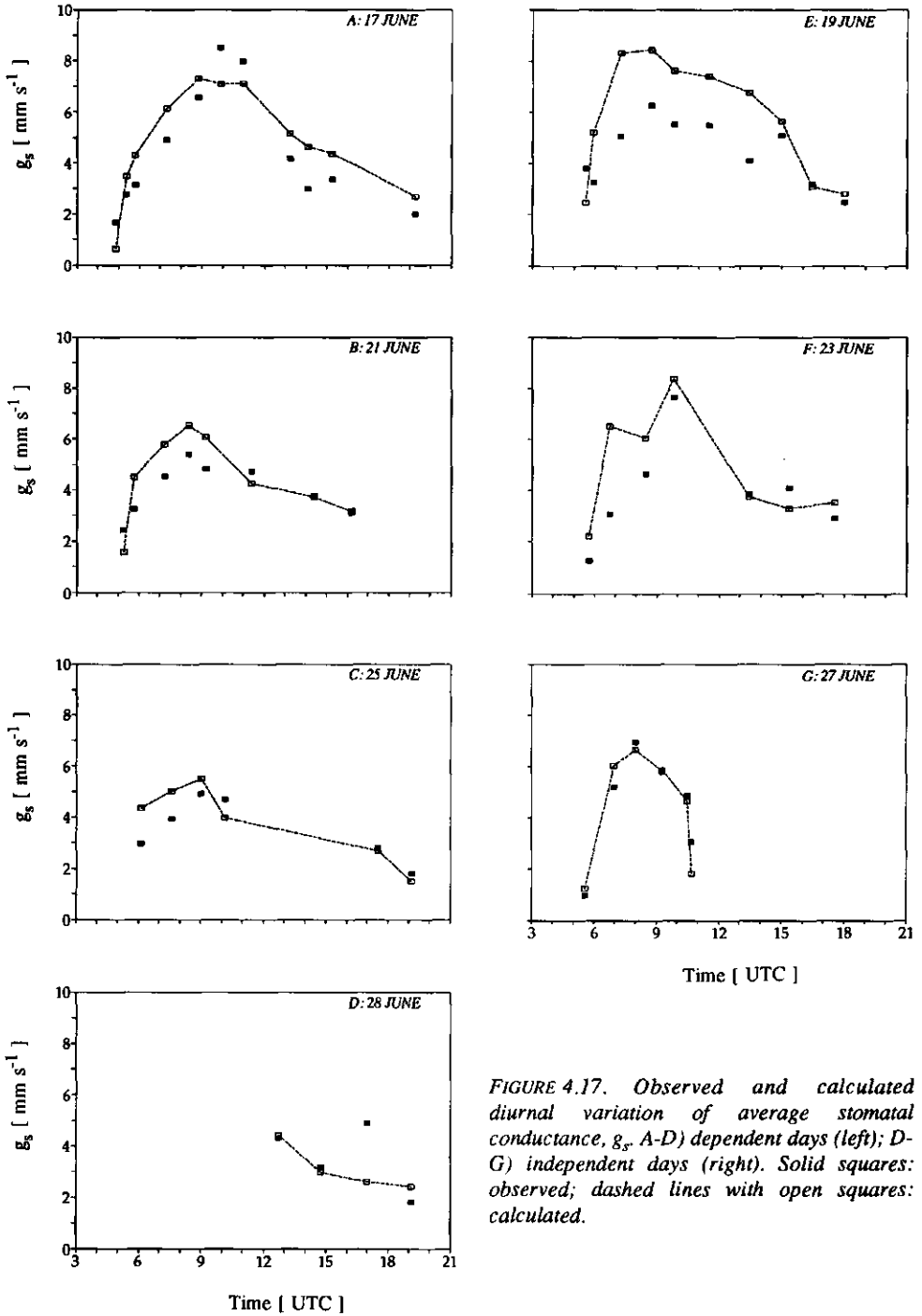


FIGURE 4.17. Observed and calculated diurnal variation of average stomatal conductance,  $g_s$ . A-D) dependent days (left); D-G) independent days (right). Solid squares: observed; dashed lines with open squares: calculated.

(1990, grapevines). Here, inspection of the diurnal variations reveals that  $g_s$  is usually overestimated in the morning. Given the fact that  $A_n$  is reasonably well simulated here, the feature may suggest that  $f_o$ , and therefore  $C_{i,vir}$ , is taken too high in the morning. It should be recalled that  $g_s$  was exceptionally high in the morning of 17 June. This feature might have triggered a rather high value of  $f_o$  during the analyses.

The worst case of overestimation of  $g_s$  is visible on 19 June. Here, the averages deviate by 20-40 %. Indeed, the clusters of data in Fig. 4.15B are related to this day. The cloudiness of 19 June (cloud cover  $\geq 4/8$  during an extended period) made the gas-exchange measurements somewhat unreliable, which might be one of the reasons for the relatively poor model performance for this day.

#### 4.6 Discussion and conclusions

The results presented in this chapter support earlier conclusions from field observations and modelling studies that  $g_s$  and  $A_n$  are correlated. Thus, a model for  $A_n$  can be used to model  $g_s$ . The advantages of such a model as compared to  $g_s$  models of the Jarvis-Stewart type (JS-models; Jarvis, 1976; Stewart, 1988) were discussed in the previous chapter. It is believed that A- $g_s$  models have more *predictive* power than JS-models, because they account for synergistic interactions between the various stimuli as well as for the effect of  $CO_2$  on the stomata. Therefore, for future meteorological research the use of A- $g_s$  models to calculate  $g_s$  or  $r_s$  is recommended.

Tuning and testing these models using field data requires simultaneous measurements of leaf photosynthesis and stomatal conductance. Thus, this type of measurement should become common practice in micrometeorological experiments. In establishing species-specific features, standard values for some of the most important parameters of the photosynthesis model may be used. These can be derived from the wealth of results from plant physiological research.

The basic assumption in A- $g_s$  models is that a correlation exists between  $A_n$  and  $g_s$ . Such a correlation has often been observed before (Goudriaan & van Laar, 1978; Louwerse, 1980; Schulze & Hall, 1982; Tenhunen *et al.*, 1987). The following observations for the grapevines studied here (*Vitis Vinifera* L. cv Airen) confirm the results of these earlier studies and provide evidence for the basic assumption mentioned above:

- younger leaves have a lower  $g_s$  as well as a lower  $A_n$  than older leaves,
- qualitatively, the diurnal variation of  $g_s$  and  $A_n$  is similar, for shaded leaves as well as for sunlit leaves,
- the method of Goudriaan & van Laar (1978) to determine  $C_{i,vir}$  is based on the correlation between  $A_n$  and  $g_s$  and could be applied with reasonable success.

$A_n$  and  $g_s$  can be coupled if  $C_s - C_i$  is known ([4.1]). A parameterization of the ratio  $f = (C_i - \Gamma) / (C_s - \Gamma)$  (Goudriaan *et al.*, 1985) seems the most convenient way to arrive at  $C_s - C_i$ . A strong linear relation was found between the ratio  $f$  and  $D_s$  (Fig. 4.10), at least between

$D_s = 6 \text{ g kg}^{-1}$  and  $D_s = 35 \text{ g kg}^{-1}$ . for the grapevines studied here. This relationship can be expressed as

$$f = 0.916 \cdot (1 - D_s/58.2) \quad r^2 = 0.959 \quad [4.9]$$

[4.9] is consistent with earlier results by Morison and Gifford (1983) and by Friend (1991). The coefficient 58.2 is the estimated value of  $D_{\max}$ , the value of  $D_s$  at which the stomata are completely closed. The coefficient 0.916 represents  $f_0$ , which is the value of  $f$  at  $D_s=0$ . The value of  $D_{\max}$  is rather high in comparison to the "standard" value derived in the preceding chapter. This may reflect the adaption of the grapevines to the warm and dry environment in which they are grown. Such an adaption may be induced by the release of plant hormones, such as ABA, which sensitize the stomata (for example, Raschke, 1987). It should be investigated whether or not relationships similar to [4.9] exist for other species, grown in a different environment. This kind of relationship provides a convenient way for parameterizing stomatal humidity responses in the context of  $A-g_s$  models (see Chapter 3). Some alternatives to this approach were also discussed in Chapter 3.

On theoretical grounds,  $f$  should deflect at values of  $D_s$  which approach  $D_{\max}$  (Chapter 3). No evidence for such a deflection was found here, probably because of the high value of  $D_{\max}$  which would suggest acclimatization of the grapevines to the dry environment. If the statement may be generalized that stomatal humidity responses acclimate to the plant's environment,  $D_s$  will seldom approach  $D_{\max}$ . Then, the deflection of  $f$  at high values of  $D_s$  may be ignored because it will hardly ever be encountered in the field. This would also confirm that  $g_c$  may be neglected in most field studies.

The complete  $A-g_s$  model satisfactorily describes the photosynthetic rate of the vines studied here. Only a limited number of the model parameters had to be adjusted to tune the model. In the other cases, standard values were successfully applied ( $\epsilon_0$ ,  $Q_{10}$  for  $g_m$  and  $A_{m,\max}$ ,  $\Gamma(@25)$ ,  $A_{m,\max}(@25)$ ). This confirms the certain general applicability of the model. Obviously, the use of non-standard parameter values would improve the model's performance, but restrict its generality.

The model performance for stomatal conductance is somewhat less than that for  $A_n$ . Nevertheless, it is similar to that of the JS-models. It is felt that the present model can be improved if the determination of parameter values is based on  $A_n$  and  $g_s$  measurements in one and the same leaf cuvette. In order to achieve this, a leaf cuvette transparent at all sides should be used.

In this chapter, the  $A-g_s$  model has been tested on leaf scale. In order to use it in meteorological models, the model has to be scaled up to the canopy level in many cases. This can be achieved by means of models such as presented by Goudriaan (1977). An example is given in the next chapter. The up-scaled model will not only describe  $g_s$  at the canopy level, but it will also describe surface fluxes of  $\text{CO}_2$ . These are additional advantages of the kind of  $g_s$  model used here.

## 5

**DIRECT IMPACT OF ATMOSPHERIC CO<sub>2</sub> ENRICHMENT ON SURFACE RESISTANCE AND REGIONAL TRANSPIRATION: SIGNIFICANCE OF THE PBL-VEGETATION INTERACTION****5.1 Introduction**

In this chapter the results of a systematic analysis of various aspects of the PBL-vegetation interaction are presented. The analysis focuses on the *prediction* of changes in the surface resistance,  $r_s$ , and the transpiration,  $\lambda E$ , at the regional scale. A doubled ambient CO<sub>2</sub> concentration is assumed to cause these changes. However, it must be stressed that it is not the intention here to give precise predictions of future changes due to CO<sub>2</sub> enrichment. Instead, it is the main goal here to identify important processes that should be taken into account in order to arrive at such predictions.

To perform the analysis, the coupled model described in Chapter 2 has been extended in three major ways:

1. Responses of the stomata to various environmental variables, including the CO<sub>2</sub> concentration, are taken into account. Thus,  $r_s$  becomes a dependent variable showing a diurnal variation, instead of being a fixed, independent variable as in the previous analysis (Chapter 2). For this purpose, the A-g<sub>s</sub> model presented in Chapter 3 and 4 is scaled up from the leaf to the canopy level.
2. The PBL model has been extended with a description of CO<sub>2</sub> concentrations and fluxes. The CO<sub>2</sub> surface flux is driven by canopy photosynthesis, evaluated by the up-scaled A-g<sub>s</sub> model.
3. Recent ideas about the parameterization of nonlocal turbulent transport of heat and tracers in the PBL have been implemented (Holtslag & Moeng, 1991).

The main features of the extensions are described in Section 5.2. A more detailed description of the background to the modifications is given in Appendix 5 and 6, along with a description of some other minor changes.

Due to the large number of variables involved in the problem, a sensitivity analysis can consist of numerous simulations. Variables and parameters can be varied individually and in combination with each other. Clearly, it is impossible to consider all the characteristics of the entire system systematically in one study. Therefore, a limited number of initial and boundary conditions - described in Section 5.3 - are applied in the analysis and only some selected aspects are addressed here. In the present study, special attention is paid to the effect of:

1. PBL feedback (see Chapter 2)
2. stomatal humidity responses
3. differences between  $C_3$  and  $C_4$  canopies
4. different atmospheric conditions
5. evolution of  $CO_2$  concentrations within the PBL
6. Leaf Area Index, LAI, and roughness length,  $z_0$

Note that, in changing to a meteorological treatment, the terminology of the micrometeorological research will be re-introduced.

## 5.2 Extensions of the coupled PBL-vegetation model

### 5.2.1 General

In the coupled model described in Chapter 2,  $r_s$  has been treated as an independent variable with a fixed value. In reality, the stomata will respond to changes in environmental conditions, so that  $r_s$  shows a diurnal variation. Therefore, the coupled model has been extended to account for the effect of stomatal behaviour on  $r_s$ . One of the factors affecting  $r_s$  is  $CO_2$ . In the problem considered in the present study, elevated  $CO_2$  causes the initial perturbation of  $r_s$ . Given the key-role of  $CO_2$ , it is important to consider the diurnal evolution of  $CO_2$  at the reference level as well. For this reason, the PBL model has been extended with a description of  $CO_2$ . The surface flux of  $CO_2$  is driven by canopy photosynthesis.

The A- $g_s$  model presented in Chapter 3 and 4 can be used to describe  $r_s$  as well as the photosynthetic rate. However, because the A- $g_s$  model applies at the leaf scale, whereas the coupled model requires a description at the canopy scale, the A- $g_s$  model has to be scaled up. In Section 5.2.2 an outline is given of how this was done in the present study.

In addition to the extension of the PBL model with a description of  $CO_2$  profiles and fluxes, the treatment of turbulent diffusion within the PBL has also been changed. A modified parameterization of the turbulent diffusion coefficient for scalars ( $K_s$ ) and the corresponding countergradient correction,  $\gamma_s$ , has been implemented to account for nonlocal turbulent transport. This was done following Holtslag & Moeng (1991), but test simulations revealed

that their parameterization of the countergradient correction does not work satisfactorily in the case of water vapour and CO<sub>2</sub>. Therefore, the new parameterization of  $\gamma_s$  for tracers has been used in an adapted form. The modifications with respect to the description of turbulent transport are outlined in Section 5.2.3. More details and a description of some other, minor changes can be found in Appendix 5.

### 5.2.2 Scaling the A-g<sub>s</sub> model up from the leaf to the canopy

The A-g<sub>s</sub> model described in the previous chapters yields photosynthetic rate, A<sub>n</sub>, at the leaf scale. The calculated A<sub>n</sub> is used to arrive at stomatal conductance, g<sub>s</sub>, so that g<sub>s</sub> also applies at the leaf scale. However, the coupled model requires *canopy* photosynthetic rate, A<sub>nc</sub>, to drive CO<sub>2</sub> fluxes in the PBL. Similarly, transpiration rate, λE, is calculated according to

$$\lambda E = \rho \lambda \frac{q^*(T_s) - q_r}{r_{av} + r_s} \quad [5.1]$$

in which r<sub>s</sub> is a *bulk* surface resistance. (The other symbols are as in Appendix 2, see also the list of symbols.) Thus, the A-g<sub>s</sub> model must be scaled up from the leaf to the canopy. In the present study, this has been done as follows.

The stomata are assumed to act parallel. Then, r<sub>s</sub> in [5.1] can be approximated by (Shuttleworth, 1976; Lhomme, 1991)

$$\frac{1}{r_s} = \int_0^{LAI} g_s dL \quad [5.2]$$

where LAI is the total leaf area index of the canopy and L is leaf area index per unit volume in the canopy. Similarly, the photosynthetic rate of the entire canopy, A<sub>nc</sub>, can be calculated from

$$A_{nc} = \int_0^{LAI} A_n dL \quad [5.3]$$

Because of the nonlinear response of A<sub>n</sub> and g<sub>s</sub> to light, it is not sufficiently accurate to calculate A<sub>nc</sub> and r<sub>s</sub> using one averaged value of the light intensity in the canopy. Therefore, the PAR profile inside the canopy is evaluated in somewhat more detail, following Goudriaan (1977, 1988), Spitters (1986) and Spitters *et al.* (1986). The treatment of the PAR regime inside the canopy is outlined in Appendix 3.

It is assumed that the light intensity profile is the principle cause of variations of A<sub>n</sub> and g<sub>s</sub> inside the canopy. Profiles of the CO<sub>2</sub> concentration, C<sub>s</sub>, the leaf temperature, T<sub>l</sub>, and specific humidity difference at the leaf surface, D<sub>s</sub>, are assumed to be much less important. Therefore, C<sub>s</sub>, T<sub>l</sub>, and D<sub>s</sub> are taken as being constant throughout the canopy. T<sub>l</sub> and D<sub>s</sub> are calculated from the energy balance equations at the effective source heights for heat and moisture, z<sub>oh</sub>



and  $z_{ov}$ , respectively (see Appendix 2), and taking  $T_1 = T_s$ . The latter notation,  $T_s$ , will be used henceforth.  $C_s$  is calculated from the  $CO_2$  concentration at  $z_1$  (denoted as  $C_1$ ), and using  $A_{nc}$  of the *previous* time step.  $C_s$  is determined at  $z_{ov}$ , which implies the assumption that  $z_{ov} = z_{oc}$ , with  $z_{oc}$  the effective sink height for  $CO_2$ .  $T_s$ ,  $D_s$ , and  $C_s$  are used to determine the parameter values in the A- $g_s$  model.

Next,  $A_n$  and  $g_s (= f(A_n)$ ; [3.16]) are calculated from the absorbed amount of PAR. The levels within the canopy for which the calculations are performed are prescribed by the integration technique used here. This integration method is the so-called three-point Gaussian integration, that prescribes three heights. Canopy totals are obtained from a weighed addition of the contribution from each of the three levels. The method is fast and very accurate as compared to other numerical integration schemes (Goudriaan, 1986).

At each level, a distinction is made between *sunlit* and *shaded* leaves (see also Appendix 3). For the sunlit leaves,  $A_n$  and  $g_s$  are averaged over all leaf angles, because the amount of absorbed radiation will depend on the leaf angle. The three-point Gaussian integration scheme is used to obtain the required average (Goudriaan, 1986). The shaded leaves are treated as one single leaf class, because effects leaf angle will be much less important in this case. The distinction between one shaded leaf class and several sunlit leaf classes usually gives results that are similar to those of very detailed models (Reynolds *et al.*, 1992). The average  $A_n$  and  $g_s$  of each level are computed from the weighed contribution of sunlit and shaded leaves. Finally,  $r_s$  and  $A_{nc}$ , given by [5.2] and [5.3], respectively, are evaluated.

### 5.2.3 Parameterization of turbulent transfer within the PBL

The PBL model has been extended with a description of  $CO_2$  concentrations and fluxes. The surface flux of  $CO_2$  is the canopy photosynthetic rate,  $A_{nc}$ , which is determined using the up-scaled A- $g_s$  model of Chapter 3 and 4, as outlined above (Section 5.2.2).

Along with the extension of the PBL model mentioned above, the parameterization of turbulent transfer has been modified. The diffusion coefficient for scalars,  $K_s$ , and the corresponding countergradient correction,  $\gamma_s$ , are now parameterized following Holtslag & Moeng (1991). They showed that in the convectively driven PBL ( $w_*/u_* \geq 2.33$ ) transport by fast, rising updrafts and slower, descending downdrafts can be included by using

$$K_s = \frac{(1 - z/h + R_s z/h)K_u K_d}{(1 - z/h)K_d + R_s(z/h)K_u} \quad [5.4]$$

where  $R_s \equiv \overline{w's'}_e / \overline{w's'}_s$ , (with  $\overline{w's'}_e$  denoting the kinematic entrainment flux of a scalar  $s$  and  $\overline{w's'}_s$  the kinematic surface flux of  $s$ ), and  $K_u$  and  $K_d$  are given below.

Under convective conditions  $R_s$  is usually negative for heat (negative entrainment flux and positive surface flux), but positive for water vapour (positive entrainment flux, positive surface flux) and  $CO_2$  (negative entrainment flux, negative surface flux).

Negative values of  $R_s$ , restrict the application of [5.4] to  $z/h < 1/(1-R_s)$ . Therefore, as proposed by Holtslag & Moeng (1991), the following parameterization is used in cases where  $R_s < 0$  (for instance, in the case of heat transport):

$$K_s = w_* h \left( \frac{z}{h} \right)^{4/3} \left( 1 - \frac{z}{h} \right)^2 \left( 1 + R_s \frac{z}{h} \right) \quad [5.5]$$

$K_u$  and  $K_d$  are diffusivities for the so-called bottom-up diffusion and top-down diffusion, respectively (see Appendix 5 for details). These are parameterized as

$$\frac{K_u}{w_* h} = \left( \frac{z}{h} \right)^{4/3} \left( 1 - \frac{z}{h} \right)^2 \quad [5.6a]$$

and

$$\frac{K_d}{w_* h} = 7 \left( \frac{z}{h} \right)^2 \left( 1 - \frac{z}{h} \right)^3 \quad [5.6b]$$

The countergradient correction,  $\gamma_s$ , is taken

$$\gamma_s = b \frac{w_* \overline{w'^2 s'}}{w'^2 h} \quad [5.7]$$

with  $b = 2$  and using

$$\overline{w'^2}^{3/2} = \left[ 1.6 u_*^2 \left( 1 - \frac{z}{h} \right) \right]^{3/2} + 1.2 w_*^3 \left( \frac{z}{h} \right) \left( 1 - 0.9 \frac{z}{h} \right)^{3/2} \quad [5.8]$$

(Holtslag & Moeng, 1991).

Contrary to the previous formulation (Troen & Mahrt, 1986; Appendix 4),  $K_s$  now depends on entrainment flux. In the new formulation  $w_*$  is used as the relevant velocity scale, instead of  $w_s$  ( $\equiv u_* / \phi_m$ , where  $\phi_m$  denotes the nondimensional gradient of the wind speed in the SL). Furthermore, it obeys the free convection limit in the SL (Panofsky & Dutton, 1984; Garratt, 1992). As in Troen & Mahrt (1986),  $\gamma_s$  is related to the surface flux. Moreover,  $\gamma_s \rightarrow 0$  if  $w_* \rightarrow 0$ .

Test simulations showed that the new parameterization for  $\gamma_s$  produces unrealistic concentration profiles for water vapour and CO<sub>2</sub>, while it works rather well for heat. Examples for water vapour and CO<sub>2</sub> profiles and an explanation of the feature are given in Appendix 5. Because of these results, the new parameterization for  $\gamma_s$  has only been applied in the case of heat. It is noted that the parameterization of heat is also the most important one because it affects PBL dynamics. For the time being, the countergradient terms of moisture and CO<sub>2</sub> are evaluated using [5.7] and [5.8] at  $z/h = 0.4$  and taking  $\gamma_s$  as constant throughout the PBL. This approach for water vapour and CO<sub>2</sub> resembles the approach by Troen and Mahrt (1986; Chapter 2). A more fundamental approach requires many more field observations and LES data and is beyond the scope of the present study.

The surface fluxes obtained with the constant countergradient term are almost equal to those resulting from the parameterizations by Holtslag & Moeng (1991). In addition, the development of PBL height, apparent from the evolution of the profiles of  $q$  and  $\text{CO}_2$ , (see Fig. A5.1) is almost the same. However, the profiles near the top of the PBL are far more realistic (Fig. A5.1).

Additional changes in the PBL-SL part of the model are:

- The entrainment coefficients for heat, water vapour and  $\text{CO}_2$  are evaluated from the modelled fluxes in the PBL,
- The Prandtl number,  $Pr$ , which determines the relationship between  $K_m$  and  $K_h$ , is adapted to the new parameterization,
- $w_*$  is used as the velocity scale to calculate  $h$ , instead of  $w_g$ ,
- The functions  $\phi_m$  and  $\phi_h$  used by Troen & Mahrt (1986) have been replaced by those used in Holtslag *et al.* (1990),
- The full integrated flux-profile relationship is used instead of the bulk-approach by Louis (1979). This requires an additional iterative procedure, but the solution is more accurate.
- Atmospheric emissivity is made dependent on water vapour content and on temperature, according to Brutsaert (1982). This parameterization replaces that of Swinbank (1963), where only temperature is used.

More details on these modifications can also be found in Appendix 5.

Results and a discussion of a test of the modified PBL model are given in Appendix 5 and 6. It may be concluded that the modified PBL model is able to simulate the state of the PBL over *extensive homogeneous areas* realistically. The analysis described in the following sections is confined to such areas.

## 5.3 Setup of the analysis

### 5.3.1 General

In the sensitivity analysis described in Chapter 2, the influence of the PBL-vegetation interaction was evaluated in a physical context, while biological processes, notably stomatal behaviour, were ignored. The extensions described in the previous section also allow the "biological feedback" to be considered. The goal of the analysis presented in this chapter is to evaluate the influence of various physical, as well as biological aspects of the biosphere-atmosphere interaction, and their relation to each other.

The analyses presented in the following sections consider changes triggered by the impact on  $r_s$  of a doubled ambient  $\text{CO}_2$  concentration, from  $340 \mu\text{mol mol}^{-1}$  to  $680 \mu\text{mol mol}^{-1}$ . Simulations for these concentrations are denoted as  $1x\text{CO}_2$  and  $2x\text{CO}_2$ , respectively. In order to compare the results of the  $1x\text{CO}_2$  and the  $2x\text{CO}_2$  simulations, the mean values of the variables,  $x$ , are calculated from the simulated diurnal evolution, using the output for each half hour between 6 and 18 LT. Relative changes,  $\Delta x$ , are then calculated as

$$\Delta x = 100 \frac{\bar{x}(@2xCO_2) - \bar{x}(@1xCO_2)}{\bar{x}(@1xCO_2)} \quad (\%) \quad [5.9]$$

where  $\bar{x}$  denotes the mean values of  $x$  between 6 and 18 LT.

Various sets of simulations were constructed, in order to be able to address the following issues by means of a comparison between the results for each set:

- As before, the influence of PBL feedback is investigated. However, in addition to its influence on transpiration ( $\lambda E/Q^*$ ), the influence of PBL feedback on stomatal behaviour ( $r_s$ ) will be considered. In Chapter 2 it was shown that the effect of PBL feedback depends strongly on the aerodynamic roughness of the surface,  $z_0$ . Therefore results are presented as a function of  $z_0$ , which facilitates the evaluation of the role of  $z_0$ . Note that  $z_0$  has been imposed as an independent variable.
- Changes of the specific humidity deficit are an important aspect of PBL feedback (see Section 1.1.3). These not only affect changes in transpiration, but also changes in  $r_s$  through the related humidity response of stomata. For this reason, special attention is paid to the influence of humidity responses.
- Leaf growth may be stimulated by elevated CO<sub>2</sub>. If so, the impact of CO<sub>2</sub> on  $r_s$  through the effect on stomatal aperture may be offset by an increased LAI. Therefore, attention is paid to the influence of LAI.
- C<sub>3</sub> and C<sub>4</sub> plants respond to elevated CO<sub>2</sub> differently. Therefore, differences between "C<sub>3</sub> canopies" and "C<sub>4</sub> canopies" will also be considered.
- Because CO<sub>2</sub> plays a key-role in the changes, the effect of a diurnal variation of the CO<sub>2</sub> concentration in the PBL, notably the concentration at  $z_p$ , is investigated in somewhat greater detail.

The differences between the sets of simulations are described in Section 5.3.3 and 5.3.4, after an outline has been given of the initial and boundary conditions applied in the analysis (Section 5.3.2).

### 5.3.2 Initial and boundary conditions

#### a) Resolution and time step

The number of grid points between 0 and 4 km is 98. The grid spacing is 10 m close to the surface and increases to 100-150 m towards the upper boundary of the model's grid. A time step of three minutes is taken.

#### b) Solar radiation

The simulations are carried out for daylight hours, between 6 and 18 LT, day 180. The solar radiation is calculated according to Holtslag & Van Ulden (1983) for 45°N, 0°E, with the atmospheric transmissivity typical of De Bilt, The Netherlands (52°06'N, 5°11'E). Fair-weather conditions are assumed with zero cloud cover. Values of  $S\downarrow$  then vary between about 100 W m<sup>-1</sup> and 850 W m<sup>-1</sup>.

*c) Initial atmospheric conditions and geostrophic wind speed*

The so-called McClatchey profiles are used as the initial conditions. These standard profiles are often used in studies of atmospheric radiative transfer (Ellingson *et al.*, 1991). They represent differences in average atmospheric conditions between latitudes and different seasons. The McClatchey profiles taken here are the Sub Arctic Summer profile (SAS), the Mid Latitude Summer profile (MLS) and the Tropical profile (TRO). The McClatchey temperature and humidity profiles are shown in Appendix 12. Clearly, the advantage of using standard profiles is that they can be readily obtained and that there is no doubt about their interpretation. Note that the profile names must not be taken too literally here, because the profiles are used as initial conditions at 6 LT, whereas, in reality, they refer to daily averages.

The initial  $\text{CO}_2$  concentration is taken  $340 \mu\text{mol mol}^{-1}$  ( $1\times\text{CO}_2$ ) and  $680 \mu\text{mol mol}^{-1}$  ( $2\times\text{CO}_2$ ), respectively. It is assumed as being constant with height. The initial wind speed in the  $x$ -direction ( $u$ ) increases logarithmically with height, from zero at the surface (height  $z_0$ ) up to  $10 \text{ m s}^{-1}$  at 1 km. Above 1 km,  $u$  remains constant with height. The initial windspeed in the  $y$ -direction is zero at all levels. The geostrophic wind speed is given a fixed value of  $10 \text{ m s}^{-1}$  in the  $x$ -direction and zero in the  $y$ -direction.

*d) Surface characteristics and parameters of the A- $g_s$  model*

The surface albedo and emissivity are chosen 0.2 and 0.97, respectively, and  $G/Q^*$  is taken 0.1 (De Bruin, 1983). The roughness length,  $z_0$ , is 0.03, 0.12, 0.48 or 2 m, while  $\ln(z_0/z_{oh}) = 2$  and  $z_{oh} = z_{ov} = z_{oc}$ . For simplicity, zero-plane displacement ( $D$ ) is taken as being zero in all cases, and the reference level,  $z_r$ , is at 10 m. The parameters in the A- $g_s$  model are as given in Table 3.2. Furthermore, LAI = 5 in most cases (exceptions are described below). The cuticular conductance,  $g_c$ , is taken as  $0.2 \text{ mm s}^{-1}$ . Using this value of  $g_c$ , the minimum photosynthetic rate ( $A_{\min} = A_n$  at  $D_s = D_{\max}$ ) and the corresponding value of  $f$  ( $f_{\min}$ ) are evaluated as described in Section 3.7.

It is noted that some combinations of surface characteristics will not occur in reality (for instance,  $z_0 = 2$  and  $D = 0$  m). However, this is not a problem here because the main goal of the analysis is to explore the importance of processes and the influence of system parameters theoretically.

### 5.3.3 Characteristics of the simulations

*a) General*

Nine sets of simulations are constructed. All sets contain simulations for  $1\times\text{CO}_2$  and for  $2\times\text{CO}_2$ . Furthermore, all sets contain simulations for  $C_3$  canopies and also for  $C_4$  canopies. Roughness length,  $z_0$ , and LAI are as mentioned above, except in Sets I and II, where LAI = 3, 4 or 5, and  $z_0 = 0.12$  m. Further initial and boundary conditions are as described above.

*b) Simulations with PBL feedback, and construction of reference cases*

First, simulations were performed with the complete coupled model. These simulations will result in a diurnal evolution of the temperature, specific humidity,  $\text{CO}_2$  concentration, and

wind speed at  $z_r$  ( $T_r$ ,  $q_r$ ,  $C_r$ , and  $u_r$ , respectively). Now, the diurnal evolution of  $T_r$ ,  $q_r$ , and  $u_r$  at the simulated current diurnal evolution of  $C_r$  ( $1xCO_2$ ) are given the status of "observations," that could have been obtained during present-day experiments. They will be called the "reference conditions."

#### c) Simulations without PBL feedback

In order to get an impression of the influence of PBL feedback the vegetation-SL model was also run separately using the reference conditions derived in the same way as has been described above. Thus, in these simulations, the diurnal evolution of  $T_r$ ,  $q_r$ , and  $u_r$  at  $z_r$  are prescribed, while  $C_r$  is given a prescribed, fixed value ( $340 \mu\text{mol mol}^{-1}$  for  $1xCO_2$  or  $680 \mu\text{mol mol}^{-1}$  for  $2xCO_2$ ). These simulations are similar to simulations where PBL feedback is ignored (for example, Martin *et al.*, 1989; Rosenberg *et al.*, 1989). It is noted that SL feedback is accounted for in all cases (see Chapter 2).

#### d) Influence of stomatal responses

In the extended model, stomatal humidity responses are taken into account by means of a parameterization related to the A-g<sub>s</sub> model (Chapter 3 and 4). In order to assess the effect of the humidity responses, the model was run with and without account being taken of these responses. In the latter case, simulations were performed with the ratio  $f=(C_1-\Gamma)/(C_5-\Gamma)$  taken as constant (0.7 for C<sub>3</sub> plants, and 0.4 for C<sub>4</sub> plants; Goudriaan *et al.*, 1985). The simulations were carried out with and without PBL feedback.

Further simulations were performed in which the diurnal variation of  $r_s$  was ignored completely. Here,  $r_s$  was imposed as an independent variable with a fixed value (see Chapter 2). The mean simulated  $r_s$  of each of the reference cases (between 6 and 18 LT) was taken as the fixed value of  $r_s$  for the  $1xCO_2$  cases. These averages were increased by 50% so they could be used for the  $2xCO_2$  cases (see, for example, Cure & Acock, 1986; Morison, 1987). Again, the simulations were carried out with and without PBL feedback.

#### e) Influence of LAI

Simulations with and without PBL feedback were performed with  $z_o = 0.12$ , while LAI = 3, 4 or 5.

#### f) Diurnal variation of CO<sub>2</sub> in the PBL

In addition to the simulations described so far, a special set of simulations was performed in order to assess the effect of the diurnal variation of CO<sub>2</sub> in the PBL. Here, the model was run with complete PBL feedback, with the exception of CO<sub>2</sub>. Complete SL feedback was allowed here, including the development of a CO<sub>2</sub> concentration gradient between  $z_r$  and the surface.

### 5.3.4 Summary of the simulations

A summary of the simulations is given in Table 5.1. Groups of simulations are denoted as the Sets I to IX. Set III to IX consist of 48 simulations each:

TABLE 5.1. Summary of the simulations. "+" denotes "with," "-" denotes "without." The results of the simulations in Set I and III for  $1xCO_2$  are the reference simulations. See text for further explanation and a description of initial and boundary conditions as well as of parameter values. Note that in all cases SL feedback is accounted for.

Simulations	PBL feedback	Photosynthesis & responses $r_s$	Humidity responses	$CO_2$ in PBL
SET I	+	+	+	+
SET II	—	+	+	+
SET III	+	+	+	+
SET IV	—	+	+	+
SET V	+	+	—	+
SET VI	—	+	—	+
SET VII	+	—	—	+
SET VIII	—	—	—	+
SET IX	+	+	+	—

- initial conditions SAS, MLS or TRO,
- $1xCO_2$  or  $2xCO_2$ ,
- $C_3$  or  $C_4$  photosynthesis,
- $z_0 = 0.03, 0.12, 0.48$  or  $2.0$  m,
- LAI = 5.

Set I and II consist of 36 simulations each:

- $z_0 = 0.12$  m,
- LAI = 3, 4, or 5.

All other characteristics are as for sets III - IX.

## 5.4 Results

Clearly, only a limited number of results can be presented here. The presentation and discussion of results will be restricted to  $r_s$ , and to  $\lambda E$  or the normalized transpiration,  $\lambda E/Q^*$  (see Chapter 2). Note that, contrary to the analysis in Chapter 2,  $r_s$  has become a dependent variable here. Results for some variables other than  $r_s$  and  $\lambda E$  are given in Appendix 13 as averages between 6 and 18 LT.

Some selected results for  $\lambda E$  and  $r_s$  will be discussed in this section. First, the influence of LAI on  $r_s$  and  $\lambda E$  is considered in Section 5.4.1, where results are presented as diurnal evolutions in order to illustrate the model's ability to simulate features typical of  $r_s$  and  $\lambda E$ . These results also appear to be able to provide a basis for the interpretation of results discussed later. In Section 5.4.2 to 5.4.4, results are presented as relative changes for elevated  $CO_2$ , from  $1xCO_2$  to  $2xCO_2$  ([5.9]). The relative changes are plotted versus  $z_0$  in order to facilitate an evaluation of the role of  $z_0$  with respect to PBL feedback. Note, that  $z_0$  is taken as being an independent variable.

5.4.1 Diurnal evolution of  $r_s$  and  $\lambda E$ , and the influence of LAI

Fig. 5.1 shows the simulated diurnal evolution of  $r_s$  and  $\lambda E$  for SAS and TRO conditions. The data depicted here refer to C<sub>3</sub> canopies under 1xCO<sub>2</sub> and 2xCO<sub>2</sub> (dotted lines and solid lines, respectively), and for LAI = 3, 4 or 5 (open squares, triangles and filled squares, respectively). In all cases  $z_0 = 0.12$  m.

Under SAS conditions the canopy encounters almost optimum conditions with  $T_s$  between 20 and 25 °C and  $D_s$  usually being less than 5 g kg<sup>-1</sup> (see Appendix 13). A slight hysteresis effect is visible, especially for  $\lambda E$ , which is due to higher temperatures and lower humidities in the afternoon. The resistances are rather low under 1xCO<sub>2</sub> and increase by about a factor 2 under 2xCO<sub>2</sub>. Different values of LAI lead to slightly different resistances and transpiration rates for 1xCO<sub>2</sub>. The differences increase somewhat under 2xCO<sub>2</sub>.

By contrast, under TRO conditions  $T_s$  is between 30 and 40 °C and  $D_s$  values may reach 25 to 30 g kg<sup>-1</sup> (see Appendix 13). A midday stomatal closure occurs in most cases under TRO conditions. Only in the case of LAI=5 and for 1xCO<sub>2</sub> is the midday stomatal closure

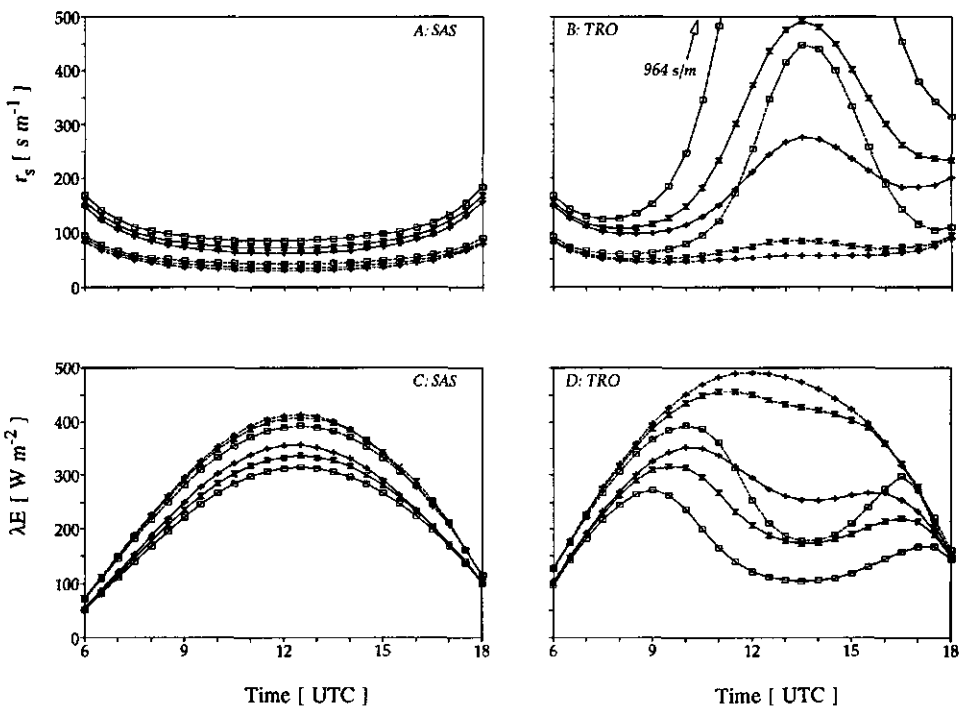


FIGURE 5.1 Effect of LAI on the diurnal evolution of  $r_s$  (A: SAS conditions and B: TRO conditions) and  $\lambda E$  (C: SAS conditions and D: TRO conditions) in the case of a C<sub>3</sub> canopy. Dashed lines: 1xCO<sub>2</sub>; solid lines: 2xCO<sub>2</sub>. Empty squares: LAI=3; Hourglasses: LAI=4; Pluses: LAI = 5.



hardly visible. Because of the higher evaporation rate, the canopy is able to maintain relatively low temperatures and also rather low values of  $D_s$ . At other values of LAI, dramatic increases in  $r_s$  are simulated. It can be seen that the influence of LAI is very strong here and it may affect predictions concerning the effect of a doubled  $\text{CO}_2$  concentration on  $r_s$  and  $\lambda E$  considerably. Part of the dramatic influence of the midday stomatal closure is related to a positive feedback mechanism: once  $T_s$  exceeds the optimum temperature of photosynthesis,  $r_s$  starts to decrease, which leads, amongst other things, to less evaporation and to even higher  $D_s$  and  $T_s$ . This mechanism will be discussed further in Section 5.6.

The simulated diurnal evolution of  $C_4$  canopies under SAS, MLS and TRO conditions is qualitatively similar to that of the  $C_3$  canopy under SAS conditions. The optimum temperature for  $C_4$  photosynthesis is hardly exceeded and, therefore, these canopies are able to maintain moderate values of  $D_s$ . The behaviour of  $C_3$  canopies under MLS conditions takes an intermediate position between SAS and TRO conditions. These cases are not shown here.

#### 5.4.2 Changes of $r_s$ and $\lambda E/Q^*$ : $C_3$ canopies

The relative change of  $r_s$  and of  $\lambda E/Q^*$  for a change from  $1\times\text{CO}_2$  to  $2\times\text{CO}_2$  in the case of  $C_3$  canopies is plotted versus  $z_0$  in Fig. 5.2. Note that for  $z_0$  a logarithmic scale is used. All data are for LAI=5. Various predictions are compared here: with or without PBL (A or C versus B or D) and with or without humidity responses (solid lines versus dashed lines).

If the stomatal humidity responses are ignored, the resulting changes in  $r_s$  are almost independent of  $z_0$  and of the atmospheric conditions. The relative change then is about 50%, which is in good agreement with the predictions by Cure & Acock (1986) and Morison (1987). However, the predicted changes are dramatically higher if humidity responses are allowed for. PBL feedback contributes significantly to this enhanced response. In addition, the differences between the atmospheric conditions also become important with PBL feedback. The additional changes of  $r_s$  are related to the concurrent changes of  $D_s$ , which intensifies the humidity responses. This effect is further analyzed in Section 5.5.3.

Dramatic increases of  $r_s$  are predicted at low  $z_0$  for the TRO conditions. This is caused by the midday stomatal closure at  $2\times\text{CO}_2$ , which was virtually absent at  $1\times\text{CO}_2$  (see Section 5.4.1). Increased  $\text{CO}_2$  causes higher values of  $r_s$  and, therefore, less transpiration and higher surface temperatures. The low value of  $z_0$  hampers the release of heat from the surface and thereby causes even higher values of  $T_s$  and  $D_s$ . This combination of circumstances highly favours the occurrence of midday stomatal closure (see also Section 5.6).

The predicted change in  $\lambda E/Q^*$  varies from -10% to -30% with PBL feedback and with humidity response. Note that the latter figure is related to an exceptionally strong increase in  $r_s$  for the TRO conditions. There are two ways in which the effect of PBL feedback can be seen from the predicted changes in  $\lambda E/Q^*$  (Figs. 5.2C and 5.2D). First, equal, and in some cases even larger changes in  $r_s$  result in smaller changes in  $\lambda E/Q^*$ . This is due to the drier and warmer atmosphere if  $\lambda E$  is smaller, which partly compensates the initial effect of the

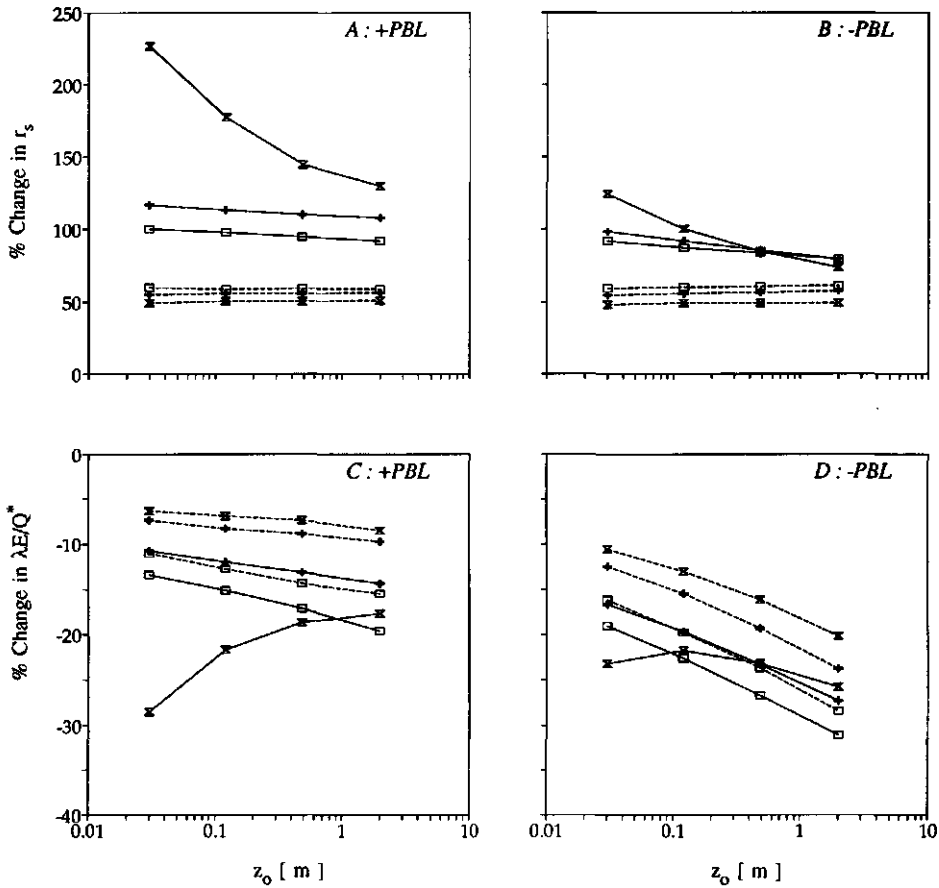


FIGURE 5.2. Predicted relative changes in the surface resistance ( $r_s$ ; A and B) and the normalized transpiration ( $\lambda E/Q^*$ ; C and D) of  $C_3$  canopies ( $LAI=5$ ) for a change in ambient  $CO_2$  from  $1 \times CO_2$  to  $2 \times CO_2$ . The changes are given versus roughness length,  $z_0$  (logarithmic scale). Left panels: with PBL feedback (A and C); right panels: SL feedback only (B and D). Solid lines: with stomatal humidity response; dashed lines: without stomatal humidity response. Squares: SAS conditions; pluses: MLS conditions; hourglasses: TRO conditions.

increased  $r_s$  on  $\lambda E$  (see Chapter 2). Second, except for the simulations with the TRO conditions, the predicted changes in  $\lambda E/Q^*$  increase with increasing  $z_0$ , but the slope is much larger without PBL feedback. It follows that, consistent with the results of Chapter 2, the difference between the results with PBL feedback and those without PBL feedback increases as  $z_0$  increases. High values of  $z_0$  result in relatively low values of  $r_a$ , so that the surface and

the atmosphere are well coupled (Jarvis & McNaughton, 1986). In other words, the atmosphere is better able to impose its changes on the surface. The TRO simulations cannot be compared in this way. Results from these simulations indicate that the processes related to plant physiology can become dominant, but, in addition, it can be seen that the importance of these processes is partly related to interaction with the PBL.

### 5.4.3 Changes of $r_s$ and $\lambda E/Q^*$ : $C_4$ canopies

The relative changes of  $r_s$  and of  $\lambda E/Q^*$  for a change in ambient  $CO_2$  from  $1xCO_2$  to  $2xCO_2$  in the case of a  $C_4$  canopy are given in Fig. 5.3. The changes have been plotted on the same scale used in Fig. 5.2, in order to facilitate a comparison with  $C_3$  canopies.

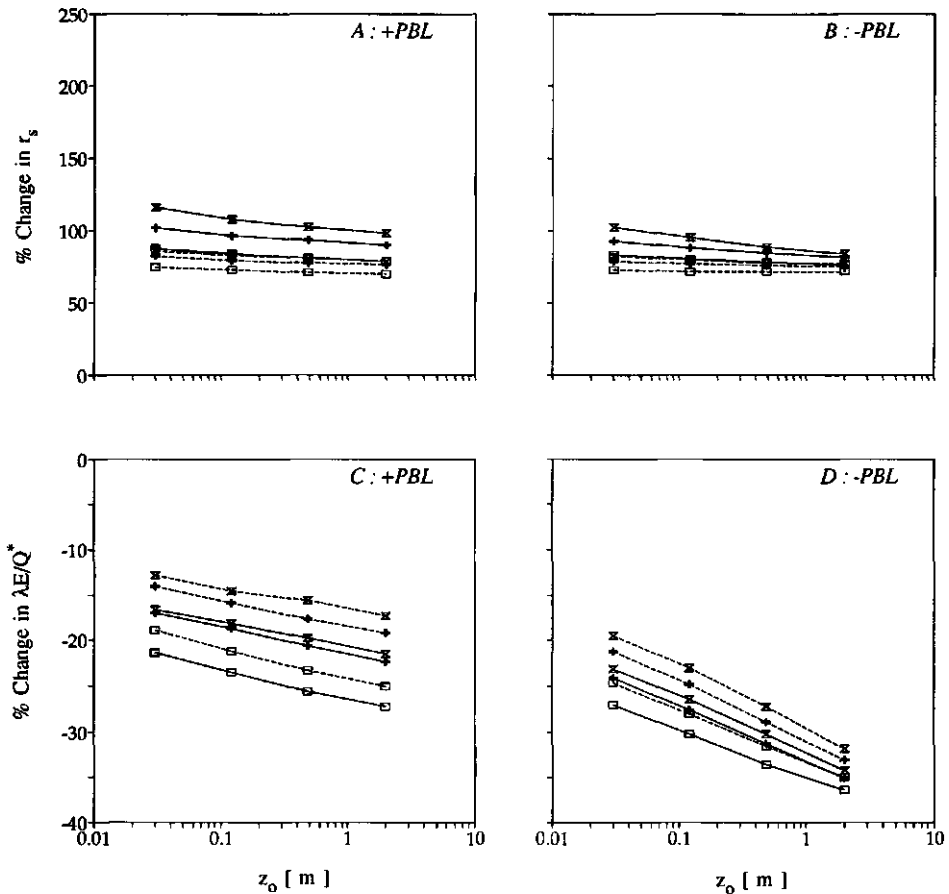


FIGURE 5.3. As in Fig. 5.2, but for  $C_4$  canopies.

For C<sub>4</sub> canopies the predicted changes in  $r_s$  without accounting for the humidity responses, about +75%, are larger than for C<sub>3</sub> canopies (Fig. 5.3 A and B versus Fig. 5.2 A and B). The predictions for C<sub>4</sub> canopies agree reasonably well with the results of the analysis by Morison (1987), who found an average change of +67% for doubled CO<sub>2</sub>. Again, accounting for the humidity deficit leads to larger changes in  $r_s$ . The interaction of the vegetation and the PBL also augments the changes and leads to somewhat larger differences between the results for the different atmospheric conditions. However, the influence of humidity responses is not as large as in the case of C<sub>3</sub> canopies. No deviating behaviour occurs for the TRO conditions. Because of the higher optimum temperature of C<sub>4</sub> photosynthesis, a rising T<sub>s</sub> leads to a decreasing  $r_s$  for a much wider range of temperatures. This results in a higher transpiration rate and, therefore, in additional cooling of the leaves, which prevents excessive heating.

The smaller range of changes in  $r_s$  leads to a smaller range of changes in  $\lambda E/Q^*$ . Predicted changes in  $\lambda E/Q^*$  range from -16% to -27% with PBL feedback and with humidity response (Figs. 5.3C and 5.3D). Larger changes in  $\lambda E$  for C<sub>4</sub> species in comparison with C<sub>3</sub> species have also been reported by Rosenberg (1981) and Cure & Acock (1986). The presence of PBL feedback is visible in the same ways as in the results for C<sub>3</sub> canopies.

#### 5.4.4 Influence of diurnal evolution of CO<sub>2</sub> at reference height

The effect of the diurnal evolution of C<sub>r</sub> on  $r_s$ ,  $\lambda E$ , and on the predicted changes can be evaluated by comparing the results of the simulations of Set III to those of Set IX (see Table 5.1). Results of this comparison are summarized in Table 5.2, where the range of obtained differences between results of the two sets of simulations is given. It can be seen that these differences are rather small. With diurnal variation of CO<sub>2</sub> at z<sub>r</sub>, C<sub>r</sub> will be smaller during daylight hours than is the case if C<sub>r</sub> remains fixed at the initial value. Therefore,  $r_s$  is somewhat larger so that  $\lambda E/Q^*$  is slightly lower in most cases. Because  $r_s$  is systematically less overestimated for 2xCO<sub>2</sub> than for 1xCO<sub>2</sub>, the predicted change in  $r_s$  is underestimated. The error introduced by ignoring the diurnal variation of C<sub>r</sub> ranges from -2.3% to -6.3%. The predicted change in  $\lambda E$  may be overestimated or underestimated, the range of errors being from -2.3% to +2.9%.

It is concluded that, in general, no serious errors are made in the prediction of relative changes in  $\lambda E/Q^*$  from daily averages if the diurnal evolution of CO<sub>2</sub> is ignored.

TABLE 5.2. Influence of the diurnal evolution of the CO<sub>2</sub> concentration at z<sub>r</sub> on  $r_s$ ,  $\lambda E/Q^*$ , and on the predicted changes in these variables. The numbers denote the minimum and the maximum relative difference between the simulations with and without CO<sub>2</sub>. The results of the calculations with diurnal evolution of CO<sub>2</sub> have been used as the reference.

Canopy	$\Delta(r_s)$ {1xCO <sub>2</sub> } [ % ]	$\Delta(r_s)$ {2xCO <sub>2</sub> } [ % ]	$\Delta(\lambda E/Q^*)$ {1xCO <sub>2</sub> } [ % ]	$\Delta(\lambda E/Q^*)$ {2xCO <sub>2</sub> } [ % ]	$\Delta(\Delta r_s)$ [ % ]	$\Delta(\Delta \lambda E/Q^*)$ [ % ]
C <sub>3</sub>	2.4,4.2	1.0,2.4	-0.9,-0.1	-0.7,-0.3	-2.3,-4.6	-2.3,+2.1
C <sub>4</sub>	2.0,4.9	0.5,1.8	-1.4,-0.9	-0.7,-0.5	-3.4,-6.3	-1.6,+2.9

## 5.5 Further analysis of the humidity responses

### 5.5.1 Introduction

The results presented in the previous section show that the stomatal humidity response may considerably enhance the initial effect of  $\text{CO}_2$  on  $r_s$ . The difference between the cases with and without humidity responses is at least as large as the difference caused by the doubled ambient  $\text{CO}_2$  concentration. The biosphere-atmosphere interaction enhances this secondary response. For these reasons, the parameterization of the humidity response is further investigated in this section.

The further analysis will be performed by considering the relative sensitivity of  $r_s$  and  $\lambda E$  to  $D_{\max}$  and  $f_o$ , respectively. Similarly, the changes of  $D_s$  which are related to changes of ambient  $\text{CO}_2$  are examined in terms of a relative sensitivity. It is recalled that the relative sensitivity of a variable  $V$  to any parameter  $x$  is defined by:

$$\Xi_{(V,x)} = \frac{\partial V}{\partial x} \frac{x}{V} \approx \frac{\Delta V}{\Delta x} \frac{x}{V} \quad [5.10]$$

(Saxton, 1975; Chapter 2). Thus, a change of  $y\%$  in  $x$  implies a change of  $\Xi_{(V,x)}$  times  $y\%$  in  $V$ . The relative sensitivities are explored theoretically and also by using results of additional simulations. Furthermore, the influence of the PBL is investigated by means of the feedback factor  $F$ , which is given by:

$$F = \frac{\Xi_{(V,x),PBL}}{\Xi_{(V,x),SL}} \quad [5.11]$$

(see Chapter 2). Here, the additional subscript PBL denotes "PBL feedback plus SL feedback" while SL denotes "SL feedback only."

### 5.5.2 Sensitivity of $r_s$ and $\lambda E/Q^*$ to $D_{\max}$ and $f_o$

#### a) Theory

The characteristics of the relative sensitivity of  $r_s$  to  $D_{\max}$  and  $f_o$  can be roughly explored as follows. If  $g_c$  and the effect of transpiration on  $A_{nc}$  may be neglected and  $R_d$  has vanished,  $r_s$  is given by

$$r_s = \frac{C_s - C_i}{1.6A_{nc}} \quad [5.12]$$

where  $C_s - C_i$  is a virtual concentration difference (Chapter 3). Note that the nonlinear character of [5.12] has been ignored, which does not cause a serious error here because the variables are either treated as a constant, or infinitesimal small changes are assumed. Furthermore

$$f = \frac{C_i - \Gamma}{C_s - \Gamma} = f_o \left(1 - \frac{D_s}{D_{\max}}\right) \quad [5.13]$$

so that

$$r_s = \frac{(C_s - \Gamma) \left(1 - f_o \left[1 - \frac{D_s}{D_{\max}}\right]\right)}{1.6A_{nc}} \quad [5.14]$$

The relative sensitivities then become

$$\Xi_{(rs, D_{\max})} \equiv \frac{\partial r_s}{\partial D_{\max}} \frac{D_{\max}}{r_s} = -f_o \frac{D_s}{D_{\max}} \frac{C_s - \Gamma}{1.6r_s A_{nc}} = -f_o \frac{D_s}{D_{\max}} \frac{1 - \Gamma/C_s}{1 - C_i/C_s} \quad [5.15]$$

and

$$\Xi_{(rs, f_o)} \equiv \frac{\partial r_s}{\partial f_o} \frac{f_o}{r_s} = -f_o \left(1 - \frac{D_s}{D_{\max}}\right) \frac{C_s - \Gamma}{1.6r_s A_{nc}} = -\frac{C_i/C_s - \Gamma/C_s}{1 - C_i/C_s} \quad [5.16]$$

for  $D_{\max}$  and  $f_o$  respectively. It is noted that the relative sensitivity of  $r_s$  to  $D_s$  (or  $D_s/D_{\max}$ ) is also given by [5.15].

[5.15] and [5.16] show that changes of  $D_{\max}$  will mainly influence the results at higher values of  $D_s$ , while changes of  $f_o$  affect the results at low values of  $D_s$ . Both sensitivities are smaller for  $C_4$  canopies than for  $C_3$  canopies because  $C_i/C_s$  for  $C_3$  plants will, in general, be larger. In other words,  $r_s$  of  $C_4$  canopies is less sensitive to humidity than is  $r_s$  of  $C_3$  canopies. Furthermore, under otherwise similar conditions, an increasing CO<sub>2</sub> concentration may slightly influence the sensitivity of  $C_3$  plants because  $A_{nc}$  will become somewhat larger. Finally,  $|\Xi_{(rs, D_{\max})}|$  and  $|\Xi_{(rs, f_o)}|$  will be larger at leaf temperatures where  $A_{nc}$  is inhibited.

The sensitivities of  $\lambda E/Q^*$  to  $D_{\max}$  and  $f_o$  and their characteristics will be a combination of [2.14] and [5.14] and [5.15], respectively. It can be shown that, as a first approximation, the sensitivities may be written as, using the Penman-Monteith equation [2.7]:

$$\Xi_{(\lambda E/Q^*, x)} \equiv \frac{\partial(\lambda E/Q^*)}{\partial x} \frac{x}{(\lambda E/Q^*)} = \frac{-1.6A_{nc}\gamma\Xi_{(rs, x)}}{(s+\gamma)r_a + \gamma(C_s - \Gamma)(1-f)} \quad [5.17]$$

where  $x$  denotes  $D_{\max}$  or  $f_o$  and other symbols are as in Chapter 2.

### b) Simulations and results

Further simulations were performed in order to determine the relative sensitivities of  $r_s$  and  $\lambda E/Q^*$  to  $D_{\max}$  and  $f_o$ , and to assess the influence of PBL feedback. First,  $D_{\max}$  was varied between 40 and 50 g kg<sup>-1</sup>, in steps of 5 g kg<sup>-1</sup>, while  $f_o$  was kept as 0.85 for  $C_3$  plants and 0.5 for  $C_4$  plants. Next,  $f_o$  was varied in steps of 0.05 between 0.80 and 0.90 for  $C_3$  plants

and between 0.45 and 0.55 for  $C_4$  plants while  $D_{\max}$  was kept as  $45 \text{ g kg}^{-1}$ . In addition, runs were performed for  $C_4$  canopies, in which the potential temperature of the initial TRO profile was increased by 5 K at each level. The simulations were performed with and without PBL feedback. Without PBL feedback the conditions at  $z_r$  were taken as in the simulations with PBL feedback, both for  $1x\text{CO}_2$  and for  $2x\text{CO}_2$ . Other conditions were as previously described (Section 5.3.2 and 5.3.3). The sensitivities were determined from finite differences between mean values for 6 to 18 LT (see also Chapter 2).

The calculated sensitivities to  $D_{\max}$  and  $f_o$  corresponded rather well to the predictions by [5.15] and [5.16] except at high temperatures, when other parameters (such as  $A_{\min}$  and  $g_c$ ) become too important to be ignored (results not shown here). Furthermore, many parameters may no longer be considered as constant. An example is  $A_{\text{nc}}$ , which, at high temperatures, dramatically decreases with decreasing  $D_{\max}$ .

The ratios  $F$  ([5.11]) of the relative sensitivities of  $r_s$  to  $D_{\max}$  and  $f_o$  are shown in Fig. 5.4 A and B and those of the relative sensitivities of  $\lambda E/Q^*$  in Fig. 5.4 C and D.  $F$  is shown as a function of  $T_s - T_{\text{opt}}$ , where  $T_s$  is the average leaf temperature in the undisturbed case, that

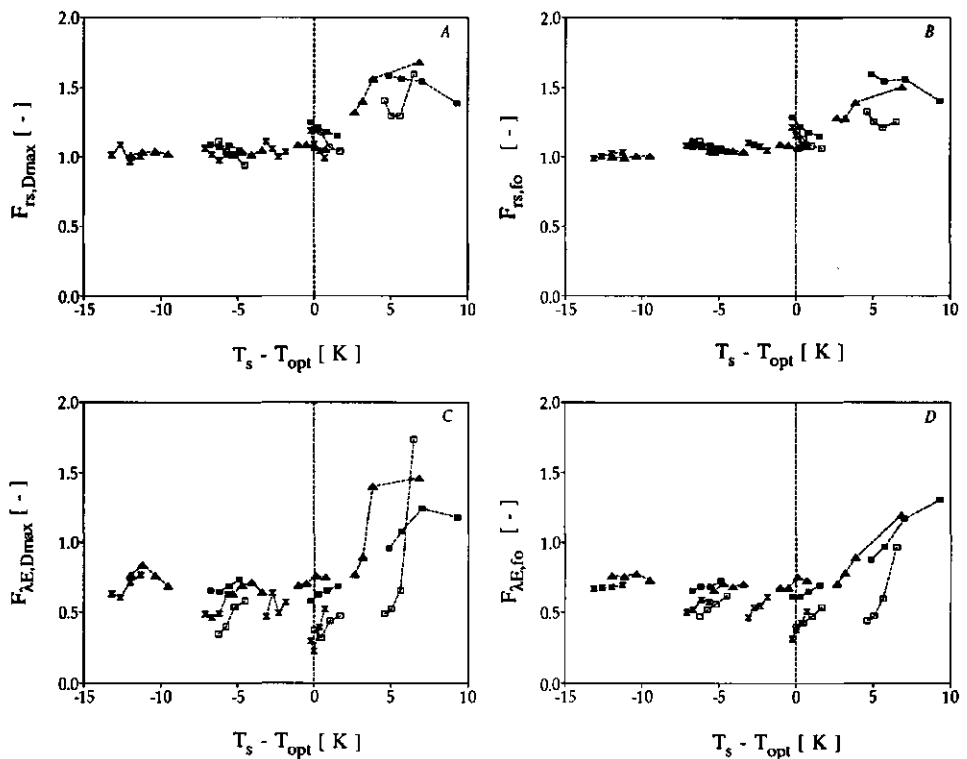


FIGURE 5.4. Feedback factor  $F$ , defined by [5.11], for the relative sensitivities of: A)  $r_s$  to  $D_{\max}$ ; B)  $r_s$  to  $f_o$ ; C)  $\lambda E$  to  $D_{\max}$ ; D)  $\lambda E$  to  $f_o$ . Open squares:  $C_3$  canopy,  $1x\text{CO}_2$ ; Solid squares:  $C_3$  canopy,  $2x\text{CO}_2$ ; Hourglasses:  $C_4$  canopy,  $1x\text{CO}_2$ ; Triangles:  $C_4$  canopy,  $2x\text{CO}_2$ .

is, using the default values for  $D_{\max}$  and  $f_o$ .  $T_{\text{opt}}$  is the estimated optimum temperature for photosynthesis. It is taken 34 °C for C<sub>4</sub> photosynthesis and 25 and 27 °C for C<sub>3</sub> photosynthesis at 1xCO<sub>2</sub> and 2xCO<sub>2</sub>, respectively. It can be seen that the sensitivities of  $r_s$  are hardly influenced by PBL feedback, up to values of the average  $T_s$  that approach  $T_{\text{opt}}$ . If  $T_s > T_{\text{opt}}$ , the influence of PBL feedback is clearly visible. Then, PBL feedback may increase the sensitivities by over 50%. The sensitivities of  $\lambda E/Q^*$  (Fig. 5.4 C and D) are reduced by PBL feedback to 30-80% of the sensitivities without PBL feedback if  $T_s < T_{\text{opt}}$ . If  $T_s > T_{\text{opt}}$ ,  $F_{\lambda E/Q^*}$  increases rapidly, especially for C<sub>3</sub> canopies (squares), and eventually becomes >1. The effect of the PBL on  $\lambda E/Q^*$  is much more pronounced than its effect on  $r_s$ . This was to be expected because the fluxes are directly influenced by the state of the PBL, while  $r_s$  is only indirectly influenced.

Both for  $r_s$  and for  $\lambda E/Q^*$ , the results confirm the existence of a positive feedback sequence if  $T_s > T_{\text{opt}}$  and in which the PBL plays a crucial role. This will be discussed further in Section 5.6.

### 5.5.3 Concurrent changes of D<sub>s</sub> and ambient CO<sub>2</sub>

#### a) Theory

To get an impression of the main controls of the relative sensitivity of D<sub>s</sub> to C<sub>r</sub>, consider, for simplicity, the sensitivity of D<sub>s</sub> to (C<sub>s</sub> - Γ). With  $\rho D_s = r_s E$ , it can be shown that, neglecting humidity responses of the stomata (f = constant) and using [5.12], [5.14], and the Penman-Monteith equation for λE ([1.1]),

$$\Xi_{(D_s, C_s - \Gamma)} \equiv \frac{\partial D_s}{\partial (C_s - \Gamma)} \frac{(C_s - \Gamma)}{D_s} = \frac{1}{1 + \frac{\gamma}{s + \gamma} \frac{(C_s - \Gamma)(1 - f)}{1.6A_{nc} r_a}} \quad [5.18]$$

According to [5.18], D<sub>s</sub> of C<sub>3</sub> canopies (1-f≈0.3) changes more than that of C<sub>4</sub> canopies (1-f≈0.6) under otherwise similar conditions. The sensitivity is smaller at higher CO<sub>2</sub> concentrations. Furthermore,  $\Xi_{(D_s, C_s - \Gamma)}$  will increase with increasing temperature and decreasing z<sub>0</sub> (that is, increasing r<sub>a</sub>).

#### b) Simulations and results

In order to determine the relative sensitivities of D<sub>s</sub> to C<sub>r</sub>, simulations were performed with the initial atmospheric CO<sub>2</sub> concentrations taken as 340 or 350 μmol mol<sup>-1</sup> in the 1xCO<sub>2</sub> cases, and 680 or 700 μmol mol<sup>-1</sup> in the 2xCO<sub>2</sub> cases, respectively. In these simulations the diurnal variation of C<sub>r</sub> was ignored so that the changes of C<sub>r</sub> were well determined. The simulations were performed with and without PBL feedback. Without PBL feedback the conditions at z<sub>r</sub> were taken as in the simulations with PBL feedback, both for 1xCO<sub>2</sub> and for 2xCO<sub>2</sub>. Other conditions were as previously described (Section 5.3.2 and 5.3.3). The sensitivities were determined from finite differences between mean values for 6 to 18 LT (see also Chapter 2).



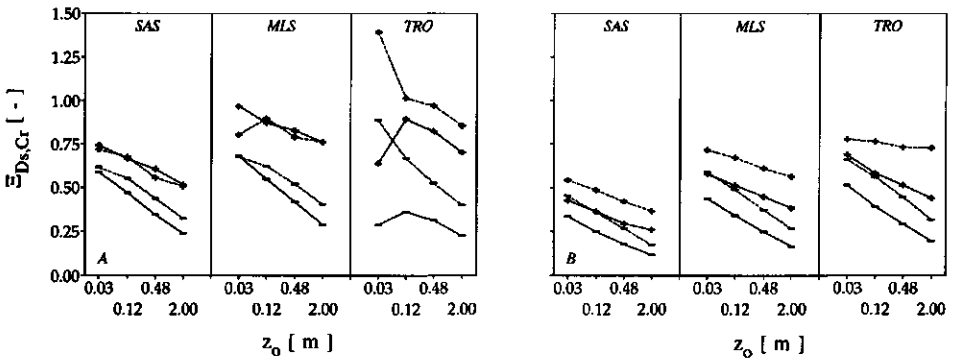
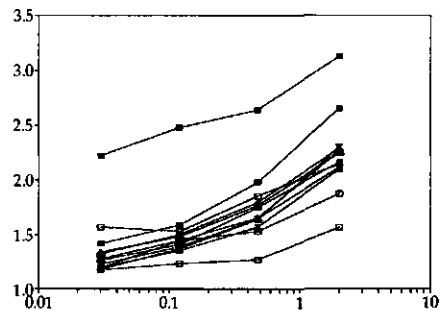


FIGURE 5.5. The relative sensitivities of  $D_s$  to  $C_r$  for A)  $C_3$  canopies and B)  $C_4$  canopies as a function of  $z_0$  (logarithmic scale). Panels from left to right: SAS conditions, MLS conditions and TRO conditions. Dotted lines:  $1xCO_2$ ; solid lines:  $2xCO_2$ . +: with PBL feedback; -: without PBL feedback.

The relative sensitivities  $\Xi_{(D_s, C_r)}$  are given in Fig. 5.5 for  $C_3$  canopies (A) and  $C_4$  canopies (B), respectively. The results with PBL feedback are shown as the curves with + and those without PBL feedback as the curves with -. Furthermore, the dashed lines and the solid lines denote the results of the  $1xCO_2$  simulations and  $2xCO_2$  simulations, respectively. The values of the ratio  $F$  are depicted in Fig. 5.6. Here, the results for the  $C_3$  canopies are represented by the squares and those of the  $C_4$  canopies by the triangles. Open symbols and closed symbols are used to denote results at  $1xCO_2$  and  $2xCO_2$ , respectively. It can be seen that  $D_s$  changes roughly between 0.1% and 1% per 1% change in  $C_r$ . The PBL clearly influences the changes of  $D_s$ . In most cases PBL feedback increases the changes in  $D_s$  by a factor 1.2 at  $z_0 = 0.03m$  up to a factor 2 at  $z_0 = 2.0 m$ . With PBL feedback, the minimum change in  $D_s$  is 0.3% per 1% change in  $C_r$ . Exceptionally high values of  $F$  are obtained for  $C_3$  canopies under TRO conditions at a doubled  $CO_2$  concentration. This confirms the important role of the PBL in the positive feedback mechanism at  $T_s > T_{opt}$ . Note that much of the variation in the relative sensitivities can be explained with reference to [5.18].

FIGURE 5.6. The ratio  $F$ , defined by [5.11], for the relative sensitivities of  $D_s$  to  $C_r$  as a function of  $z_0$  (logarithmic scale). Squares:  $C_3$  canopies; Triangles,  $C_4$  canopies. Shaded symbols:  $1xCO_2$ ; Black symbols:  $2xCO_2$ .



## 5.6 Discussion

### 5.6.1 Significance of PBL-vegetation interaction at the regional scale

The present study shows that the interaction between the PBL and vegetation has a strong influence on changes in  $r_s$  and  $\lambda E/Q^*$ . Therefore, PBL feedback must be accounted for if changes in  $r_s$  and  $\lambda E/Q^*$  are to be *predicted at the regional scale*. The cases considered in this study apply to changes which are due to the direct effect of elevated ambient CO<sub>2</sub> on the stomata. However, it is expected that similar conclusions can be made in cases where other disturbances at the surface are considered. Examples were given in Chapter 2.

In addition, the results of the present study indicate that  $r_s$  may change by at least 100%. This prediction is a factor 1½ or more greater than earlier predictions based on results of plant-physiological research. Reports from such research quote 50%-75% as a reasonable estimate for an "average plant" (Cure & Acock, 1986; Morison, 1987). The reason for the difference is that the primary response to elevated CO<sub>2</sub> indirectly produces a strong, secondary humidity response. This secondary response causes  $r_s$  to increase more than what might have been expected from a change in CO<sub>2</sub> alone. Most of the secondary effect on the stomata is due to SL feedback, but PBL feedback enhances it. Without PBL feedback, a 1% change in the CO<sub>2</sub> concentration at the reference level (10 m) is accompanied by an increase in  $D_s$  of typically between 0.1% and 1%. The present study suggests that PBL feedback increases these changes by a factor of between 1.2 at low values of  $z_o$  and 2 or higher at high values of  $z_o$ . Results from previous plant physiological research obtained from controlled environment experiments and from experiments at small scale field plots can therefore not be used *directly* to predict changes of  $r_s$  for extensive vegetated surfaces from given changes in the CO<sub>2</sub> concentration alone. SL feedback as well as PBL feedback must be accounted for.

Results from the coupled model indicate that, under an approximately doubled ambient CO<sub>2</sub> concentration, the regional transpiration of dense, well-watered canopies may be reduced by 10% - 30%. The resulting change depends, amongst other things, on atmospheric conditions, aerodynamic roughness and plant class (C<sub>3</sub> or C<sub>4</sub>). The impact of the PBL on the resulting changes is twofold. First, a negative PBL feedback strongly moderates the changes in transpiration which are due to the (enlarged) change of  $r_s$ . This conclusion is consistent with the conclusion of Chapter 2. Second, PBL feedback together with SL feedback controls changes within the vegetation, notably changes in  $D_s$ . These changes trigger a secondary effect on  $r_s$  by which the primary changes are enlarged. This is a positive feedback mechanism.

The positive feedback mechanism was not considered in earlier predictions, including the predictions made in Chapter 2, and those by De Bruin & Jacobs (1993). Also, it was not considered by Jarvis & McNaughton (1986), Gifford (1986) and Eamus (1991), who argued that the effect of CO<sub>2</sub> as a global anti-transpirant is insignificant due to the many *negative* feedbacks. However, a final conclusion about the importance of CO<sub>2</sub> as an anti-transpirant can only be made if all the significant feedbacks, both positive and negative, are taken into

account. These include feedbacks provided by the interaction between the vegetation and the soil. Furthermore, a variety of plant physiological feedbacks may be present, for example, enhanced root growth (Stulen & Den Hertog, 1993), allocation of photosynthetic products (Stitt, 1991) with possible effects on the photosynthesis characteristics (Long *et al.*, 1993), and decreases in the number of stomata per unit leaf area (Woodward, 1993). Much work has to be done in this field, and an interdisciplinary approach is required here.

The results of this study are in qualitative agreement with the  $\Omega$  concept of Jarvis & McNaughton (1986) as far as the influence of roughness on PBL feedback is concerned. It is recalled that  $\Omega$  is a decoupling coefficient defined by (McNaughton & Jarvis, 1983; Jarvis & McNaughton, 1986):

$$\Omega = \left[ 1 + \frac{\gamma}{s + \gamma} \frac{r_s}{r_a} \right]^{-1} \quad [5.19]$$

The atmosphere and the surface are well coupled if  $\Omega$  is low, for example, in the case of rough surfaces where  $r_a$  is low. As such,  $\Omega$  describes the degree to which changes at  $z_r$  will be imposed on the surface. This depends not only on (the changes in)  $r_a$ , but also on  $r_s$  and on temperature. Consistent with this approach, it was found here that the influence of the PBL is larger at higher  $z_0$ . From the results presented in the present chapter, this can be seen in two ways. First, PBL feedback reduces the slope of the relation between the predicted changes of  $\lambda E/Q^*$  and  $z_0$ . Second, the effect of the PBL on changes in  $D_s$  that are triggered by changes in  $C_r$  is larger at higher values of  $z_0$ . Other examples are given in Chapter 2. However, the  $\Omega$  concept should be used with caution, because of its severe limitations. For instance, in Chapter 2 it was argued that  $\Omega$  is a sensitivity and, therefore, depends on the degree of coupling itself. In addition, the influence of PBL feedback on the sensitivities of  $\lambda E/Q^*$  to  $r_a$  and  $r_s$  were found not to be entirely consistent with the  $\Omega$  concept. Another limitation includes the limited scope of [5.19], that is,  $\Omega$  can never account for the many nonlinear feedback processes which are encountered in scaling up from the stomatal pore to the region (McNaughton & Jarvis, 1991).

## 5.6.2 Controls in the PBL-vegetation interaction

### a) Control diagram

For a further discussion of the results, it may be helpful to consider the different interactions by means of a control diagram such as presented by McNaughton & Jarvis (1991). They used this type of diagram to illustrate the effects of up-scaling on the control of transpiration by stomatal resistance. Here, it will be used qualitatively as an aid in the discussion of the results presented in the previous sections.

Figure 5.7 presents the control diagram of the processes *in the context of the current vegetation model*. The feedbacks are included by means of the controls  $\partial x/\partial y$ , called "gain" by McNaughton & Jarvis (1991). Changes of the system variables,  $dx$  and  $dy$ , are influenced by other changes and are controlled by the gains. For example, the change in  $r_s$ ,  $dr_s$ , results

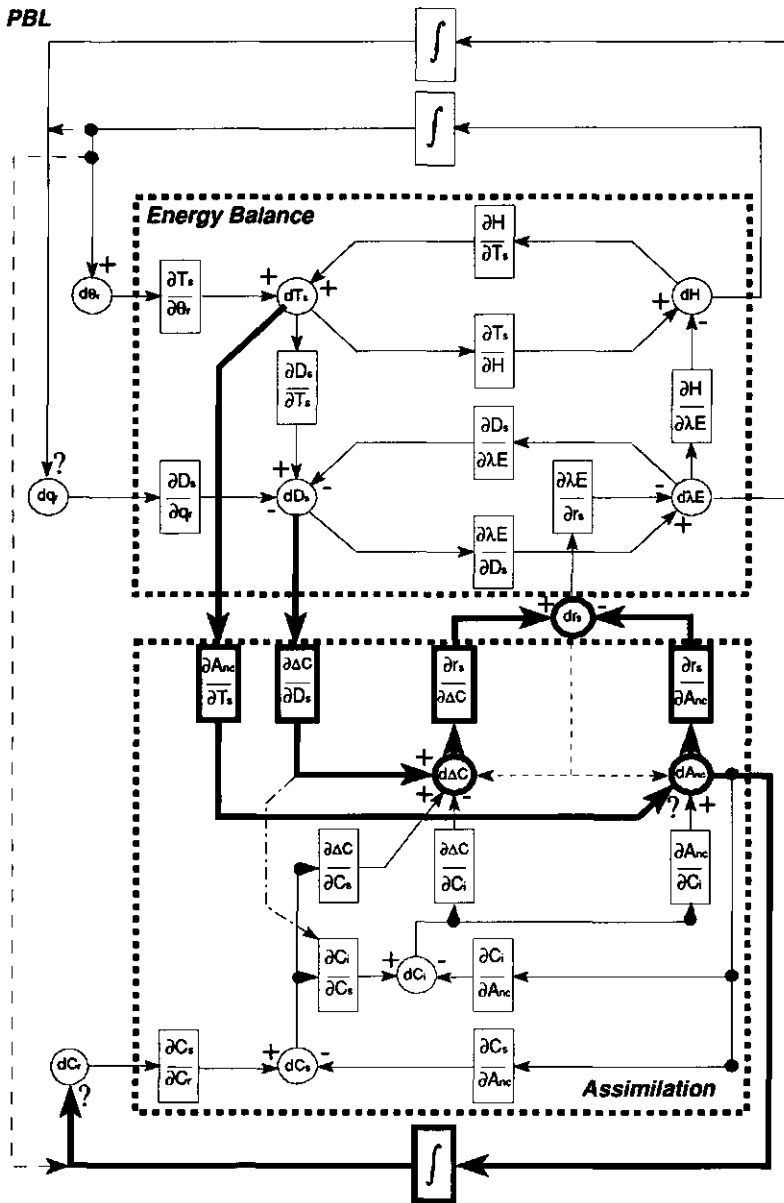
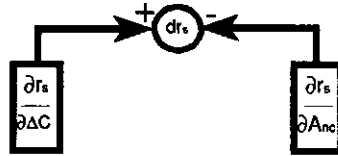


FIGURE 5.7. Partial representation of the controls of the surface resistance,  $r_s$ , and the regional transpiration,  $\lambda E$ , accounted for by the current PBL-vegetation model. Essential differences with the control diagram by McNaughton & Jarvis (1991) are indicated by means of the bold lines. Boxes represent the controls or gains, circles represent changes. Signs indicate the sign of the gain. The dashed-dotted arrow symbolizes that the humidity response is parameterized through an effect on  $\partial C_i / \partial C_s$ . The dotted arrows symbolize the effect of  $r_s$  on  $A_{nc}$  and on  $\Delta C$  is implicit in the model. The total effect of the nonlinear controls in the PBL is indicated by means of the integral symbols. Effects of a changing wind speed, available energy and externally driven processes are not included here.

from a change in  $A_{nc}$ ,  $dA_{nc}$ , and from a change of the concentration difference  $\Delta C$ ,  $d\Delta C$ , (with  $\Delta C = C_s - C_i$ ). This is depicted in the diagram as follows:



The plus and the minus signs indicate the sign of the gain and the effect of  $dy$  on  $dx$ . If the gain  $\partial x/\partial y$  is positive,  $x$  increases if  $y$  increases and it decreases if  $y$  decreases. Each of the controls can be determined as the fractional change at otherwise unchanged conditions, which makes them a sensitivity as defined by [2.6]. The total change  $dx$  is given by  $dy$  as controlled by the gains. In the example given above:

$$dr_s = \left( \frac{\partial r_s}{\partial \Delta C} \right)_{A_{nc}} d\Delta C + \left( \frac{\partial r_s}{\partial A_{nc}} \right)_{\Delta C} dA_{nc} \quad [5.20]$$

The upper part of the control diagram in Fig. 5.7 is the energy balance part. It depicts, in essence, SL feedback (see Fig. 2.1A). The lower part is the assimilation part, which shows "biological feedback."  $r_s$  is one of the links between the two parts. The outer part is the PBL part, which basically depicts PBL feedback (see Fig. 2.1B). The present diagram is equivalent to a synthesis of the diagrams given by McNaughton and Jarvis (1991). Below, it is discussed in more detail.

Essential differences with the control diagrams presented by McNaughton & Jarvis (1991) are indicated by means of the bold lines. Here,  $r_s$  is controlled by  $A_{nc}$  and  $\Delta C$ . Furthermore,  $A_{nc}$  depends on  $T_s$ , and the humidity response is coupled to the assimilation model through the parameterization of  $C_i/C_s$  as a function of  $D_s$ . This provides a much stronger link between the assimilation part (the lower part of the diagram) and the energy balance part (the upper part) than in McNaughton & Jarvis (1991). A third difference is the influence of  $\text{CO}_2$  in the PBL feedback. Although  $\text{CO}_2$  seems to have little effect on the results of this study, its contribution to PBL feedback has been depicted for completeness. The effect of  $r_s$  on  $A_{nc}$  and  $\Delta C$  is not explicit in the model; it is implicit through assumptions about the control  $\partial C_i/\partial C_s = k = f(D_s)$  (see Chapter 3 and 4). This is shown by means of the dotted lines starting at  $dr_s$ .

The complete system is depicted as a closed system. In reality, externally driven changes of  $\theta_r$ ,  $q_r$ , and  $C_r$  are present. Furthermore, there will be an exchange with the free atmosphere. These features are not described in the diagram. The control of changes in conditions at the reference level by the processes in the PBL are depicted in a highly simplified form. These changes depend on the integral of the changes in the fluxes  $H$ ,  $\lambda E$ , and  $A_{nc}$ , as indicated in the control boxes. In addition, the controls depend on a number of nonlinear processes of

which PBL growth and the concurrent entrainment process are the most important. The latter process is interesting in particular, because it depends on H (McNaughton & Jarvis, 1991; see also Fig. 2.1B).

Some other simplifications have also been made for clarity. For example, initially independent influences, such as that of PAR on  $A_{nc}$ , the effect of  $Q^*$  on  $T_s$ , the influence of wind speed as well as the influence of LAI have been omitted. Furthermore, the effect of  $D_s$  has been included as an influence on  $\Delta C$ . In reality, it has an influence on the sensitivity  $\partial C_i / \partial C_s = k$ . This is indicated by the dashed arrow starting at  $\partial \Delta C / \partial D_s$ .

In order to discuss the results presented in Section 5.4 and 5.5, consider the consequences of an increase of the ambient CO<sub>2</sub> concentration,  $C_r$ , by means of the control diagram presented above (Fig. 5.7). Assume that no further external perturbations are present.

*b) Primary effect on  $r_s$*

The increase of  $C_r$  will result in an increase of  $\Delta C$  through changes in  $C_s$  as well as in  $C_i$ . The latter changes depend on changes in the resistances (for example,  $r_a$  and  $r_s$ ), implicit in  $\partial C_i / \partial C_r$  and  $\partial C_i / \partial C_s$ . They depend also on concurrent changes in  $A_{nc}$ , which is shown as the gains  $\partial C_s / \partial A_{nc}$  and  $\partial C_i / \partial A_{nc}$ .  $dC_i$  is also controlled by the important gain  $\partial C_i / \partial C_s = k$ . Because  $k < 1$ ,  $dC_i < dC_s$ . Therefore and because  $\partial \Delta C / \partial C_s = 1$  and  $\partial \Delta C / \partial C_i = -1$ , the effect of an increase in  $C_r$  is to increase  $\Delta C$ . This leads to an increase in  $r_s$ . Because  $k$  is larger for  $C_3$  plants than for  $C_4$  plants,  $d\Delta C$  will be smaller for  $C_3$  canopies. Thus, the contribution of  $d\Delta C$  to  $dr_s$  will be smaller for  $C_3$  canopies than for  $C_4$  canopies. Furthermore, it can be seen that  $r_s$  is more sensitive to  $C_r$  at higher values of  $D_s$ , because  $k$  decreases as  $D_s$  increases (see Chapter 3 and 4). This conclusion is consistent with most of the evidence from plant physiological research as reviewed by Tyree & Alexander (1993). However, according to the present model,  $k$  will increase again towards very high values of  $D_s$  (Chapter 4), which de-sensitizes the stomata again. This would be consistent with reports that the sensitivity to  $C_r$  is less at high values of  $D_s$  (Tyree & Alexander, 1993). Thus, the current modelling approach may be able to combine the two features.

The rise of  $r_s$  as discussed in the previous paragraph will be compensated by an increasing  $A_{nc}$ , which is controlled by  $\partial A_{nc} / \partial C_i$ . This gain is the average slope of the  $C_i$  response curve of photosynthesis between  $C_i$  and  $C_i + dC_i$ . At the current value of  $C_r$ , the actual  $C_i$  will be found beyond the quasi-linear part of the curve (see Chapter 3). Thus, it may be expected that the relative increase in  $A_{nc}$  will be less than that of  $C_i$ , so that  $dA_{nc}$  will not be able to entirely compensate for  $d\Delta C$ . Indeed, in the case of  $C_4$  canopies the increase of  $A_{nc}$  due to a rising  $C_r$  is very small (see Appendix 13). The increase is somewhat larger for  $C_3$  canopies.

The reasoning in the previous paragraphs is valid if  $k$  remains constant, that is, if there is no humidity response that affects  $\partial \Delta C / \partial D_s$ . Then, it follows that  $r_s$  of  $C_4$  plants increases more than that of  $C_3$  plants ( $\approx 75\%$  versus  $\approx 50\%$ ). This is because the change of  $\Delta C$  is larger, but the compensation due to the increase of  $A_{nc}$  is smaller. The results presented in Section 5.5.2 for the simulations without stomatal humidity response are consistent with this reasoning (Fig.

5.2 and 5.3, dashed lines). These changes are consistent with the predictions by Cure & Acock (1986) and Morison (1987). However, Morison (1987) found no significant difference between  $C_3$  and  $C_4$  plants with respect to the effect of  $CO_2$  on the stomata, but  $D_s$  was probably not controlled in most of the cases he discusses. Furthermore, he considers the effect of  $CO_2$  on  $g_s$ , which may obscure changes in  $r_s$ . Stronger decreases of  $\lambda E$  for  $C_4$  species have been reported by Rosenberg (1981) and Cure & Acock (1986). These indirectly confirm the results of this study with respect to  $r_s$ .

*c) Effect on  $\lambda E$ , and SL feedback*

An increase of  $r_s$  as discussed above will have the following consequences, represented in the energy balance part of the control diagram. First,  $\lambda E$  will decrease. If all other circumstances remain equal, this amount of energy is now available to the sensible heat flux,  $H$ , which therefore increases. This can only be achieved if  $T_s$  increases. As a consequence,  $D_s$  increases as well, and this stimulates  $\lambda E$  somewhat ( $\partial\lambda E/\partial D_s$ ). Without feedback to the assimilation part, that is, without the humidity responses and the effect of the temperature on  $A_{nc}$ , an equilibrium will be established in which the original change of  $\lambda E$  will have decreased somewhat. Thus, it is a negative feedback. This sequence of feedbacks is part of SL feedback (Chapter 2).

The equilibrium will be influenced by the aerodynamic resistance,  $r_a$  (see Chapter 2 and Appendix 2), which affects the gain  $\partial H/\partial T_s$  and  $\partial T_s/\partial H$ . (Note that the latter gain can also be represented by a gain  $\partial T_s/\partial \lambda E$ .) If  $r_a$  is high, for instance, at low values of  $z_0$  and at a low wind speed, the release of heat from the surface is hampered. This leads to relatively high values of  $T_s$  and of  $D_s$ . In its turn, this stimulates  $\lambda E$  more, so that the sensitivity of  $\lambda E$  to  $r_s$  is reduced (see also [2.14]). Note that the higher  $T_s$  can have important consequences for the biological feedback which is discussed later.

LAI influences the SL feedback through its effect on  $r_s$  and therefore on the gain  $\partial D_s/\partial \lambda E$ . It can be shown that this gain is proportional to  $r_s$ . Because  $r_s$  is lower at high LAI, the increase in  $D_s$  due to the decrease in  $\lambda E$  is less at higher values of LAI ( $\partial D_s/\partial \lambda E$  is negative). This mechanism helps to prevent the occurrence of midday stomatal closure.

The SL feedback will also be influenced by the radiation components (shortwave, longwave). These will not be discussed here. Furthermore changes at the reference level,  $dT_r$  and  $dq_r$  are of importance. These changes are part of the PBL feedback which will be discussed below.

*d) Coupling between energy balance and physiological processes: secondary effect on  $r_s$*

Now consider the impact of the interaction between the assimilation part and the energy balance part through the effect of  $D_s$  on  $\Delta C$  and of  $T_s$  on  $A_{nc}$  if  $r_s$  has increased so that  $\lambda E$  has decreased (see above). The changes cause  $D_s$  and, therefore,  $\Delta C$  to increase as well, which augments the original perturbation of  $r_s$ . Thus, the humidity response introduces a *positive feedback* on  $r_s$ . As was explained above, LAI will decrease the magnitude of this positive feedback.

The total impact of this positive feedback depends on the leaf temperature which also increases. If  $T_s < T_{opt}$ , the gain  $\partial A_{nc}/\partial T_s$  is positive. Then the additional increase in  $\Delta C$  through  $dD_s$  is accompanied by an additional increase in  $A_{nc}$  through  $dT_s$ , which provides a negative feedback on  $r_s$ . It follows that the system is stabilized somewhat. However, if  $T_s > T_{opt}$ , the gain  $\partial A_{nc}/\partial T_s$  is negative and so,  $A_{nc}$  decreases, by which  $r_s$  increases. This provides a positive feedback on  $r_s$ , by which the system is destabilized.  $C_4$  plants are somewhat protected from this mechanism because their stomata are less sensitive to humidity (Section 5.5) and because of their higher optimum temperature (Section 3.4). This explains the tremendous differences between the results for  $C_3$  plants and those of  $C_4$  plants under TRO conditions (Section 5.4.1 and 5.4.2). Furthermore, it is consistent with the notion that  $C_4$  plants are better adapted to warmer environments than are  $C_3$  plants. Note that the increase of the optimum temperature for  $C_3$  plants under  $2\times CO_2$  (see Section 3.4) will also protect  $C_3$  plants somewhat against this mechanism.

The value of  $z_0$  will now be important because of its effect on  $r_a$ . As has been explained earlier, higher values of  $r_a$  lead to higher surface temperature. Therefore,  $T_{opt}$  is exceeded earlier, which triggers the positive feedback mechanism at an earlier stage. This explains the large dependence of the results on  $z_0$  under the TRO conditions. Furthermore, it confirms the importance of  $z_0$  and the related roughness lengths for heat and moisture in meteorological studies.

#### e) PBL feedback

The processes in the PBL are schematically outlined in the outer part of the diagram (see also Fig. 2.1B). The extent to which the conditions at  $z_r$  are affected are determined by the height of the PBL and by its growth, which determines the entrainment. The latter process depends on  $H$  and affects the temperature as well as the humidity. Therefore, the entrainment will be an important factor in the impact of humidity responses. The impact of PBL feedback depends on a complicated set of nonlinear processes in the PBL. Perhaps the only way to estimate it properly is by means of model simulations such as in this study.

The PBL feedback on the fluxes is negative, that is, the initial changes in the fluxes are decreased by PBL feedback. This is clearly visible from the results presented in Chapter 2, and from a comparison of the changes in  $\lambda E/Q^*$  at a fixed value for the change in  $r_s$  (Chapter 5). If  $\lambda E$  decreases,  $H$  must increase. Thus, the PBL not only becomes drier, but also warmer as compared to the undisturbed situation. This stimulates  $\lambda E$  and hampers  $H$ . Up to this point, the results are consistent with those of Chapter 2.

However, the changes at the reference level also induce changes at the surface. These changes at the surface are larger if PBL feedback is present. This can be seen from the results in Section 5.5.3, where it was shown that the changes in  $D_s$  are typically larger by a factor of between 1.2 to 2 if PBL feedback is accounted for. Therefore, the PBL provides a positive feedback on  $r_s$  through the humidity response.  $D_s$  will change partly through a drying of the atmosphere which will be felt at the surface, and partly through an increase of  $T_s$ . The latter feature is partly due to SL feedback and partly to PBL feedback. It was shown above that the



change in  $T_s$  may provide either a negative feedback on  $r_s$  ( $T_s < T_{opt}$ ) or a positive feedback ( $T_s > T_{opt}$ ). The results presented here clearly show that once  $T_s > T_{opt}$ , PBL feedback enlarges the original positive feedback. It then enhances the sensitivity of  $r_s$  to humidity. This was demonstrated in Section 5.5.2, where the ratio  $F$  ([5.11]) for the sensitivity of  $r_s$  to  $D_{max}$  and to  $f_0$  remained about 1 if  $T_s < T_{opt}$ , but became larger than 1 if  $T_s > T_{opt}$ . In such cases, PBL feedback can result in even *larger* changes in  $\lambda E/Q^*$  than without PBL feedback (see Fig. 5.2).

### 5.6.3 Simulation of stomatal responses

The discussion given above will be valid for any extensive, densely vegetated surface of which  $r_s$  increases with increasing  $D_s$  and of which the response of  $r_s$  to  $T_s$  can be described by means of an optimum curve. The way that the model mimics these responses does not affect the principle behind the conclusions. The model used in this study is only one of the ways of achieving this. Up to now, it has been based on a limited number of observations (Chapter 3 and 4) and its generality has yet to be established.

In the present study, an increase of the ambient  $CO_2$  concentration was taken as the principle cause of an initial increase of  $r_s$ . However, the conclusions about the influence of the PBL-vegetation interaction on  $r_s$  is expected to be valid for any disturbance that causes the stomata to close, for example, a drying of the soil. In order to test this hypothesis, the present model should be extended with a model for the interaction between canopies and processes in the soil.

The main quantitative differences found here are related to midday stomatal closure, which occurs if the optimum temperature of photosynthesis,  $T_{opt}$ , is exceeded. This seems to suggest that it is a temperature response and not a humidity response. However, it can easily be demonstrated that low values of  $D_s$  prevent stomatal closure if  $T_s > T_{opt}$  while high values of  $D_s$  trigger stomatal closure if  $T_s < T_{opt}$  (Section 3.7). This agrees with observations in controlled chamber experiments (Schulze *et al.*, 1987) and in field experiment (Tenhunen *et al.*, 1987). Thus, the feature results from a combined effect of a temperature and a humidity response.

In order to describe the stomatal responses, the characteristics of average plants were used. However, plants may adapt these responses to the circumstances they are usually exposed to. The vines studied in the previous chapter might be an example of such an adaptation. These plants are grown under the extremely dry and warm conditions of central Spain. The stomatal conductance of these plants had a much lower sensitivity to  $D_s$ ,  $D_{max}$  being about  $60 \text{ g kg}^{-1}$ . Furthermore, their temperature optimum extended over temperatures that ranged from 25 to almost  $40^\circ\text{C}$ . A less pronounced midday stomatal closure would have been obtained if these characteristics were used. Also, other important adaptations may be related to higher  $CO_2$  (for example, Long *et al.*, 1993; Woodward, 1993).

Using average plant-physiological characteristics,  $r_s$  resembled the surface resistance of well-watered agricultural crops and grasslands of the mid-latitudes (Russel, 1980; McNaughton &

Jarvis, 1983).  $r_s$  was hardly dependent on the roughness length. Therefore, the results for the rough surfaces cannot be taken to be representative for forest, notably coniferous forest. These canopies generally have a higher  $r_s$  than other canopies (Jarvis *et al.*, 1976; McNaughton & Jarvis, 1983; Shuttleworth, 1989). Some special features have to be accounted for in such cases. The guard cells of the stomata of conifers are sunk below the epidermis and the subsidiary cells, which are often thickened with wax (Allaway & Milthorpe, 1976; Sack, 1987). Therefore, the minimum  $r_s$  will be much higher for such plants (see, for example, Choudhury & Monteith, 1986). At similar photosynthetic rates, low values of  $C_i/C_s$  may be obtained. For example, for Douglas fir (*Pseudotsuga menziesii*) values of about 0.5 are reported at almost saturating light intensities (Price & Black, 1990; Van Hove *et al.*, 1992). Using a lower value for  $f_0$  together with C<sub>3</sub> photosynthesis would increase  $r_s$ , and therefore  $T_s$  and  $D_s$ . Together with a lower albedo (0.1 instead of 0.2; Gash *et al.*, 1989; Shuttleworth, 1989) this would have produced a much more realistic values of  $r_s$  for forest. It should also be investigated whether a description of  $r_s$  of coniferous forest by means of an A-g<sub>s</sub> model can be made consistent with the observation that this type of vegetation is relatively insensitive to CO<sub>2</sub> (Shugart, 1986; Eamus & Jarvis, 1989), for instance, by taking high values of mesophyll conductance,  $g_m$ .

The description of the CO<sub>2</sub> fluxes in the PBL was an important extension of the present coupled model. These fluxes were found to have only a small effect on  $r_s$  and  $\lambda E$ . However, the results of this study were mainly expressed as averages. If a detailed and accurate description of processes in the canopy is required, the fluxes in the PBL might contribute significantly to the results.

In the evaluation of the effect of LAI it was found that what are initially small differences can become very important under the influence of PBL feedback. This results in a large impact on the *prediction of changes*. Thus, a re-evaluation of the influence of the canopies micro-climate may be necessary. This requires the use of detailed canopy models (Goudriaan, 1977; El-Kilani, 1991; Reynolds, 1992) and perhaps a modern description of turbulence within canopies (Finnigan & Raupach, 1987). Also, it might be necessary to include effects such as those of leaf age or development stage (Chapter 4), and soil respiration. Whether or not these extensions are useful can probably only be evaluated properly by means of *coupled PBL-vegetation* models.

#### 5.6.4 Final remarks

The fact that the conclusions of the previous sections are only valid for extensive canopies need not be as limiting as may appear at first sight. Clearly, the restriction is related to the use of a 1D model. However, the humidity response is a quite common response (Lösch & Tenhunen, 1981; Choudhury & Monteith, 1986; Grantz, 1991). In addition, the stomata of many plants, though not all, respond to CO<sub>2</sub> by reducing their aperture (Cure & Acock 1986; Raschke, 1986; Morison, 1987). Therefore, these responses may be considered as large-scale responses, although the surface consists of different canopies. This consolidates the main conclusions on PBL-vegetation interaction.

The problem now becomes one of averaging with respect to parameters such as the albedo and the roughness length. The importance of this problem is clearly recognized in the scientific community (see Shuttleworth, 1991b; Bolle *et al.*, 1993). The problem becomes the more intriguing because the value of these parameters may prevent or invoke the occurrence of the positive feedback sequence discussed in the previous sections. This implies that an averaging procedure which gives an adequate description of the regional fluxes under one set of circumstances may be useless under another set, for example, if in reality one field reaches the stage of positive feedback, and another does not, while the chosen parameter values prevent positive feedback in all cases.

Furthermore, it has to be established how PBL dynamics is affected by surface inhomogeneities. These problems may be investigated by means of mesoscale models (see Pinty *et al.*, 1989; Segal & Arritt 1992) or by LES models (see Moeng & Wyngaard, 1989; Schumann, 1989). The outcome of such studies can be parameterized and incorporated in 1D PBL models (Holtslag & Moeng, 1991) which need less computing facilities and are easily accessible. Although these models will certainly not give the answer to all questions, they can be used as a valuable tool in performing systematic sensitivity analysis. This strategy was followed in this study.

Finally, the present results and the discussion are valid for fair-weather summer conditions, when the PBL usually is in the convective state. Simulations for other, as well as different atmospheric conditions may also be necessary.

## 5.7 Summary of conclusions

This study reveals that:

*The interaction between the PBL and the vegetation* has a significant influence on changes in  $r_s$  and  $\lambda E/Q^*$  at the regional scale. The conditions at the reference level as well as those within an extensive canopy are affected by the PBL. The coupling between the PBL and the surface is stronger in the case of rougher surfaces. The PBL feedback is negative for the fluxes, but usually positive for  $r_s$ .

*The humidity response and the temperature response* are key responses in the prediction of changes. The humidity response provides a positive feedback on a disturbance of  $r_s$ . The feedback of the temperature response is positive if  $T_s > T_{opt}$  or negative if  $T_s < T_{opt}$ . The positive feedbacks are, in general, magnified by the PBL. Changes of  $r_s$  are accompanied by changes of  $D_s$ . Therefore, the humidity response causes much larger changes of  $r_s$  than may be expected from plant physiological research in controlled environments or at small scale field plots. The PBL affects the concurrent changes of  $D_s$ . Thus, the impact of the increased  $CO_2$  concentration on  $r_s$  and  $\lambda E$  of extensive vegetated surfaces can only be estimated by means of coupled PBL-vegetation models, which should perhaps be extended with a description of the soil.

*C*<sub>3</sub> and *C*<sub>4</sub> canopies will exhibit similar changes of  $r_s$  and  $\lambda E/Q^*$  at the regional scale as long as  $T_s < T_{opt}$ . The initial response of  $r_s$  of *C*<sub>4</sub> canopies is larger, but its sensitivity to  $D_s$  is smaller. Furthermore, the change of  $D_s$  which will occur together with a change of the CO<sub>2</sub> concentration is expected to be somewhat less for *C*<sub>4</sub> canopies.

Differences in atmospheric conditions can have a significant impact on the changes in  $r_s$  if they cause differences in  $T_s - T_{opt}$ . Furthermore, they influence the impact of PBL feedback. Differences in the vertical structure may become important because of their effect on entrainment.

CO<sub>2</sub> fluxes in the PBL only have a small negative effect on the daily averaged  $r_s$  (< 5%) and a small positive effect on  $\lambda E/Q^*$  (< 1.5%). Their impact on the predicted change for a doubling of the ambient CO<sub>2</sub> concentration is less than -7% of the predicted relative change in the case of  $r_s$  and between -3% and +3% in the case of  $\lambda E/Q^*$ .

The LAI and  $z_o$  are parameters the value of which partly control the occurrence of a significant positive feedback on  $r_s$  through their impact on the conditions at the surface. Small initial differences between canopies can become important under the influence of PBL feedback.

## Samenvatting

### Direct effect van de toenemende atmosferische CO<sub>2</sub> concentratie op de regionale transpiratie

#### *Achtergrond en afbakening van het onderzoek*

Verdamping speelt een sleutelrol in onder andere meteorologische, hydrologische en planten-fysiologische processen. Landbouwkundige praktijk en waterbeheer in een bepaald gebied zullen aanzienlijk wijzigen als de verdamping er verandert. Daarnaast beïnvloedt verdamping in hoge mate de overdracht van warmte en waterdamp tussen het aardoppervlak en de atmosfeer, en is waterdamp het voornaamste "broeikasgas". Daardoor is zowel het lokale, het regionale als het mondiale klimaat gevoelig voor veranderingen in de verdamping.

Het onderwerp van dit onderzoek is de vraag hoe veranderingen in de verdamping voorspeld kunnen worden. Daarbij gaat de aandacht vooral uit naar de directe gevolgen van de invloed van het stijgende atmosferische CO<sub>2</sub> gehalte op planten. Ook wordt enige aandacht geschonken aan veranderingen als gevolg van andere wijzigingen aan het oppervlak, zoals ontbossing. Het onderzoek is beperkt tot de verdamping van dichte, droge, goed van water voorziene, uitgestrekte vegetaties. Omdat het overgrote deel van de verdamping van zulke vegetaties bestaat uit de zogenaamde transpiratie, zijn alleen effecten hierop beschouwd. De later te bespreken analyses en resultaten gelden voor mooie, zomerse dagen. Op zulke dagen transpireren goed van water voorziene gewassen het meest.

Transpiratie is de verdamping van door planten uit de bodem opgenomen water. Dit water verdampt aan het oppervlak van cellen die met lucht in contact staan. Vervolgens ontsnapt het water naar de atmosfeer. Ter beperking van het waterverlies bezitten landplanten een voor water en CO<sub>2</sub> vrijwel ondoordringbare opperhuid. Om toch de opname van het voor fotosynthese noodzakelijke CO<sub>2</sub> mogelijk te maken zijn in de opperhuid zogenaamde huidmondjes aanwezig. Het overgrote deel van het transpiratiewater verlaat de plant via de openingen in de huidmondjes, terwijl CO<sub>2</sub> erdoor binnen komt. Bij dit transport treedt een weerstand op, de huidmondjesweerstand, die groter is naarmate de opening kleiner is. De openingstoestand van de huidmondjes, en daarmee huidmondjesweerstand en transpiratiesnelheid, wordt aangepast aan een scala aan omgevings- en plantfactoren, waaronder CO<sub>2</sub>, licht, temperatuur en luchtvochtigheid. Daarbij zal de plant de verhouding tussen transpiratie en fotosynthese optimaliseren. Door alle huidmondjesweerstand van een gewas samen te nemen verkrijgt men de oppervlakteweerstand. Deze kan opgevat worden als een plantenfysiologisch bepaalde eigenschap van het oppervlak, die afhangt van CO<sub>2</sub> en andere omgevingsfactoren en die de totale transpiratiesnelheid van vegetaties sterk beïnvloedt.

Uit plantenfysiologisch onderzoek is bekend dat CO<sub>2</sub> de huidmondjes bij veel plantesoorten enigszins doet sluiten. De oppervlakteweerstand neemt dan toe, en de transpiratie zou dus afnemen wanneer het CO<sub>2</sub> gehalte van de atmosfeer stijgt. Het hier beschreven onderzoek is met name gericht op dit zogenoemde directe effect van een hoger atmosferisch CO<sub>2</sub> gehalte op de transpiratie.

*Aanpak: principe, gekozen modellen en koppeling*

Rekening houdend met oppervlakteweerstand en andere oppervlakte-eigenschappen, zoals de mate waarin zonlicht gereflecteerd wordt (albedo) en de ruwheid, kan de transpiratie berekend worden aan de hand van de toestand van de omgeving en de instraling door de zon. De toestand van de omgeving wordt doorgaans bepaald op enige hoogte boven het oppervlak, het referentieniveau. De variabelen die gebruikt worden bij de berekening van de transpiratie, zoals temperatuur en luchtvochtigheid op referentieniveau, zijn echter zelf afhankelijk van de transpiratie. Daarom is het niet correct om, zoals in eerder uitgevoerde analyses, bij het voorspellen van veranderingen in de transpiratie aan te nemen dat de randvoorwaarden op referentieniveau in de gewijzigde situatie gelijk zijn aan die in de uitgangssituatie.

In de atmosfeer zal met name de onderste laag beïnvloed worden door de overdracht van warmte en waterdamp naar de atmosfeer. Deze laag heet de (planetaire) grenslaag (afgekort: PG; hoogte: 1 à 2 kilometer) en bevat het referentieniveau. Als de transpiratie afneemt zal de PG niet alleen relatief droog blijven, maar ook relatief warm omdat er bij een verminderde transpiratie meer energie over blijft voor verwarming van de PG. Het totale effect is een toename van het vochtdeficiet (het verschil tussen de hoeveelheid vocht die de lucht maximaal kan bevatten (deze neemt toe met de temperatuur) en de werkelijke hoeveelheid vocht in de lucht). Het toegenomen vochtdeficiet zal de transpiratie weer stimuleren. Er is dus sprake van een negatieve terugkoppeling: het primaire effect op de transpiratie wordt gedempt. Deze interactie tussen vegetaties en de PG is vooral belangrijk is op de regionale schaal (10 tot 100 kilometer horizontaal, 1-5 kilometer verticaal). Daarom, en omdat processen op de regionale schaal de koppeling vormen tussen het grootschalige (mondiale) en kleinschalige (lokale) weer en klimaat, is de regionale transpiratie als uitgangspunt voor analyses genomen.

De consequentie van de bovenbeschreven vegetatie-atmosfeer interactie is, dat een voorspelling van eventuele veranderingen in de regionale transpiratie alleen kan gebeuren met behulp van een gekoppeld vegetatie-atmosfeer model. In dit onderzoek is het belang van de interactie voor het eerst systematisch onderzocht op basis van een gekoppeld model met een gedetailleerde beschrijving van de PG. Gekozen is voor een koppeling tussen het in de meteorologie gangbare "groot blad" model voor de vegetatie (Monteith, 1965) en het model van Troen & Mahrt (1986) voor de PG. Met het vegetatiemodel, waarin het gewas wordt beschouwd als één groot blad met dezelfde oppervlakte-eigenschappen als het nagebootste gewas, wordt onder andere de transpiratie berekend. Het model voor de PG geeft een beschrijving van de verticale structuur van de atmosfeer (ééndimensionaal), per laag van 25 à 125 meter, tot een totale hoogte van vier à vijf kilometer. Uitgaande van een beginsituatie en van bepaalde randvoorwaarden worden voor elke laag de veranderingen in temperatuur, luchtvochtigheid en windsnelheid berekend. De ontwikkeling van de PG is daarbij sterk afhankelijk van de in het vegetatiemodel gesimuleerde uitwisselingsprocessen aan het oppervlak, waaronder warmtetransport en transpiratie. Deze worden op hun beurt beïnvloed door de ontwikkelingen in de PG, met name die op referentieniveau. In het gebruikte model voor de PG wordt onder andere rekening gehouden met de bijdrage van wervels ter grootte van de PG aan het totale transport van warmte en waterdamp. Zulke wervels worden voornamelijk in stand gehouden met behulp van warmte die aan het oppervlak vrij komt.

Zowel het gewasmodel als het grenslaagmodel zijn in het verleden uitvoerig beschreven en getest. Het resulterende gekoppelde model is gedetailleerd, maar relatief eenvoudig. Dit model kan gebruikt worden op een *personal* computer. Het kan in uiteenlopende disciplines (meteorologie, biologie, milieukunde, enzovoort) als onderzoeksgereedschap dienen.

#### *Eerste analyse*

In eerste instantie is een systematische analyse van de regionale transpiratie uitgevoerd, waarbij per simulatie de oppervlakteweerstand werd gevarieerd zonder rekening te houden met een dagelijkse gang hierin. Hierdoor wordt het fysiologische karakter van deze eigenschap uitgeschakeld. Ook de invloed van ruwheidsveranderingen en albedo-veranderingen is onderzocht. Veranderingen in de transpiratie als gevolg van wijzigingen in genoemde oppervlakte-eigenschappen zijn berekend met en zonder PG. Met PG bedragen de veranderingen in regionale transpiratie door wijzigingen in oppervlakteweerstand of ruwheid slechts 40% à 80% van de veranderingen zonder PG. Veranderingen door wijzigingen in albedo zijn 25% tot 250% groter met grenslaag. De invloed van de PG blijkt niet alleen van de atmosferische omstandigheden af te hangen, maar ook van het type oppervlak (bijvoorbeeld gras, bos). De invloed van de interactie neemt af met een afnemende oppervlakteweerstand en ruwheid van het oppervlak en is daarom groter bij een bos dan bij een grasland.

#### *Model voor de huidmondjesweerstand*

Het plantenfysiologisch karakter van de oppervlakteweerstand kan nagebootst worden met behulp van een model dat het effect van CO<sub>2</sub> en andere factoren op de huidmondjes simuleert. Bovendien moet de onderlinge samenhang in de reacties beschreven worden, temeer daar CO<sub>2</sub> bekend staat als een factor die de reactie op andere factoren sterk beïnvloedt. De in de meteorologie gangbare modellen bieden hier geen uitkomst. Noodgedwongen wordt in deze modellen het effect van CO<sub>2</sub> meestal verwaarloosd en beperkt hun geldigheid zich tot de huidige CO<sub>2</sub> concentratie van de atmosfeer.

Het in dit onderzoek toegepaste weerstandsmodel is gebaseerd op de vaak waargenomen correlatie tussen fotosynthesesnelheid (de snelheid waarmee CO<sub>2</sub> door de plant wordt opgenomen) en huidmondjesgeleiding (inverse van de weerstand). Deze geleiding wordt dan berekend uit de verhouding tussen de fotosynthesesnelheid en het verschil in de CO<sub>2</sub> concentratie binnen en buiten het blad. Het voor dit doel gebruikte fotosynthesemodel (Goudriaan *et al.*, 1985) is goed in staat de invloed van CO<sub>2</sub>, licht en temperatuur op de fotosynthese, alsmede de samenhang tussen de invloeden te beschrijven. Vanwege de koppeling tussen fotosynthesesnelheid en huidmondjesgeleiding gelden deze eigenschappen automatisch voor de berekende geleiding. Simulatie van de reactie van huidmondjes op luchtvochtigheid vereist echter een aanvulling. Deze is afgeleid uit waarnemingen die tijdens een veldexperiment in Spanje zijn uitgevoerd. Het experiment vond plaats onder droge omstandigheden, waarbij de onderzochte planten (druif, *Vitis Vinifera* L. cv. Airen) steeds redelijk goed van water voorzien bleven en nauwelijks stress ondervonden. De waarnemingen geven een sterk, bijna lineair verband te zien tussen het vochtdeficiet aan het bladoppervlak en de verhouding tussen de CO<sub>2</sub> concentratie binnen en buiten het blad. Dit resultaat is gebruikt om de reactie van huidmondjes op luchtvochtigheid in het model na te kunnen

bootsen. Het resulterende model blijkt zowel fotosynthesesnelheid als huidmondjesgedrag van de onderzochte planten redelijk te beschrijven. Ook worden algemene karakteristieken van de reactie van huidmondjesgeleiding op luchtvochtigheid redelijk beschreven.

#### *Uitbreidingen gekoppeld model*

In de volgende fase van het onderzoek is het bestaande gekoppelde model uitgebreid. Op de eerste plaats is het model voor de fotosynthese en huidmondjesgeleiding opgeschaald van bladniveau naar gewasniveau en ingebouwd in het gekoppeld model. Daarin wordt de oppervlakteweerstand nu berekend aan de hand van omgevingsfactoren ( $\text{CO}_2$ , licht, temperatuur en luchtvochtigheid). Bovendien wordt gewasfotosynthese gesimuleerd. Op de tweede plaats worden in het grenslaagdeel nu ook  $\text{CO}_2$ -transporten en -concentraties berekend. Deze worden aangestuurd door de gewasfotosynthese. Op de derde plaats zijn recente ideeën (Holtslag & Moeng, 1991) over het transport van warmte, waterdamp en  $\text{CO}_2$  in de PG verwerkt. Met name de beschrijving van de bijdrage van grote wervels aan het totale transport is aangepast. Het resultaat is een gekoppeld model dat de belangrijkste aspecten van de interactie tussen vegetaties en de atmosfeer gedetailleerd beschrijft.

#### *Tweede analyse en effecten van een verdubbelde atmosferische $\text{CO}_2$ concentratie*

Met het uitgebreide gekoppelde model zijn simulaties uitgevoerd voor de huidige atmosferische  $\text{CO}_2$  concentratie en voor een verdubbelde concentratie. In beide gevallen zijn simulaties uitgevoerd met en zonder PG. Het grote verschil met de eerder beschreven analyses is dat nu rekening gehouden is met het plantenfysiologische karakter van de oppervlakteweerstand. De nieuwe resultaten hebben de cruciale rol van de vegetatie-atmosfeer interactie bevestigd. Ten eerste dempt deze interactie veranderingen in de transpiratie die het gevolg zijn van een wijzigende oppervlakteweerstand, waarbij de mate van demping afhankelijk is van de atmosferische omstandigheden en van het beschouwde oppervlak (gras, bos, enzovoort). Ten tweede brengt de interactie veranderingen teweeg in omstandigheden binnen het gewas, met name in het vochtdeficiet. De daarmee gepaard gaande reactie van de huidmondjes versterken het primaire effect van  $\text{CO}_2$  op de oppervlakteweerstand: hier is dus sprake van een positieve terugkoppeling. Resultaten van kleinschalig plantenfysiologisch onderzoek in het laboratorium of in het veld kunnen daarom niet zonder meer vertaald worden naar uitgestrekte vegetaties. De analyses van dit onderzoek geven aan dat, voor de omstandigheden beschouwd in dit onderzoek, de totale relatieve toename van de oppervlakteweerstand kan oplopen tot 100 à 120%. Zonder grenslaag en het effect van een toegenomen vochtdeficiet in het gewas zou deze stijging slechts 50 à 80% bedragen, wat overeenkomt met eerder gerapporteerde resultaten van plantenfysiologisch onderzoek. Het in dit onderzoek gevonden uiteindelijke resultaat voor de regionale transpiratie is een relatieve afname van 10 à 30%. De uiteindelijke afname is sterk afhankelijk van de ruwheid, in combinatie met de temperatuur en de luchtvochtigheid binnen het gewas en in de atmosfeer, en van het soort plant.

Kleine verschillen tussen gewassen kunnen door de vele gekoppelde niet-lineaire processen uiteindelijk aanzienlijke verschillen in oppervlakteweerstand en transpiratie tot gevolg hebben, gerekend over een dag. Dit is met name het geval als de verschillen leiden tot overschrijding van de voor fotosynthese optimale temperatuur. Dan treedt een extra, positieve terugkoppeling



in werking. Voor planten met een hoge optimum temperatuur zal dit effect relatief onbelangrijk zijn. Ook meer bladoppervlak kan dit helpen voorkómen. Bovendien is de ruwheid een cruciale eigenschap omdat deze de uitwisseling van warmte en waterdamp sterk beïnvloedt, en daarmee de temperatuur in het gewas.

Schattingen van veranderingen in de regionale transpiratie zullen van geval tot geval gemaakt moeten worden met behulp van gekoppelde modellen. Mogelijk moet de interactie tussen planten en de bodem ook ingebouwd worden en is een wat meer gedetailleerde beschrijving van de vegetatie noodzakelijk. Het nut van zulke uitbreidingen kan waarschijnlijk alleen juist beoordeeld worden als de interactie met de PG is verdisconteerd.

Het principe achter bovenstaande conclusies is naar verwachting onafhankelijk van de aard van de hier gekozen modellen, zolang de dynamiek van de grenslaag goed beschreven kan worden met een ééndimensionaal model. Effecten gerelateerd aan overgangen tussen twee of meerdere soorten oppervlak zullen verder onderzocht moeten worden. Ook zouden simulaties uitgevoerd moeten worden voor andere meteorologische situaties.

## Summary

### Direct impact of atmospheric CO<sub>2</sub> enrichment on regional transpiration

#### *Background and delimitation of the present study*

Evaporation is a key-process in meteorology, hydrology and plant-physiology. If evaporation in a specific region changes, agriculture and water management of that region will also change significantly. Evaporation is an important component of the surface energy balance and, in addition, water vapour is the most important of the greenhouse gases. Thus, local, regional, and global climate is very sensitive to evaporation.

The prediction of changes in the evaporation of vegetated land-surfaces is the subject of the present study. To a large extent, the study focuses on the consequences of the direct impact of elevated CO<sub>2</sub> on plants. Attention is also given to the consequences of other direct changes at surface level, such as deforestation. The study is confined to changes in the main component of evaporation in dense, well-watered, but dry canopies: transpiration. The analyses and results discussed later apply to fair-weather conditions typical of a summer day. On such days, the transpiration rate of well-watered canopies is relatively high.

Transpiration is the evaporation of water that has been taken up from the soil. The water evaporates at the walls of cells in contact with internal air. Hereafter, it escapes into the atmosphere. In order to prevent excessive water loss, land-plants contain an epidermis that is almost impermeable to water and to CO<sub>2</sub>. To ensure the uptake of CO<sub>2</sub> required for photosynthesis, the epidermis contains stomata. Virtually all transpired water escapes into the air surround the leaf through the stomatal pore and CO<sub>2</sub> enters the leaf through this same pore. The resistance to diffusion through the stomatal pore, called stomatal resistance, increases with a decreasing stomatal aperture, and this controls the diffusion rate. In its turn, stomatal aperture responds to many plant and environmental factors, such as CO<sub>2</sub>, light, temperature and the humidity of the air. It can be adjusted in accordance with the conditions of the leaf's environment. In this way, plants tend to optimize the ratio of transpiration to CO<sub>2</sub> uptake. All stomatal resistances in a canopy can be integrated to yield the surface resistance. The surface resistance can be regarded as a surface characteristic that is related to plant physiological processes which depend on environmental conditions, and which controls, to a large extent, the transpiration rate of the canopy.

Plant physiological research has revealed that the stomatal resistance of many plant species tends to increase as the CO<sub>2</sub> content of the air increases. Thus, surface resistance is expected to increase as well and this implies a decrease of transpiration if the ambient CO<sub>2</sub> concentration increases. The present study focuses on this so-called direct effect of CO<sub>2</sub> on the transpiration of extensive vegetation.

#### *Approach: principle, selected models and coupling*

Transpiration can be calculated from routine weather data if the surface characteristics, such as the surface resistance, the albedo, and aerodynamic roughness length, are also known. The

environmental variables used refer to conditions at some height above the surface, which is the reference height. However, transpiration is expressed as a set of variables, including temperature and humidity at the reference height, which depend on transpiration. Therefore, changes in transpiration cannot be *predicted* using the same boundary conditions at the reference level for the new situation at the surface. The atmospheric layer adjacent to the Earth's surface, the Planetary Boundary Layer (PBL, with a typical height of 1-2 km), is particularly affected by the exchange processes at the surface, including transpiration. If transpiration decreases, the PBL will remain relatively dry, and also relatively warm because more energy is available to warm the PBL. Thus, the humidity deficit is increased and this stimulates transpiration. This negative feedback, called PBL feedback, is particularly important at the regional scale (horizontal scale: 10-100 km; vertical scale: 1-5 km) and is due to a large set of coupled, nonlinear processes. For this reason, and because processes at the regional scale provide the link between global and local scale processes, transpiration is considered at the regional scale in this study.

Because of the interaction between vegetation and the atmosphere, a proper prediction of changes in regional transpiration can only be achieved by using a coupled vegetation-PBL model. In the present study, relatively simple but physically realistic models have been selected. Vegetation is described by the Penman-Monteith big leaf model (Monteith, 1965), which is widely used in meteorological research. This model has been coupled to a one dimensional model for the PBL (Troen & Mahrt, 1986), which describes the vertical structure of the atmosphere up to about a height of four kilometres, in layers of 25 to 125 meters each. The PBL model accounts for nonlocal turbulent transport within the PBL. The eddies responsible for this transport have a size similar to the height of the PBL and are fed by the input of energy at the surface. Both the vegetation model and the PBL model have been used and discussed extensively by others. In this study the two models have been coupled, which results in a detailed PBL-vegetation model. The PBL development simulated by the coupled model is driven by the energy exchange at the surface. This energy exchange, of which transpiration is a major component is evaluated in the vegetation part of the model, using the conditions at the reference level. The PBL part of the model describes the concurrent changes at reference level which in turn affect the exchange of energy. Modifications of the atmospheric layer between the surface and the reference height, the surface layer, are also taken into account in the present model. The model runs on a personal computer and can be used as a research tool in various disciplines, including meteorology and biology, and in air pollution studies.

#### *First analysis*

First, a systematic analysis has been performed of regional transpiration in which the plant physiological character of the surface resistance was ignored. Thus, the surface resistance was treated as if it were an independent variable with a fixed value. The sensitivity of regional transpiration to surface resistance, and the sensitivity to aerodynamic resistance (related to roughness) and albedo were investigated. Runs were performed with and without PBL feedback. If the processes in the PBL are taken into account, sensitivity to surface resistance and aerodynamic resistance is reduced to between 40 and 80 percent of the value which

would have been obtained if PBL feedback had been ignored. By contrast, the sensitivity to albedo increases by 25 to 250 percent if atmospheric feedback is included. The influence of PBL feedback not only depends on atmospheric conditions, but also on the surface characteristics. It increases with increasing surface roughness and with increasing surface resistance. Therefore, it is more important in the case of forest than in the case of grassland.

#### *Leaf conductance model*

Stomatal responses to environmental conditions can be accounted for by means of a model that simulates stomatal responses to  $\text{CO}_2$  as well as responses to other important variables. Furthermore, the interactions between the various responses cannot be ignored, because  $\text{CO}_2$  is well-known for its effect on the stomatal responses to other variables. The models which are at present most widely used in meteorology are, in most cases, not able to describe the response to  $\text{CO}_2$ , nor can they describe the interactions between responses. Thus, their validity is restricted to the current atmospheric  $\text{CO}_2$  concentration.

The resistance model used in the present study is based on the often observed correlation between photosynthetic rate and stomatal conductance. This implies that stomatal conductance can be determined from the photosynthetic rate and the difference between the  $\text{CO}_2$  concentration inside the leaf and at the leaf's surface. The photosynthesis model used for this purpose is able to describe most of the well-known characteristics of the photosynthetic response to  $\text{CO}_2$ , light and temperature, as well as the interaction of the responses. Assuming the existence of a relationship between photosynthetic rate and stomatal conductance, the characteristics of the photosynthesis model automatically apply to the calculated conductance. However, the stomatal response to air humidity requires an additional parameterization. Such a parameterization has been derived from data obtained during a field experiment in Spain. The experiment was performed under semi-arid conditions. However, the plants investigated here (grapevines, *Vitis Vinifera* L. cv. Airen) were well-watered and unstressed. The experimental data revealed a strong, almost linear relationship between the humidity deficit at the leaf surface and the ratio of the  $\text{CO}_2$  concentration inside the leaf and at the surface of the leaf. In the present study, this relationship is used to mimic stomatal humidity responses. The resulting photosynthesis-conductance model describes photosynthesis and the stomatal conductance of the grapevines reasonably well. Sample calculations also indicate that general characteristics of the humidity responses are simulated satisfactorily using the new parameterization.

#### *Extensions of the coupled model*

Subsequently, the coupled model mentioned above was extended in three major respects. First, the photosynthesis-conductance model already referred to has been scaled up from the leaf to the canopy and implemented in the vegetation part of the coupled model to yield surface resistance. Thus, the surface resistance is now determined using environmental variables, notably  $\text{CO}_2$ , light, temperature and the specific humidity of the air. The canopy photosynthetic rate is also evaluated. Second,  $\text{CO}_2$  concentration and transport are now described in the PBL model. These are driven by the canopy photosynthesis. Third, recent views (Holtslag & Moeng, 1991) on the transport of heat, water vapour and  $\text{CO}_2$  in the PBL

have also been included. In particular, the parameterization of nonlocal turbulent transport has been adapted. The result of the extensions is a coupled vegetation-PBL model that describes the most important aspects of the vegetation-atmosphere interaction in considerable detail.

#### *Second analysis and impact of a doubled atmospheric CO<sub>2</sub> concentration*

Using the extended model, simulations were performed for the current and a doubled atmospheric CO<sub>2</sub> concentration. In both cases, runs were performed with and without PBL feedback. Analysis of the results for regional transpiration have confirmed the crucial role of the vegetation-atmosphere interaction. First, changes in transpiration due to a changing surface resistance are damped by the PBL and the influence of the PBL depends strongly on the atmospheric conditions and on the surface type (grass, forest, *et cetera*). Second, the interaction leads to changes within the canopy, in particular changes of the specific humidity deficit. The concurrent stomatal responses enhance the primary effect of CO<sub>2</sub> on surface resistance. Due to this positive feedback mechanism, results from small-scale plant physiological research in controlled environments or small field plots cannot be translated into changes in the surface resistance of extensive canopies while ignoring the vegetation-atmosphere interaction. For the conditions applied in this research, the relative increase in surface resistance due to doubled ambient CO<sub>2</sub> can become as much as 100 to 120 percent. By contrast, without PBL feedback and stomatal responses to humidity deficit, a relative increase of only 50 to 80 is found here, which agrees well with results from previous plant-physiological research. The resulting effect on regional transpiration as found by means of the complete coupled model is a decrease of 10 to 30 percent. The actual change depends on the surface roughness and on the temperature and humidity of air in the canopy and in the PBL, and also on plant class (C<sub>3</sub> or C<sub>4</sub>).

Due to the many coupled nonlinear processes involved in the problem, small differences between canopies can result in rather significant differences with respect to daily averaged surface resistance and regional transpiration. This is especially true if the optimum temperature for photosynthesis is exceeded. An additional positive feedback is then present. This effect will be rather insignificant for plants with a high optimum temperature and more leaf area may help to avoid the phenomenon. Roughness is a crucial factor here because, to a large extent, it controls the exchange of water vapour and heat between the canopy and the atmosphere and thus controls the canopy temperature.

Estimates of changes in regional transpiration will have to be carried out separately for every specific case. It is possible that the interaction between soil and canopy will have to be accounted for and a somewhat more detailed description of the vegetation may also be required. The significance of such model extensions can probably only be assessed properly if atmospheric feedback is accounted for.

The principle behind the conclusions given above is not expected to depend on the models selected here, as long as PBL dynamics can be described by means of a one dimensional model. Effects related to surface inhomogeneities should be further investigated and more, as well as different meteorological conditions should be considered.

## Appendix 1 Anatomy of a leaf

Fig. A1.1 schematically depicts a cross section of a leaf with stomata at its *abaxial* surface (a *hypostomatous* leaf). *Stomata* are *pores* surrounded by *guard cells*. They are located in the *epidermis* of aerial parts of plants (Sack, 1987). At the atmospheric side, the epidermis is covered with a *cuticle*. The cuticle has a low permeability to water and also to  $\text{CO}_2$  (Schönherr, 1976; Ziegler, 1987). The guard cells are surrounded by one or more *subsidiary cells* that differ from other epidermal cells in size, shape, arrangement and structure. The space behind a stoma is called *sub-stomatal cavity*. It is a special representative of the many *intercellular spaces* between the *mesophyll cells* (Sack, 1987). The mesophyll cells contain *chloroplasts*, where the actual  $\text{CO}_2$  fixation occurs. Unlike other epidermal cells, guard cells usually contain chloroplasts.

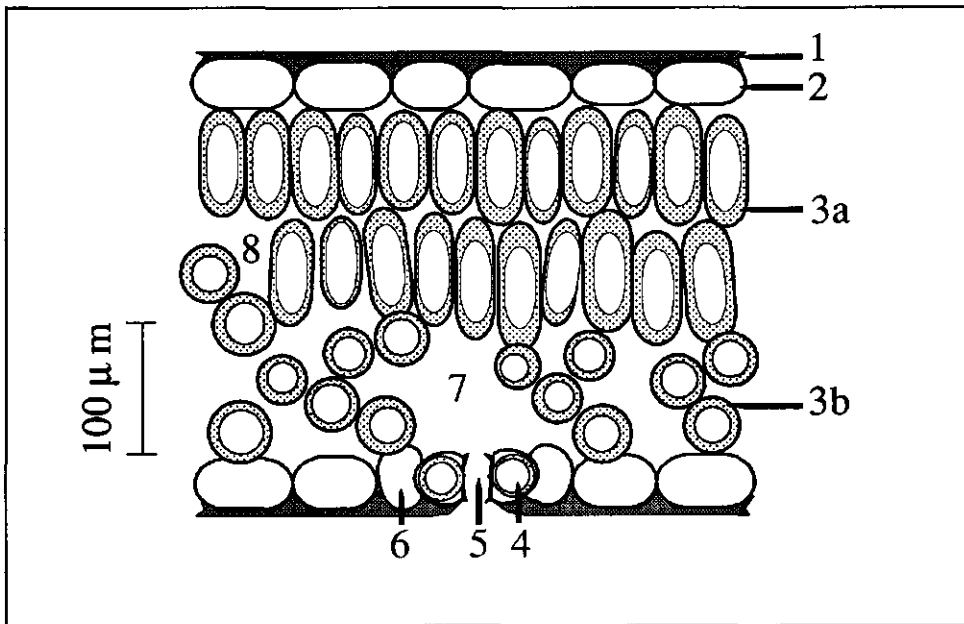


FIGURE A1.1. Schematic representation of a transverse section through a leaf (after Nobel, 1991). 1 (shaded area)=cuticle; 2=epidermis; 3=mesophyll (a: palisade; b: spongy); 4=guard cell; 5=stomatal pore; 6=subsidiary cell; 7=sub-stomatal cavity; 8=intercellular air space. Dotted areas indicate occurrence of chloroplasts.

## Appendix 2 The vegetation—surface-layer model

Vegetation is described by the Penman-Monteith big-leaf model (Monteith, 1965). The canopy is considered as one big leaf with the same surface characteristics (albedo, aerodynamic roughness, surface resistance, emissivity, etc.) as the canopy represented by the model. The air in the stomata is assumed to be saturated with water vapour.

The energy that drives the processes at the surface is provided by the net radiation:

$$Q^* - G = H - \lambda E \quad [A2.1]$$

where  $Q^*$  is the net radiation,  $H$  is the sensible heat flux,  $\lambda E$  the latent heat flux, and  $G$  (which will simply be referred to as "soil heat flux") contains the soil heat flux, the photosynthesis and other storage and metabolic terms, so that  $Q^* - G$  is the available energy for  $H$  and  $\lambda E$ .

In terms of incoming and outgoing shortwave and longwave radiation  $Q^*$  is parameterized:

$$Q^* = (1 - a)S\downarrow + L\downarrow - L\uparrow \quad [A2.2]$$

where  $S\downarrow$  is the solar radiation,  $a$  is the surface albedo,  $L\downarrow$  is the downward longwave radiation and  $L\uparrow$  the upward longwave radiation;  $L\downarrow$  is given by:

$$L\downarrow = \epsilon_a \sigma T_r^4 \quad [A2.3a]$$

where  $\sigma$  is the Stefan-Boltzmann constant ( $5.67 \times 10^{-8} \text{ W m}^{-2} \text{ K}^{-4}$ ) and  $T_r$  is the temperature at the reference level in K. The emissivity of the air,  $\epsilon_a$ , is parameterized as  $\epsilon_a = kT^2$ , with  $k = 9.46 \times 10^{-6} \text{ K}^{-2}$  (Swinbank, 1964). The upward longwave radiation is taken

$$L\uparrow = \epsilon_s \sigma T_s^4 \quad [A2.3b]$$

in which  $T_s$  is the surface temperature (K) and  $\epsilon_s$  is the emissivity of the surface (taken 0.97, Brutsaert, 1982).

The sensible and latent heat fluxes are defined as

$$H = \rho C_p \frac{\theta_s - \theta_r}{r_{ah}} \quad [A2.4a]$$

$$\lambda E = \rho \lambda \frac{q^*(T_s) - q_r}{r_{av} + r_s} \quad [A2.4b]$$

where  $\rho$  is the density of dry air,  $C_p$  is the heat capacity of the air at constant pressure ( $1005 \text{ J kg}^{-1} \text{ K}^{-1}$ ),  $r_{ah}$  and  $r_{av}$  are the aerodynamic resistances to heat and water vapour transport, respectively, and  $\lambda$  the latent heat of vaporization ( $2.46 \times 10^6 \text{ J kg}^{-1}$ ). Given  $T_r$ ,  $q_r$ ,  $r_{ah}$ ,  $r_{av}$  and  $G$ , the system A2.1-A2.4 is solved numerically for  $T_s$  with  $S\downarrow$  as the driving force. This approach avoids errors due to the linearization that leads to the Penman-Monteith equation ([1.1], [2.7]; cf. Paw U & Gao, 1988; MacArthur, 1990).

G is parameterized as

$$G = \begin{cases} \alpha Q^*, & S \downarrow \geq 100 \text{ W m}^{-2} \\ \frac{1}{3} Q_i^* - \frac{1}{4} H, & S \downarrow < 100 \text{ W m}^{-2} \end{cases} \quad [\text{A2.5}]$$

with  $\alpha \equiv G/Q^*$  is the soil heat flux coefficient (taken 0.07) and  $Q_i^*$  is the isothermal net radiation defined as  $(\epsilon_s - \epsilon_a)\sigma T_r^4$ . The parameterization closely follows De Bruin (1983) and Holtslag & De Bruin (1988).

Between  $z_r$  and  $z_o$ , the aerodynamic resistances to heat and water vapour transport ( $r_a$ ) are assumed equal and are calculated following Louis (1979). The bulk transfer coefficients for momentum and for heat and moisture ( $C_m$  and  $C_h$ , respectively) are calculated as

$$C_x = C_n f \left( Ri_b, \frac{z}{z_o} \right) \quad [\text{A2.6}]$$

where  $C_n$  is the bulk transfer coefficient for neutral conditions,  $Ri_b$  is the Richardson bulk number, and the subscript x denotes "m" for momentum transport and "h" for heat and water vapour transport. The regression function,  $f$ , is fitted on the flux profile relationships. The functions proposed by Louis *et al.* (1982) are taken for *unstable* conditions. These functions fit the Dyer & Hicks (1970) stability functions. For *stable* conditions the function proposed by Holtslag & Beljaars (1988) is used. Their function is consistent with the stability correction proposed by Holtslag & De Bruin (1988). Now  $r_a$  is calculated from

$$r_a = \frac{1}{C_h u_r} \quad [\text{A2.7}]$$

In the case of rough surfaces ( $z_o > 0.5$  m, arbitrarily) the excess resistances ( $r_{bh}$ , between  $z_o$  and  $z_{oh}$ , and  $r_{bv}$ , between  $z_o$  and  $z_{ov}$ , for heat and water vapour, respectively;  $z_{oh}$  and  $z_{ov}$  denote the effective source height for heat and moisture, respectively; Thom, 1975) are parameterized following Stewart and Thom (1973). For other surfaces it is assumed that  $z_{oh} = z_{ov}$  and  $\ln(z_o/z_{oh}) = 2$  (Garrat & Hicks, 1973). Stability effects on  $r_{bh}$  and  $r_{bv}$  are neglected. Knowing the excess resistances,  $r_{ah} = r_a + r_{bh}$  and  $r_{av} = r_a + r_{bv}$ .



### Appendix 3 Extension of the vegetation model: PAR within the canopy

A spherical leaf angle distribution is assumed, that is, every leaf inclination has the same probability. The amount of PAR absorbed by the canopy is taken 47% of the global radiation,  $S\downarrow$  ( $I \approx 0.5S\downarrow$ ; Ross, 1975; Goudriaan, 1977). This allows for a reflection of 6% of the incident PAR. The dependence of the canopy reflection on the elevation of the sun (Goudriaan, 1977; Spitters, 1986) is ignored. The amount of PAR entering the canopy is divided into direct light and diffuse light, according to the approximations given by Spitters *et al.* (1986). Within the canopy, the flux density of both components is assumed to decrease exponentially according to

$$I_a(L) = -\frac{dI}{dL} = K_x I_t \text{EXP}(-K_x L) \quad [\text{A3.1}]$$

where  $I_a(L)$  is the absorbed amount of PAR at each level (diffuse or direct),  $K_x$  is an extinction coefficient (with  $x$  denoting "dr" for direct light and "df" for diffuse light), and the subscript  $t$  denotes "at the top of the canopy." The extinction coefficients for direct light and diffuse light are taken

$$K_{dr} = K_{bl} \sqrt{1 - s_l} = \frac{0.5}{\text{SIN}(\beta)} \sqrt{1 - s_l} \quad [\text{A3.2a}]$$

and

$$K_{df} = 0.8 \sqrt{1 - s_l} \quad [\text{A3.2b}]$$

respectively. Here,  $K_{bl} = 0.5/\text{SIN}(\beta)$  is the extinction coefficient for "black leaves," (with  $\beta$  denoting the elevation of the sun), and  $s_l$  is the scattering coefficient of green leaves for PAR (taken 0.2; Goudriaan, 1977).

Direct light that hits a leaf is either absorbed or reflected as *diffuse radiation*. This *secondary source* of diffuse radiation contributes to the total amount of diffuse radiation in the canopy. *Shaded* leaves only absorb the total background diffuse radiation from the primary and the secondary source. *Sunlit* leaves also absorb the amount of direct light that is not scattered (Goudriaan, 1977; Spitters, 1986). The fraction of sunlit leaf area at any particular level,  $f_{sl}$ , is equal to the fraction of direct light reaching that level. Then:

$$f_{sl} = e^{-K_{bl}L} \quad \text{and} \quad f_{sh} = 1 - f_{sl} \quad [\text{A3.3}]$$

where  $f_{sh}$  is the fraction of shaded leaves.

## Appendix 4 The planetary boundary layer model

### a) Description

The PBL model (Troen & Mahrt, 1986; Mahrt *et al.*, 1987) is a 1D, multilayer, first-order closure model. The tendency of an entity,  $s$ , is evaluated according to

$$\frac{\partial s}{\partial t} = \frac{\partial}{\partial z} \left( K_s \frac{\partial s}{\partial z} - \gamma_s \right) \quad [\text{A4.1}]$$

where  $K_s$  is the appropriate turbulent diffusion coefficient,  $t$  is time, and  $z$  is height. The countergradient correction,  $\gamma_s$ , is included to account for nonlocal turbulent mixing (Deardorff, 1972). It is taken zero for momentum. For heat and moisture,  $\gamma_s$  is defined below.

For momentum transport  $K_s = K_m$  is calculated from

$$K_m = \frac{\kappa u_* z}{\phi_m(z/L_v)} \left( 1 - \frac{z}{h} \right)^2 \quad [\text{A4.2}]$$

where  $u_*$  is the friction velocity,  $\kappa$  is the Von Kármán constant (0.40),  $h$  is the PBL depth,  $\phi_m(z/L_v)$  is the dimensionless wind shear, with  $L_v$  denoting virtual Monin-Obukhov length. As in Troen & Mahrt (1986)  $\phi_m$  is taken

$$\phi_m(z/L_v) = 1 + 4.7 \frac{z}{L_v} \quad [\text{A4.3a}]$$

under *stable* conditions ( $z/L_v > 0$ ) and

$$\phi_m(z/L_v) = \left( 1 - 7 \frac{z}{L_v} \right)^{-1/3} \quad [\text{A4.3b}]$$

for *unstable and neutral* conditions ( $z/L_v \leq 0$ ). For heat and water vapour,  $K_s = K_m/\text{Pr}$ , where  $\text{Pr}$  is the Prandtl number. At the top of the surface layer (height:  $z_s$ ;  $z_s/h = 0.1$ ) the surface fluxes and the fluxes in the PBL are matched, so that

$$\text{Pr} = \frac{\phi_h(z/L_v)}{\phi_m(z/L_v)} + C \kappa \frac{z}{h} \quad [\text{A4.4}]$$

where  $C$  is a constant of proportionality (see below). Above  $z_s$ ,  $\text{Pr}$  is assumed constant (Troen & Mahrt, 1986; Mahrt *et al.*, 1987). The characteristic velocity scale,  $w_s$ , is defined as

$$w_s \equiv \frac{u_*}{\phi_m(z/L_v)} \quad [\text{A4.5}]$$

for  $z > z_s$ , so that  $K_m$  becomes

$$K_m = w_s \kappa z \left( 1 - \frac{z}{h} \right)^2 \quad [\text{A4.6}]$$

Here,  $\phi_m$  is evaluated at  $z_s$ . Using  $w_s$ , both turbulent mixing produced by shear and turbulent mixing produced by buoyancy are included, and a continuous transition between stable and unstable conditions is obtained (Troen & Mahrt, 1986).

The PBL depth,  $h$ , is diagnosed using a bulk Richardson formulation:

$$h = \frac{Ri_{cr} \theta_{ov} |V(h)|^2}{g(\theta_v(h) - \theta_s)} \quad [A4.7]$$

where  $Ri_{cr}$  is the critical Richardson bulk number (taken 0.25),  $\theta_{ov}$  is a reference virtual potential temperature (K),  $V(h)$  is the wind speed at the top of the PBL,  $g$  is the gravitational acceleration ( $9.81 \text{ m s}^{-2}$ ),  $\theta_v(h)$  is the virtual potential temperature at the top of the PBL, and  $\theta_s$  the near-surface potential temperature. In the convective boundary layer,  $h$  will be found slightly above the well mixed layer, which implies an entrainment layer. By putting the power in [A4.2] equal to 2, the entrainment sensible heat flux is modelled to be a reasonable fraction (10-40%) of surface sensible heat flux (Troen & Mahrt, 1986; cf. Tennekes, 1973; Tennekes & Driedonks, 1981; Caughey, 1982).

For *unstable* conditions,  $\theta_s$  is chosen to be a measure of the temperature of the thermals that account for most of the transport in the convective PBL by letting:

$$\theta_s = \theta_v(z_1) + \frac{C}{w_s} \left( \frac{H}{\rho C_p} \right), \quad z/L_v < 0 \quad [A4.8]$$

in which  $\theta_v(z_1)$  is the virtual potential temperature at the lowest model level, and  $C$  is taken 6.5, as in Troen & Mahrt (1986). The second term at the rhs of [A4.8] can be considered as the scaled temperature excess of the thermals, corresponding to the thermal turnover time  $h/w_s$  (Troen & Mahrt, 1986). Now,  $\gamma_s$  is related to the kinematic surface flux of  $s$ ,  $S$ , by

$$\gamma_s = C \frac{S}{hw_s} \quad [A4.9]$$

For *stable* conditions  $\theta_s = \theta_v(z_1)$  and  $\gamma_s$  is taken zero.

#### b) Coupling, initial and boundary conditions

The PBL model has been coupled to the vegetation-SL model by taking  $z_0$  of the latter model as the lowest level of the PBL part (at  $D + 50 \text{ m}$ , where  $D$  is the displacement height). The coupled model is run with a grid of 52 levels between 0 and 4 km. The grid spacing varies from 25 m between 0 and 150 m to 125 m between 3.5 and 4 km. The time step is two minutes. The model requires initial profiles of: wind velocities in the  $x$  and  $y$  direction,  $u$  and  $v$ , respectively; vertical velocity,  $w$ ; potential temperature,  $\theta$ ; specific humidity,  $q$ . Furthermore, beside a set of surface parameters ( $a$ ,  $z_0$ , etc.), a set of various parameters like geographic position,  $Ri_{cr}$ , etc., has to be specified.

At every time,  $t$ ,  $S\downarrow$ , cloud cover and geostrophic wind speed are used as the forcings. First, the surface fluxes of momentum, heat and water vapour as well as  $T_s$  and  $q_s$  are computed in the vegetation-SL part. These are used as input in the PBL part, where  $h$  is estimated and the diffusivity profiles are determined. Then, the tendencies of  $u$ ,  $v$ ,  $\theta$  and  $q$  at every grid level are calculated and used to evaluate the new PBL profiles for these variables. In the next time step, the updated conditions at  $z_0$  and updated values of the forcings are used as input in the vegetation-SL part, etc..

## Appendix 5 Modifications of the PBL model (Chapter 5)

### a) Turbulent diffusion coefficient for heat, $K_h$ (Holtslag & Moeng, 1991)

The description of  $K_h$  is based on a parameterization of the transport term and the pressure covariance term in the vertical heat flux equation, written as:

$$\frac{\partial \overline{w'\theta'}}{\partial t} = - \underbrace{\frac{\partial \overline{w'^2\theta'}}{\partial z}}_{(I)} - \underbrace{\overline{w'^2} \frac{\partial \overline{\theta}}{\partial z}}_{(II)} + \underbrace{\beta g \overline{\theta'^2}}_{(III)} - \underbrace{\frac{1}{\rho_o} \frac{\overline{\theta' \partial p'}}{\partial z}}_{(IV)} \quad [A5.1]$$

where primes denote fluctuations and overbars denote ensemble averages,  $\beta g$  = the buoyancy parameter ( $g/\theta_o$ , with  $\theta_o$  a reference potential temperature) and  $\rho_o$  is the air density at the reference state. At the rhs of [A5.1], (I) is the turbulent transport term, (II) is the mean gradient production, (III) is the buoyant production and (IV) is the pressure covariance term. Data of Large Eddy Simulations (LES) by Moeng & Wyngaard (1989) suggest:

$$(I) \approx (IV) + b \frac{w_*^2 \theta_{*,c}}{h} \quad [A5.2]$$

with  $b \approx 2$ . In [A5.2]  $\theta_{*,c}$  is the convective temperature scale defined by

$$\theta_{*,c} \equiv \frac{\overline{w'\theta'_s}}{w_*} \quad [A5.3]$$

where  $\overline{w'\theta'_s}$  is the kinematic surface heat flux. Also, (IV) is parameterized as

$$IV = -a\beta g \overline{\theta'^2} - \frac{\overline{w'\theta'}}{\tau} \quad [A5.4]$$

where  $a$  is a constant ( $\approx 1/2$ ), and  $\tau$  is the return to isotropy time scale (Moeng & Wyngaard, 1986). Then, (substituting [A5.2] and [A5.4] in [A5.1]):

$$\frac{\overline{w'\theta'}}{\tau} \approx - \frac{\overline{w'^2}}{2} \frac{\partial \overline{\theta}}{\partial z} + \frac{b}{2} \frac{w_*^2 \theta_{*,c}}{h} \quad [A5.5]$$

By comparing [A5.5] to the modelled heat flux, given by

$$\overline{w'\theta'} = -K_h \left( \frac{\partial \overline{\theta}}{\partial z} - \gamma_\theta \right) \quad [A5.6]$$

it follows that:

$$K_h = \overline{w'^2} \frac{\tau}{2} \quad [A5.7]$$

and

$$\gamma_\theta = b \frac{w_*^2 \theta_{*,c}}{\overline{w'^2} h} \quad [A5.8]$$

$\overline{w'^2}$  is further parameterized using data of the Air Mass Transformation Experiment (AMTEX; Lenschow *et al.*, 1980) and LES by Moeng & Wyngaard (1989):

$$(\overline{w'^2})^{3/2} = \left[ 1.6 u_*^2 \left( 1 - \frac{z}{h} \right) \right]^{3/2} + 1.2 w_*^3 \left( \frac{z}{h} \right) \left( 1 - 0.9 \frac{z}{h} \right)^{3/2} \quad [\text{A5.9}]$$

In addition,  $K_h$  is parameterized as

$$K_h = w_* h \left( \frac{z}{h} \right)^{4/3} \left( 1 - \frac{z}{h} \right)^2 \left( 1 + R_h \frac{z}{h} \right) \quad [\text{A5.10}]$$

where  $R_h$  is the ratio of the entrainment flux of heat to the surface flux of heat.

*b) Bottom-up and top-down diffusion and generalization*

In the convective PBL, the total flux of a scalar,  $s$ , can be thought of to consist of a "bottom-up" flux,  $\overline{w's'}_u$ , and a "top-down" flux,  $\overline{w's'}_d$ . Within this conceptual framework, bottom-up diffusion is driven by the surface flux,  $\overline{w's'}_s$ , with zero entrainment flux, and top-down diffusion is driven by the entrainment flux,  $\overline{w's'}_e$ , with zero surface flux. Under quasi-stationary conditions and without advection the total flux at a level in the PBL can be written as a linear combination of  $\overline{w's'}_s$  and  $\overline{w's'}_e$ , so that (Wyngaard & Brost, 1984)

$$\overline{w's'}_x = \left( 1 - \frac{z}{h} \right) \overline{w's'}_s + \left( \frac{z}{h} \right) \overline{w's'}_e = \overline{w's'}_u + \overline{w's'}_d \quad [\text{A5.11}]$$

By analogy with [A5.6], the individual fluxes are written as

$$\overline{w's'}_x = -K_x \left( \frac{\partial s_x}{\partial z} - \gamma_x \right) \quad [\text{A5.12}]$$

where the subscript  $x=u$  for the bottom-up case and  $x=d$  for the bottom-down case. The scalar gradients are defined by

$$\frac{\partial s_x}{\partial z} = \frac{-\overline{w's'}_y}{w_* h} g_x \quad [\text{A5.13}]$$

with  $g_x$  a dimensionless gradient of  $s$ , and the subscript  $y=s$  for the bottom-up case and  $y=e$  for the top-down case. The total mean gradient of  $s$  is given by

$$\frac{\partial s}{\partial z} = \frac{-(\overline{w's'}_s g_u + \overline{w's'}_e g_d)}{w_* h} \quad [\text{A5.14}]$$

(Wyngaard & Brost, 1984).  $g_u$  and  $g_d$  are different because of the asymmetry in the bottom-up and the top-down diffusion (Wyngaard & Brost, 1984; Wyngaard, 1987).

LES data of Moeng & Wyngaard (1984) suggest that  $\gamma_d \approx 0$  while  $\gamma_u$  may be taken, by analogy with [A5.8]:

$$\gamma_u = b_u \frac{w_* \overline{w's'}_s}{w'^2 h} \quad [\text{A5.15}]$$

where  $b_u \approx 2$ . Holtslag & Moeng (1991) show that  $K_u$  and  $K_d$  can be parameterized as

$$\frac{K_u}{w_* h} = \left(\frac{z}{h}\right)^{4/3} \left(1 - \frac{z}{h}\right)^2 \quad [\text{A5.16a}]$$

and

$$\frac{K_d}{w_* h} = 7 \left(\frac{z}{h}\right)^2 \left(1 - \frac{z}{h}\right)^3 \quad [\text{A5.16b}]$$

respectively. Finally, using

$$\overline{w's'} = -K_s \left(\frac{\partial s}{\partial z} - \gamma_s\right) \quad [\text{A5.17}]$$

and [A5.11], [A5.12], [A5.15] and [A5.16], the total diffusion coefficient,  $K_s$ , reads

$$K_s = \frac{(1 - z/h + R_s z/h) K_u K_d}{(1 - z/h) K_d + R_s (z/h) K_u} \quad [\text{A5.18}]$$

where  $R_s \equiv \overline{w's'}_e / \overline{w's'}_s$ . Usually,  $R_s < 0$  for heat and  $R_s > 0$  for water vapour and  $\text{CO}_2$ .

Negative values of  $R_s$  restrict the application of [A5.18] to  $z/h < 1/(1-R_s)$ . Therefore, [A5.10] is used instead of [A5.18] if  $R_s < 0$  (for example, for heat). Finally,

$$\gamma_s = b \frac{w_* \overline{w's'}_s}{w'^2 h} \quad [\text{A5.19}]$$

with  $b = 2$ .

Test simulations revealed that the new parameterization causes unrealistic profiles of water vapour and  $\text{CO}_2$  (Fig. A5.1). Probably, the parameterization in [A5.6] does not apply in the case of moisture and  $\text{CO}_2$ , which implies that [A5.19] is also incorrect. Contrary to the entrainment flux of heat, the entrainment flux of moisture is positive (dry air is transported downward). Then, the countergradient profile in the upper part of the PBL becomes mirrored in comparison with respect to that of heat. The hypothesis is supported by field data and LES data showing that, in the upper part of the PBL, the pressure correlation term ((IV) in [A5.1]) in the heat and moisture flux budgets are mirrored (Lenschow *et al.*, 1980; Stull, 1988). Similar arguments are valid in the case of  $\text{CO}_2$ . Therefore, the countergradient terms of water vapour and  $\text{CO}_2$  are calculated using [A5.8] and [A5.9] at  $z/h = 0.4$  and taking them constant throughout the PBL. This approach resembles that of Troen and Mahrt (1986; Appendix 4) and yields virtually the same results, except that the profiles of water vapour and  $\text{CO}_2$  are much improved (Fig. A5.1).

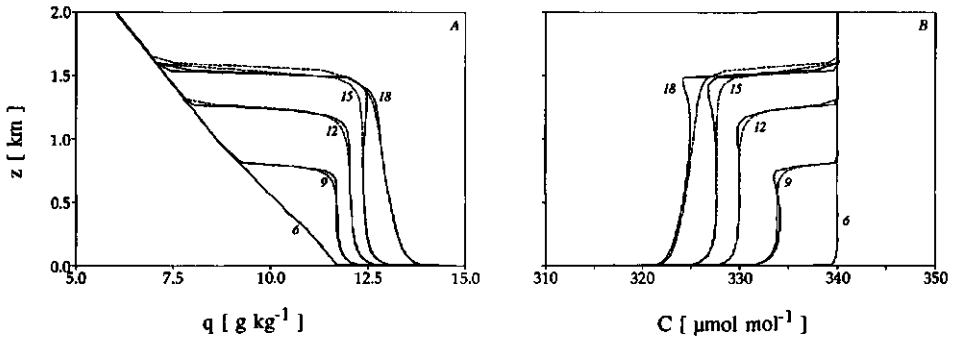


FIGURE A5.1. Simulated profiles of specific humidity ( $q$ ; in A) and  $\text{CO}_2$  concentration ( $C$ ; in B) using: 1) [A5.8] and [A5.9] (Holtslag & Moeng, 1991: solid lines) or 2) [A5.8] and [A5.9] for  $z/h = 0.4$  throughout the PBL (dashed lines). Initial conditions: MLS (see Section 5.3 and Appendix 12). Labels indicate Local Time (LT).

c) Diffusion coefficient for momentum

As before (see Appendix 4) it is assumed that  $K_h = K_m/Pr$ . However, it can be shown that  $Pr$  now becomes (matching the fluxes of the SL and the PBL):

$$\frac{K_m}{K_h} = Pr = \frac{\phi_h(z/L_v)}{\phi_m(z/L_v)} - \frac{\gamma_\theta K z}{\theta_* \phi_m(z/L_v)} \quad [\text{A5.20}]$$

$Pr$  is assumed constant above the SL and is evaluated using [A5.22] at  $z = 0.1h$ .

d) Transition from a convective PBL to a stable PBL

To provide a smooth transition between the stably stratified PBL and the convective PBL the values of  $K_s$  are interpolated between the Holtslag & Moeng (1991) parameterization (denoted by  $K_s(\text{H\&M})$ ) ([A5.10] or [A5.18]) and the parameterization by Troen & Mahrt (1986) ( $K_s(\text{T\&M})$ ; Appendix 4, [A4.2]) by taking

$$K_s = F_i K_s(\text{T\&M}) + (1 - F_i) K_s(\text{H\&M}) \quad [\text{A5.21}]$$

with

$$F_i = \sqrt{\frac{2.33 - w_*/u_*}{2.33}}; \quad w_*/u_* < 2.33 \quad [\text{A5.22}]$$

e) Entrainment ratios

In the present study, the entrainment ratio for the heat flux,  $R_h$ , is estimated as the ratio of the minimum heat flux in the PBL to the surface heat flux. This approach is consistent with the definitions given by Wyngaard & Brost (1984). The level where the minimum heat flux occurs,  $z_{H\text{min}}$ , will be found somewhat below  $h$ . The entrainment ratios,  $R_s$ , for water vapour and  $\text{CO}_2$  can also be calculated from the fluxes at  $z_{H\text{min}}$ . However, test simulations revealed that  $R_s$  is prone to fluctuations of a numerical nature. Therefore, the fluxes at  $z/z_{H\text{min}} = 0.8$  are used. The fluxes at this lower level are corrected for the height difference with  $z_{H\text{min}}$

(using [A5.11]). Also,  $R_h$  and  $R_s$  are updated only every ten time steps instead of every single time step. Resulting entrainment ratios show a daily trend. They are usually between -0.1 and -0.4 for heat, and between 0 and 3 for water vapour and  $CO_2$ .

f) Velocity scale and thermal temperature excess

For convective conditions, the relevant velocity scale in the new parameterization becomes  $w_*$  instead of  $w_s$  ( $\equiv u_* / \phi_m$ ; see [A4.5]). Therefore, the scaled thermal temperature excess,  $\theta_T$ , used to estimate  $h$  (see Appendix 4) is now estimated from

$$\theta_T = C \frac{\overline{w'\theta'}_s}{w_*} \tag{A5.23}$$

Here,  $C$  is taken 5 (cf. Holtslag & Moeng, 1991).

g) Other changes

Following Holtslag *et al.* (1990), the functions  $\phi_m$  and  $\phi_h$  for *unstable* conditions are taken

$$\phi_m = \left( 1 - 15 \frac{z}{L_v} \right)^{-1/3} \tag{A5.24a}$$

and

$$\phi_h = \left( 1 - 15 \frac{z}{L_v} \right)^{-1/2} \tag{A5.24b}$$

respectively. Furthermore, the bulk transfer approach of Louis (1979) is replaced by the fully integrated flux-profile relationships, according to which

$$r_a = \frac{\left[ \ln \left( \frac{z_r - D}{z_o} \right) - \Psi_m(\zeta_r) + \Psi_m(\zeta_o) \right] \left[ \ln \left( \frac{z_r - D}{z_o} \right) - \Psi_h(\zeta_r) + \Psi_h(\zeta_o) \right]}{\kappa^2 u_r(z_r - D) [\theta_s(z_o) - \theta_r]} \tag{A5.25}$$

[A5.25] replaces [A2.7]. In [A5.25]

$$\Psi_x = \int_0^{\zeta} \frac{1 - \phi_x(\zeta')}{\zeta'} d\zeta' \tag{A5.26}$$

(Paulson, 1970),  $\zeta_r = (z_r - D)/L_v$ ,  $\zeta_o = z_o/L_v$  and  $x = m$  or  $h$ . As before, it is assumed that  $r_a$  also applies to moisture and  $CO_2$ .

Finally, to calculate the effective atmospheric emissivity for longwave radiation,  $\epsilon_a$ , the parameterization of Brutsaert (1982) replaces that of Swinbank (1963). Then

$$\epsilon_a = 1.24 \left( \frac{e_r}{T_r} \right)^{1/7} \tag{A5.27}$$

where  $e_r$  is the water vapour pressure at the reference level.



## Appendix 6 Test of the modified PBL model

### a) Initial and boundary conditions

The initial conditions for the simulations presented here are the radiosonde observations from EFEDA (Bolle *et al.*, 1993; see also Section 3.2.1), 11 and 23 June ("Golden Days"). Average observed wind speed (x and y direction) between a height of 3 and 4 km (upper part of the PBL model grid) was taken as the geostrophic wind speed. Every time step, the imposed geostrophic wind was interpolated from these averages. The vertical wind speed was assumed zero. Observed global radiation was used to drive the exchange at the surface. For the experimental area,  $z_0$  may be taken 0.1 m and the albedo 25%.  $G/Q^*$ ,  $z_0/z_{oh}$ , and  $r_s$  were adjusted so that  $H$ , and  $Q^*$ , were rather well simulated. Then, the calculated energy balance will be in agreement with the observed one, so that it can be regarded as an imposed lower boundary condition of the PBL model.

### b) Results

Results of the simulations are shown in Fig. A6.1, where they are compared to observations. Fig. A6.1 A and B depict the simulated and the observed PBL height,  $h$ , for 11 and 23 June, respectively. Here,  $h$  was determined from radiosonde observations. The model's formalism was used in order to avoid methodological differences. It can be seen that the simulated boundary layer height is in reasonable agreement with the observations.

In Fig. A6.1 C and D profiles of  $\theta$  are shown. Note that height is normalized with  $h$ . It can be seen that the simulated profiles are realistic with respect to their shape. Furthermore, on both days, the evolution of the  $\theta$  profile is reasonably well simulated, until 12 UTC. Hereafter, the simulations clearly deviate from the observations.

Finally, in Fig. A6.1 E and F the profiles of  $q$  are depicted. The model produces slightly tilted profiles, which is in agreement with the observations. However, the evolution of the  $q$  profiles are rather poorly simulated.

### c) Discussion

Large scale advection, possibly caused by meso-scale circulations, is probably the reason for the deviation between modelled and observed profiles. For example, between 12 and 15 UTC on 23 June (Fig. A6.1D), an average heat flux of at least  $500 \text{ W m}^{-2}$  would be required to explain the observed 2 K increase of  $\theta$  within the PBL, with  $h = 2.5\text{--}3 \text{ km}$ . Less than half of that flux ( $\approx 225 \text{ W m}^{-2}$ ) was actually observed at the surface (data not shown). Also,  $\lambda E$  as observed at the surface cannot explain the observed evolution of  $q$  within the PBL. For instance, between 9 and 12 UTC on 11 June,  $h$  increases from about 0.6 km to about 2 km. The average  $q$  in the lowest 2 km increases with about  $0.11 \text{ g kg}^{-1}$  in the model profiles. This corresponds to  $\lambda E = 50$  to  $60 \text{ W m}^{-2}$ . By contrast, the average observed  $q$  below 2 km increases by about  $0.42 \text{ g kg}^{-1}$ , corresponding to  $\lambda E \approx 200 \text{ W m}^{-2}$ . Observed  $\lambda E$  at the surface was at most  $100 \text{ W m}^{-2}$  during this period (data not shown). For  $q$ , the influence of advection can also be seen as follows. In the observed and the simulated evolution the PBL becomes drier during the day. This is caused by the entrainment of the dry air from above the PBL, that is not compensated by  $\lambda E$  at the surface. If the  $\lambda E$  at the surface is very small, as is the case here, and if PBL growth stops, the humidity in the PBL must remain about the same if no other source of dry air is present. The results of the simulations are consistent with this reasoning. By contrast, the observed profiles continue to dry.

d) Conclusion

The PBL model realistically simulates the evolution of the PBL of areas where meso-scale circulations and large-scale advection may be neglected, that is, of extensive areas.

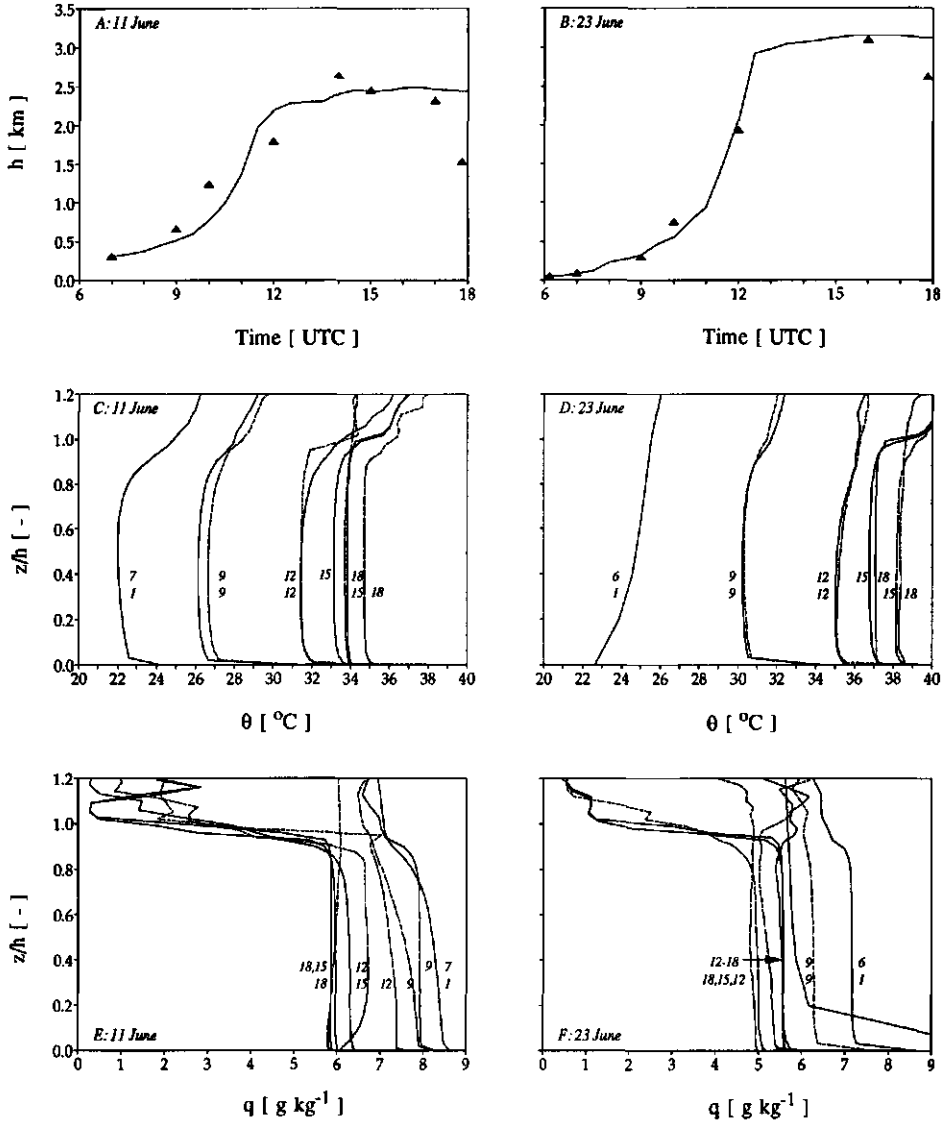


FIGURE A6.1. Results from the modified PBL model: comparison of calculated and observed PBL height ( $h$ : A and B), potential temperature profiles ( $\theta$ : C and D), and specific humidity profiles ( $q$ : E and F). Initial conditions and observations: EFEDA (Bolle et al., 1993). Solid lines represent model calculations, triangles and dashed lines represent observations. Labels denote time (UTC). Upper time labels refer to simulated profiles (solid lines) and lower time labels refer to observed profiles (dashed lines). "I" indicates "Initial profile". Note that normalized height ( $z/h$ ) is used in the case of the profiles.

## Appendix 7 The closed box model

### a) Description

The closed box model represents the PBL by a box with height  $h$ , containing well mixed air in the mixed layer (ML). Here, the potential temperature,  $\theta_m$ , the specific humidity,  $q_m$ , and the wind speed are assumed constant with height. The SL, where vertical gradients of  $\theta$ ,  $q$  and the wind speed occur, extends up to a height  $z_s$ . The box is nonpermeable to heat and water vapour, but transparent to radiation. Furthermore, a soil heat flux is allowed through the floor of the box.  $\theta_m$  and  $q_m$  are changed such that:

$$\frac{d\theta_m}{dt} = \frac{H}{\rho C_p h} \quad \text{and} \quad \frac{dq_m}{dt} = \frac{E}{\rho h} \quad [\text{A7.1}]$$

respectively. Obviously, the choice of  $h$  is critical. Also, only convective conditions are described.

### b) Coupling, initial and boundary conditions for the simulations presented in Chapter 2

The box model is coupled to the big-leaf model (Appendix 2) by taking  $z_r = z_s$ . The height of the box,  $h$ , and the surface characteristics like  $a$ ,  $z_0$  and  $r_s$  have to be specified. The average PBL depth from the simulations with the model of Troen & Mahrt (1986) is taken as the value for  $h$ ;  $u_r$  is assumed to be the wind speed of the well mixed air. It is determined as described in Section 2.3. From the radiosonde data of 6.00 UTC the average temperature and humidity between  $z_r$  and  $h$  are taken as the initial temperature and humidity.

The model runs with a time step of 2 minutes and a reference level at  $z_r = D + 50$  m. At every time,  $t$ ,  $S\downarrow$  (clear sky; Holtlag & Van Ulden, 1983) is used as the driving force.  $H$  and  $\lambda E$  from the vegetation part are used to evaluate the new values of  $\theta_m$  and  $q_m$ , which enables computation of the fluxes in the next time step, etc.

## Appendix 8 Temperature responses

### a) $CO_2$ compensation concentration, $\Gamma$

It can be shown that  $\Gamma$  of  $C_3$  plants, in the absence of dark respiration, can be evaluated from (Farquhar *et al.*, 1980, Collatz *et al.*, 1991):

$$\Gamma = \frac{[O_2]}{2\tau} \quad [A8.1]$$

Here,  $\tau$  describes the ratio of the oxygenase to the carboxylase activity of Rubisco. Thus, the temperature dependence of  $\Gamma$  can be described by means of the temperature dependence of  $\tau$ .  $\tau \approx 2500$  with  $Q_{10} \approx 0.6$  (Jensen, 1990; Collatz *et al.*, 1991).

Brooks & Farquhar (1985) proposed the following function to account for temperature effects on  $\Gamma$  in the absence of dark respiration (at 210  $\mu\text{mol mol}^{-1}$  ambient  $O_2$ ):

$$\Gamma = 44.7 + 1.88(T - 25) + 0.036(T - 25)^2 \quad [A8.2]$$

In the present study, the temperature dependence of  $\Gamma$  is described by means of a  $Q_{10}$  response function:

$$\Gamma = \Gamma(@25) \cdot Q_{10}^{(0.1(T-25))} \quad [A8.3]$$

If in [A8.3]  $Q_{10}$  is taken 1.5, and  $\Gamma(@25)$  is taken 45  $\mu\text{mol mol}^{-1}$  for  $C_3$  plants and 3  $\mu\text{mol mol}^{-1}$  for  $C_4$  plants, respectively, [A8.1]-[A8.3] give similar values for  $\Gamma$  up to about 35  $^{\circ}\text{C}$ , while [A8.3] leads to values intermediate to those of [A8.1] and [A8.2] at higher temperatures. The present parameterization for  $C_3$  plants is compared to [A8.1] and [A8.2] in Fig. A8.1.

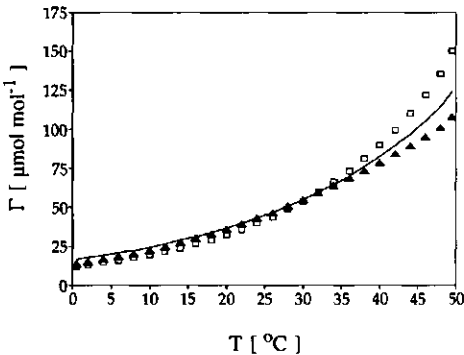


FIGURE A8.1. Temperature response of  $CO_2$  compensation concentration,  $\Gamma$ , for  $C_3$  plants, without dark respiration, at 21% ambient  $O_2$ . Solid line: present parameterization ([A8.3] with  $\Gamma(@25) = 45 \mu\text{mol mol}^{-1}$  and  $Q_{10}=1.5$ ); Squares: [A8.1] (Brooks & Farquhar, 1985); triangles: [A8.2] with  $\tau = 2500$ ,  $Q_{10} = 0.6$  (Jensen, 1990; Collatz *et al.*, 1991).

### b) Maximum photosynthetic capacity, $A_{m,max}$

The temperature responses of  $A_{m,max}$  is assumed to be given by (Collatz *et al.*, 1992):

$$X(T) = \frac{\frac{T - 25}{10} \cdot X(@25) \cdot Q_{10}^{\frac{T - 25}{10}}}{(1 + \text{EXP}(0.3(T_1 - T)))(1 + \text{EXP}(0.3(T - T_2)))} \quad [A8.4]$$

where  $X$  denotes  $A_{m,max}$  or  $g_m$  and  $T_1$  and  $T_2$  denote temperatures that enable a description

of temperature inhibition characteristics.  $A_{m,max}$  is assumed proportional to the maximum catalytic capacity of Rubisco,  $V_{cmax}$ , where  $V_{cmax}$  is a function of the activity of Rubisco as well as of its total amount present in the leaf. Thus,  $A_{m,max} = k \cdot V_{cmax}$ , with  $k=0.5$  for  $C_3$  species (Collatz *et al.*, 1991) and  $k=1$  for  $C_4$  species (Collatz *et al.*, 1992). Then, the temperature dependence of  $A_{m,max}$  corresponds to that of  $V_{cmax}$ .  $V_{cmax}(@25)$  may be taken  $4.3 \text{ mg m}^{-2} \text{ s}^{-1}$  with  $Q_{10} = 2.2$  for  $C_3$  plants (Farquhar *et al.*, 1980).

$A_{m,max}$  of  $C_3$  plants is assumed to be less inhibited at lower temperatures than  $A_{m,max}$  of  $C_4$  plants. Therefore,  $T_1$  is taken  $8^\circ\text{C}$  for  $C_3$  plants and  $13^\circ\text{C}$  for  $C_4$  plants.  $T_2$  is taken  $38^\circ\text{C}$  for both plant types, which results in the about same temperature optimum for  $A_{m,max}$ . Then, at high light intensity and high  $\text{CO}_2$  concentration, where  $A_n \rightarrow A_{m,max}$ , the temperature response of  $C_3$  and  $C_4$  plants will become similar (Berry & Raison, 1982). Now, using  $Q_{10}=2$  for  $C_3$  and  $C_4$  species, the temperature characteristic of  $A_{m,max}$ , given by [A8.4], corresponds well to that of  $k \cdot V_{cmax}$  if  $A_{m,max}(@25) = 2.2 \text{ mg m}^{-2} \text{ s}$  for  $C_3$  plants (cf. Farquhar *et al.*, 1980) and  $A_{m,max}(@25) = 1.7 \text{ mg m}^{-2} \text{ s}$  for  $C_4$  plants (cf. Collatz *et al.*, 1992).

In Fig. A8.2 the resulting temperature response of  $A_{m,max}$  is compared to the responses given by Collatz *et al.* (1991,1992). The parameterizations resemble each other at a temperature less than  $30^\circ\text{C}$ . However, the present parameterization results in a stronger inhibition for  $C_3$  plants at a high temperature, accompanied by a lower maximum  $A_{m,max}$ . For  $C_4$  plants, the reverse is true. These differences with the parameterizations by Collatz (1991, 1992) are considered to be reasonable.

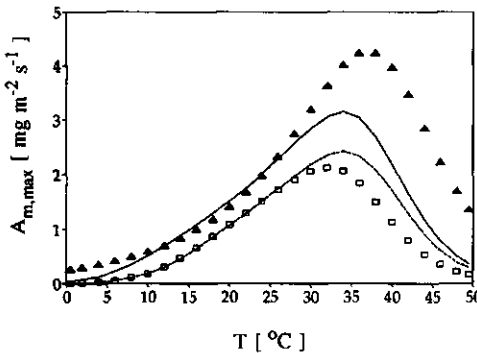


FIGURE A8.2. Temperature response of maximum photosynthetic capacity,  $A_{m,max}$ . Solid line: present parameterization for  $C_3$  plants; Dashed line: present parameterization for  $C_4$  plants; Triangles: for  $C_3$  plants according to Collatz *et al.* (1991); Squares: for  $C_4$  plants according to Collatz *et al.* (1992).

### c) Mesophyll conductance, $g_m$

$g_m$  is the slope of the  $\text{CO}_2$  response curve of photosynthesis at low  $C_i$  and high light intensity. For  $C_3$  species, this slope can be conveniently evaluated at  $C_i = \Gamma$  (Farquhar *et al.*, 1980):

$$\frac{dA_n}{dC_i} = g_m = \frac{V_{cmax}}{\Gamma + K_c \left(1 + \frac{O}{K_o}\right)} \quad [\text{A8.5}]$$

Here,  $K_c$  and  $K_o$  are Michaelis constants for  $\text{CO}_2$  and  $\text{O}_2$ , respectively, and  $O$  denotes the partial pressure of  $\text{O}_2$ . It can be seen that the temperature response of  $g_m$  will be the result of the temperature dependence of  $A_{m,max}$  ( $\approx V_{cmax}/2$ ; see b),  $\Gamma$ ,  $K_c$  and  $K_o$ . Here,  $A_{m,max}$  and  $\Gamma$  are determined as described above.  $K_c$  and  $K_o$  are taken, following Farquhar *et al.* (1980),

$K_o(@25) = 330 \text{ mmol mol}^{-1}$  with  $Q_{10} = 1.6$ , and  $K_c = 460 \text{ } \mu\text{mol mol}^{-1}$ , with  $Q_{10}=2.2$ , and without temperature inhibition ([A8.3]). In the present study, the resulting temperature dependence of  $g_m$  is assumed to be given by [A8.4]. Then, using  $Q_{10} = 2$ , [A8.5] can be approximated by [A8.4] with  $g_m(@25) = 7 \text{ mm s}^{-1}$ ,  $T_1 = 5 \text{ }^\circ\text{C}$  and  $T_2 = 28 \text{ }^\circ\text{C}$ .

For  $C_4$  species, the response of  $A_n$  to  $C_i$  at low  $C_i$  can be calculated as (Collatz *et al.*, 1992):

$$A_n = k C_i \quad \text{[A8.6]}$$

which results in  $dA_n/dC_i = g_m = k$ . Again using  $Q_{10}=2$ ,  $g_m$  and [A8.6] are matched by taking  $g_m(@25) = 17.5 \text{ mm s}^{-1}$ ,  $T_1 = 13 \text{ }^\circ\text{C}$  and  $T_2 = 36 \text{ }^\circ\text{C}$  (cf. Collatz *et al.*, 1992).

In Fig. A8.3, the present parameterizations of  $g_m$  are compared to [A8.5] and to  $k$  in [A8.6].

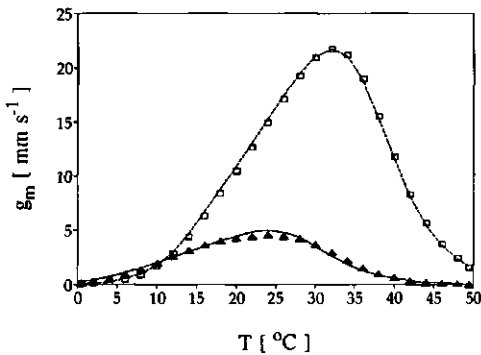


FIGURE A8.3. Temperature response of mesophyll conductance,  $g_m$ . Solid line: present parameterization for  $C_3$  plants; Dashed line: present parameterization for  $C_4$  plants; Triangles: [A8.5] ( $C_3$  plants; Farquhar *et al.*, 1980) with temperature response functions according to Collatz *et al.* (1992); Squares:  $k$  in [A8.6] ( $C_4$  plants; Collatz *et al.*, 1992).

## Appendix 9 Characterization of micrometeorological conditions during EFEDA, site Tomelloso

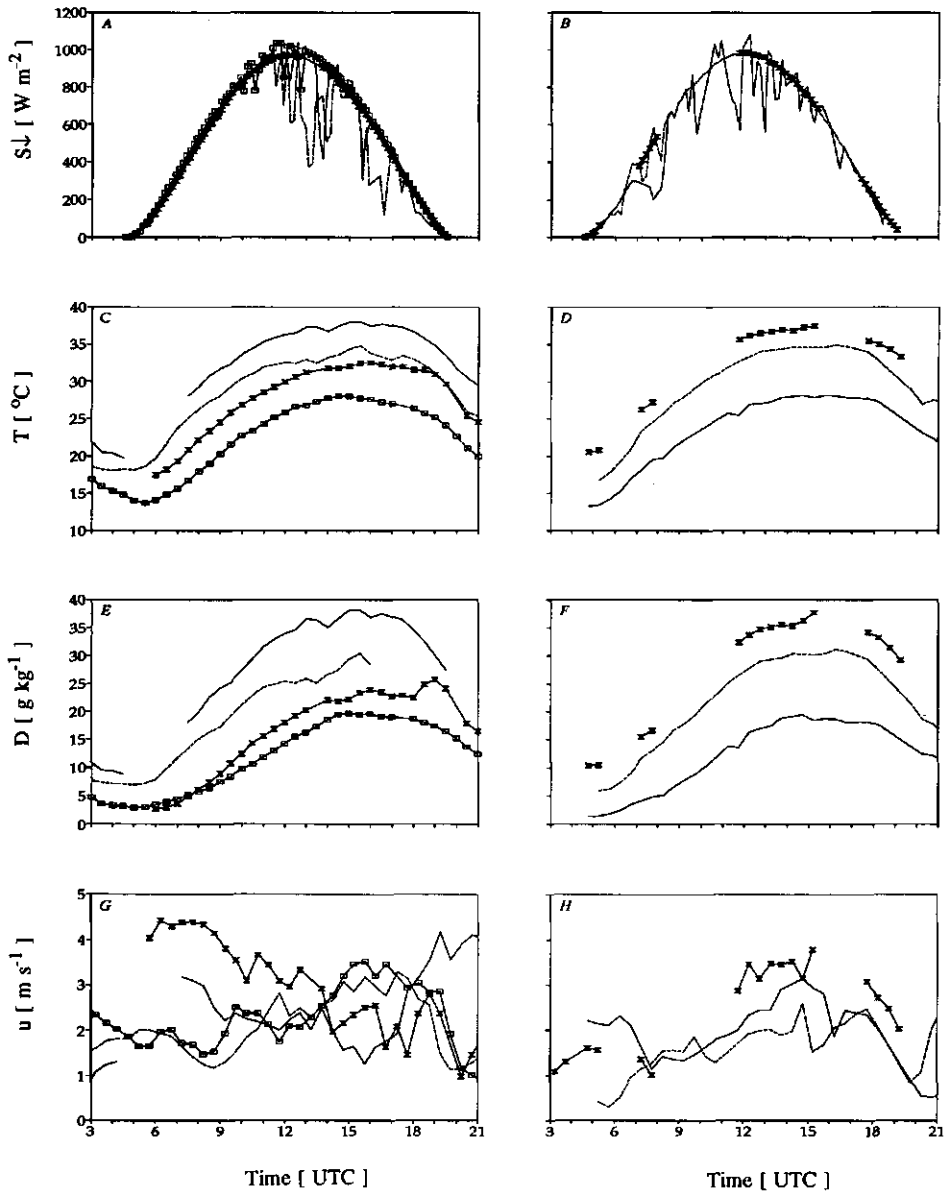


FIGURE A9.1. A, B: global radiation ( $S\downarrow$ ) (Kipp Solarimeter, type CM 5, height 6 m); C, D: temperature ( $T$ ), and E, F: specific humidity deficit ( $D$ ) (aspirated psychrometers equipped with PT100 resistance elements, height 1.4 m); G, H: wind speed ( $u$ ) (cup anemometer, height 1.4 m). Left panels: 17 June (solid with hourglasses), 21 June (dashed), 25 June (solid) and 28 June (solid with squares); right panels: 19 June (solid), 23 June (dashed), 27 June (solid with hourglasses). A description of EFEDA can be found in Bolle et al. (1993).

## Appendix 10 Response test of gas exchange system

In order to test the stabilization of the concentration difference in the leaf cuvette, a sunlit leaf was enclosed during two minutes and a half. During the first minute, values were recorded after every 10 seconds. Hereafter, values were recorded at 90 s, 120 s and 150 s. The measured  $\text{CO}_2$  concentration difference and the apparent net photosynthetic rate, resulting from these differences, are depicted in Fig. A10.1. Furthermore, the corresponding specific humidity difference at the leaf surface and stomatal conductance are shown in Fig. A10.2.

FIGURE A10.1. Results of gas exchange response test. Observed  $\text{CO}_2$  concentration difference ( $\Delta C$ , solid with squares, left ordinate) and apparent net photosynthetic rate ( $A_n$ , dashed with triangles, right ordinate) versus time ( $t$ ). The vertical lines indicate the time interval in which observations usually were recorded.

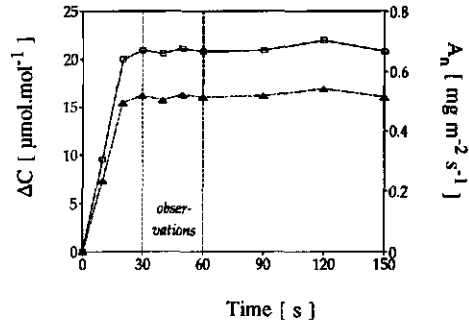
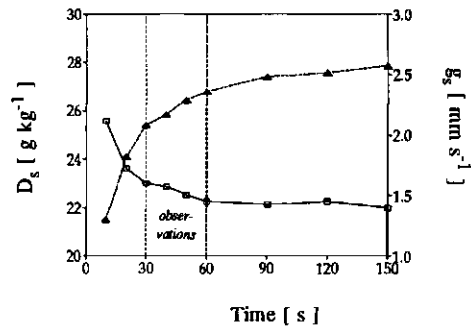


FIGURE A10.2. As in Fig. A10.1 but for the specific humidity difference at the leaf surface ( $D_s$ , solid with squares, left ordinate), and for stomatal conductance ( $g_s$ , dashed with triangles, right ordinate).





## Appendix 11 Gas exchange calculations

### a) Influence of transpiration on air flow through the cuvette and on CO<sub>2</sub> concentration

Due to the addition of water vapour to the air stream in the cuvette the flow will be altered according to (Ball, 1987):

$$F_o = \frac{F_r(1 - w_r)}{(1 - w_o)} \quad [\text{A11.1}]$$

where  $F$  is the air flow ( $\text{mol s}^{-1}$ ),  $w$  the water vapour concentration ( $\text{mol mol}^{-1}$ ) and the subscripts  $i$  and  $r$  denote "reference" (towards cuvette), and "out" (from cuvette), respectively. The mole fractions  $w$  are calculated from the measured relative humidity, the saturation vapour pressure at the measured temperature, and the atmospheric pressure. The CO<sub>2</sub> mole fraction will also be affected by humidification. To take this effect into account, the CO<sub>2</sub> concentration of the reference air ( $c_r$ ,  $\text{mol mol}^{-1}$ ) is corrected using:

$$c_{r,c} = \frac{c_r(1 - w_o)}{(1 - w_r)} \quad [\text{A11.2}]$$

(Ball, 1987) where  $c_{r,c}$  denotes the corrected reference concentration.

### b) Net photosynthetic rate, $A_n$ , and transpiration rate, $E$ (Ball, 1987)

After stabilization of the CO<sub>2</sub> concentration difference between the reference air and the sample air,  $A_n$  can be determined from:

$$A_n = \frac{(F_r c_{r,c} - F_o c_o)}{L_a} \quad [\text{A11.3}]$$

with  $A_n$  in  $\text{mol m}^{-2} \text{s}^{-1}$  and with  $L_a$  denoting the leaf area enclosed by the cuvette. Furthermore, the transpiration rate can be evaluated from:

$$E = \frac{F_r (w_o - w_r)}{L_a (1 - w_o)} \quad [\text{A11.4}]$$

where the transpiration rate  $E$  is also in  $\text{mol m}^{-2} \text{s}^{-1}$ .

### c) Photosynthetically active radiation, PAR

The amount of PAR absorbed by the leaf,  $I_l$ , is calculated from the amount of PAR measured outside the leaf cuvette,  $I_o$ , assuming a cuvette transmittance of 85% (Van Kleef, 1991). Furthermore, it is assumed that the PAR absorptivity of the leaves is 80% (Goudriaan, 1977), so that:

$$I_l = 0.68I_o \quad [\text{A11.5}]$$

The total amount of solar radiation absorbed by the leaf,  $S\downarrow_l$ , is calculated from the measured incident PAR, assuming that 50% of the solar radiation is PAR and 50% is Near Infra Red radiation (NIR), so that  $S\downarrow = 2I_o$  (Ross, 1975; Goudriaan, 1977). The transmittance of the cuvette to NIR is 0.6 (Van Kleef, 1991), and the absorptivity of the leaf to NIR is taken 0.2 (Goudriaan, 1977). Thus:

$$S\downarrow_l = 0.68I_o(\text{PAR}) + 0.12I_o(\text{NIR}) = 0.8I_o \quad [\text{A11.6}]$$

d) Leaf temperature,  $T_l$ 

The leaf temperature,  $T_l$ , is calculated from the energy balance of the leaf, using:

$$T_l = T_{cuv} + \frac{S\downarrow_l - \lambda E}{\frac{\rho C_p}{r_{bh}} + 4\sigma T_{cuv}^3} \quad [A11.7]$$

where the temperature of the air in the cuvette,  $T_{cuv}$ , and  $T_l$  are in Kelvin and where  $E$  is in  $\text{kg m}^{-2} \text{s}^{-1}$  again. Furthermore,  $r_{bh}$  denotes the aerodynamic resistance to heat transfer ( $20.0 \text{ s m}^{-1}$ ; Van Kleeef, 1991). Other symbols are as in Appendix 2.

e) stomatal conductance,  $g_s$ 

$g_s$  is evaluated from the water vapour content in the sub-stomatal cavities, assuming that the air in the cavities is saturated with water vapour, so that:

$$g_s = \frac{E}{\rho(q^*(T_l) - q_{cuv}) - E r_{bv}} \quad [A11.8]$$

where  $q_{cuv}$  is the specific humidity of the air in the cuvette and  $r_{bv}$  is the aerodynamic resistance to water vapour diffusion ( $18.6 \text{ s m}^{-1}$ ).

f)  $\text{CO}_2$  concentration at the leaf surface,  $C_s$  and internal  $\text{CO}_2$  concentration,  $C_i$ 

Finally, the  $\text{CO}_2$  concentration at the surface of the leaf,  $C_s$ , and the intercellular  $\text{CO}_2$  concentration,  $C_i$ , are evaluated using:

$$C_s = \frac{(g_{bc} - \frac{E}{2\rho\epsilon})C_{cuv} - A_n}{g_{bc} + \frac{E}{2\rho\epsilon}} \quad [A11.9]$$

and

$$C_i = \frac{(g_{sc} - \frac{E}{2\rho\epsilon})C_s - A_n}{g_{sc} + \frac{E}{2\rho\epsilon}} \quad [A11.10]$$

where  $g_{bc}$  is the aerodynamic conductance for  $\text{CO}_2$  (taken  $1/r_{av}$ ) and  $g_{sc} = 1.6g_s$  is the stomatal conductance for  $\text{CO}_2$ .

Appendix 12 McClatchey profiles (specific humidity and potential temperature)

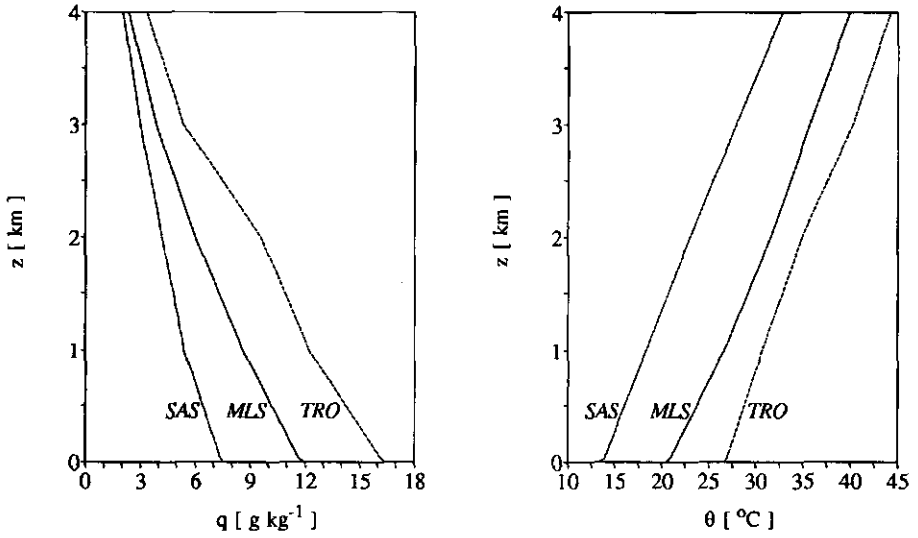


FIGURE A12.1. McClatchey specific humidity profiles ( $q$ ; left) and potential temperature profiles ( $\theta$ , right): Sub Arctic Summer (SAS), Mid Latitude Summer (MLS), and Tropical (TRO).

Appendix 13 Results from sensitivity analyses (Chapter 5)

This appendix contains results of the sensitivity analyses presented in Chapter 5. Symbols are as defined in the list of symbols. Note that CO<sub>2</sub> concentration is given in mg m<sup>-3</sup>, and A<sub>nc</sub> in µg m<sup>-2</sup> s<sup>-1</sup>. Futhermore:

- Pho = photosynthesis mechanism (C<sub>3</sub> or C<sub>4</sub>);
- Ini = initial conditions (SASn, MLSn or TROn. Here n = 1 or 2, denoting 1xCO<sub>2</sub> and 2xCO<sub>2</sub> respectively).

The various sets are described in Section 5.3 and Table 5.1. Codes defining the sets are:

- with or without PBL feedback: + or - PBL;
- with or without A-g<sub>s</sub> model: + or - A;
- with or without humidity response: + or - D;
- with PBL feedback but without CO<sub>2</sub> fluxes and concentrations within the PBL: +PBL(-CO<sub>2</sub> fluxes).

See Chapter 5 for further explanation.

Set I: +PBL, +A, +D, z<sub>0</sub>=0.12m.

Pho	Ini	LAI	Q*	H	λE	A <sub>nc</sub>	r <sub>s</sub>	T <sub>l</sub>	D <sub>l</sub>	C <sub>s</sub>	C <sub>i</sub> /C <sub>s</sub>	T <sub>r</sub>	q <sub>r</sub>	C <sub>r</sub>	U <sub>r</sub>	r <sub>a</sub>	h
C3	SAS1	3	419	99	278	1143	51	20.3	4.7	479	0.79	18.1	7.9	598	6.0	17.3	1295
C3	MLS1	3	439	67	328	1070	52	26.6	5.9	474	0.79	25.0	12.8	580	5.8	18.3	1085
C3	TRO1	3	437	132	261	612	113	33.7	15.1	496	0.70	31.0	15.5	581	5.8	17.7	1518
C3	SAS2	3	410	147	222	1448	102	22.0	7.5	999	0.73	19.0	7.3	1214	6.2	16.2	1468
C3	MLS2	3	426	122	261	1338	119	28.9	11.0	996	0.68	26.2	11.7	1183	6.0	16.9	1308
C3	TRO2	3	420	213	165	695	280	36.6	23.5	1028	0.59	32.4	14.3	1174	6.2	15.7	1818
C3	SAS1	4	421	91	287	1182	44	20.0	4.2	476	0.80	18.0	7.9	596	6.0	17.4	1261
C3	MLS1	4	441	59	338	1103	44	26.2	5.0	472	0.80	24.7	13.0	579	5.7	18.7	1047
C3	TRO1	4	451	55	351	866	67	31.2	8.5	483	0.76	29.9	16.5	576	5.8	18.7	1285
C3	SAS2	4	412	136	235	1474	88	21.7	6.9	997	0.74	18.8	7.5	1214	6.1	16.4	1428
C3	MLS2	4	430	104	283	1383	96	28.2	9.4	992	0.71	25.8	12.0	1182	6.0	17.3	1238
C3	TRO2	4	428	168	217	855	198	35.2	19.3	1019	0.61	31.8	14.8	1172	6.1	16.4	1695
C3	SAS1	5	421	87	292	1160	41	19.8	4.0	477	0.81	17.9	8.0	597	6.0	17.5	1248
C3	MLS1	5	442	55	343	1064	40	26.0	4.7	473	0.80	24.6	13.1	580	5.7	18.7	1025
C3	TRO1	5	454	41	367	892	56	30.6	7.1	481	0.78	29.6	16.8	576	5.8	19.0	1219
C3	SAS2	5	413	130	242	1420	82	21.4	6.5	998	0.75	18.7	7.5	1214	6.1	16.5	1410
C3	MLS2	5	432	95	294	1315	86	27.8	8.6	993	0.72	25.7	12.2	1183	5.9	17.4	1205
C3	TRO2	5	435	131	260	950	154	34.0	16.1	1012	0.64	31.3	15.2	1171	6.0	16.9	1586
C4	SAS1	3	407	160	207	1317	123	22.5	8.3	480	0.42	19.3	7.2	597	6.2	16.0	1520
C4	MLS1	3	430	106	281	1428	103	28.4	9.8	467	0.40	26.0	11.9	576	6.0	17.1	1260
C4	TRO1	3	445	74	327	1428	101	32.2	11.3	465	0.39	30.5	15.9	567	6.1	17.4	1410
C4	SAS2	3	398	211	147	1421	230	24.2	11.1	1010	0.38	20.0	6.8	1216	6.4	15.2	1670
C4	MLS2	3	417	165	210	1488	209	30.6	14.9	999	0.34	27.1	11.0	1181	6.2	15.9	1472
C4	TRO2	3	430	147	240	1447	221	35.0	18.5	999	0.30	31.8	14.7	1164	6.3	16.0	1700
C4	SAS1	4	409	150	218	1355	109	22.2	7.8	478	0.42	19.1	7.3	596	6.2	16.1	1486
C4	MLS1	4	431	97	291	1432	92	28.0	9.0	466	0.41	25.8	12.1	575	6.0	17.2	1225
C4	TRO1	4	447	65	338	1415	88	31.9	10.3	465	0.40	30.3	16.1	567	6.1	17.6	1365
C4	SAS2	4	400	201	159	1443	203	23.8	10.6	1008	0.39	19.9	6.8	1215	6.3	15.3	1647
C4	MLS2	4	419	153	224	1464	183	30.2	13.9	998	0.35	26.9	11.1	1182	6.2	16.1	1432
C4	TRO2	4	433	131	259	1424	189	34.4	17.0	998	0.32	31.6	14.9	1164	6.3	16.2	1646
C4	SAS1	5	410	145	224	1324	101	22.0	7.5	479	0.42	19.0	7.3	597	6.2	16.2	1471
C4	MLS1	5	432	93	296	1353	86	27.8	8.6	468	0.41	25.7	12.2	577	6.0	17.3	1209
C4	TRO1	5	448	60	343	1312	83	31.7	9.8	468	0.40	30.2	16.2	569	6.1	17.7	1337
C4	SAS2	5	401	195	166	1389	187	23.6	10.2	1009	0.39	19.8	6.9	1216	6.3	15.4	1622
C4	MLS2	5	421	146	232	1351	169	29.9	13.3	1001	0.36	26.8	11.2	1183	6.2	16.2	1404
C4	TRO2	5	435	121	270	1297	172	34.1	16.1	1001	0.33	31.4	15.0	1166	6.3	16.4	1608

158 Appendix 13

Set II: +PBL, +A, +D,  $z_0=0.12m$ .

Pho	Ini	LAI	$Q^*$	H	$\lambda E$	$A_{h,c}$	$r_s$	$T_1$	$D_1$	$C_s$	$C_1/C_s$	$T_r$	$q_r$	$C_r$	$U_r$	$r_a$	h
C3	SAS1	3	419	102	275	1160	53	20.4	4.8	496	0.79	18.1	7.9	618	6.0	17.2	-
C3	MLS1	3	439	71	324	1091	54	26.6	6.0	495	0.78	25.0	12.8	604	5.8	18.2	-
C3	TRO1	3	437	134	258	619	115	33.7	15.2	506	0.70	31.0	15.5	592	5.8	17.7	-
C3	SAS2	3	419	102	275	1160	53	20.4	4.8	496	0.79	18.1	7.9	618	6.0	17.2	-
C3	MLS2	3	439	71	324	1091	54	26.6	6.0	495	0.78	25.0	12.8	604	5.8	18.2	-
C3	TRO2	3	437	134	258	619	115	33.7	15.2	506	0.70	31.0	15.5	592	5.8	17.7	-
C3	SAS1	4	420	94	284	1201	46	20.0	4.3	495	0.80	18.0	7.9	619	6.0	17.4	-
C3	MLS1	4	441	63	334	1126	46	26.3	5.2	494	0.79	24.7	13.0	605	5.7	18.6	-
C3	TRO1	4	450	58	347	879	69	31.3	8.7	499	0.76	29.9	16.5	594	5.8	18.6	-
C3	SAS2	4	420	94	284	1201	46	20.0	4.3	495	0.80	18.0	7.9	619	6.0	17.4	-
C3	MLS2	4	441	63	334	1126	46	26.3	5.2	494	0.79	24.7	13.0	605	5.7	18.6	-
C3	TRO2	4	450	58	347	879	69	31.3	8.7	499	0.76	29.9	16.5	594	5.8	18.6	-
C3	SAS1	5	421	90	289	1177	43	19.9	4.0	495	0.80	17.9	8.0	619	6.0	17.5	-
C3	MLS1	5	441	58	339	1085	42	26.1	4.8	494	0.80	24.6	13.1	605	5.7	18.6	-
C3	TRO1	5	453	45	363	907	57	30.7	7.3	497	0.77	29.6	16.8	595	5.8	19.0	-
C3	SAS2	5	415	151	222	1428	80	21.1	5.8	1016	0.76	17.9	8.0	1238	6.0	16.5	-
C3	MLS2	5	434	121	269	1331	81	27.4	7.3	1014	0.74	24.6	13.1	1210	5.7	17.4	-
C3	TRO2	5	443	124	274	1130	114	32.4	11.1	1019	0.69	29.6	16.8	1190	5.8	17.3	-
C4	SAS1	3	407	163	203	1323	126	22.6	8.4	496	0.41	19.3	7.2	616	6.2	15.9	-
C4	MLS1	3	429	111	275	1435	108	28.5	10.0	490	0.40	26.0	11.9	602	6.0	17.0	-
C4	TRO1	3	437	134	258	619	115	33.7	15.2	506	0.70	31.0	15.5	592	5.8	17.7	-
C4	SAS2	3	407	163	203	1323	126	22.6	8.4	496	0.41	19.3	7.2	616	6.2	15.9	-
C4	MLS2	3	429	111	275	1435	108	28.5	10.0	490	0.40	26.0	11.9	602	6.0	17.0	-
C4	TRO2	3	444	80	320	1433	105	32.4	11.6	489	0.38	30.5	15.9	593	6.1	17.3	-
C4	SAS1	4	409	154	214	1361	112	22.3	7.9	495	0.42	19.1	7.3	616	6.2	16.0	-
C4	MLS1	4	431	103	285	1436	96	28.1	9.2	490	0.41	25.8	12.1	603	6.0	17.2	-
C4	TRO1	4	446	70	331	1418	93	32.0	10.6	488	0.39	30.3	16.1	594	6.1	17.6	-
C4	SAS2	4	409	154	214	1361	112	22.3	7.9	495	0.42	19.1	7.3	616	6.2	16.0	-
C4	MLS2	4	431	103	285	1436	96	28.1	9.2	490	0.41	25.8	12.1	603	6.0	17.2	-
C4	TRO2	4	446	70	331	1418	93	32.0	10.6	488	0.39	30.3	16.1	594	6.1	17.6	-
C4	SAS1	5	410	149	220	1329	105	22.1	7.6	496	0.42	19.0	7.3	616	6.2	16.1	-
C4	MLS1	5	432	98	291	1355	90	27.9	8.8	491	0.41	25.7	12.2	603	6.0	17.2	-
C4	TRO1	5	447	66	337	1312	86	31.8	10.0	490	0.40	30.2	16.1	594	6.1	17.7	-
C4	SAS2	5	403	211	152	1387	189	23.2	9.4	1022	0.40	19.0	7.3	1233	6.2	15.5	-
C4	MLS2	5	423	174	207	1358	169	29.4	11.7	1019	0.38	25.7	12.2	1206	6.0	16.2	-
C4	TRO2	5	437	150	242	1297	169	33.5	14.0	1018	0.35	30.2	16.1	1188	6.1	16.3	-

## Set III: +PBL, +A, +D, LAI=5.

Pho	Ini	$z_0$	$Q^*$	H	$\lambda E$	An,c	$r_s$	$T_1$	$D_1$	$C_s$	$C_1/C_s$	$T_r$	$q_r$	$C_r$	$U_r$	$r_a$	h
C3	SAS1	0.03	417	87	288	1152	39	20.5	3.7	469	0.81	17.9	8.0	597	6.9	26.1	1244
C3	MLS1	0.03	438	58	336	1035	40	26.7	4.6	467	0.81	24.7	13.0	581	6.7	27.5	1043
C3	TRO1	0.03	449	52	352	818	61	31.5	7.7	478	0.77	29.8	16.6	577	6.7	28.0	1264
C3	SAS2	0.03	409	123	245	1417	79	22.1	6.4	988	0.75	18.6	7.6	1214	7.0	24.9	1379
C3	MLS2	0.03	428	94	291	1288	87	28.5	8.6	985	0.72	25.6	12.2	1183	6.8	26.0	1195
C3	TRO2	0.03	420	165	213	721	199	36.3	21.3	1021	0.62	31.7	14.8	1174	6.9	24.9	1686
C3	SAS1	0.12	421	87	292	1160	41	19.8	4.0	477	0.81	17.9	8.0	597	6.0	17.5	1248
C3	MLS1	0.12	442	55	343	1064	40	26.0	4.7	473	0.80	24.6	13.1	580	5.7	18.7	1025
C3	TRO1	0.12	454	41	367	892	56	30.6	7.1	481	0.78	29.6	16.8	576	5.8	19.0	1219
C3	SAS2	0.12	413	130	242	1420	82	21.4	6.5	998	0.75	18.7	7.5	1214	6.1	16.5	1410
C3	MLS2	0.12	432	95	294	1315	86	27.8	8.6	993	0.72	25.7	12.2	1183	5.9	17.4	1205
C3	TRO2	0.12	435	131	260	950	154	34.0	16.1	1012	0.64	31.3	15.2	1171	6.0	16.9	1586
C3	SAS1	0.48	425	88	295	1163	43	19.3	4.2	484	0.80	17.9	8.0	597	4.7	10.5	1252
C3	MLS1	0.48	445	52	349	1087	41	25.5	4.8	479	0.80	24.5	13.2	579	4.5	11.3	1012
C3	TRO1	0.48	457	34	377	939	53	30.0	6.9	484	0.78	29.4	17.1	574	4.5	11.6	1178
C3	SAS2	0.48	417	137	238	1419	84	20.8	6.6	1006	0.75	18.8	7.5	1216	4.9	9.7	1434
C3	MLS2	0.48	436	98	295	1333	86	27.3	8.7	1000	0.72	25.7	12.2	1183	4.7	10.4	1235
C3	TRO2	0.48	443	111	287	1106	130	32.7	13.8	1010	0.66	31.0	15.4	1170	4.8	10.2	1533
C3	SAS1	2.00	428	89	296	1163	45	18.8	4.4	491	0.80	17.9	8.1	598	3.0	4.7	1248
C3	MLS1	2.00	448	51	352	1104	42	25.0	5.0	484	0.80	24.4	13.4	579	2.7	5.3	996
C3	TRO1	2.00	460	31	383	973	52	29.6	6.8	488	0.78	29.2	17.3	573	2.7	5.5	1134
C3	SAS2	2.00	420	146	233	1414	86	20.3	6.7	1014	0.75	18.9	7.4	1218	3.1	4.4	1459
C3	MLS2	2.00	439	101	294	1347	87	26.8	8.7	1008	0.72	25.7	12.1	1185	2.9	4.7	1218
C3	TRO2	2.00	448	104	299	1186	119	31.9	12.8	1013	0.67	30.9	15.6	1170	3.0	4.7	1499
C4	SAS1	0.03	406	135	230	1340	96	22.7	7.3	468	0.43	18.8	7.4	595	7.1	24.4	1427
C4	MLS1	0.03	429	89	297	1351	82	28.4	8.3	458	0.42	25.6	12.2	576	6.9	25.8	1183
C4	TRO1	0.03	445	60	341	1306	80	32.1	9.4	458	0.41	30.2	16.1	569	6.9	26.6	1331
C4	SAS2	0.03	396	180	177	1400	181	24.5	10.5	1000	0.39	19.5	7.0	1215	7.1	23.5	1572
C4	MLS2	0.03	416	136	238	1344	166	30.6	13.4	992	0.36	26.6	11.4	1183	7.0	24.5	1367
C4	TRO2	0.03	430	114	273	1293	173	34.7	16.3	992	0.33	31.3	15.1	1166	7.1	24.8	1571
C4	SAS1	0.12	410	145	224	1324	101	22.0	7.5	479	0.42	19.0	7.3	597	6.2	16.2	1471
C4	MLS1	0.12	432	93	296	1353	86	27.8	8.6	468	0.41	25.7	12.2	577	6.0	17.3	1209
C4	TRO1	0.12	448	60	343	1312	83	31.7	9.8	468	0.40	30.2	16.1	569	6.1	17.7	1337
C4	SAS2	0.12	401	195	166	1389	187	23.6	10.2	1009	0.39	19.8	6.9	1216	6.3	15.4	1622
C4	MLS2	0.12	421	146	232	1351	169	29.9	13.3	1001	0.36	26.8	11.2	1183	6.2	16.2	1404
C4	TRO2	0.12	435	121	270	1297	172	34.1	16.1	1001	0.33	31.4	15.0	1166	6.3	16.4	1608
C4	SAS1	0.48	414	156	217	1306	106	21.4	7.6	487	0.42	19.2	7.2	598	5.0	9.5	1513
C4	MLS1	0.48	435	97	295	1354	89	27.3	8.9	478	0.41	25.8	12.1	577	4.8	10.3	1227
C4	TRO1	0.48	451	61	345	1316	85	31.3	10.1	477	0.40	30.2	16.2	569	4.8	10.6	1342
C4	SAS2	0.48	406	209	156	1372	193	22.8	9.9	1017	0.40	20.0	6.8	1218	5.1	9.0	1669
C4	MLS2	0.48	425	156	226	1356	172	29.3	13.1	1009	0.36	27.0	11.1	1185	4.9	9.6	1445
C4	TRO2	0.48	439	129	266	1301	172	33.5	15.9	1009	0.33	31.6	14.9	1167	5.0	9.6	1647
C4	SAS1	2.00	417	167	208	1285	111	20.8	7.6	496	0.42	19.3	7.2	600	3.1	4.2	1540
C4	MLS1	2.00	438	102	292	1353	92	26.9	9.0	486	0.41	25.9	12.0	579	3.0	4.7	1239
C4	TRO1	2.00	453	64	344	1319	87	30.9	10.3	485	0.39	30.2	16.2	570	3.0	4.7	1338
C4	SAS2	2.00	410	224	145	1351	199	22.1	9.5	1025	0.40	20.1	6.7	1222	3.3	4.0	1709
C4	MLS2	2.00	429	167	218	1360	174	28.7	12.9	1017	0.36	27.1	11.0	1188	3.1	4.3	1482
C4	TRO2	2.00	443	138	261	1304	173	33.0	15.6	1016	0.33	31.7	14.8	1170	3.2	4.3	1668

Set IV: -PBL, +A, +D, LAI=5.

Pho	Ini	$z_0$	$Q^*$	H	$\lambda E$	An,c	$r_s$	$T_1$	$D_1$	$C_e$	$C_i/C_s$	$T_r$	$q_r$	$C_r$	$U_r$	$r_a$	h
C3	SAS1	0.03	417	89	286	1170	41	20.6	3.8	487	0.81	17.9	8.0	619	6.9	26.0	-
C3	MLS1	0.03	438	61	333	1056	42	26.7	4.7	487	0.80	24.7	13.0	605	6.7	27.5	-
C3	TRO1	0.03	448	55	349	828	63	31.6	7.9	493	0.77	29.8	16.6	594	6.7	27.9	-
C3	SAS2	0.03	410	139	230	1426	78	21.9	5.9	1008	0.76	17.9	8.0	1238	6.9	24.9	-
C3	MLS2	0.03	429	113	273	1305	83	28.2	7.6	1007	0.74	24.7	13.0	1209	6.7	26.0	-
C3	TRO2	0.03	433	140	249	948	141	34.0	13.8	1019	0.67	29.8	16.6	1189	6.7	25.6	-
C3	SAS1	0.12	421	90	289	1177	43	19.9	4.0	495	0.80	17.9	8.0	619	6.0	17.5	-
C3	MLS1	0.12	441	58	339	1085	42	26.1	4.8	494	0.80	24.6	13.1	605	5.7	18.6	-
C3	TRO1	0.12	453	45	363	907	57	30.7	7.3	497	0.77	29.6	16.8	595	5.8	19.0	-
C3	SAS2	0.12	415	151	222	1428	80	21.1	5.8	1016	0.76	17.9	8.0	1238	6.0	16.5	-
C3	MLS2	0.12	434	121	269	1331	81	27.4	7.3	1014	0.74	24.6	13.1	1210	5.7	17.4	-
C3	TRO2	0.12	443	124	274	1130	114	32.4	11.1	1019	0.69	29.6	16.8	1190	5.8	17.3	-
C3	SAS1	0.48	425	91	291	1179	44	19.3	4.3	502	0.80	17.9	8.0	619	4.7	10.5	-
C3	MLS1	0.48	445	56	344	1108	43	25.5	4.9	501	0.79	24.5	13.2	605	4.5	11.2	-
C3	TRO1	0.48	457	38	373	956	55	30.1	7.1	503	0.77	29.4	17.1	595	4.5	11.5	-
C3	SAS2	0.48	419	165	212	1424	82	20.3	5.7	1023	0.76	17.9	8.0	1238	4.7	9.8	-
C3	MLS2	0.48	438	133	262	1350	79	26.6	7.0	1021	0.74	24.5	13.2	1210	4.5	10.3	-
C3	TRO2	0.48	449	124	280	1217	101	31.4	9.8	1022	0.71	29.4	17.1	1191	4.5	10.4	-
C3	SAS1	2.00	428	93	292	1178	46	18.8	4.4	508	0.79	17.9	8.1	619	3.0	4.7	-
C3	MLS1	2.00	447	57	346	1125	43	25.1	5.0	507	0.79	24.4	13.4	605	2.7	5.3	-
C3	TRO1	2.00	459	36	378	993	53	29.6	6.9	507	0.77	29.2	17.3	596	2.7	5.4	-
C3	SAS2	2.00	424	181	200	1416	83	19.5	5.4	1028	0.77	17.9	8.1	1238	3.0	4.3	-
C3	MLS2	2.00	443	148	251	1365	77	25.9	6.5	1026	0.75	24.4	13.4	1211	2.7	4.7	-
C3	TRO2	2.00	454	131	278	1267	92	30.5	8.8	1027	0.72	29.2	17.3	1192	2.7	4.7	-
C4	SAS1	0.03	405	138	227	1346	100	22.8	7.4	486	0.42	18.8	7.4	617	7.1	24.3	-
C4	MLS1	0.03	428	93	292	1352	86	28.5	8.5	481	0.41	25.6	12.2	603	6.9	25.8	-
C4	TRO1	0.03	444	64	336	1306	84	32.3	9.7	480	0.40	30.2	16.1	594	6.9	26.4	-
C4	SAS2	0.03	397	194	164	1401	183	24.2	9.8	1015	0.40	18.8	7.4	1234	7.1	23.4	-
C4	MLS2	0.03	417	158	218	1349	167	30.2	12.2	1011	0.37	25.6	12.2	1206	6.9	24.4	-
C4	TRO2	0.03	431	137	251	1293	170	34.3	14.7	1010	0.34	30.2	16.1	1188	6.9	24.7	-
C4	SAS1	0.12	410	149	220	1329	105	22.1	7.6	496	0.42	19.0	7.3	616	6.2	16.1	-
C4	MLS1	0.12	432	98	291	1355	90	27.9	8.8	491	0.41	25.7	12.2	603	6.0	17.2	-
C4	TRO1	0.12	447	66	337	1312	86	31.8	10.0	490	0.40	30.2	16.1	594	6.1	17.7	-
C4	SAS2	0.12	403	211	152	1387	189	23.2	9.4	1022	0.40	19.0	7.3	1233	6.2	15.5	-
C4	MLS2	0.12	423	174	207	1358	169	29.4	11.7	1019	0.38	25.7	12.2	1206	6.0	16.2	-
C4	TRO2	0.12	437	150	242	1297	169	33.5	14.0	1018	0.35	30.2	16.1	1188	6.1	16.3	-
C4	SAS1	0.48	413	159	213	1310	109	21.5	7.6	503	0.42	19.2	7.2	616	5.0	9.5	-
C4	MLS1	0.48	435	103	289	1355	93	27.4	9.0	500	0.41	25.8	12.1	603	4.8	10.2	-
C4	TRO1	0.48	450	68	338	1316	89	31.4	10.3	499	0.39	30.2	16.2	594	4.8	10.5	-
C4	SAS2	0.48	409	228	140	1367	195	22.3	8.9	1027	0.41	19.2	7.2	1232	5.0	9.1	-
C4	MLS2	0.48	428	190	195	1365	171	28.6	11.2	1024	0.38	25.8	12.1	1205	4.8	9.5	-
C4	TRO2	0.48	442	166	232	1302	168	32.7	13.3	1024	0.36	30.2	16.2	1188	4.8	9.6	-
C4	SAS1	2.00	417	171	204	1289	114	20.9	7.6	509	0.42	19.3	7.2	616	3.1	4.2	-
C4	MLS1	2.00	438	109	285	1354	95	27.0	9.2	507	0.41	25.9	12.0	602	3.0	4.6	-
C4	TRO1	2.00	453	72	336	1319	91	31.0	10.5	506	0.39	30.2	16.2	594	3.1	4.7	-
C4	SAS2	2.00	414	245	128	1341	201	21.4	8.4	1031	0.41	19.3	7.2	1232	3.1	4.0	-
C4	MLS2	2.00	433	207	183	1369	173	27.8	10.6	1029	0.39	25.9	12.0	1205	3.0	4.3	-
C4	TRO2	2.00	447	184	218	1307	167	31.9	12.5	1029	0.37	30.2	16.2	1188	3.1	4.2	-

Set V: +PBL, +A, -D, LAI=5.

Pho	Ini	z <sub>0</sub>	Q'	H	ΔE	An,c	r <sub>s</sub>	T <sub>1</sub>	D <sub>1</sub>	C <sub>s</sub>	C <sub>1</sub> /C <sub>s</sub>	T <sub>r</sub>	q <sub>r</sub>	C <sub>r</sub>	U <sub>r</sub>	r <sub>a</sub>	h
C3	SAS1	0.03	414	101	272	1137	54	21.2	4.8	472	0.74	18.2	7.8	598	6.9	25.5	1300
C3	MLS1	0.03	435	68	324	1016	53	27.2	5.8	470	0.75	25.0	12.7	582	6.8	26.9	1090
C3	TRO1	0.03	449	48	356	844	63	31.4	7.7	478	0.76	29.9	16.5	577	6.8	27.4	1268
C3	SAS2	0.03	408	127	240	1415	85	22.4	6.7	989	0.72	18.7	7.5	1214	7.0	24.7	1396
C3	MLS2	0.03	429	89	297	1303	82	28.3	8.2	984	0.73	25.5	12.3	1183	6.9	26.0	1180
C3	TRO2	0.03	443	69	329	1154	93	32.6	10.6	989	0.73	30.4	16.0	1167	6.9	26.4	1373
C3	SAS1	0.12	418	102	274	1147	55	20.5	5.0	480	0.74	18.2	7.8	598	6.1	17.0	1311
C3	MLS1	0.12	439	65	330	1048	52	26.5	5.8	476	0.75	25.0	12.8	581	5.8	18.2	1084
C3	TRO1	0.12	453	42	365	898	60	30.8	7.5	481	0.76	29.7	16.7	576	5.9	18.7	1235
C3	SAS2	0.12	412	134	237	1419	88	21.6	6.8	999	0.72	18.8	7.4	1215	6.2	16.3	1430
C3	MLS2	0.12	433	90	300	1324	81	27.7	8.2	992	0.72	25.6	12.3	1182	6.0	17.4	1188
C3	TRO2	0.12	447	66	336	1205	90	31.9	10.4	994	0.73	30.3	16.0	1166	6.0	17.7	1366
C3	SAS1	0.48	422	104	275	1152	56	19.9	5.1	487	0.73	18.3	7.8	598	4.8	10.1	1320
C3	MLS1	0.48	443	63	335	1073	52	26.0	5.9	481	0.75	24.9	12.9	580	4.5	11.1	1067
C3	TRO1	0.48	456	37	374	939	58	30.2	7.4	485	0.75	29.5	16.9	575	4.6	11.3	1200
C3	SAS2	0.48	416	141	233	1418	90	21.0	6.9	1007	0.72	18.9	7.4	1216	5.0	9.6	1454
C3	MLS2	0.48	437	90	303	1339	81	27.1	8.3	999	0.72	25.6	12.3	1183	4.7	10.4	1195
C3	TRO2	0.48	451	63	342	1240	87	31.3	10.3	1000	0.73	30.3	16.1	1166	4.8	10.5	1348
C3	SAS1	2.00	425	107	275	1154	58	19.3	5.2	493	0.73	18.3	7.8	599	3.0	4.6	1324
C3	MLS1	2.00	445	62	339	1093	52	25.5	6.0	487	0.74	24.8	13.0	581	2.8	5.2	1052
C3	TRO1	2.00	459	33	380	970	57	29.8	7.4	489	0.75	29.4	17.2	574	2.8	5.3	1170
C3	SAS2	2.00	419	149	228	1414	92	20.4	6.9	1015	0.72	19.1	7.3	1219	3.1	4.4	1484
C3	MLS2	2.00	440	92	303	1352	82	26.6	8.4	1006	0.72	25.6	12.2	1184	2.9	4.8	1196
C3	TRO2	2.00	453	63	345	1266	86	30.9	10.2	1006	0.73	30.2	16.3	1167	3.0	4.8	1329
C4	SAS1	0.03	406	136	229	1339	98	22.7	7.4	468	0.41	18.8	7.4	596	7.1	24.3	1432
C4	MLS1	0.03	429	89	297	1352	82	28.4	8.3	457	0.41	25.6	12.2	576	6.9	25.9	1185
C4	TRO1	0.03	445	58	342	1308	78	32.1	9.3	457	0.41	30.2	16.2	568	6.9	26.6	1327
C4	SAS2	0.03	397	175	182	1399	171	24.3	10.2	999	0.40	19.5	7.0	1215	7.1	23.6	1562
C4	MLS2	0.03	418	128	249	1345	150	30.2	12.6	991	0.40	26.4	11.5	1183	7.0	24.7	1338
C4	TRO2	0.03	434	100	291	1289	146	34.1	14.6	990	0.40	31.0	15.3	1166	7.1	25.1	1518
C4	SAS1	0.12	410	146	223	1323	103	22.1	7.5	479	0.40	19.0	7.3	597	6.2	16.1	1475
C4	MLS1	0.12	432	92	297	1355	85	27.8	8.6	468	0.41	25.7	12.2	576	6.0	17.3	1209
C4	TRO1	0.12	449	58	346	1313	80	31.6	9.6	468	0.41	30.2	16.2	569	6.1	17.8	1331
C4	SAS2	0.12	402	190	172	1388	178	23.5	10.0	1008	0.40	19.7	6.9	1216	6.3	15.4	1612
C4	MLS2	0.12	422	136	244	1352	153	29.6	12.5	1000	0.40	26.6	11.4	1183	6.2	16.3	1380
C4	TRO2	0.12	438	106	289	1292	147	33.5	14.6	999	0.40	31.2	15.2	1166	6.2	16.6	1553
C4	SAS1	0.48	414	156	216	1304	107	21.4	7.6	488	0.40	19.2	7.2	598	5.0	9.5	1517
C4	MLS1	0.48	436	95	297	1355	88	27.3	8.8	478	0.41	25.8	12.1	577	4.8	10.3	1226
C4	TRO1	0.48	451	58	348	1317	82	31.2	9.8	477	0.41	30.2	16.3	569	4.8	10.7	1322
C4	SAS2	0.48	407	205	161	1371	184	22.7	9.7	1016	0.40	19.9	6.8	1218	5.1	9.0	1660
C4	MLS2	0.48	426	146	238	1357	156	29.0	12.5	1008	0.40	26.8	11.2	1184	4.9	9.7	1413
C4	TRO2	0.48	442	112	286	1295	148	33.0	14.6	1007	0.40	31.3	15.2	1167	5.0	9.8	1580
C4	SAS1	2.00	417	168	207	1284	112	20.9	7.6	496	0.40	19.4	7.2	600	3.2	4.2	1543
C4	MLS1	2.00	438	100	295	1354	90	26.9	8.9	486	0.41	25.8	12.1	578	3.0	4.7	1234
C4	TRO1	2.00	454	60	349	1320	84	30.8	10.0	485	0.41	30.1	16.3	570	3.0	4.8	1325
C4	SAS2	2.00	411	220	150	1350	191	22.0	9.4	1024	0.40	20.1	6.7	1222	3.3	4.0	1700
C4	MLS2	2.00	430	156	231	1361	159	28.4	12.4	1016	0.40	27.0	11.1	1188	3.1	4.4	1447
C4	TRO2	2.00	445	119	281	1299	150	32.5	14.5	1014	0.40	31.4	15.1	1169	3.2	4.4	1599



162 Appendix 13

Set VI: -PBL, +A, -D, LAI=5.

Pho	Ini	$z_p$	$Q^*$	H	$\lambda E$	An,c	$r_s$	$T_1$	$D_1$	$C_s$	$C_1/C_s$	$T_r$	$q_r$	$C_r$	$U_r$	$r_a$	h
C3	SAS1	0.03	414	111	262	1156	55	21.2	4.7	489	0.74	17.9	8.0	619	6.9	25.4	-
C3	MLS1	0.03	435	78	313	1037	54	27.2	5.7	489	0.75	24.7	13.0	605	6.7	26.9	-
C3	TRO1	0.03	448	51	353	859	64	31.5	7.7	492	0.76	29.8	16.6	594	6.7	27.8	-
C3	SAS2	0.03	408	148	219	1424	88	22.1	6.3	1009	0.72	17.9	8.0	1238	6.9	24.7	-
C3	MLS2	0.03	429	112	273	1313	83	28.2	7.6	1007	0.72	24.7	13.0	1209	6.7	25.9	-
C3	TRO2	0.03	442	85	313	1166	94	32.5	10.1	1007	0.73	29.8	16.6	1189	6.7	26.7	-
C3	SAS1	0.12	418	116	260	1165	56	20.4	4.8	497	0.73	17.9	8.0	619	6.0	17.0	-
C3	MLS1	0.12	439	80	315	1070	53	26.5	5.7	496	0.75	24.6	13.1	605	5.7	18.1	-
C3	TRO1	0.12	453	48	359	915	61	30.8	7.5	498	0.75	29.6	16.8	595	5.8	18.8	-
C3	SAS2	0.12	413	163	209	1426	90	21.3	6.2	1017	0.72	17.9	8.0	1238	6.0	16.4	-
C3	MLS2	0.12	433	124	266	1335	83	27.4	7.4	1015	0.72	24.6	13.1	1210	5.7	17.3	-
C3	TRO2	0.12	447	91	311	1218	90	31.8	9.6	1014	0.73	29.6	16.8	1190	5.8	17.8	-
C3	SAS1	0.48	422	123	257	1168	58	19.7	4.9	503	0.73	17.9	8.0	619	4.7	10.1	-
C3	MLS1	0.48	442	83	316	1096	53	25.9	5.7	502	0.74	24.5	13.2	605	4.5	10.9	-
C3	TRO1	0.48	456	46	365	958	59	30.3	7.4	503	0.75	29.4	17.1	595	4.5	11.3	-
C3	SAS2	0.48	418	180	196	1423	93	20.5	6.0	1024	0.72	17.9	8.0	1238	4.7	9.7	-
C3	MLS2	0.48	438	139	255	1353	83	26.7	7.1	1021	0.72	24.5	13.2	1210	4.5	10.2	-
C3	TRO2	0.48	451	101	305	1255	88	31.1	9.2	1021	0.73	29.4	17.1	1191	4.5	10.6	-
C3	SAS1	2.00	426	132	251	1168	60	19.1	4.9	509	0.73	17.9	8.1	619	3.0	4.5	-
C3	MLS1	2.00	445	90	311	1116	54	25.4	5.6	508	0.74	24.4	13.4	605	2.7	5.0	-
C3	TRO1	2.00	459	48	365	992	58	29.8	7.2	508	0.75	29.2	17.3	596	2.7	5.3	-
C3	SAS2	2.00	423	200	180	1414	96	19.7	5.7	1029	0.72	17.9	8.1	1238	3.0	4.3	-
C3	MLS2	2.00	442	159	238	1366	84	26.0	6.7	1027	0.72	24.4	13.4	1211	2.7	4.6	-
C3	TRO2	2.00	455	117	292	1282	86	30.4	8.6	1026	0.73	29.2	17.3	1192	2.7	4.8	-
C4	SAS1	0.03	405	139	225	1344	101	22.8	7.5	486	0.40	18.8	7.4	617	7.1	24.3	-
C4	MLS1	0.03	428	93	292	1354	86	28.5	8.5	481	0.41	25.6	12.2	603	6.9	25.7	-
C4	TRO1	0.03	445	61	339	1308	82	32.2	9.6	480	0.41	30.2	16.1	594	6.9	26.5	-
C4	SAS2	0.03	398	190	168	1400	175	24.1	9.6	1014	0.40	18.8	7.4	1234	7.1	23.5	-
C4	MLS2	0.03	419	150	227	1350	153	30.0	11.7	1010	0.40	25.6	12.2	1206	6.9	24.5	-
C4	TRO2	0.03	434	122	268	1290	149	33.9	13.7	1009	0.40	30.2	16.1	1188	6.9	25.0	-
C4	SAS1	0.12	410	150	219	1327	106	22.1	7.6	496	0.40	19.0	7.3	616	6.2	16.1	-
C4	MLS1	0.12	432	97	292	1356	89	27.9	8.7	491	0.41	25.7	12.2	603	6.0	17.3	-
C4	TRO1	0.12	448	61	342	1313	83	31.7	9.8	490	0.41	30.2	16.1	594	6.1	17.7	-
C4	SAS2	0.12	404	207	156	1386	182	23.1	9.2	1022	0.40	19.0	7.3	1233	6.2	15.5	-
C4	MLS2	0.12	424	164	217	1358	157	29.2	11.4	1018	0.40	25.7	12.2	1206	6.0	16.3	-
C4	TRO2	0.12	439	135	260	1295	150	33.2	13.3	1017	0.40	30.2	16.1	1188	6.1	16.5	-
C4	SAS1	0.48	413	160	212	1308	110	21.5	7.6	503	0.40	19.2	7.2	616	5.0	9.5	-
C4	MLS1	0.48	435	100	291	1357	91	27.4	8.9	500	0.41	25.8	12.1	603	4.8	10.3	-
C4	TRO1	0.48	451	61	345	1316	85	31.3	10.1	499	0.41	30.2	16.2	594	4.8	10.6	-
C4	SAS2	0.48	409	225	143	1366	189	22.2	8.8	1027	0.40	19.2	7.2	1232	5.0	9.1	-
C4	MLS2	0.48	429	181	205	1365	160	28.4	11.0	1024	0.40	25.8	12.1	1205	4.8	9.6	-
C4	TRO2	0.48	443	150	248	1300	151	32.5	12.9	1023	0.40	30.2	16.2	1188	4.8	9.7	-
C4	SAS1	2.00	417	172	203	1287	114	20.9	7.6	509	0.40	19.3	7.2	616	3.1	4.2	-
C4	MLS1	2.00	438	105	289	1356	93	26.9	9.1	506	0.41	25.9	12.0	602	3.0	4.7	-
C4	TRO1	2.00	453	62	346	1319	87	30.9	10.3	506	0.41	30.2	16.2	594	3.1	4.7	-
C4	SAS2	2.00	414	242	131	1340	196	21.4	8.4	1031	0.40	19.3	7.2	1232	3.1	4.0	-
C4	MLS2	2.00	433	198	192	1369	164	27.7	10.5	1029	0.40	25.9	12.0	1205	3.0	4.3	-
C4	TRO2	2.00	448	169	233	1306	153	31.8	12.3	1028	0.40	30.2	16.2	1188	3.1	4.3	-

Set VII: +PBL, -A, -D, LAI=5.

Pho	Ini	z <sub>0</sub>	Q*	H	λE	An,c	r <sub>s</sub>	T <sub>1</sub>	D <sub>1</sub>	C <sub>s</sub>	C <sub>1</sub> /C <sub>s</sub>	T <sub>r</sub>	q <sub>r</sub>	C <sub>r</sub>	U <sub>r</sub>	r <sub>a</sub>	h
C3	SAS1	0.03	417	90	286	-	39	20.6	3.8	-	-	17.9	8.0	-	6.8	26.3	1251
C3	MLS1	0.03	438	60	334	-	40	26.7	4.7	-	-	24.8	13.0	-	6.6	27.9	1053
C3	TRO1	0.03	449	50	354	-	61	31.5	7.7	-	-	29.9	16.6	-	6.7	28.1	1272
C3	SAS2	0.03	413	109	262	-	59	21.5	5.3	-	-	18.3	7.8	-	6.9	25.6	1330
C3	MLS2	0.03	433	76	313	-	60	27.6	6.6	-	-	25.2	12.6	-	6.7	27.1	1128
C3	TRO2	0.03	442	71	327	-	91	32.6	10.6	-	-	30.4	16.0	-	6.8	26.9	1388
C3	SAS1	0.12	421	91	288	-	41	19.9	4.1	-	-	17.9	8.0	-	5.9	17.8	1257
C3	MLS1	0.12	442	57	340	-	40	26.1	4.8	-	-	24.7	13.1	-	5.6	19.0	1045
C3	TRO1	0.12	454	42	367	-	56	30.7	7.2	-	-	29.7	16.8	-	5.8	19.1	1234
C3	SAS2	0.12	417	115	260	-	62	20.8	5.5	-	-	18.4	7.7	-	6.0	17.2	1359
C3	MLS2	0.12	437	77	317	-	60	27.0	6.7	-	-	25.2	12.7	-	5.7	18.5	1131
C3	TRO2	0.12	448	66	337	-	83	31.8	10.0	-	-	30.3	16.2	-	5.8	18.4	1361
C3	SAS1	0.48	425	93	289	-	43	19.4	4.3	-	-	18.0	8.1	-	4.6	10.7	1275
C3	MLS1	0.48	445	54	346	-	41	25.6	4.9	-	-	24.6	13.2	-	4.4	11.5	1029
C3	TRO1	0.48	457	36	376	-	53	30.1	7.1	-	-	29.5	17.0	-	4.5	11.7	1209
C3	SAS2	0.48	420	120	258	-	65	20.3	5.7	-	-	18.5	7.7	-	4.7	10.2	1380
C3	MLS2	0.48	440	76	320	-	61	26.5	6.9	-	-	25.2	12.7	-	4.5	11.1	1137
C3	TRO2	0.48	452	62	344	-	80	31.2	9.7	-	-	30.2	16.3	-	4.6	11.1	1349
C3	SAS1	2.00	428	94	291	-	45	18.9	4.5	-	-	18.0	8.1	-	2.9	4.8	1281
C3	MLS1	2.00	448	52	351	-	42	25.1	5.1	-	-	24.5	13.4	-	2.7	5.4	1020
C3	TRO1	2.00	460	31	383	-	52	29.7	7.0	-	-	29.3	17.3	-	2.8	5.4	1164
C3	SAS2	2.00	423	128	253	-	68	19.8	5.8	-	-	18.6	7.7	-	2.9	4.7	1408
C3	MLS2	2.00	443	76	322	-	63	26.0	7.0	-	-	25.2	12.7	-	2.8	5.1	1141
C3	TRO2	2.00	455	60	349	-	77	30.7	9.6	-	-	30.1	16.5	-	2.8	5.2	1325
C4	SAS1	0.03	405	139	226	-	96	22.8	7.5	-	-	18.8	7.4	-	7.0	24.8	1444
C4	MLS1	0.03	428	92	293	-	82	28.4	8.5	-	-	25.6	12.2	-	6.7	26.5	1200
C4	TRO1	0.03	445	64	336	-	80	32.2	9.6	-	-	30.2	16.2	-	6.7	27.4	1349
C4	SAS2	0.03	399	168	191	-	145	24.0	9.6	-	-	19.3	7.1	-	7.0	24.1	1539
C4	MLS2	0.03	421	118	261	-	123	29.7	11.4	-	-	26.2	11.7	-	6.8	25.6	1299
C4	TRO2	0.03	437	90	304	-	120	33.5	13.0	-	-	30.8	15.6	-	6.9	26.2	1476
C4	SAS1	0.12	410	150	218	-	101	22.1	7.6	-	-	19.0	7.4	-	6.1	16.5	1488
C4	MLS1	0.12	432	97	292	-	86	27.9	8.8	-	-	25.7	12.2	-	5.8	17.8	1230
C4	TRO1	0.12	448	65	337	-	83	31.8	9.9	-	-	30.2	16.2	-	5.8	18.4	1359
C4	SAS2	0.12	404	183	181	-	152	23.2	9.5	-	-	19.6	7.0	-	6.2	15.8	1591
C4	MLS2	0.12	425	127	255	-	129	29.1	11.5	-	-	26.4	11.6	-	5.9	17.1	1342
C4	TRO2	0.12	441	97	300	-	124	33.0	13.3	-	-	30.9	15.6	-	6.0	17.6	1504
C4	SAS1	0.48	414	162	210	-	106	21.5	7.7	-	-	19.2	7.3	-	4.8	9.7	1522
C4	MLS1	0.48	435	102	289	-	89	27.4	9.0	-	-	25.8	12.1	-	4.6	10.7	1251
C4	TRO1	0.48	451	67	338	-	85	31.4	10.2	-	-	30.3	16.2	-	4.6	11.0	1382
C4	SAS2	0.48	408	198	169	-	160	22.5	9.3	-	-	19.8	6.9	-	5.0	9.3	1640
C4	MLS2	0.48	429	137	249	-	133	28.6	11.6	-	-	26.6	11.5	-	4.7	10.1	1385
C4	TRO2	0.48	444	103	297	-	127	32.6	13.5	-	-	31.0	15.5	-	4.8	10.3	1542
C4	SAS1	2.00	417	175	201	-	111	20.9	7.6	-	-	19.4	7.2	-	3.0	4.4	1559
C4	MLS1	2.00	438	107	286	-	92	27.0	9.2	-	-	25.9	12.0	-	2.9	4.8	1268
C4	TRO1	2.00	453	71	337	-	87	31.0	10.4	-	-	30.3	16.3	-	2.8	5.1	1383
C4	SAS2	2.00	412	213	158	-	167	21.8	9.0	-	-	20.0	6.8	-	3.1	4.2	1671
C4	MLS2	2.00	432	148	240	-	138	28.1	11.6	-	-	26.7	11.3	-	2.9	4.6	1421
C4	TRO2	2.00	447	111	291	-	131	32.2	13.5	-	-	31.2	15.4	-	3.0	4.7	1576

Set VIII: -PBL, -A, -D, LAI=5.

Pho	Ini	$z_0$	$Q^*$	H	$\lambda E$	$An_r c$	$r_s$	$T_s$	$D_s$	$C_s$	$C_s/C_s$	$T_r$	$q_r$	$C_r$	$U_r$	$r_a$	h
C3	SAS1	0.03	417	90	285	-	39	20.5	3.8	-	-	17.9	8.0	-	6.9	26.1	-
C3	MLS1	0.03	438	61	333	-	40	26.7	4.7	-	-	24.7	13.0	-	6.7	27.6	-
C3	TRO1	0.03	449	50	354	-	61	31.5	7.6	-	-	29.8	16.6	-	6.7	28.0	-
C3	SAS2	0.03	412	101	270	-	59	21.5	5.4	-	-	18.6	7.6	-	7.0	25.5	-
C3	MLS2	0.03	433	64	326	-	60	27.6	6.9	-	-	25.6	12.2	-	6.8	27.0	-
C3	TRO2	0.03	443	38	361	-	91	32.9	11.8	-	-	31.7	14.8	-	6.9	27.8	-
C3	SAS1	0.12	421	91	288	-	41	19.9	4.0	-	-	17.9	8.0	-	6.0	17.6	-
C3	MLS1	0.12	442	58	339	-	40	26.0	4.8	-	-	24.6	13.1	-	5.7	18.7	-
C3	TRO1	0.12	453	43	365	-	56	30.7	7.2	-	-	29.6	16.8	-	5.8	19.0	-
C3	SAS2	0.12	416	104	271	-	62	20.9	5.7	-	-	18.7	7.5	-	6.1	17.0	-
C3	MLS2	0.12	437	58	335	-	60	27.0	7.1	-	-	25.7	12.2	-	5.9	18.2	-
C3	TRO2	0.12	448	32	371	-	83	32.0	11.0	-	-	31.3	15.2	-	6.0	18.8	-
C3	SAS1	0.48	425	93	289	-	43	19.3	4.3	-	-	17.9	8.0	-	4.7	10.5	-
C3	MLS1	0.48	445	57	344	-	41	25.5	4.9	-	-	24.5	13.2	-	4.5	11.3	-
C3	TRO1	0.48	457	38	373	-	53	30.1	7.0	-	-	29.4	17.1	-	4.5	11.6	-
C3	SAS2	0.48	419	107	271	-	65	20.4	6.0	-	-	18.8	7.5	-	4.9	10.0	-
C3	MLS2	0.48	440	52	344	-	61	26.6	7.4	-	-	25.7	12.2	-	4.7	11.0	-
C3	TRO2	0.48	451	26	380	-	80	31.4	10.8	-	-	31.0	15.4	-	4.8	11.2	-
C3	SAS1	2.00	428	96	289	-	45	18.8	4.4	-	-	17.9	8.1	-	3.0	4.8	-
C3	MLS1	2.00	448	58	344	-	42	25.0	5.0	-	-	24.4	13.4	-	2.7	5.4	-
C3	TRO1	2.00	460	37	377	-	52	29.6	6.9	-	-	29.2	17.3	-	2.7	5.5	-
C3	SAS2	2.00	422	111	269	-	68	19.9	6.2	-	-	18.9	7.4	-	3.1	4.6	-
C3	MLS2	2.00	442	46	352	-	63	26.2	7.7	-	-	25.7	12.1	-	2.9	5.1	-
C3	TRO2	2.00	454	17	391	-	77	31.0	10.7	-	-	30.9	15.6	-	3.0	5.2	-
C4	SAS1	0.03	406	139	226	-	96	22.7	7.5	-	-	18.8	7.4	-	7.1	24.4	-
C4	MLS1	0.03	428	92	293	-	82	28.4	8.5	-	-	25.6	12.2	-	6.9	25.9	-
C4	TRO1	0.03	445	63	337	-	80	32.1	9.6	-	-	30.2	16.1	-	6.9	26.7	-
C4	SAS2	0.03	398	163	195	-	145	24.1	9.8	-	-	19.5	7.0	-	7.2	23.9	-
C4	MLS2	0.03	421	108	271	-	123	29.8	11.8	-	-	26.6	11.4	-	7.0	25.2	-
C4	TRO2	0.03	437	76	317	-	120	33.6	13.6	-	-	31.3	15.1	-	7.1	25.8	-
C4	SAS1	0.12	410	151	218	-	101	22.1	7.6	-	-	19.0	7.3	-	6.2	16.2	-
C4	MLS1	0.12	432	98	291	-	86	27.9	8.7	-	-	25.7	12.2	-	6.0	17.4	-
C4	TRO1	0.12	448	65	338	-	83	31.7	9.9	-	-	30.2	16.1	-	6.1	17.8	-
C4	SAS2	0.12	403	178	185	-	152	23.3	9.7	-	-	19.8	6.9	-	6.3	15.6	-
C4	MLS2	0.12	424	115	266	-	129	29.3	12.1	-	-	26.8	11.2	-	6.2	16.7	-
C4	TRO2	0.12	440	80	317	-	124	33.2	14.0	-	-	31.4	15.0	-	6.3	17.1	-
C4	SAS1	0.48	413	162	210	-	106	21.5	7.7	-	-	19.2	7.2	-	5.0	9.5	-
C4	MLS1	0.48	435	103	288	-	89	27.4	9.0	-	-	25.8	12.1	-	4.8	10.3	-
C4	TRO1	0.48	451	67	338	-	85	31.3	10.2	-	-	30.2	16.2	-	4.8	10.6	-
C4	SAS2	0.48	407	193	174	-	160	22.6	9.6	-	-	20.0	6.8	-	5.1	9.1	-
C4	MLS2	0.48	428	124	261	-	133	28.8	12.2	-	-	27.0	11.1	-	4.9	9.9	-
C4	TRO2	0.48	443	84	315	-	127	32.8	14.3	-	-	31.6	14.9	-	5.0	10.1	-
C4	SAS1	2.00	417	175	200	-	111	20.9	7.6	-	-	19.3	7.2	-	3.1	4.2	-
C4	MLS1	2.00	438	111	283	-	92	26.9	9.1	-	-	25.9	12.0	-	3.0	4.7	-
C4	TRO1	2.00	453	72	336	-	87	30.9	10.4	-	-	30.2	16.2	-	3.1	4.7	-
C4	SAS2	2.00	411	207	163	-	167	21.9	9.3	-	-	20.1	6.7	-	3.3	4.1	-
C4	MLS2	2.00	431	133	254	-	138	28.4	12.3	-	-	27.1	11.0	-	3.1	4.5	-
C4	TRO2	2.00	446	89	312	-	131	32.5	14.5	-	-	31.7	14.8	-	3.2	4.5	-

Set IX: +PBL (-CO<sub>2</sub> fluxes), +A, +D, LAI=5.

Pho	Ini	z <sub>0</sub>	Q <sup>*</sup>	H	λE	An,c	r <sub>s</sub>	T <sub>1</sub>	D <sub>1</sub>	C <sub>s</sub>	C <sub>i</sub> /C <sub>s</sub>	T <sub>r</sub>	q <sub>r</sub>	C <sub>r</sub>	U <sub>r</sub>	r <sub>a</sub>	h
C3	SAS1	0.03	417	89	287	1170	41	20.6	3.8	487	0.81	17.9	8.0	619	6.9	26.0	1247
C3	MLS1	0.03	438	60	334	1056	42	26.7	4.7	487	0.80	24.8	13.0	605	6.7	27.5	1048
C3	TRO1	0.03	448	54	349	825	63	31.6	8.0	493	0.77	29.9	16.5	594	6.7	27.9	1283
C3	SAS2	0.03	409	124	243	1422	80	22.2	6.4	1006	0.75	18.6	7.6	1235	7.0	24.9	1381
C3	MLS2	0.03	427	95	289	1293	89	28.6	8.8	1005	0.72	25.6	12.2	1206	6.8	26.0	1200
C3	TRO2	0.03	420	166	212	721	201	36.4	21.4	1028	0.62	31.7	14.8	1182	6.9	24.8	1688
C3	SAS1	0.12	421	89	290	1177	43	19.9	4.1	495	0.80	17.9	8.0	619	6.0	17.4	1252
C3	MLS1	0.12	442	58	340	1085	42	26.1	4.8	494	0.80	24.7	13.1	605	5.7	18.7	1030
C3	TRO1	0.12	453	44	364	905	57	30.7	7.3	497	0.77	29.7	16.8	595	5.8	18.9	1225
C3	SAS2	0.12	413	131	240	1425	83	21.5	6.6	1015	0.75	18.7	7.5	1234	6.1	16.5	1414
C3	MLS2	0.12	432	97	291	1320	88	27.9	8.8	1013	0.72	25.7	12.2	1206	5.9	17.4	1210
C3	TRO2	0.12	434	133	258	949	156	34.1	16.2	1023	0.64	31.3	15.2	1183	6.0	16.9	1589
C3	SAS1	0.48	424	89	293	1179	44	19.3	4.3	502	0.80	17.9	8.0	619	4.8	10.4	1256
C3	MLS1	0.48	445	55	346	1107	43	25.6	5.0	501	0.79	24.6	13.2	605	4.5	11.4	1017
C3	TRO1	0.48	457	37	373	954	55	30.1	7.2	503	0.77	29.5	17.0	595	4.5	11.6	1185
C3	SAS2	0.48	417	139	236	1423	85	20.9	6.7	1021	0.74	18.8	7.4	1234	4.9	9.7	1437
C3	MLS2	0.48	435	100	292	1337	88	27.3	8.8	1019	0.72	25.7	12.1	1205	4.7	10.4	1219
C3	TRO2	0.48	443	113	285	1108	132	32.7	13.9	1023	0.65	31.0	15.4	1184	4.8	10.2	1537
C3	SAS1	2.00	427	91	294	1178	46	18.8	4.5	508	0.79	17.9	8.0	619	3.0	4.7	1254
C3	MLS1	2.00	447	53	349	1124	43	25.1	5.1	507	0.79	24.5	13.3	605	2.7	5.3	1010
C3	TRO1	2.00	459	32	381	991	54	29.7	7.1	508	0.77	29.3	17.3	596	2.8	5.3	1152
C3	SAS2	2.00	420	147	231	1418	87	20.3	6.7	1027	0.74	19.0	7.4	1233	3.1	4.4	1465
C3	MLS2	2.00	438	103	292	1351	88	26.8	8.8	1025	0.72	25.8	12.1	1205	2.9	4.7	1222
C3	TRO2	2.00	448	106	297	1189	120	31.9	12.9	1026	0.66	30.9	15.5	1185	3.0	4.6	1502
C4	SAS1	0.03	405	137	228	1345	100	22.8	7.5	486	0.42	18.8	7.4	617	7.1	24.3	1433
C4	MLS1	0.03	428	92	293	1352	86	28.5	8.6	481	0.41	25.6	12.2	603	6.9	25.9	1196
C4	TRO1	0.03	444	63	337	1306	84	32.3	9.8	480	0.40	30.2	16.1	594	6.9	26.5	1339
C4	SAS2	0.03	396	181	175	1401	183	24.5	10.5	1013	0.39	19.5	7.0	1231	7.2	23.5	1574
C4	MLS2	0.03	416	137	237	1344	169	30.6	13.5	1009	0.36	26.6	11.4	1202	7.0	24.5	1371
C4	TRO2	0.03	430	116	271	1293	176	34.8	16.5	1008	0.33	31.3	15.1	1183	7.1	24.8	1584
C4	SAS1	0.12	410	148	221	1329	105	22.1	7.6	496	0.42	19.0	7.3	616	6.2	16.1	1476
C4	MLS1	0.12	432	96	292	1355	90	27.9	8.9	491	0.41	25.7	12.1	603	6.0	17.3	1217
C4	TRO1	0.12	448	64	339	1312	86	31.8	10.1	490	0.40	30.3	16.1	594	6.1	17.7	1346
C4	SAS2	0.12	401	196	165	1389	189	23.7	10.2	1021	0.39	19.8	6.9	1230	6.3	15.4	1624
C4	MLS2	0.12	420	147	231	1350	171	30.0	13.4	1017	0.36	26.8	11.2	1201	6.2	16.1	1414
C4	TRO2	0.12	435	123	268	1297	175	34.1	16.2	1016	0.33	31.4	15.0	1183	6.3	16.3	1612
C4	SAS1	0.48	413	158	213	1310	109	21.5	7.7	503	0.42	19.2	7.2	616	5.0	9.5	1518
C4	MLS1	0.48	435	101	291	1355	93	27.5	9.1	500	0.41	25.9	12.0	602	4.8	10.3	1236
C4	TRO1	0.48	450	65	340	1316	89	31.4	10.4	499	0.39	30.3	16.1	594	4.8	10.5	1353
C4	SAS2	0.48	406	210	155	1373	194	22.8	9.9	1026	0.40	20.0	6.8	1229	5.1	9.0	1670
C4	MLS2	0.48	424	158	224	1356	174	29.3	13.2	1023	0.36	27.0	11.1	1200	4.9	9.6	1448
C4	TRO2	0.48	439	131	264	1301	174	33.5	16.0	1022	0.33	31.6	14.9	1182	5.0	9.6	1650
C4	SAS1	2.00	417	170	205	1289	113	20.9	7.7	509	0.42	19.4	7.2	616	3.1	4.3	1544
C4	MLS1	2.00	437	106	288	1354	95	27.0	9.3	506	0.41	25.9	12.0	602	3.0	4.6	1255
C4	TRO1	2.00	452	68	339	1319	91	31.0	10.6	506	0.39	30.3	16.1	594	3.0	4.8	1358
C4	SAS2	2.00	410	225	145	1351	200	22.1	9.5	1030	0.40	20.1	6.7	1228	3.3	4.0	1709
C4	MLS2	2.00	428	169	217	1360	176	28.7	13.0	1028	0.36	27.1	11.0	1200	3.1	4.3	1484
C4	TRO2	2.00	442	139	259	1304	174	33.0	15.7	1027	0.33	31.7	14.8	1182	3.2	4.3	1671

## References

- Allaway, W.G. and F.L. Milthorpe, 1976: Structure and Functioning of Stomata. In: T.T. Kozlowski (Ed.), *Water Deficits and Plant Growth, Vol. IV*. Academic Press, New York, 57-102.
- Amthor, J.S., 1989: *Respiration and crop productivity*. Springer Verlag, New York.
- André, J.C., J.P. Goutorbe & A. Perrier, 1986: HAPEX-MOBILHY: A hydrologic atmospheric experiment for the study of water budget and evaporation flux at the climatic scale. *Bull. Amer. Meteor. Soc.*, **67**, 138-144.
- André, J.C., J.P. Goutorbe, A. Perrier, F. Becker, P. Bessemoulin, P. Bougeault, Y. Brunet, W. Brutseart, T. Carlson, R. Cuenca, J. Gash, J. Gelpe, P. Hildebrand, J.-P. Lagouarde, C. Lloyd, L. Mahrt, P. Mascart, C. Mazaudier, J. Noilhan, C. Otlé, M. Payen, T. Phulpin, R. Stull, J. Shuttleworth, T. Schmugge, O. Taconet, C. Tarrieu, R.-M. Thepenier, C. Valencogne, D. Vidal-Madjar & A. Weill, 1988: Evaporation over land surfaces: first results from HAPEX-MOBILHY special observing period. *Ann. Geophys.*, **6**, 477-492.
- Aphalo, P.J. & P.G. Jarvis, 1991: Do stomata respond to relative humidity? *Plant, Cell and Environment*, **14**, 127-132.
- Aron, D.I., 1977: Photosynthesis 1950-1975: Changing Concepts and Perspectives. In: A. Trebst, & M. Avron (Eds.), *Encyclopedia of Plant Physiology, New Series, Vol. 5: Photosynthesis I: Photosynthetic Electron Transport and Photophosphorylation*. Springer Verlag, Berlin, 7-56.
- Baldocchi, D., 1989: Canopy-atmosphere water vapour exchange: can we scale from a leaf to a canopy? In: *IAHS publication 177: Proc. of a workshop on the estimation of areal evapotranspiration, Vancouver, B.C., Canada, August 1987*, IAHS press, Wallingford, 21-41.
- Baldocchi, D.D., R.J. Luxmoore & J.L. Hatfield, 1991: Discerning forest from trees: an essay on scaling stomatal conductance. *Agric. For. Meteorol.*, **54**, 197-226.
- Ball, J.T., 1987: Calculations related to gas exchange. In: E. Zeiger, G.D. Farquhar and I.R. Cowan (Eds.), *Stomatal Function*. Stanford University Press, Stanford, 445-476.
- Ball, J.T., I.E. Woodrow & J.A. Berry, 1987: A model predicting stomatal conductance and its contribution to the control of photosynthesis under different environmental conditions. In: J. Biggins (Ed.), *Progress in Photosynthesis Research, Vol. IV*. Martinus Nijhoff Publishers, Dordrecht, 221-224.
- Bascham, J.A., 1979: The Reductive Pentose Phosphate Cycle and Its Regulation. In: Gibbs, M. & E. Latzko, *Encyclopedia of Plant Physiology, New Series, Vol. 6: Photosynthesis II, Photosynthetic Carbon Metabolism and Related Processes*. Springer-Verlag, Berlin, 9-29.
- Beer, S., 1986: The fixation of inorganic carbon in plant cells. In: H.Z. Enoch, & B.A. Kimball (Eds.) *Carbon Dioxide Enrichment of Greenhouse Crops. Volume II: Physiology, Yield and Economics*. CRC-Press Inc., Boca Raton, 3-11.
- Berry, J.A. & J.K. Raison, 1982: Responses of Macrophytes to Temperature. In: O.L. Lange, P.S. Nobel, C.B. Osmond & H. Ziegler (Eds.), *Encyclopedia of Plant Physiology, New Series, Vol. 12B, Physiological Plant Ecology II*. Springer Verlag, Berlin, 277-338.
- Beven, K., 1979: A sensitivity analysis of the Penman-Monteith actual evapotranspiration estimates. *J. Hydrol.*, **44**, 169-190.
- Bolle, H.-J., J.-C. André, J.L. Arrue, H.K. Barth, P. Bessemoulin, A. Brasa, H.A.R. de Bruin, J. Cruces, G. Dugdale, E.T. Engman, D.L. Evans, R. Frantechi, F. Fiedler, A. van de Griend, A.C. Imeson, A. Jochum, P. Kabat, T. Kratzsch, J.-P. Lagouarde, I. Langer, R. Llamas, E. Lopez-Baeza, J. Melia Miralles, L.S. Muniosguren, F. Nerry, J. Noilhan, H.R. Oliver, R. Roth, S.S. Saatchi, J. Sanchez Diaz, M. de Santa Olalla, W.J. Shuttleworth, H. Sogaard, H. Stricker, J. Thomes, M. Vauclin and D. Wickland, 1993: EFEDA: European field experiment in a desertification-threatened area. *Ann. Geophys.*, **11**, 173-189.
- Bowes, G., 1991: Growth and elevated CO<sub>2</sub>: photosynthetic responses mediated through rubisco. *Plant, Cell and Environment*, **14**, 795-806.

- Bradford, K.J. and T.C. Hsiao, 1982: Physiological responses to moderate water stress. In: O.L. Lange, P.S. Nobel, C.B. Osmond & H. Ziegler (Eds.), *Encyclopedia of Plant Physiology, New Series, Vol. 12B, Physiological Plant Ecology II*. Springer Verlag, Berlin, 263-324.
- Bravdo, B.-A., 1986: Effect of CO<sub>2</sub> on photosynthesis of C<sub>3</sub> plants. In: H.Z. Enoch, & B.A. Kimball (Eds.) *Carbon Dioxide Enrichment of Greenhouse Crops. Volume II: Physiology, Yield and Economics*. CRC-Press Inc., Boca Raton, 13-27.
- Brooks, A. & G.D. Farquhar, 1985: Effect of temperature on the CO<sub>2</sub>/O<sub>2</sub> specificity of ribulose-1,5-biphosphate carboxylase/oxygenase and the rate of respiration in the light, estimates from gas-exchange measurements on spinach. *Planta*, **165**, 397-406.
- Brutsaert, W., 1982: *Evaporation into the atmosphere*. D. Reidel Publishing Company, Dordrecht.
- Brutsaert, W., 1986: Catchment-scale evaporation and the atmospheric boundary layer. *Water Resour. Res.*, **22**, 39-45.
- Burrows, F.J. and F.L. Milthorpe, 1976: Stomatal conductance in the control of gas exchange. In: T.T. Kozlowski (Ed.), *Water Deficits and Plant Growth, Vol IV*. Academic Press, New York, 103-152.
- Canvin, D.T., 1979: Photorespiration: comparison between C<sub>3</sub> and C<sub>4</sub> plants. In: Gibbs, M. & E. Latzko, *Encyclopedia of Plant Physiology, New Series, Vol. 6: Photosynthesis II, Photosynthetic Carbon Metabolism and Related Processes*. Springer-Verlag, Berlin, 368-396.
- Canvin, D.T., 1990: Photorespiration and CO<sub>2</sub>-concentrating mechanisms. In: Dennis, D.T. & D.M. Turpin (Eds.), *Plant Physiology, Biochemistry and Molecular Biology*. Longman Scientific & Technical, Harlow, 253-273.
- Caughey, S.J., 1981: Observed characteristics of the atmospheric boundary layer. In: F.T.M. Nieuwstadt & H. van Dop (Eds.), *Atmospheric turbulence and air pollution modelling*, D. Reidel Publishing Company, Dordrecht, 107-158.
- Choudhury, B.J. & J.L. Monteith, 1986: Implications of stomatal response to saturation deficit for the heat balance of vegetation. *Agric. For. Meteorol.*, **36**, 215-225.
- Claussen, M., 1990: Area-averaging of surface fluxes in a neutrally stratified, horizontally inhomogeneous atmospheric boundary layer. *Atmospheric Environment*, **24A**, 1349-1360.
- Coleman, G. & D.G. DeCoursey, 1976: Sensitivity and model variance analysis applied to some evaporation and evapotranspiration models. *Water Resour. Res.*, **12-5**, 873-879.
- Collatz, G.J., J.T. Ball, C. Grivet & J.A. Berry, 1991: Physiological and environmental regulation of stomatal conductance, photosynthesis and transpiration: a model that includes a laminar boundary layer. *Agric. For. Meteorol.*, **54**, 107-136.
- Collatz, G.J., M. Ribas-Carbo & J.A. Ball, 1992: Coupled photosynthesis-stomatal conductance model for leaves of C<sub>4</sub> plants. *Aust. J. Plant Physiol.*, **19**, 519-538.
- Cowan, I.R., 1982: Regulation of water use in relation to carbon gain in higher plants. In: O.L. Lange, P.S. Nobel, C.B. Osmond & H. Ziegler (Eds.), *Encyclopedia of Plant Physiology, New Series, Vol. 12B, Physiological Plant Ecology II*. Springer Verlag, Berlin, 589-615.
- Cure, J.D. and B. Acock, 1986: Crop responses to carbon dioxide doubling: a literature survey. *Agric. For. Meteorol.*, **38**, 127-145.
- Deardorff, J.W., 1972: Theoretical expression for the countergradient vertical heat flux. *J. Geophys. Res.*, **77**, 5900-5904.
- De Bruin, H.A.R., 1983: A model for the Priestley-Taylor parameter  $\alpha$ . *J. Climate Appl. Meteor.*, **22**, 572-578.
- De Bruin, H.A.R., 1989: Physical aspects of the planetary boundary layer with special reference to regional evapotranspiration. In: *IAHS publication 177: Proc. of a workshop on the estimation of areal evapotranspiration, Vancouver, B.C., Canada, August 1987*, IAHS press, Wallingford, 117-132.
- De Bruin, H.A.R., N.J. Bink & L.J.M. Kroon, 1991: Fluxes in the surface layer under advective conditions. In: T.J. Schmugge & J.C. André (Eds.), *Measurement and Parameterization of Land Surface Evaporation Fluxes*. Springer Verlag, New York, 157-169.
- De Bruin, H.A.R. & C.M.J. Jacobs, 1989: Forests and regional scale processes. *Phil. Trans. R. met. Soc.*, **B 324**, 393-406.

- De Bruin, H.A.R. & C.M.J. Jacobs, 1993: Impact of CO<sub>2</sub> enrichment on the regional evapotranspiration of agro-ecosystems, a theoretical and numerical modelling study. *Vegetatio* **104/105**, 307-318.
- Dickinson, R.E., A. Henderson-Sellers, C. Rosenzweig and P.J. Sellers, 1991: Evapotranspiration models with canopy resistance for use in climate models, a review. *Agric. For. Meteorol.*, **54**, 373-388.
- Dubbe, D.R., G.D. Farquhar & K. Raschke, 1978: Effect of Abscisic Acid on the gain of the feedback loop involving carbon dioxide and stomata. *Plant Physiol.*, **62**, 413-417.
- Dyer, A.J. & B.B. Hicks, 1970: Flux-gradient relationships in the constant flux layer. *Quart. J. Roy. Meteor. Soc.*, **96**, 715-721.
- Eamus, D., 1991: The interaction of rising CO<sub>2</sub> and temperature with water use efficiency. *Plant, Cell and Environment*, **14**, 843-852.
- Eamus, D. & P.G. Jarvis, 1989: The direct effects of increase in the global atmospheric CO<sub>2</sub> concentration on natural and commercial temperate trees and forests. *Advances in Ecological Research*, **19**, 1-55.
- Ehleringer, J. & O. Björkman, 1977: Quantum yields for CO<sub>2</sub> uptake in C<sub>3</sub> and C<sub>4</sub> plants, dependence on temperature, CO<sub>2</sub> and O<sub>2</sub> concentration. *Plant Physiol.*, **59**, 86-90.
- El-kilani, R.M.M., 1991: Some aspects of energy exchange processes in a plant canopy. *Proc. 20<sup>th</sup> conference on agricultural and forest meteorology, Salt Lake City, Utah*, AMS, Boston, 3-6.
- Ellingson, R.G., J. Ellis & S. Fels, 1991: The intercomparison of radiation codes used in climate models: long wave results. *J. Geophys. Res.*, **96**, 8929-8953.
- Enoch, H.Z. & B.A. Kimball (Eds.), 1986: *Carbon Dioxide Enrichment of Greenhouse Crops. Volume II: Physiology, Yield and Economics*. CRC-Press Inc., Boca Raton.
- Farquhar, G.D., 1978: Feedforward responses of stomata to humidity. *Aust. J. Plant Physiol.*, **5**, 787-800.
- Farquhar, G.D., S. von Caemmerer & J.A. Berry, 1980: A biochemical model of photosynthetic CO<sub>2</sub> assimilation in leaves of C<sub>3</sub> species. *Planta*, **149**, 78-90.
- Farquhar, G.D. & T.D. Sharkey, 1982: Stomatal Conductance and Photosynthesis. *Ann. Rev. Plant Physiol.*, **33**, 317-345.
- Farquhar, G.D. & S.C. Wong, 1984: An empirical model of stomatal conductance. *Aust. J. Plant Physiol.*, **11**, 191-209.
- Field, C.B., 1987: Leaf-age effects on stomatal conductance. In: E. Zeiger, G.D. Farquhar and I.R. Cowan (Eds.), *Stomatal Function*. Stanford University Press, Stanford, California, 367-384.
- Finnigan, J.J. & M.R. Raupach, 1987: Transfer processes in plant canopies in relation to stomatal characteristics. In: E. Zeiger, G.D. Farquhar and I.R. Cowan (Eds.), *Stomatal Function*. Stanford University Press, Stanford, California, 385-429.
- Friend, A.D., 1991: Use of a model of photosynthesis and leaf microenvironment to predict optimal stomatal conductance and leaf nitrogen partitioning. *Plant, Cell and Environment*, **14**, 895-905.
- Fuentes, J.D. & K.M. King, 1989: Leaf photosynthesis and leaf conductance of maize grown hydroponically and in soil under field conditions. *Agric. For. Meteorol.*, **45**, 155-166.
- Gaastra, P., 1959: Photosynthesis of crop plants as influenced by light, carbon dioxide, temperature and stomatal diffusion resistance. *Meded. Landbouwhogeschool, Wageningen*, **59**, 1-68.
- Gaastra, P., 1962: Photosynthesis of leaves and field crop. *Neth. J. Agric. Sci.*, **10**, 311-324.
- Garratt, J.R., 1992: *The atmospheric boundary layer*. Cambridge University Press.
- Garratt, J.R., 1993: Sensitivity of climate simulations to land-surface and atmospheric boundary-layer treatments — A Review. *J. of Clim.*, **6**, 419-449.
- Garratt, J.R. & B.B. Hicks, 1973: Momentum, heat and water vapour transfer to and from natural and artificial surfaces. *Quart. J. Roy. Meteor. Soc.*, **99**, 680-687.
- Gash, J.H.C., W.J. Lloyd, C.R. André, J.C. Goutorbe & J. Gelpe, 1989: Micrometeorological measurements in Les Landes Forest during HAPEX-MOBILHY. *Agric. For. Meteorol.*, **46**, 131-147.
- Gates, D.M., 1980: *Biophysical Ecology*. Springer Verlag, New York.

- Gifford, R.M., 1988: Direct effects of higher carbon dioxide concentrations on vegetation. In: G.I. Pearman (Ed.), *Greenhouse. Planning for climate change*. Brill, Leiden, 506-519.
- Gollan, T., J.B. Passioura & R. Munns, 1986: Soil water status affects the stomatal conductance of fully turgid wheat and sunflower leaves. *Aust. J. Plant Physiol.*, **13**, 459-464.
- Gollan, T., U. Schurr & E.-D. Schulze, 1992: Stomatal response to drying soil in relation to changes in the xylem sap composition of *Helianthus Annuus*. I. The Concentration of Cations, Anions, Amino Acids in, and pH of, the Xylem Sap. *Plant, Cell & Environment*, **15**, 551-560.
- Goudriaan, J., 1977: *Crop micrometeorology: a simulation study*. Pudoc, Wageningen.
- Goudriaan, J., 1986: A simple and fast numerical method for the computation of daily totals of crop photosynthesis. *Agric. For. Meteorol.*, **38**, 249-254.
- Goudriaan, J., 1988: The bare bones of leaf-angle distribution in radiation models for canopy photosynthesis and energy exchange. *Agric. For. Meteorol.*, **43**, 155-169.
- Goudriaan, J., & H.H. van Laar, 1978: Relations between leaf resistance, CO<sub>2</sub>-concentration and CO<sub>2</sub>-assimilation in maize, beans, lalang grass and sunflower. *Photosynthetica*, **12**, 241-249.
- Goudriaan, J., H.H. van Laar, H. van Keulen & W. Louwse, 1985: Photosynthesis, CO<sub>2</sub> and plant production. In: W. Day & R.K. Atkin (Eds.), *Wheat growth and modelling. NATO ASI Series, Series A, Vol 86*. Plenum Press, New York, 107-122.
- Goudriaan, J., and M.H. Unsworth, 1990: Implications of increasing carbon dioxide and climate change for agricultural productivity and water resources. In: *Impact of carbon dioxide, trace gases and climate change on global agriculture*, ASA Special Publication no. 53., ASA Madison, 111-130.
- Graham, D. & E.A. Chapman, 1979: Interactions between photosynthesis and respiration in higher plants. In: M. Gibbs & E. Latzko (Eds.), *Encyclopedia of Plant Physiology, New Series, Vol. 6: Photosynthesis II, Photosynthetic Carbon Metabolism and Related Processes*. Springer Verlag, Berlin, 150-162.
- Grantz, D.A., 1990: Plant response to atmospheric humidity. *Plant, Cell and Environment*, **13**, 667-679.
- Grantz, D.A. & F.A. Meinzer, 1990: Stomatal responses to humidity in a sugarcane field: simultaneous porometric and micrometeorological measurements. *Plant, Cell and Environment*, **13**, 27-37.
- Grantz, D.A. & F.A. Meinzer, 1991: Regulation of transpiration in field-grown sugarcane: evaluation of the stomatal response to humidity with Bowen ratio technique. *Agric. For. Meteorol.*, **53**, 169-183.
- Harley, P.C., R.B. Thomas, J.F. Reynolds, & B.R. Strain, 1992: Modelling photosynthesis of cotton grown in elevated CO<sub>2</sub>. *Plant, Cell and Environment*, **15**, 271-282.
- Hildebrand, P.H., 1988: Flux and sounding data from the NCAR King Air Aircraft during HAPEX. *NCAR Technical Note*, NCAR/TN-319+STR, NCAR, Boulder.
- Holtslag, A.A.M. & A.C.M. Beljaars, 1988: Surface flux parameterization schemes: developments and experiences at KNMI. *Royal Netherlands Meteorological Institute Scientific Reports WR-nr 88-06*, De Bilt.
- Holtslag, A.A.M. & H.A.R. De Bruin, 1988: Applied modelling of the nighttime surface energy balance over land. *J. Climate. appl. Met.*, **27**, 689-704.
- Holtslag, A.A.M., E.I.F. De Bruijn & H.-L. Pan, 1990: A high resolution air mass transformation model for short-range weather forecasting. *Mon. Wea. Rev.*, **118**, 1561-1575.
- Holtslag, A.A.M. & C.-H. Moeng, 1991: Eddy diffusivity and countergradient transport in the convective atmospheric boundary layer. *J. Atmos. Sci.*, **48**, 1690-1698.
- Holtslag, A.A.M. & A.P. Van Ulden, 1983: A simple scheme for daytime estimates of the surface fluxes from routine weather data. *J. Climate appl. Met.*, **22**, 517-529.
- Houghton, J.T., Jenkins, G.J. & Ephraums, J.J. (Eds.), 1990: *Climatic Change. The IPCC scientific assessment. Final report of working group I of the IPCC*. University Press, Cambridge.
- Idso, S.B., 1989: *Carbon dioxide and global change: Earth in transition*. IBR Press, Tempe, Arizona.
- Jacobs, C.M.J. & H.A.R. De Bruin, 1992: The sensitivity of regional transpiration to land-surface characteristics: significance of feedback. *J. of Clim.*, **5**, 683-698.



- Jacobs, C.M.J., H.A.R. De Bruin & A. Verhoef, 1991: The effects of surface inhomogeneities on the surface fluxes and on the development of the planetary boundary layer. *Ann. Geophys.*, **9**, 510-520.
- Jarman, P.D., 1974: The diffusion of carbon dioxide and water vapour through stomata. *J. Exp. Bot.*, **25**, 927-936.
- Jarvis, P.G., 1971: The estimation of resistances to carbon dioxide transfer. In: Z. Šesták, J. Čatský & P.G. Jarvis (Eds.), *plant photosynthetic production, manual of methods*. Dr. W. Junk N.V. Publishers, The Hague, 566-631.
- Jarvis, P.G., 1976: The interpretation of leaf water potential and stomatal conductance found in canopies in the field. *Phil. Trans. R. Soc. Lond., B.*, **273**, 593-610.
- Jarvis, P.G., 1986: Stomatal control of transpiration: scaling up from pore to paddock. In: C. Rosenzweig & R. Dickinson (Eds.), *Climate Vegetation Interactions, Proceedings of a workshop held at NASA/Goddard Space Flight Center, Greenbelt, Maryland, January 27-29 1986* UCAR Report OIES-2.
- Jarvis, P.G. & K.G. McNaughton, 1986: Stomatal control of transpiration: scaling up from leaf to region. *Adv. ecol. Res.* **15**, 1-49.
- Jarvis, P.G. & J.I.L. Morison, 1981: The control of transpiration and photosynthesis by the stomata. In: P.G. Jarvis & T.A. Mansfield (Eds.), *Stomatal Physiology*. Cambridge University Press, Cambridge, 247-279.
- Jensen, R.G., 1990: Ribulose 1, 5-biphosphate carboxylase/oxygenase: mechanism, activation, and regulation. In: D.T. Dennis & D.H. Turpin (Eds.), *Plant physiology, biochemistry and molecular biology*, Longman Scientific & Technical, Harlow, 224-238.
- Jones, H.G., 1985: Partitioning stomatal and non-stomatal limitations to photosynthesis. *Plant, Cell and Environment*, **8**, 95-104.
- Kim, J. & S.B. Verma, 1991: Modeling canopy photosynthesis: scaling up from a leaf to canopy in a temperate grassland ecosystem. *Agric. For. Meteorol.*, **57**, 187-208.
- Kimball, B.A., 1986: CO<sub>2</sub> stimulation of growth and yield under environmental restraints. In: Enoch, H.Z. and B.A. Kimball (Eds.), *Carbon Dioxide Enrichment of Greenhouse Crops. Volume II: Physiology, Yield and Economics*. CRC-Press Inc., Boca Raton, 53-67.
- Kimball, B.A., J.R. Mauney, F.S. Nakayama & S.B. Idso, 1993: Effects of increasing atmospheric CO<sub>2</sub> on vegetation. In: Rozema, J., H. Lambers, S.C. van der Geijn & M.L. Cambridge (Eds.), *CO<sub>2</sub> and Biosphere*. Advances in vegetation science 14, Kluwer Academic Publishers, Dordrecht, 65-75.
- Lange, O.L., R. Lösch, E.-D. Schulze & L. Kappen, 1971: Responses of stomata to changes in humidity. *Planta*, **100**, 76-86.
- Leegood, R.C. & C.B. Osmond, 1990: The flux of metabolites in C<sub>4</sub> and CAM plants. In: D.T. Dennis & D.H. Turpin (Eds.), *Plant physiology, biochemistry and molecular biology*, Longman Scientific & Technical, Harlow, 274-297.
- Lemon, E.R., (Ed.), 1983: *CO<sub>2</sub> and plants*. Westview Press, Boulder, Colorado.
- Lenschow, D.H., J.C. Wyngaard & W.T. Pennell, 1980: Mean-field and second-moment budgets in a baroclinic, convective boundary layer. *J. Atmos. Sci.*, **37**, 1313-1326.
- Leuning, R., 1983: Transport of gases into leaves. *Plant, Cell and Environment*, **6**, 181-194.
- Leuning, R., 1990: Modelling stomatal behaviour and photosynthesis of *Eucalyptus grandis*. *Aust. J. Plant Physiol.*, **17**, 150-175.
- Lhomme, J.-P., 1991: The concept of canopy resistance: historical survey and comparison of different approaches. *Agric. For. Meteorol.*, **54**, 227-240.
- Long, S.P., 1991: Modification of the response of photosynthetic productivity to rising temperature by atmospheric CO<sub>2</sub> concentrations: has its importance been underestimated? *Plant, Cell and Environment*, **14**, 729-739.
- Long, S.P., Baker, N.R. & C.A. Raines, 1993: Analysing the responses of photosynthetic CO<sub>2</sub> assimilation to long-term elevation of atmospheric CO<sub>2</sub> concentration. In: Rozema, J., H. Lambers, S.C. van der Geijn & M.L. Cambridge (Eds.), *CO<sub>2</sub> and Biosphere*. Advances in vegetation science 14, Kluwer Academic Publishers, Dordrecht, 33-45.

- Lösch, R. & J.D. Tenhunen, 1981: Stomatal responses to humidity - phenomenon and mechanism. In: P.G. Jarvis & T.A. Mansfield (Eds.), *Stomatal Physiology*. Cambridge University Press, Cambridge, 137-161.
- Louis, J.-F., 1979: A parametric model of vertical eddy fluxes in the atmosphere. *Boundary-Layer Met.*, **17**, 187-202.
- Louis, J.-F., M. Tiedtke, & J.F. Geleyn, 1982: A short history of the PBL parameterization at ECMWF. Workshop on Boundary Layer parameterisation, 25-27 November 1981, ECMWF, Reading.
- Louwerse, W., 1980: Effects of CO<sub>2</sub> concentration and irradiance on the stomatal behaviour of maize, barley and sunflower plants in the field. *Plant, Cell and Environment*, **3**, 391-398.
- Luxmoore, R.J., J.L. Stolzy & J.T. Holdeman, 1981: Sensitivity of a soil-plant-atmosphere model to changes in air temperature, dew point temperature and solar radiation. *Agric. Meteorol.*, **23**, 115-129.
- Lynn, B.H. & T.N. Carlson, 1990: A stomatal resistance model illustrating plant vs. external control of transpiration. *Agric. For. Meteorol.*, **52**, 5-43.
- Mahrt, L., H.-L. Pan, P. Ruscher & C.-T. Chu, 1987: Boundary layer parameterization for a Global Spectral Model. Rep. AFGL-TR-87-0246 of the Air Force Geophysics Laboratory.
- Mansfield, T.A., A.J. Travis & R.G. Jarvis, 1981: Responses to light and carbon dioxide. In: P.G. Jarvis & T.A. Mansfield (Eds.), *Stomatal Physiology*. Cambridge University Press, Cambridge, 121-135.
- Mascart, P., O. Taconet, J.-P. Pinty & M.B. Mehrez, 1991: Canopy resistance formulation and its effect in mesoscale models: a HAPEX perspective. *Agric. For. Meteorol.*, **54**, 319-351.
- Mason, P.J., 1988: The formation of areally-averaged roughness lengths. *Quart. J. Roy. Meteor. Soc.*, **114**, 399-420.
- Martin, P., N.J. Rosenberg & M.S. McKenny, 1989: Sensitivity of evapotranspiration in a wheat field, a forest and a grassland to changes in climatic and direct effects of carbon dioxide. *Climatic Change*, **14**, 117-151.
- McArthur, A.J., 1990: An accurate solution to the Penman equation. *Agric. For. Meteorol.*, **51**, 87-92.
- McCree, K.J., 1981: Photosynthetically Active Radiation. In: A. Pirson & M.H. Zimmerman (Eds.), *Encyclopedia of plant physiology, New Series, Vol 12A*: Berlin, Springer Verlag, 41-54.
- McCuen, R.H., 1974: A sensitivity analysis of procedures used for estimating evaporation. *Water Resour. Bull.*, **10**, 486-497.
- McNaughton, K.G., 1976: Evaporation and advection I: evaporation from extensive homogeneous areas. *Quart. J. Roy. Meteor. Soc.*, **102**, 181-191.
- McNaughton, K.G., 1989: Regional interactions between canopies and the atmosphere. In: G. Russell, B. Marshall and P.G. Jarvis (Eds.), *Plant canopies: their growth, form and function, SEB seminar series, 31*, Cambridge University Press, Cambridge, 63-81.
- McNaughton, K.G. & P.G. Jarvis, 1983: Predicting effects of vegetation changes on transpiration and evaporation. In: T.T. Kozlowski (Ed.), *Water deficits and plant growth, vol. 7*, 1-47, Academic Press, New York.
- McNaughton, K.G. & P.G. Jarvis, 1991: Effects of spatial scale on stomatal control of transpiration. *Agric. For. Meteorol.*, **54**, 279-301.
- McNaughton, K.G. & T.W. Spriggs, 1986: A mixed layer model for regional evaporation. *Boundary-Layer Met.*, **34**, 243-262, 1986.
- McNaughton, K.G. & T.W. Spriggs, 1989: An evaluation of the Priestley and Taylor equation and the complementary relationship using results from a mixed-layer model of the convective boundary layer. In: *IAHS publication 177: Proc. of a workshop on the estimation of areal evapotranspiration, Vancouver, B.C., Canada, August 1987*, IAHS press, Wallingford, 89-103.
- Mead, R. & R.N. Cumow, 1983: *Statistical methods in agriculture and experimental biology*. Chapman & Hall, London (1<sup>st</sup> Edition).
- Meidner, H. and T.A. Mansfield, 1968: *Physiology of Stomata*. McGraw-Hill, London.
- Meinzer, F.C., 1982: The effect of light on stomatal control of gas exchange in Douglas fir (*Pseudotsuga Menziesii*) saplings. *Oecologia*, **54**, 270-274.

- Mintz, Y., 1984: The sensitivity of numerically simulated climates to land-surface boundary conditions. In: J.T. Houghton (Ed.), *The Global Climate*. C.U.P, Cambridge, 79-106.
- Moeng, C.-H. & J.C. Wyngaard, 1986: An analysis of closures for pressure-scalar covariances in the convective boundary layer. *J. Atmos. Sci.*, **43**, 2499-2513.
- Moeng, C.-H. & J.C. Wyngaard, 1989: Evaluation of turbulent transport and dissipation closures in second-order modeling. *J. Atmos. Sci.*, **46**, 2311-2331.
- Monteith, J.L., 1963: Gas exchange in plant communities. In: L.T. Evans (Ed.), *Environmental Control of Plant Growth*. Academic Press, New York, 95-112.
- Monteith, J.L., 1965: Evaporation and the environment. *Symp. Soc. Exp. Biol.* **19**, 205-234.
- Monteith, J.L., 1991: Conservative behaviour in the response of crops to water and light. In: R. Rabbinge, J. Goudriaan, H. van Keulen, F.W.T. Penning de Vries & H.H. van Laar (Eds.), *Theoretical production ecology: reflections and prospects*, Pudoc, Wageningen.
- Monteith, J.L., 1993: The exchange of water and carbon by crops in a mediterranean climate. *Irrig. Sci.*, **14**, 85-91.
- Monteith, J.L., G.S. Campbell & E.A. Potter, 1988: Theory and performance of a dynamic diffusion porometer. *Agric. For. Meteorol.*, **44**, 27-38.
- Monteith, J.L. & M.H. Unsworth, 1990: *Principles of environmental physics* (2<sup>nd</sup> Ed.). Arnold, London.
- Morison, J.I.L., 1987: Stomatal response to CO<sub>2</sub>. In: E. Zeiger, G.D. Farquhar and I.R. Cowan (Eds.), *Stomatal Function*. Stanford University Press, Stanford, California, 229-251.
- Morison, J.I.L. & R.M. Gifford, 1983: Stomatal sensitivity to carbon dioxide and humidity: a comparison of two C<sub>3</sub> and two C<sub>4</sub> grass species. *Plant Physiology*, **71**, 789-796.
- Mott, K.A., 1988: Do stomata respond to CO<sub>2</sub> concentrations other than intercellular? *Plant Physiol.*, **86**, 200-203.
- Mott, K.A. & D.F. Parkhurst, 1991: Stomatal responses to humidity in air and helox. *Plant, Cell and Environment* **14**, 509-515.
- Ng, P.A.P. & P.G. Jarvis. 1980: Hysteresis in the response of stomatal conductance in *Pinus Sylvestris* L. needles to light: observations and a hypothesis. *Plant, Cell and Environment*, **3**, 207-216.
- Nobel, P.S., 1991: *Physiochemical and environmental plant physiology*. Academic Press Inc., San Diego.
- Noilhan, J. & S. Planton, 1989: A simple parameterization of land surface processes for meteorological models. *Monthly Weather Rev.*, **117**, 536-549.
- Nonami, H., E.-D. Schulze & H. Ziegler, 1990: Mechanisms of stomatal movements in response to air humidity, irradiance and xylem water potential. *Planta*, **183**, 57-64.
- Norman, J.M. & Polley, H.W., 1989: Canopy photosynthesis. In: W.R. Briggs (Ed.), *Photosynthesis*, Allan R. Liss, New York, 227-241.
- Pan, H.-L. & L. Mahrt, 1987: Interactions between soil hydrology and boundary-layer development. *Boundary-Layer Meteorol.*, **38**, 185-202.
- Panofsky, H.A., & J.A. Dutton, 1984: *Atmospheric turbulence; models and methods for engineering applications*. Wiley & Sons, New York.
- Parry, M.L., T.R. Carter & N.T. Konijn (Eds.), 1988: The impact of climatic variations on agriculture, Volume 1 & 2. Kluwer, Dordrecht.
- Paulson, C.A., 1970: The mathematical representation of wind speed and temperature profiles in the unstable atmospheric surface layer. *J. Appl. Meteor.*, **9**, 857-861.
- Paw U, K.T. & W. Gao, 1988: Application of solutions to nonlinear energy budget equations. *Agric. For. Meteorol.* **43**, 121-145.
- Pearcy, R.W. and O. Björkman 1983: Physiological effects. In: E.R. Lemon (Ed.), *CO<sub>2</sub> and plants*. Westview Press, Boulder, Colorado, 65-105.
- Pearcy, R.W. & J. Ehleringer, 1984: Comparative ecophysiology of C<sub>3</sub> and C<sub>4</sub> plants. *Plant, Cell and Environment*, **7**, 1-13.
- Pearman, G.I. & J.R. Garratt, 1973: Carbon dioxide measurements above a wheat crop. I. Observations of vertical gradients and concentrations. *Agric. Meteorol.*, **12**, 13-25.

- Pinty, J.P., P. Mascart, E. Richard & R. Rosset, 1989: An investigation of mesoscale flows induced by vegetation inhomogeneities using an evapotranspiration model calibrated against HAPEX--MOBILHY data. *J. Appl. Meteor.*, **29**, 976-982.
- Price, D.T. & T.A. Black, 1990: Effects of short-term variation in weather on diurnal canopy CO<sub>2</sub> flux and evapotranspiration of a juvenile Douglas-fir stand. *Agric. For. Meteorol.*, **50**, 139-158.
- Radmer, R.J. & B. Kok, 1977: Light conversion efficiency in photosynthesis. In: A. Trebst & M. Avron (Eds.), *Encyclopedia of Plant Physiology, New Series, Vol. 5: Photosynthesis I, Photosynthetic Electron Transport and Photophosphorylation*. Springer Verlag, Berlin, 125-136.
- Raschke, K., 1979: Movements of stomata. In: W. Haupt & M.E. Feinleib (Eds.) *Encyclopedia of Plant Physiology, New Series, Vol. 7, Physiology of Movements*. Springer-Verlag, Berlin, 381-444.
- Raschke, K., 1986: The influence of the CO<sub>2</sub> content of the ambient air on stomatal conductance and the CO<sub>2</sub> concentration in leaves. In: Enoch, H.Z. and B.A. Kimball (Eds.) *Carbon Dioxide Enrichment of Greenhouse Crops. Volume II: Physiology, Yield and Economics*. CRC-Press Inc., Boca Raton, 87-102.
- Raschke, K., 1987: Action of abscisic acid on guard cells. In: E. Zeiger, G.D. Farquhar and I.R. Cowan (Eds.), *Stomatal Function*. Stanford University Press, Stanford, California, 253-279.
- Raupach, M.R., 1991: Vegetation-atmosphere interaction in homogeneous and heterogeneous terrain: some implications of mixed-layer dynamics. *Vegetatio* **91**, 105-120.
- Ray, T.B. & C.C. Black, 1979: The C<sub>4</sub> pathway and its regulation. In: M. Gibbs & E. Latzko (Eds.), *Encyclopedia of Plant Physiology, New Series, Vol. 6: Photosynthesis II, Photosynthetic Carbon Metabolism and Related Processes*. Springer Verlag, Berlin, 77-101.
- Reicosky, D.C., 1989: Diurnal and seasonal trends in carbon dioxide concentrations in corn and soybean canopies as affected by tillage and irrigation. *Agric. For. Meteorol.*, **48**, 285-303.
- Reynolds, J.F., J.L. Chen, P.C. Harley, D.W. Hilbert, R.L. Dougherty & J.D. Tenhunen, 1992: Modeling the effects of elevated CO<sub>2</sub> on plants: extrapolating leaf response to a canopy. *Agric. For. Meteorol.*, **61**, 69-94.
- Rodrigues, M.L., M.M. Chaves, R. Wendler, M.M. David, W.P. Quick, R.C. Leegood, M. Stitt & J.S. Pereira, 1993: Osmotic adjustment in water stressed grapevine leaves in relation to carbon assimilation. *Aust. J. Plant Physiol.*, **20**, 309-321.
- Rosenberg, N.J., 1981: The increasing CO<sub>2</sub> concentration in the atmosphere and its implication on agricultural productivity. I. Effects on photosynthesis, transpiration and water use efficiency. *Climatic Change*, **3**, 265-279.
- Rosenberg, N.J., M.S. McKenny & P. Martin, 1989: Evapotranspiration in a greenhouse-warmed world: a review and a simulation. *Agric. For. Meteorol.*, **47**, 303-320.
- Ross, J., 1975: Radiative transfer in plant communities. In: Monteith, J.L. (Ed.), *Vegetation and the atmosphere, Vol. 1., principles*, Academic Press, New York, 13-55.
- Rowntree, P.R., 1991: Atmospheric parameterization schemes for evaporation over land, basic concepts and climate modelling aspects. In: T.J. Schmugge & J.C. André (Eds.), *Measurement and Parameterization of Land Surface Evaporation Fluxes*, Springer Verlag, New York, 5-29.
- Rozema, J., H. Lambers, S.C. van der Geijn & M.L. Cambridge (Eds.), 1993: *CO<sub>2</sub> and Biosphere*. Advances in vegetation science 14, Kluwer Academic Publishers, Dordrecht.
- Ruckdeschel, F.R., 1981: *Basic scientific subroutines*. Byte, Peterborough.
- Russel, G., 1980: Crop evaporation, surface resistance and soil water status. *Agric. Meteorol.*, **21**, 213-226.
- Sack, F.D., 1987: The development and structure of stomata. In: E. Zeiger, G.D. Farquhar and I.R. Cowan (Eds.), *Stomatal Function*. Stanford University Press, Stanford, 59-89.
- Saxton, K.E., 1975: Sensitivity analyses of the combination evapotranspiration equation. *Agric. Meteorol.*, **15**, 343-353.
- Schmugge, T.J. & J.C. André (Eds.), 1991: *Measurement and Parameterization of Land Surface Evaporation Fluxes*. Springer Verlag, New York.

- Schönherr, J., 1976: Water permeability of cuticular membranes. In: O.L. Lange, L. Kappen & E.-D. Schulze (Eds.), *Water and plant life, problems and modern approaches*. Springer Verlag Berlin-Heidelberg, 148-159.
- Schulze, E.-D., & A.E. Hall, 1982: Stomatal responses, water loss and CO<sub>2</sub> assimilation rates of plants in contrasting environments. In: O.L. Lange, P.S. Nobel, C.B. Osmond & H. Ziegler (Eds.), *Encyclopedia of Plant Physiology, New Series, Vol. 12B, Physiological Plant Ecology II*. Springer Verlag, Berlin, 181-230.
- Schulze, E.-D., N.C. Turner, T. Gollan & K.A. Shackel, 1987: Stomatal responses to air humidity and soil drought. In: E. Zeiger, G.D. Farquhar and I.R. Cowan (Eds.), *Stomatal Function*. Stanford University Press, Stanford, California, 311-321.
- Schumann, U., 1989: Large-eddy simulation of turbulent diffusion with chemical reactions in the convective boundary layer. *Atmospheric Environment*, **23**, 1713-1727.
- Segal, M & R.W. Arritt, 1992: Nonclassical mesoscale circulations caused by surface sensible heat flux gradients. *Bull. Amer. Meteor. Soc.*, **73**, 1593-1604.
- Segal, M., R. Avissar, M.C. McCumber & R.A. Pielke, 1988: Evaluation of vegetation effects on the generation and modification of mesoscale circulation. *J. Atmos. Sci.*, **45**, 2268-2292.
- Segal, M., J.R. Garratt, G. Kallos & R.A. Pielke, 1989: The impact of wet soil and canopy temperatures on daytime boundary-layer growth. *J. Atmos. Sci.*, **46**, 3673-3684.
- Sellers, P.J. & J.L. Dorman, 1987: Testing the Simple Biosphere Model (SiB) using point micrometeorological and biophysical data. *J. Appl. Meteor.*, **26**, 622-651.
- Sharkey, T.D. & T. Ogawa, 1987: Stomatal responses to light. In: E. Zeiger, G.D. Farquhar and I.R. Cowan (Eds.), *Stomatal Function*. Stanford University Press, Stanford, California, 195-208.
- Shugart, H.H., M.Ya Antonovski, P.G. Jarvis & A.P. Sandford, 1986: CO<sub>2</sub>, climatic change and forest ecosystems. In: B. Bolin, B.R. Döös, J. Jäger and R.A. Warrick (Eds.), *The greenhouse effect, climatic change, and ecosystems*. Scope 29, Wiley & Sons, New York, 475-521.
- Shuttleworth, W.J., 1976: A one-dimensional theoretical description of the vegetation-atmosphere interaction. *Bound.-Layer Meteorol.*, **10**, 273-302.
- Shuttleworth, W.J., 1988: Macrohydrology - the new challenge for process hydrology. *J. Hydrology*, **100**, 31-56.
- Shuttleworth, W.J., 1989: Micrometeorology of temperate and tropical forest. *Phil. Trans. R. Soc. Lond.*, **B 324**, 299-334.
- Shuttleworth, W.J., 1991a: Evaporation models in hydrology. In: Schmugge, T.J. & J.C. André (Eds.), *Measurement and Parameterization of Land Surface Evaporation Fluxes*. Springer Verlag, New York, 93-120.
- Shuttleworth, W.J., 1991b: Insight from large-scale observational studies of land/atmosphere interactions. *Surveys in Geophysics*, **12**, 3-30.
- Shuttleworth, W.J. & J.S. Wallace, 1985: Evaporation from sparse crops-an energy combination theory. *Quart. J. Roy. Meteor. Soc.*, **111**, 839-855.
- Spitters, C.J.T., 1986: Separating the diffuse and direct component of global radiation and its implications for modeling canopy photosynthesis. Part II: Calculation of canopy photosynthesis. *Agric. For. Meteorol.*, **38**, 231-242.
- Spitters, C.J.T., H.A.J.M. Toussaint & J. Goudriaan, 1986: Separating the diffuse and direct component of global radiation and its implications for modeling canopy photosynthesis. Part I: Components of incoming radiation. *Agric. For. Meteorol.*, **38**, 217-230.
- Stanghellini, C., 1987: *Transpiration of greenhouse crops, an aid to climate management*. Thesis, IMAG, Wageningen.
- Stewart, J.B., 1983: A discussion of the relationships between the principal forms of the combination equation for estimating crop evaporation. *Agric. Meteorol.*, **30**, 111-127.
- Stewart, J.B., 1988: Modelling surface conductance of pine forest, *Agric. For. Meteorol.*, **43**, 19-35.
- Stewart, J.B., & A.S. Thom, 1973: Energy budgets in pine forests. *Quart. J. Roy. Meteor. Soc.*, **99**, 154-170.

- Stigter, C.J., 1972: Leaf diffusion resistance to water vapour and its direct measurement, I. Introduction and review concerning relevant factors and methods. *Meded. Landbouwhoges. Wageningen*, 72-3, 1-47.
- Stigter, C.J., J. Birnie & B. Lammers, 1973: Leaf diffusion resistance to water vapour and its direct measurement, II. design, calibration and pertinent theory of an improved leaf diffusion resistance meter. *Meded. Landbouwhoges. Wageningen*, 73-15, 1-55.
- Stigter, C.J. & Lammers, 1974: Leaf diffusion resistance to water vapour and its direct measurement, III. results regarding the improved diffusion porometer in growth rooms and fields of Indian Corn (*Zea Mays*). *Meded. Landbouwhoges. Wageningen*, 74-21, 1-76.
- Stitt, M., 1991: Rising CO<sub>2</sub> levels and their potential significance for carbon flow in photosynthetic cells. *Plant, Cell and Environment*, 14, 741-762.
- Strain, B.R. & J.D. Cure, 1985: *Direct effects of increasing CO<sub>2</sub> on vegetation*. US dept. of energy, DOE/ER-0238, Washington DC.
- Stryer, L., 1981: *Biochemistry* (2<sup>nd</sup> edition). W.H. Freeman and Company, San Francisco.
- Stulen, I. & J. Den Hertog, 1993: Root growth and functioning under atmospheric CO<sub>2</sub> enrichment. In: Rozema, J., H. Lambers, S.C. van der Geijn & M.L. Cambridge (Eds.): *CO<sub>2</sub> and Biosphere*. Advances in vegetation science 14, Kluwer Academic Publishers, Dordrecht, 99-115.
- Stull, R.B., 1988: *An introduction to boundary layer meteorology*. Kluwer Academic Publishers, Dordrecht.
- Swinbank, W.C., 1963: Long-wave radiation from clear skies. *Quart. J. Roy. Meteor. Soc.*, 89, 339-348.
- Thom, A.S. & H.R. Oliver, 1977: On Penman's equation for estimating regional evaporation. *Quart. J. Roy. Meteor. Soc.*, 103, 345-357.
- Ten Berge, H.F.M., 1990: Heat and water transfer at the bare top soil and in the lower atmosphere. *Simulation monographs*, 33, Pudoc, Wageningen.
- Tenhunen, J.D., R.W. Pearcy & O.L. Lange, 1987: Diurnal variations in leaf conductance and gas exchange in natural environments. In: E. Zeiger, G.D. Farquhar and I.R. Cowan (Eds.), *Stomatal Function*. Stanford University Press, Stanford, California, 323-351.
- Tennekes, H., 1973: A model for the dynamics of the inversion above a convective boundary layer. *J. Atmos. Sci.*, 30, 558-567.
- Tennekes, H., & A.G.M. Driedonks, 1981: Basic entrainment equations for the atmospheric boundary layer. *Boundary-Layer Meteorol.*, 20, 515-531.
- Thom, A.S., 1975: Momentum, mass and heat exchange of plant communities. In: Monteith (Ed.), *Vegetation and the atmosphere, Vol. 1, principles*, Academic Press Inc., New York, 57-109.
- Thornley, J.H.M., 1976: *Mathematical models in plant physiology*. Academic Press, London.
- Tolbert, N.E. & I. Zeltich, 1983: Carbon metabolism. In: E.R. Lemon (Ed.), *CO<sub>2</sub> and plants*. Westview Press, Boulder, Colorado, 65-105.
- Troen, I.B. & L. Mahrt, 1986: A simple model of the atmospheric boundary layer, sensitivity to surface evaporation. *Boundary-Layer Meteorol.*, 37, 129-148.
- Turner, N.C., 1991: Measurement and influence of environmental and plant factors on stomatal conductance in the field. *Agric. For. Meteorol.*, 54, 137-154.
- Tyree, M.T., & J.D. Alexander, 1993: Plant water relations and the effects of elevated CO<sub>2</sub>: a review and suggestions for future research. In: Rozema, J., H. Lambers, S.C. van der Geijn & M.L. Cambridge (Eds.), *CO<sub>2</sub> and Biosphere*. Advances in vegetation science 14, Kluwer Academic Publishers, Dordrecht, 47-62.
- Van der Laan, P., 1982: *TS 6 (Verdelingsvrije methoden)* (Dutch text). Available from: Dept. of Mathematics, Agricultural University, Wageningen.
- Van Heemst, 1986: Potential crop production. In: H. van Keulen & J. Wolf (Eds.), *Modelling of agricultural production: weather, soil and crops*. Simulation Monographs, Pudoc, Wageningen.
- Van Hove, L.W.A., 1989: The mechanism of NH<sub>3</sub> and SO<sub>2</sub> uptake by leaves and its physiological effects. *Thesis*, Agricultural University, Wageningen.

- Van Hove, L.W.A., M.E. Bossen, M.G.J. Mensink & O. Van Kooten, 1992: Physiological effects of a long term exposure to low concentrations of  $\text{NH}_3$ ,  $\text{NO}_2$  and  $\text{SO}_2$  on Douglas fir (*Pseudotsuga Menziesii*). *Physiol. Plant.*, **86**, 559-567.
- Van Kleef, 1991: *Handleiding Bladfotosynthesemeter* (Dutch text). Available from: CABO-DLO, Wageningen.
- Verma, S.B. & N.J. Rosenberg, 1976: Vertical profiles of carbon dioxide concentration un stable stratification. *Agric. Meteorol.*, **16**, 359-369.
- Von Caemmerer, S. & G.D. Farquhar, 1981: Some relationships between the biochemistry of photosynthesis and the gas exchange of leaves. *Planta*, **153**, 376-387.
- Warrick, R.A., R.M. Gifford & M.L. Parry, 1986:  $\text{CO}_2$ , climatic change and agriculture. Assessing the response of food crops to the direct effects of increased  $\text{CO}_2$  and climatic change. In: B. Bolin, B.R. Döös, J. Jäger and R.A. Warrick (Eds.), *The greenhouse effect, climatic change, and ecosystems*. Scope 29, Wiley & Sons, New York, 393-473.
- Wieringa, J., 1986: Roughness-dependent geographical interpolation of surface wind speed averages. *Quart. J. Roy. Meteor. Soc.*, **112**, 867-889.
- Wilson, M.F., A. Henderson-Sellers, R.E. Dickinson & P.J. Kennedy, 1987: Sensitivity of the Biosphere-Atmosphere Transfer Scheme (BATS) to the inclusion of variable soil characteristics. *J. Clim. Appl. Meteor.* **26**, 341-362.
- Winkel, T. & S. Rambal 1990: Stomatal conductance of some grapevines growing in the field under Mediterranean environment. *Agric. For. Meteorol.*, **51**, 107-121.
- Wong, S.C., I.R. Cowan & G.D. Farquhar, 1979: Stomatal conductance correlates with photosynthetic capacity. *Nature*, **282**, 424-426.
- Woodward, F.I., 1993: Plant responses to past concentrations of  $\text{CO}_2$ . In: Rozema, J., H. Lambers, S.C. van der Geijn & M.L. Cambridge (Eds.),  *$\text{CO}_2$  and Biosphere*. Advances in vegetation science 14, Kluwer Academic Publishers, Dordrecht, 145-155.
- Wyngaard, J.C., 1987: A physical mechanism for the asymmetry in top-down and bottom-up diffusion. *J. Atmos. Sci.*, **44**, 1083-1087.
- Wyngaard, J.C. & R.A. Brost, 1984: Top-down and bottom-up diffusion of a scalar in the convective boundary layer. *J. Atmos. Sci.*, **41**, 102-112.
- Zeiger, E., M. Iino, K.-I. Shimazaki & T. Ogawa, 1987: The blue-light response of stomata: mechanism and function. In: E. Zeiger, G.D. Farquhar and I.R. Cowan (Eds.), *Stomatal Function*. Stanford University Press, Stanford, California, 209-227.
- Ziegler, H., 1987: The evolution of stomata. In: E. Zeiger, G.D. Farquhar & I.R. Cowan (Eds.), *Stomatal function*. Stanford University Press, Stanford, 29-57.

## Curriculum Vitae

Cornelis Maria Johannes Jacobs werd geboren op 27 februari 1961 in Tegelen. In 1979 behaalde hij aan het St. Thomacollege te Venlo het diploma Gymnasium-β. Later in dat jaar begon hij de studie Milieuhygiëne aan de toenmalige Landbouwhogeschool te Wageningen. De kandidaatsfase en de eerste fase van de doctoraalstudie stonden in het teken van de arbeidshygiëne. Na een stage voor de Regenboogfractie van het Europe Parlement maakte hij de definitieve overstap naar de buitenluchthygiëne en de meteorologie. De studie werd in januari 1987 afgerond met als hoofdvakken luchthygiëne en meteorologie, en met gezondheidsleer als bijvak. Vervolgens was hij drie maanden in dienst van het kersverse Meteo Consult b.v. te Wageningen. Daar verrichtte hij een adviserend onderzoek ten behoeve van de Stichting Onderzoek Wereldvoedselvoorziening (SOW) en de Beleids Commissie Remote Sensing (BCRS), naar de toepasbaarheid van Meteosat-waarnemingen voor het schatten van neerslaghoeveelheden in Zambia. In de zomer van 1987 begon hij als erkend gewetensbezwaarde aan zijn vervangende dienst als onderzoeksassistent bij de sectie Weerkunde van de toenmalige vakgroep Natuur- en Weerkunde van de Landbouwuniversiteit. In die tijd is zijn speciale belangstelling voor de grenslaagmeteorologie en de micrometeorologie gewekt. In februari 1989 zwaaide hij af, waarna hij op zaterdag 1 april van dat jaar als onderzoeker in opleiding (OIO) in dienst trad van de Nederlandse Organisatie voor Wetenschappelijk Onderzoek (NWO). Gedurende de jaren daarna werkte hij bij de vakgroep Meteorologie van de Landbouwuniversiteit aan het onderzoek dat in dit proefschrift beschreven is.